Publishing House ASV

begell house, inc. publishers

PAACH

Scientific coordination is carried out by the Russian Academy of Architecture and Construction Sciences (RAACS)

Volume 15 • Issue 3 • 2019

ISSN 2588-0195 (Online)
ISSN 2587-9618 (Print) Continues ISSN 1524-5845

International Journal for

Computational Civil and Structural Engineering

Международный журнал по расчету гражданских и строительных конструкций

http://raasn.ru/public.php
http://ijccse.iasv.ru

DOI: 10.22337/2587-9618
GICID: 71.0000.1500.2830

PUBLISHER

ASV Publishing House
(ООО «Издательство АСВ»)
19/1,12, Yaroslavskoe Shosse, 120338, Moscow, Russia
Tel. +7(925)084-74-24; E-mail: iasv@iasv.ru; Интернет-сайт: http://iasv.ru/

ADVISORY EDITORIAL BOARD

TECHNICAL EDITOR

EDITORIAL TEAM

INVITED REVIEWERS

AIMS AND SCOPE

The aim of the Journal is to advance the research and practice in structural engineering through the application of computational methods. The Journal will publish original papers and educational articles of general value to the field that will bridge the gap between high-performance construction materials, large-scale engineering systems and advanced methods of analysis.

The scope of the Journal includes papers on computer methods in the areas of structural engineering, civil engineering materials and problems concerned with multiple physical processes interacting at multiple spatial and temporal scales. The Journal is intended to be of interest and use to researches and practitioners in academic, governmental and industrial communities.

ОБЩАЯ ИНФОРМАЦИЯ О ЖУРНАЛЕ

International Journal for Computational Civil and Structural Engineering

(Международный журнал по расчету гражданских и строительных конструкций)

Международный научный журнал "International Journal for Computational Civil and Structural Engineering (Международный журнал по расчету гражданских и строительных конструкций)" (IJCCSE) является ведущим научным периодическим изданием по направлению «Инженерные и технические науки», издаваемым, начиная с 1999 года (ISSN 2588-0195 (Online); ISSN 2587-9618 (Print) Continues ISSN 1524-5845). В журнале на высоком научно-техническом уровне рассматриваются проблемы численного и компьютерного моделирования в строительстве, актуальные вопросы разработки, исследования, развития, верификации, апробации и приложений численных, численно-аналитических методов, программно-алгоритмического обеспечения и выполнения автоматизированного проектирования, мониторинга и комплексного наукоемкого расчетно-теоретического и экспериментального обоснования напряженно-деформированного (и иного) состояния, прочности, устойчивости, надежности и безопасности ответственных объектов гражданского и промышленного строительства, энергетики, машиностроения, транспорта, биотехнологий и других высокотехнологичных отраслей.

В редакционный совет журнала входят известные российские и зарубежные деятели науки и техники (в том числе академики, члены-корреспонденты, иностранные члены, почетные члены и советники Российской академии архитектуры и строительных наук). Основной критерий отбора статей для публикации в журнале − их высокий научный уровень, соответствие которому определяется в ходе высококвалифицированного рецензирования и объективной экспертизы, поступающих в редакцию материалов.

Журнал входит в Перечень ВАК РФ ведущих рецензируемых научных изданий, в которых должны быть опубликованы основные научные результаты диссертаций на соискание ученой степени кандидата наук, на соискание ученой степени доктора наук по научным специальностям и соответствующим им отраслям науки:

- 01.02.04 – Механика деформируемого твердого тела (технические науки),
- 05.13.18 – Математическое моделирование численные методы и комплексы программ (технические науки),
- 05.23.01 – Строительные конструкции, здания и сооружения (технические науки),
- 05.23.02 – Основания и фундаменты, подземные сооружения (технические науки),
- 05.23.05 – Строительные материалы и изделия (технические науки),
- 05.23.07 – Гидротехническое строительство (технические науки),
- 05.23.17 – Строительная механика (технические науки).

В Российской Федерации журнал индексируется Российским индексом научного цитирования (РИНЦ).

Журнал входит в базу данных Russian Science Citation Index (RSCI), полностью интегрированную с платформой Web of Science. Журнал имеет международный статус и высылается в ведущие библиотеки и научные организации мира.

Издатели журнала – *Издательство Ассоциации строительных высших учебных заведений /АСВ/* (Россия, г. Москва) и до 2017 года *Издательский дом Begell House Inc.* (США, г. Нью-Йорк). Официальными партнерами издания является *Российская академия архитектуры и строительных наук* (*РААСН*), осуществляющая научное курирование издания, и *Научно-исследовательский центр СтаДиО* (ЗАО НИЦ СтаДиО).

Цели журнала – демонстрировать в публикациях российскому и международному профессиональному сообществу новейшие достижения науки в области вычислительных ме-

тодов решения фундаментальных и прикладных технических задач, прежде всего в области строительства.

Задачи журнала:

- предоставление российским и зарубежным ученым и специалистам возможности публиковать результаты своих исследований;
- привлечение внимания к наиболее актуальным, перспективным, прорывным и интересным направлениям развития и приложений численных и численно-аналитических методов решения фундаментальных и прикладных технических задач, совершенствования технологий математического, компьютерного моделирования, разработки и верификации реализующего программно-алгоритмического обеспечения;
- обеспечение обмена мнениями между исследователями из разных регионов и государств.

Тематика журнала. К рассмотрению и публикации в журнале принимаются аналитические материалы, научные статьи, обзоры, рецензии и отзывы на научные публикации по фундаментальным и прикладным вопросам технических наук, прежде всего в области строительства. В журнале также публикуются информационные материалы, освещающие научные мероприятия и передовые достижения Российской академии архитектуры и строительных наук, научно-образовательных и проектно-конструкторских организаций.

Тематика статей, принимаемых к публикации в журнале, соответствует его названию и охватывает направления научных исследований в области разработки, исследования и приложений численных и численно-аналитических методов, программного обеспечения, технологий компьютерного моделирования в решении прикладных задач в области строительства, а также соответствующие профильные специальности, представленные в диссертационных советах профильных образовательных организациях высшего образования.

Редакционная политика. Политика редакционной коллегии журнала базируется на современных юридических требованиях в отношении авторского права, законности, плагиата и клеветы, изложенных в законодательстве Российской Федерации, и этических принципах, поддерживаемых сообществом ведущих издателей научной периодики.

За публикацию статей плата с авторов не взымается. Публикация статей в журнале бесплатная. На платной основе в журнале могут быть опубликованы материалы рекламного характера, имеющие прямое отношение к тематике журнала.

Журнал предоставляет непосредственный открытый доступ к своему контенту, исходя из следующего принципа: свободный открытый доступ к результатам исследований способствует увеличению глобального обмена знаниями.

Индексирование. Публикации в журнале входят в системы расчетов индексов цитирования авторов и журналов. «Индекс цитирования» — числовой показатель, характеризующий значимость данной статьи и вычисляющийся на основе последующих публикаций, ссылающихся на данную работу.

Авторам. Прежде чем направить статью в редакцию журнала, авторам следует ознакомиться со всеми материалами, размещенными в разделах сайта журнала (интернет-сайт Российской академии архитектуры и строительных наук (http://raasn.ru); подраздел «Издания РААСН» или интернет-сайт Издательства АСВ (http://iasv.ru); подраздел «Журнал IJCCSE»): с основной информацией о журнале, его целями и задачами, составом редакционной коллегии и редакционного совета, редакционной политикой, порядком рецензирования направляемых в журнал статей, сведениями о соблюдении редакционной этики, о политике авторского права и лицензирования, о представлении журнала в информационных системах (индексировании), информацией о подписке на журнал, контактными данными и пр. Журнал рабо-

Рецензирование. Все научные статьи, поступившие в редакцию журнала, проходят обязательное двойное слепое рецензирование (рецензент не знает авторов рукописи, авторы рукописи не знаю рецензентов).

Заимствования и плагиат. Редакционная коллегия журнала при рассмотрении статьи проводит проверку материала с помощью системы «Антиплагиат». В случае обнаружения многочисленных заимствований редакция действует в соответствии с правилами COPE.

Подписка. Журнал зарегистрирован в Федеральном агентстве по средствам массовой информации и охраны культурного наследия Российской Федерации. Индекс в общероссийском каталоге РОСПЕЧАТЬ − 18076.

По вопросам подписки на международный научный журнал “International Journal for Computational Civil and Structural Engineering (Международный журнал по расчету гражданских и строительных конструкций)” обращайтесь в Агентство «Роспечать» (Официальный сайт в сети Интернет: http://www.rosp.ru/) или в издательство Ассоциации строительных вузов (АСВ) в соответствии со следующими контактными данными:

ООО «Издательство АСВ»

Юридический адрес: 129337, Россия, г. Москва, Ярославское ш., д. 26, офис 705;

Фактический адрес: 129337, Россия, г. Москва, Ярославское ш., д. 19, корп. 1, 5 этаж, офис 12;

Телефоны: +7 (925) 084-74-24, +7 (926) 010-91-33;

Интернет-сайт: www.iasv.ru. Адрес электронной почты: iasv@iasv.ru.

Контактная информация. По всем вопросам работы редакции, рецензирования, согласования правки текстов и публикации статей следует обращаться к главному редактору журнала члену-корреспонденту РААСН *Сидорову Владимиру Николаевичу* (адреса электронной почты: sidorov.vladimir@gmail.com, sidorov@iasv.ru, iasv@iasv.ru, sidorov@raasn.ru) или к техническому редактору журнала советнику РААСН *Кайтукову Таймуразу Батразовичу* (адреса электронной почты: tkaytukov@gmail.com; kaytukov@raasn.ru). Кроме того, по указанным вопросам, а также по вопросам размещения в журнале рекламных материалов можно обращаться к генеральному директору ООО «Издательство АСВ» *Никитиной Надежде Сергеевне* (адреса электронной почты: iasv@iasv.ru, nsnikitina@mail.ru, ijccse@iasv.ru).

Журнал становится технологичнее. Издательство АСВ с сентября 2016 года является членом Международной ассоциации издателей научной литературы (Publishers International Linking Association (PILA)), осуществляющей свою деятельность на платформе CrossRef. Оригинальным статьям, публикуемым в журнале, будут присваиваться уникальные номера (индексы DOI – Digital Object Identifier), что значительно облегчит поиск метаданных и местонахождение полнотекстового произведения. DOI – это система определения научного контента в сети Интернет.

С октября 2016 года стал возможен прием статей на рассмотрение и рецензирование через онлайн систему приема статей Open Journal Systems на сайте журнала (электронная редакция): http://ijccse.iasv.ru/index.php/IJCCSE.

Автор имеет возможность следить за продвижением статьи в редакции журнала в личном кабинете Open Journal Systems и получать соответствующие уведомления по электронной почте.

В феврале 2018 года журнал был зарегистрирован в Directory of open access journals (DOAJ) (это один из самых известных поисковых сервисов в мире, который предоставляет открытый доступ к материалам и индексирует не только заголовки журналов, но и научные статьи), в сентябре 2018 года включен в продукты EBSCO Publishing.

International Journal for
Computational Civil and Structural Engineering
(Международный журнал по расчету гражданских и строительных конструкций)
Volume 15, Issue 3 ***2019***

Scientific coordination is carried out by the Russian Academy of Architecture and Construction Sciences (RAACS)

CONTENTS

International Journal for
Computational Civil and Structural Engineering
(Международный журнал по расчету гражданских и строительных конструкций)
Volume 15, Issue 3 ***2019***

Scientific coordination is carried out by the Russian Academy of Architecture and Construction Sciences (RAACS)

СОДЕРЖАНИЕ

DOI:10.22337/2587-9618-2019-15-3-14-39

STRUCTURES OF THE HIGH-RISE BUILDING "LAKHTA CENTER" IN SAINT-PETERSBURG

Elena A. Ilyukhina [1], Sergey I. Lakhman [2], Alexey B. Miller [3], Vladimir I. Travush [2, 4]

[1] Joint Stock Company "Multifunctional complex Lakhta Center", Saint-Petersburg, RUSSIA
[2] Close Joint Stock Company "Planning Institute of Residential and Public Buildings", Moscow, RUSSIA
[3] Public Joint Stock Company Gazprom, Saint-Petersburg, RUSSIA
[4] Russian Academy of Architecture and Construction Sciences, Moscow, RUSSIA

Abstract: The "Lakhta Center" skyscraper that built up in Saint-Petersburg on the coast of Baltic sea at the end of 2018 is the highest building of Europe. The tower has 87 floors above the ground and 2 underground floors. The distinctive paper is devoted to structures of this skyscraper. Particularly piled foundation, building structures of the underground part (substructure), building structures of the aboveground part (building superstructure), designs of steel-reinforced concrete columns, design of slabs, structural analysis, some loads and impacts, aerodynamic tests, engineering-geological research, testing of steel-reinforced concrete columns, glass racks and structural health monitoring are under consideration.

Keywords: high-rise building "Lakhta Center", building structures, steel-reinforced concrete columns, loads and impacts, structural analysis, structural-health monitoring

КОНСТРУКЦИИ ВЫСОТНОГО ЗДАНИЯ «ЛАХТА ЦЕНТР» В САНКТ-ПЕТЕРБУРГЕ

Е.А. Илюхина [1], С.И. Лахман [2], А.Б. Миллер [3], В.И. Травуш [2, 4]

[1] АО «Многофункциональный комплекс Лахта Центр», г. Санкт-Петербург, РОССИЯ
[2] ЗАО «Городской проектный институт жилых и общественных зданий», г. Москва, РОССИЯ
[3] ПАО «Газпром», г. Москва, РОССИЯ
[4] Российская академия архитектуры и строительных наук, г. Москва, РОССИЯ

Аннотация: Построенный в конце 2018 года небоскреб «Лахта Центр» высотой 462 метра, расположенный в городе Санкт-Петербурге на берегу Балтийского моря, является самым высоким зданием в Европе. Башня имеет 87 надземных этажей и 2 подземных этажа. В настоящей статье рассматриваются конструкции этого высотного здания, в частности, приводится информация о свайном основании, конструкциях подземной части, конструкциях надземной части, конструкциях сталежелезобетонных колонн, конструкциях перекрытий, кратко описаны проведенные расчеты строительных конструкций и определение некоторых видов нагрузок, аэродинамические испытания, инженерно-геологические исследования, испытания сталежелезобетонных колонн, стеклянные стойки, реализованная система мониторинга объекта.

Ключевые слова: высотное здание «Лахта Центр», строительные конструкции, сталежелезобетонные колонны, нагрузки и воздействия, расчетное обоснование, мониторинг

1. GENERAL INFORMATION

The Lakhta Center skyscraper (tower) that built up in Saint-Petersburg on the coast of Baltic sea at the end of 2018 is the highest building of Europe. The tower has 87 floors above the ground and 2 underground floors.

In the plan, the tower is pentagonal star, the beams of which go apart from the central core, the building takes twisted conical form. Slabs of the overlap made of five square "petals" interconnected by the circle central core. Through the height of the building square "petals" rotate around their own axes counterclockwise for 0.82 degree at each floor (Figures 1, 2, 3, 4).

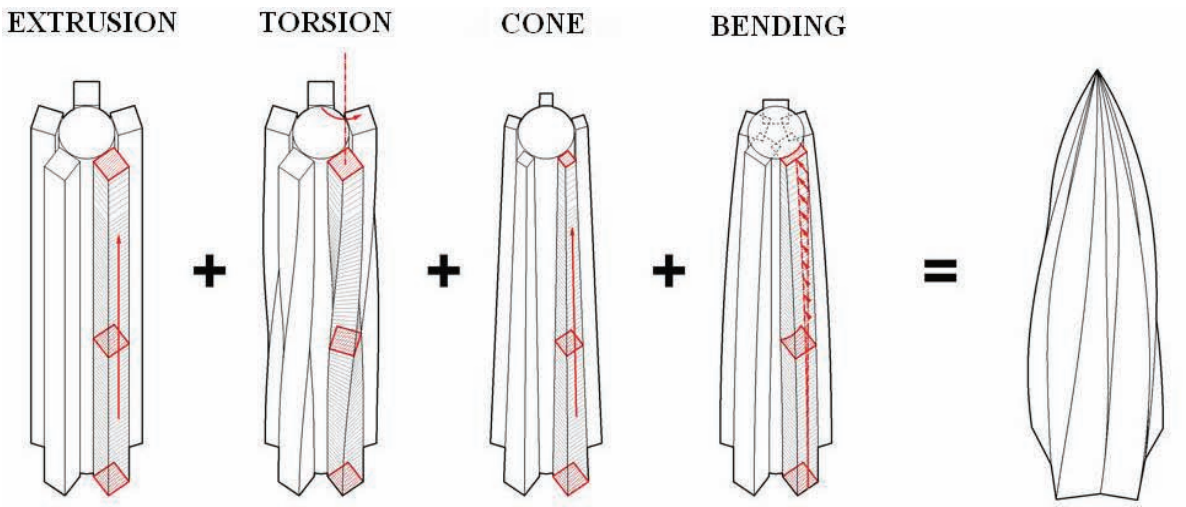

Figure 1. Scheme for obtaining of the tower geometry.

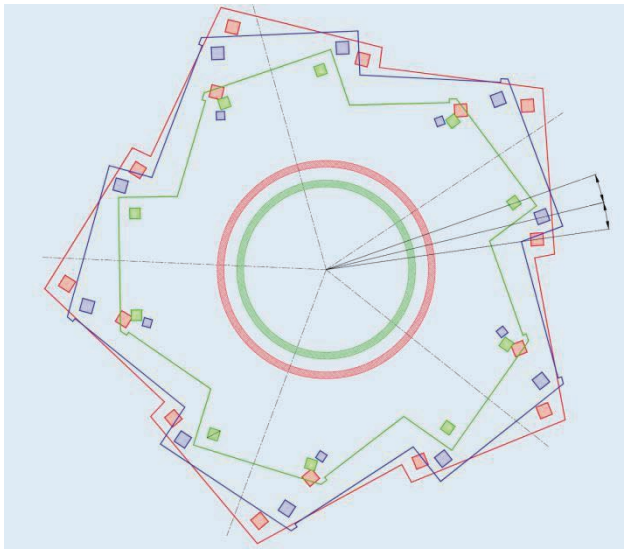

Figure 2. Combined plans of the 19, 39 and 59 floors.

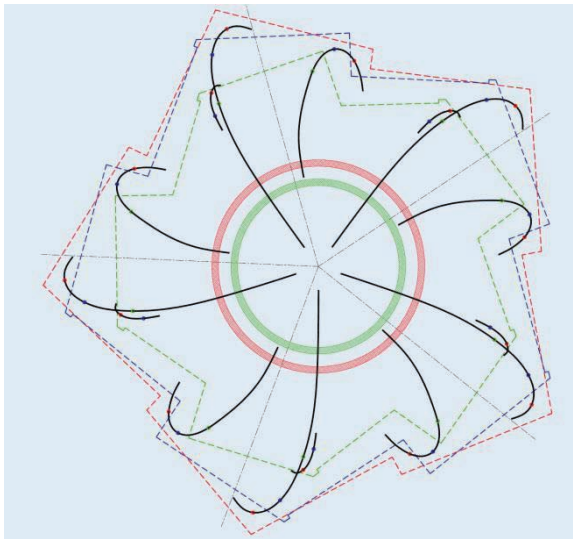

Figure 3. Combined plans of the 19, 39 and 59 floors.

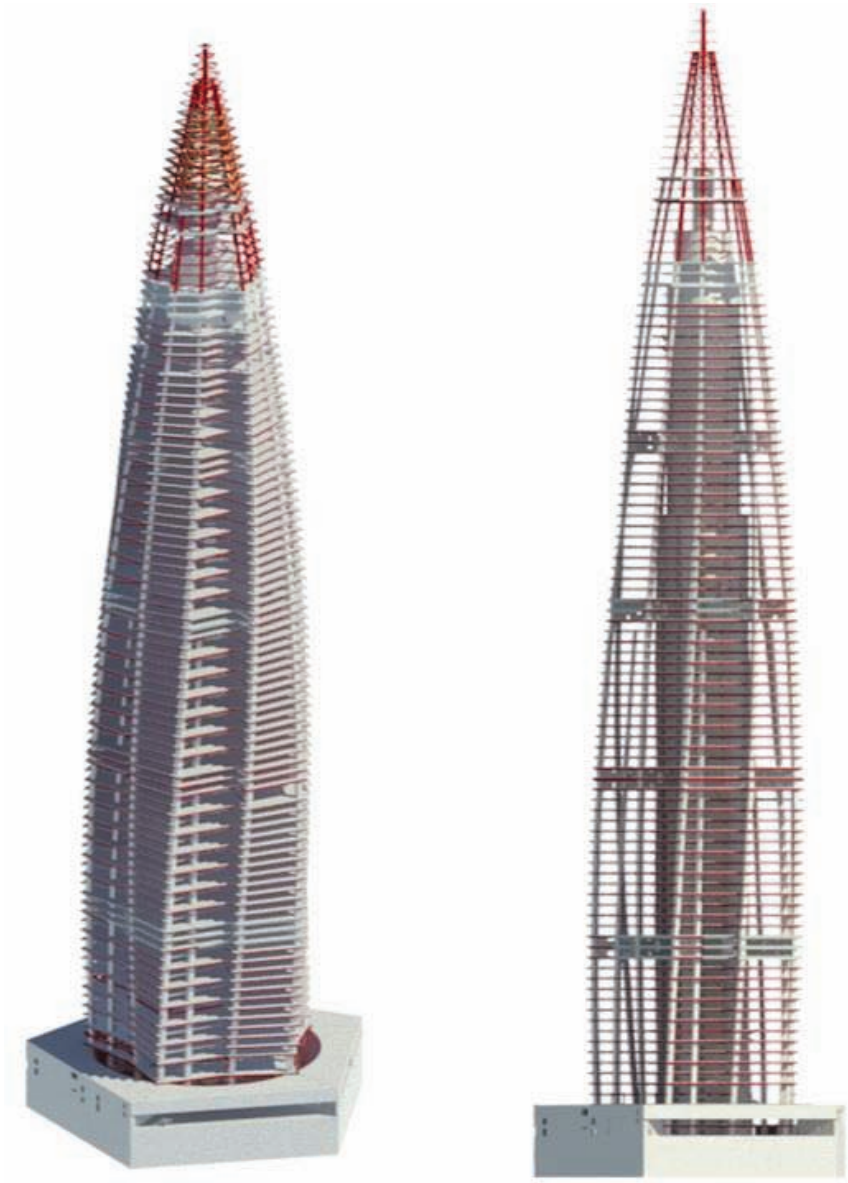

Figure 4. General view.

2. PILED FOUNDATION

In accordance with results of geotechnical survey, the following layers are in the ground (from the top to the bottom, as it is shown in Figure 5):

- interlaminating weak layers of banded clays, sandy loam and sand (specimens 1-4);
- moraine (specimens 5,6);
- Vendian clay (specimens 7-9);
- Sandstone with layers of siltstone and mudstone (specimen 10).

Since the top layers of ground had low deformation modulus and strength, it was decided to use pile foundation supported on a Vendian clay. In order to decrease deflection of the foundation slab and efforts in the outer pile rows it were conducted calculations of pile field with different length of piles. As result, piled foundation of the tower consists of 264 bored piles of 2000 mm diameter and 55 or 65 m length, placed with step from 4 to 6 meters (Figure 6). Since piles were bored from ground surface, the fact depth of the piles were 72 and 82 m respectively (Figure 7).

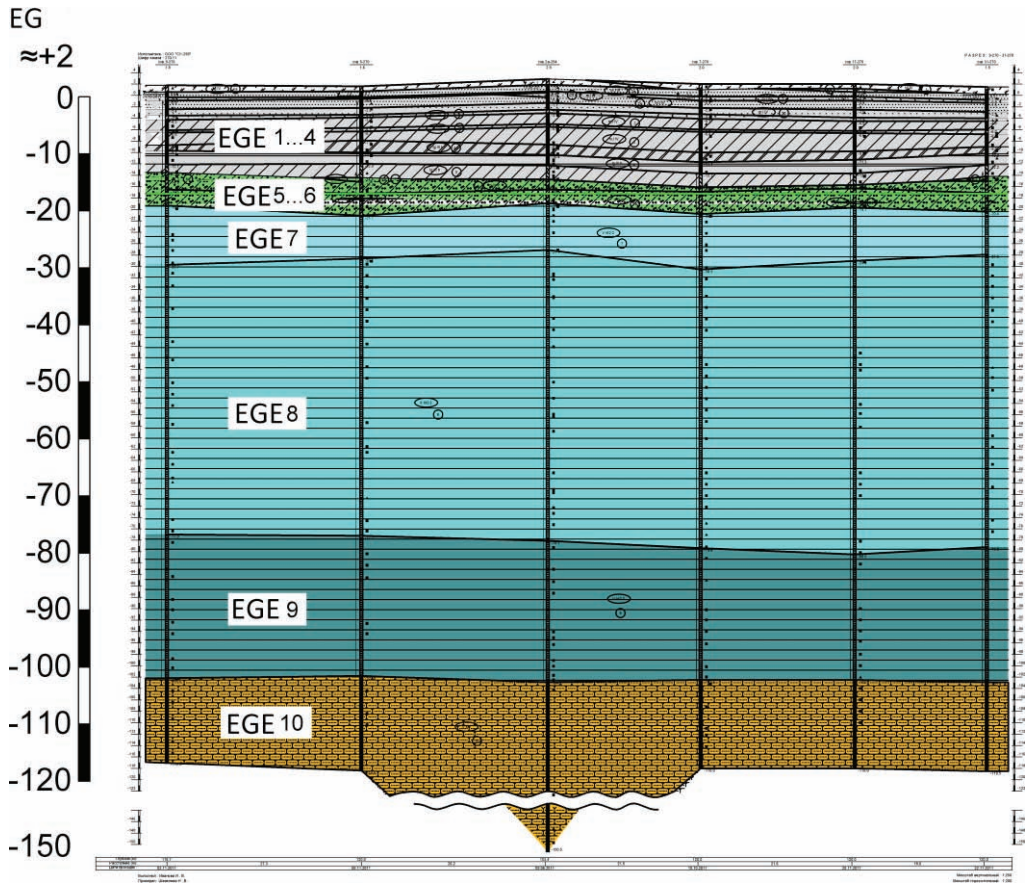

Figure 5. Layers of ground under the tower (EGE – Engineering and geological element; EG – Existing grade).

Calculated loadbearing capacity of a pile of 55 m length was 36000 kN in accordance with regulatory documents and 64000 kN obtained by experiment. Calculated load bearing capacity of a pile of 65 m length was 43000 kN in accordance with regulatory documents and 77000 kN obtained by experiment. The average calculated loading on a pile was 25450 kN.

3. BUILDING STRUCTURES OF THE UNDERGROUND PART

The underground floors of the building in the plan have the shape of an equilateral pentagon with a length of each side 57.5 m. In the center of the building there is a central core with a down part diameter of 26.0 m.

The weight of the building from standard loads, including the weight of the box foundation, is 4,930,000 kN. Initial calculations to determine the required thickness of the foundation slab showed that, in order to obtain uniformity of sediments, a traditional foundation slab even 7-8 meters thick is not enough. The draft under the core was about 180 mm, while at the periphery the size of the draft was about 60 mm. Therefore, it was decided to create a box foundation that provided a more economical solution. The calculations showed that such a foundation has high rigidity (the difference in sediment between the core zone and the periphery does not exceed 25-30 mm), the average pressure under the base of the tower foundation from standard loads was 870 kPa.

The bottom plate, located at a relative mark of -17.650 m, has a thickness of 3600 mm, the top plate, located at a relative mark of -4.650 m, is made 2000 mm thick. The joint work of the lower and upper slabs of the box foundation is ensured by 10 stiffness diaphragms 2500 mm thick, diverging from the building core in the radial direction (Figures 7, 8).

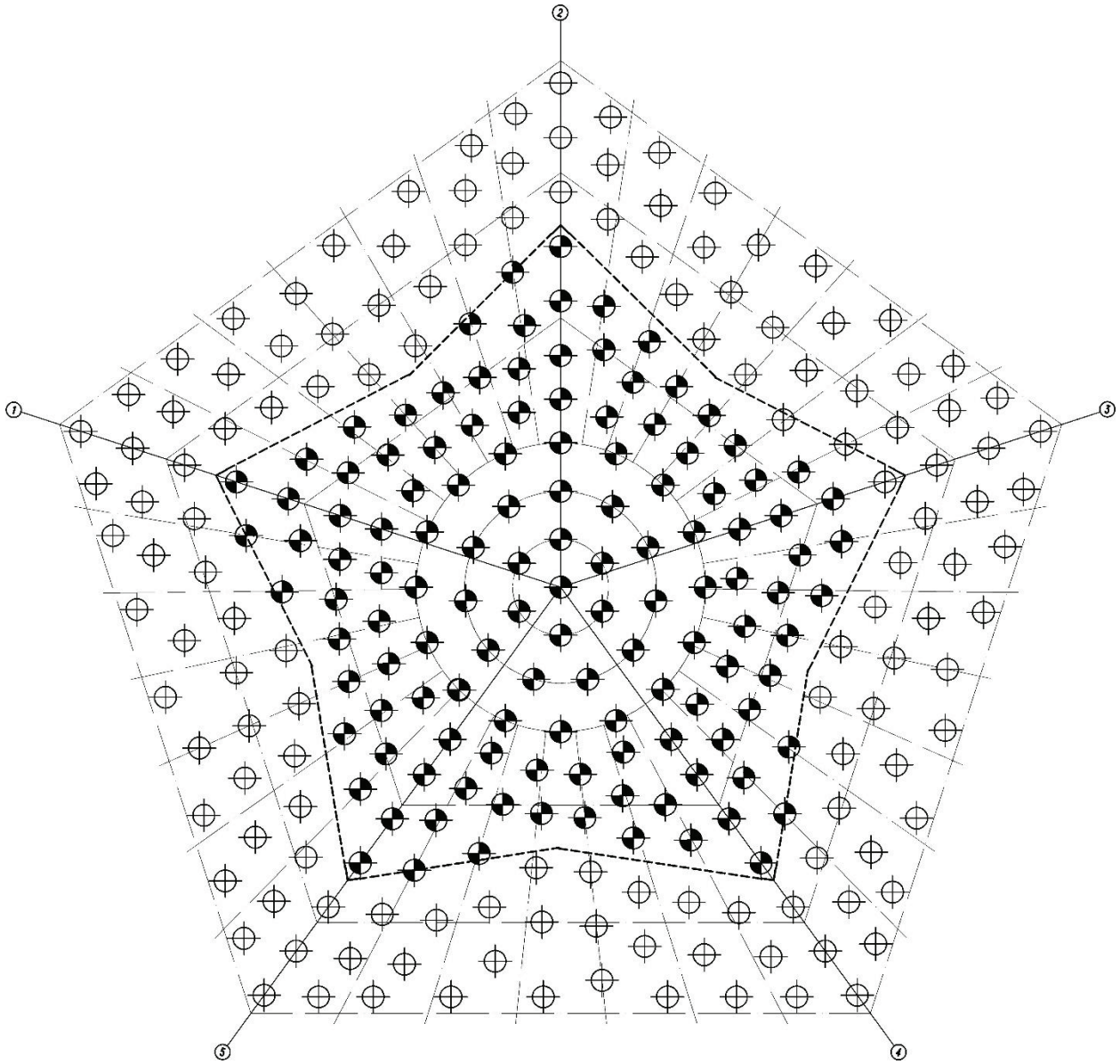

Figure 6. Piled foundation of the tower.

For the perception of large tensile forces, which amount to 23000 kN/m, the lower foundation plate is reinforced with 15 reinforcing meshes in height with rods with a diameter of 32 mm from A500C steel, spaced 150 mm apart. In the protective layers of the concrete slab at a distance of 25 mm from the upper and lower surfaces installed anti-shrink mesh with cells 100 x 100 mm. Between the upper and lower slabs of the box foundation there is a middle slab 0.4 m thick.

4. BUILDING STRUCTURES OF THE ABOVEGROUND PART

The underground part of the tower building is separated from the rest of the Lakhta Center complex by a sedimentary expansion joint. The aboveground part of the building at the 1st floor level is inscribed in a pentagon with a side length (between the axis of the columns) of 35.2 m (Figure 10). Up to the 16th floor, the dimensions of each subsequent floor of the aboveground part of the building increase.

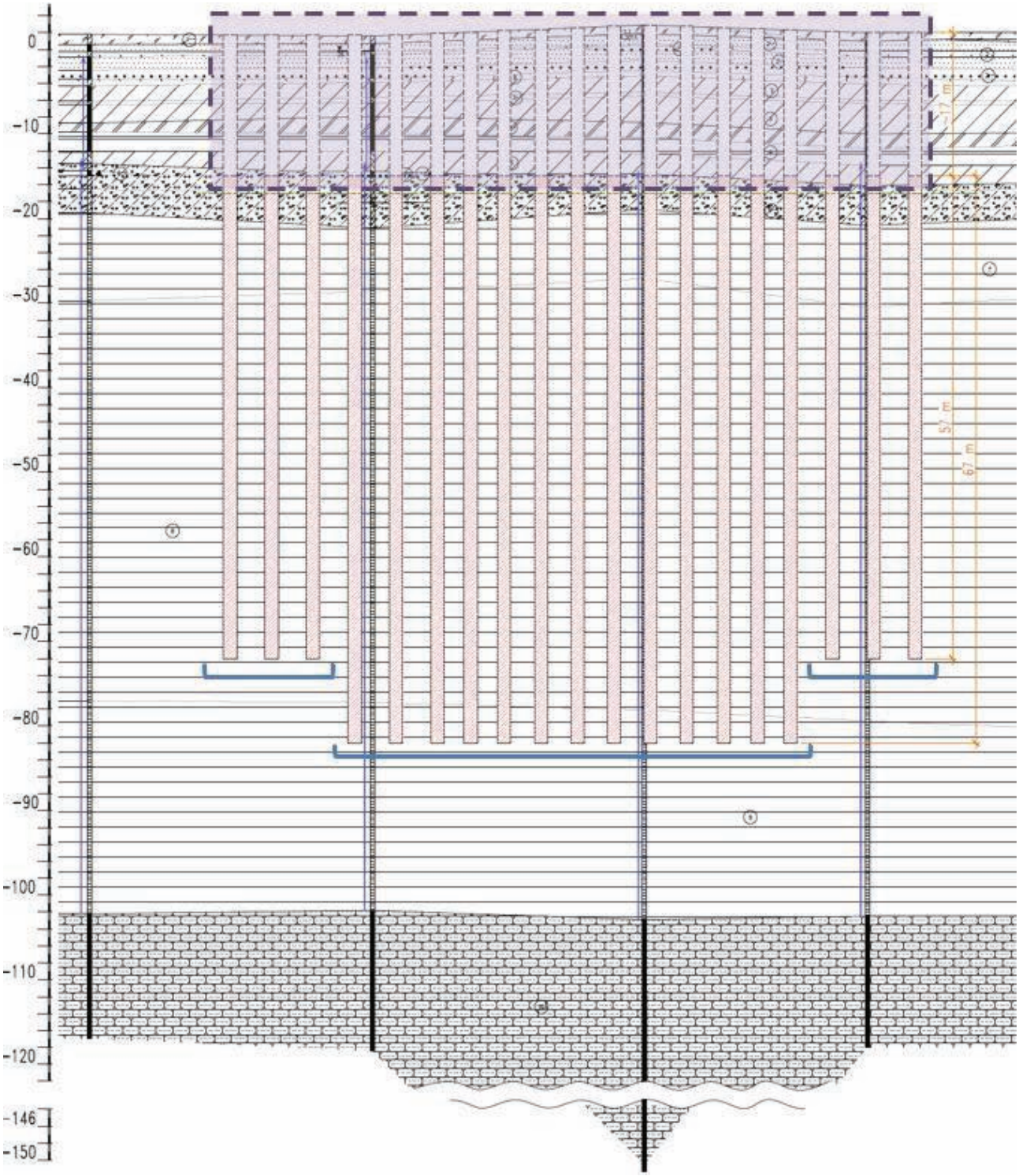

Figure 7. Piled foundation of the tower.

The maximum length of the side of the pentagon at the level of the 16th floor is 36.6 m. After the 16th floor, each subsequent floor of the aboveground part of the building is reduced in size. The length of the side of the pentagon at the level of the upper 86th floor is 19 m.

The structural scheme of the building is a core and frames.

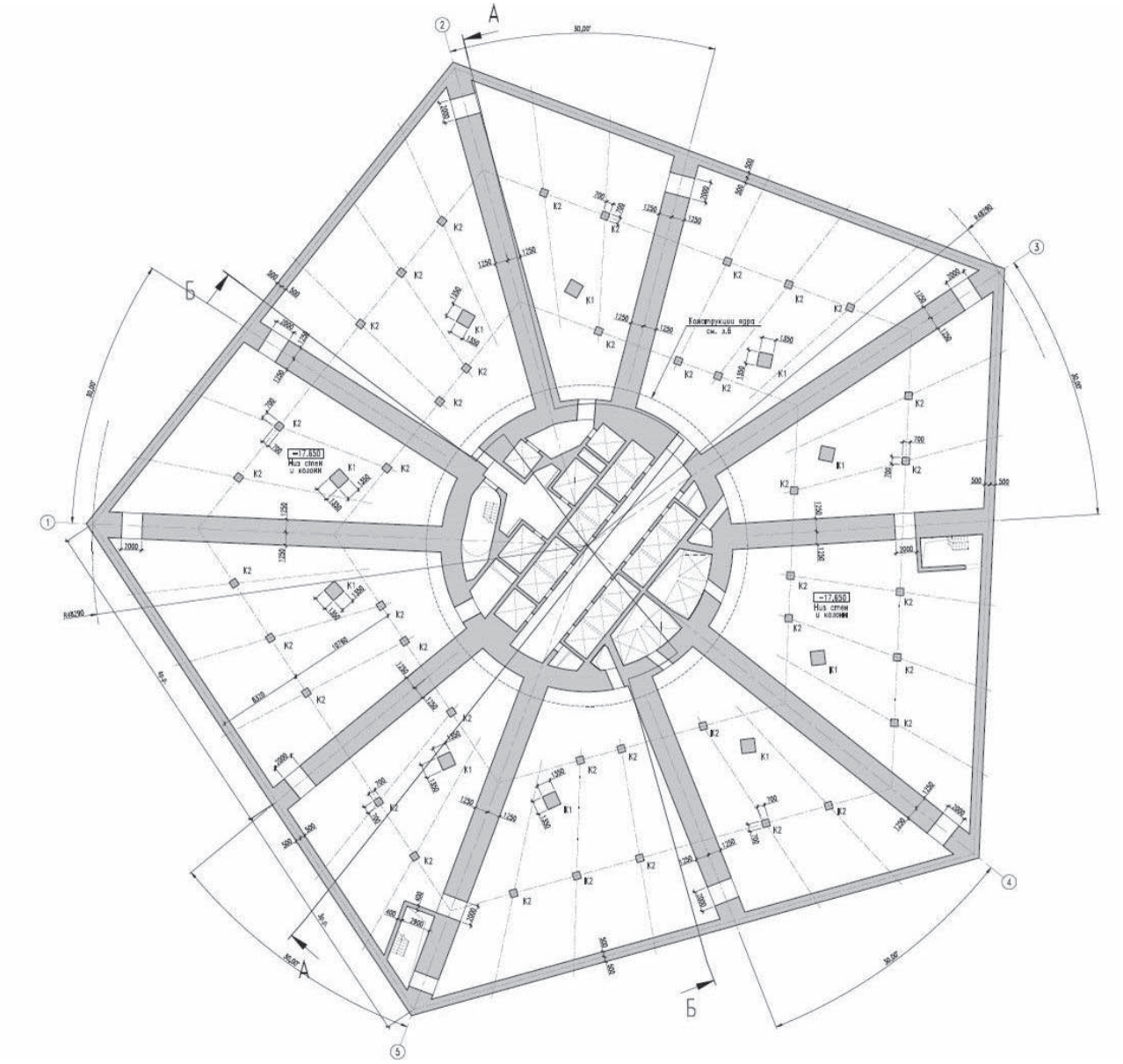

Figure 8. Walls and columns of the lower level of the box foundation of the tower.

The load bearing structures of the tower are the central reinforced concrete core and 10 steel-reinforced concrete columns around the perimeter. In order to reduce spans in the building, another 5 steel-reinforced concrete columns were introduced until the level of the 56th floor.

The central reinforced concrete core of a round shape is the main supporting structural element of the tower. The core perceives vertical and horizontal loads, including constant torsion caused by the shape of the building, and transfers them to the foundation.

The thickness of the outer walls of the core at -3 and -2 floors is 2500 mm, on the -1 and 1 floors it is 2000 mm, on the 2nd and 3rd floors it is 1700 mm, on the 4th and 5th floors it is 1400 mm, on the 6th and 7th floors it is 1100 mm, from 8 to 67 floors it is 800 mm, from 68 to 80 floors it is 600 mm, from 81 to 89 floors it is 400 mm. The thickness of the outer walls of the core is determined both by the calculation conditions for all types of impacts, and by the design requirements (the number and location of holes and openings, the multiplicity of the pitch of reinforcing meshes, etc.).

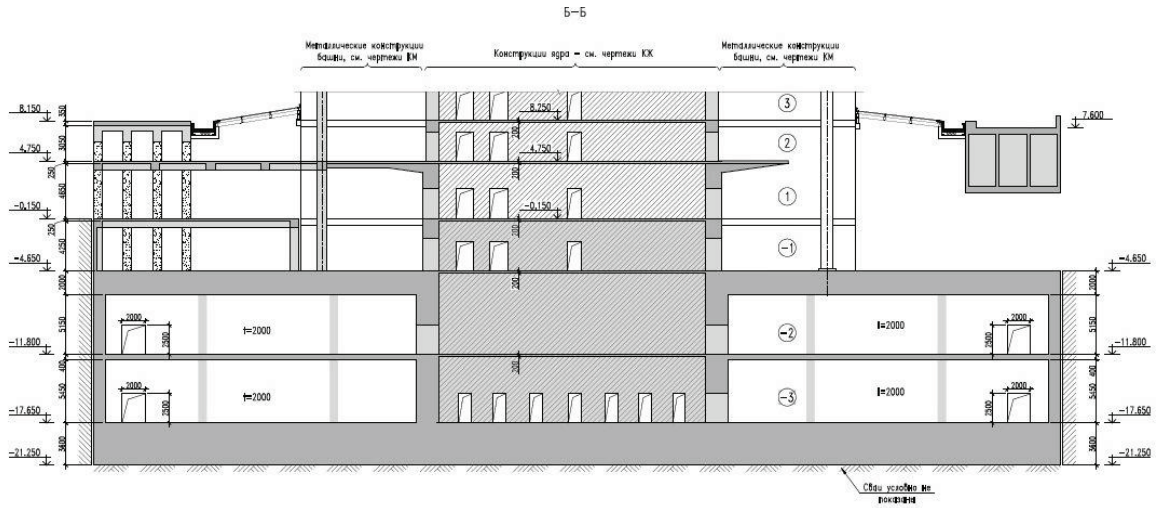

Figure 9. Structures of building core of the tower.

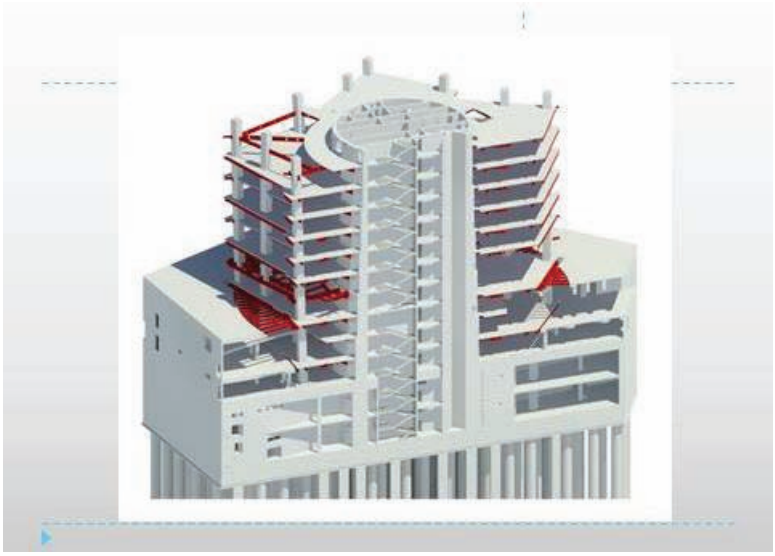

Figure 10. The aboveground part of the tower (Fragment).

The outer diameter of the core from the 8th to the 58th floor is 26.1 m; starting from the level of the 59th floor to the 80th floor, the outer diameter of the core decreases to 21.0 m.

5. DESIGNS OF STEEL-REINFORCED CONCRETE COLUMNS

Steel-reinforced concrete columns consist of a metal core, flexible reinforcement and concrete of class B80. The core material of the columns is HISTAR 460 Russia steel manufactured by ArcelorMittal. The cores of the columns are made of cross-section from HL series I-beams according to ASTM A6/A6M-12 and T-sections obtained by dividing of HL I-beams. Elements of the column core are welded with waist fillet welds (Figure 11).

In accordance with the architectural concept of the tower, steel-reinforced concrete columns are arranged in a spiral, thereby repeating the twisted surface of the building’s facade. The rotation of the axis of the metal core of the column is made at the levels of odd floors. The joint at the level of fracture of the core of the column is performed on the flange sheets. For direct transmission of the horizontal component of the force at the point of fracture of the axis of the column, this factory joint of the core of the column is performed at the level of the slab.

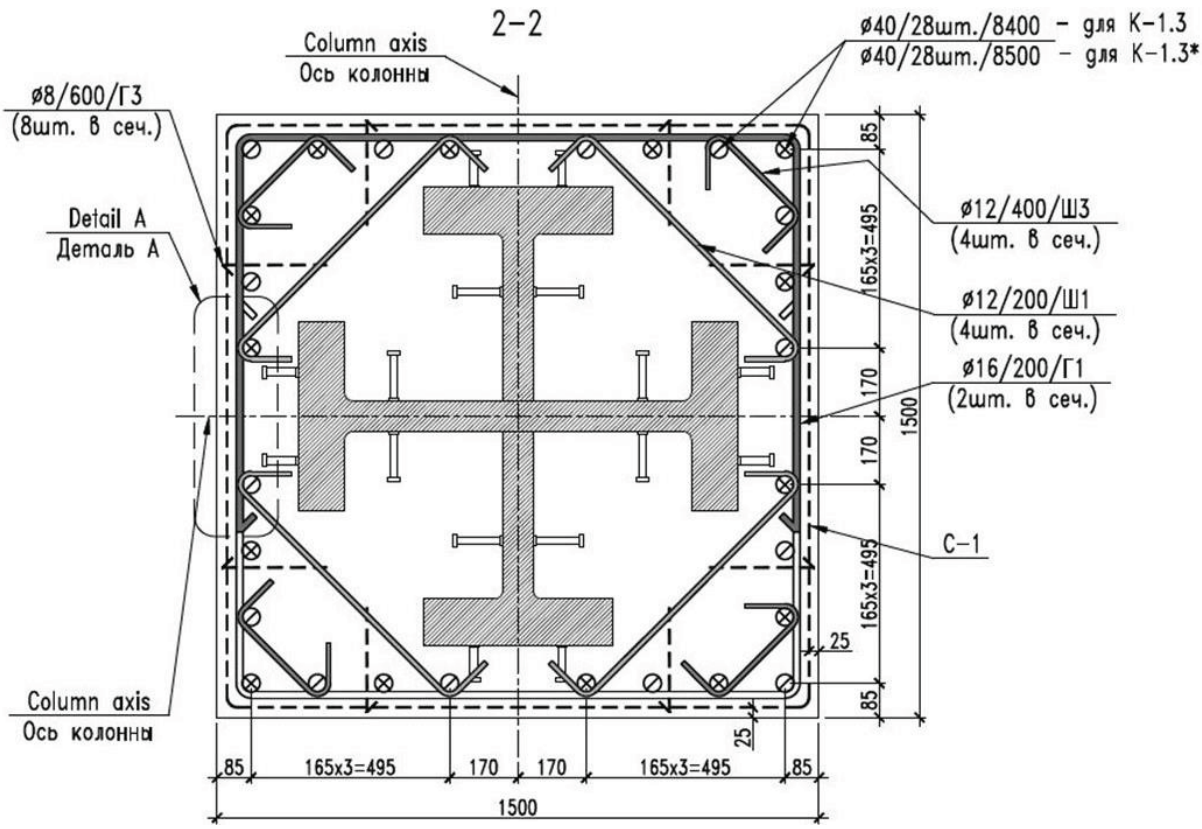

Figure 11. Column core of the tower.

The assembly joint of the column core is carried out in another place, 1200 mm above the floor slab. Mounting joints of metal cores are performed on bolts and are located every two floors of the building. The compressive forces in the assembly joints of the cores are transmitted through the milled ends of the elements, the tensile forces (occurring when calculating for progressive collapse) are transmitted through the lining of steel C345-3 on high-strength bolts M30 strength class 10.9.

To ensure the joint work of the steel core of the column with reinforced concrete, flexible stops (stud bolts) were installed on the core at the manufacturing plant.

In steel-reinforced concrete columns, concrete of class C80 for compressive strength is applied. For a relatively uniform transfer of the load more than 160,000 kN from the column to the foundation, the column base was developed, consisting of 7 plates, 40 mm thick. The space between the lower edge of the base of the column and the upper edge of the foundation slab was filled with high-strength material EMACO S55. Due to the fact that the column is tilted in the space around the steel base, a monolithic reinforced concrete box is arranged that perceives the horizontal component of the force in the column (Figure 12).

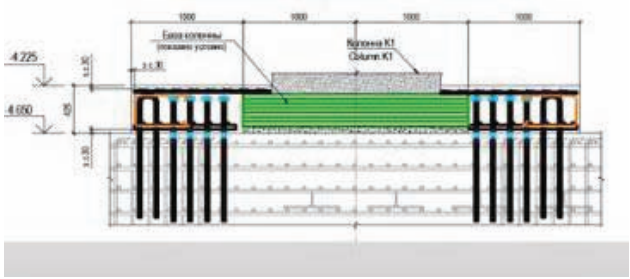

Figure 12. Concrete base coating.

Due to the fact that the ratio of the core diameter to the height of the building is about 1/17, the rigidity only of the core was not enough to satisfy the requirements of the norms for the horizontal deviation of the top of the building and the maximum acceleration of the oscillations of the upper floors (comfort of stay).

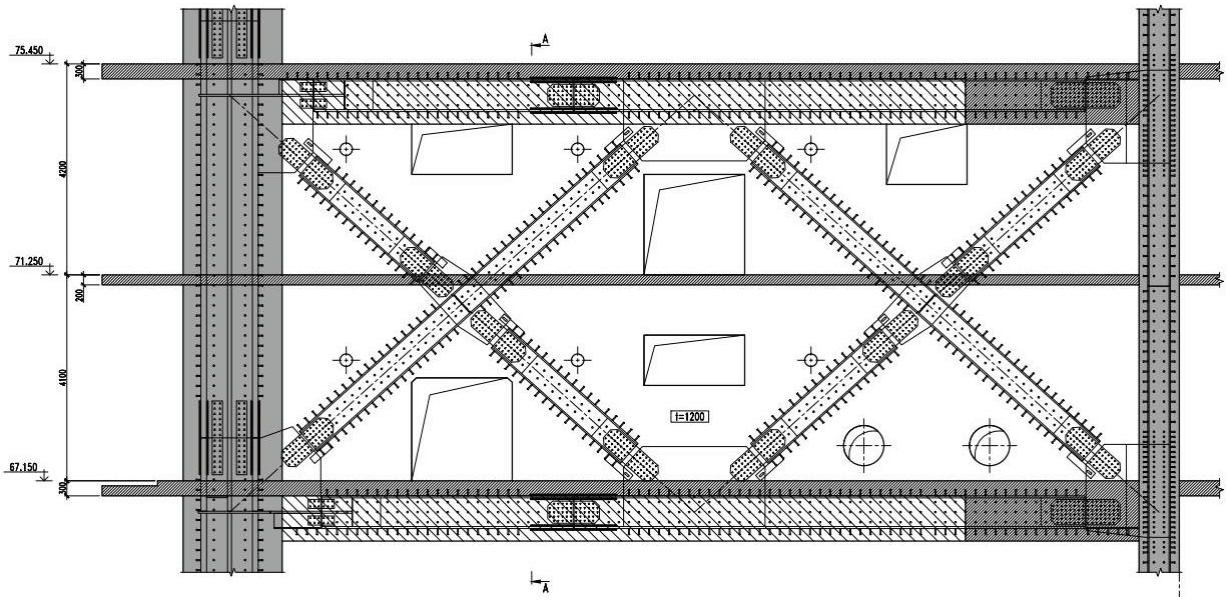

Figure 13. Connection of outriggers to core and columns.

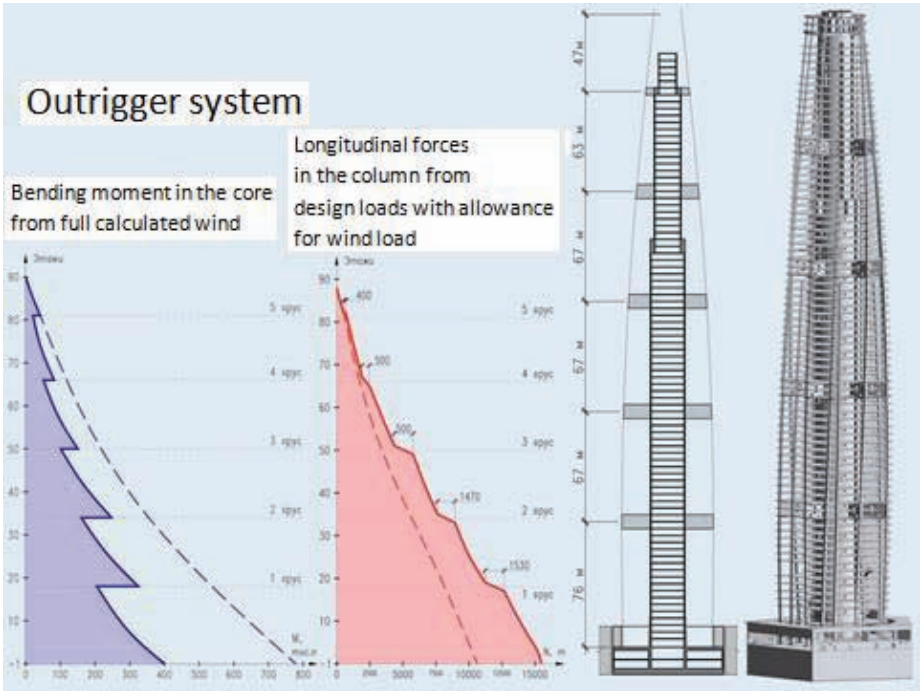

Figure 14. Outrigger system. Bending moment in the core from full calculated wind (left). Longitudinal forces in the column from design loads with allowance for wind load (right).

Additional rigidity of the building and its resistance to progressive collapse is provided by two-story outriggers located at the height of the tower at levels 17–18, 33–34, 49–50, and 65–66 technical floors (Figure 4). At each of these levels, outriggers are connected to core and 10 columns (Figure 13). The distribution plate above the 80th floor works as the top outrigger of the building. The introduction of outriggers made it possible to reduce the horizontal movement of the top of the building from the action of wind loads and to ensure the comfort of staying on the upper floors of the tower.

Figure 14 shows the values of bending moments in the central core, excluding and taking into account the inclusion of outriggers.

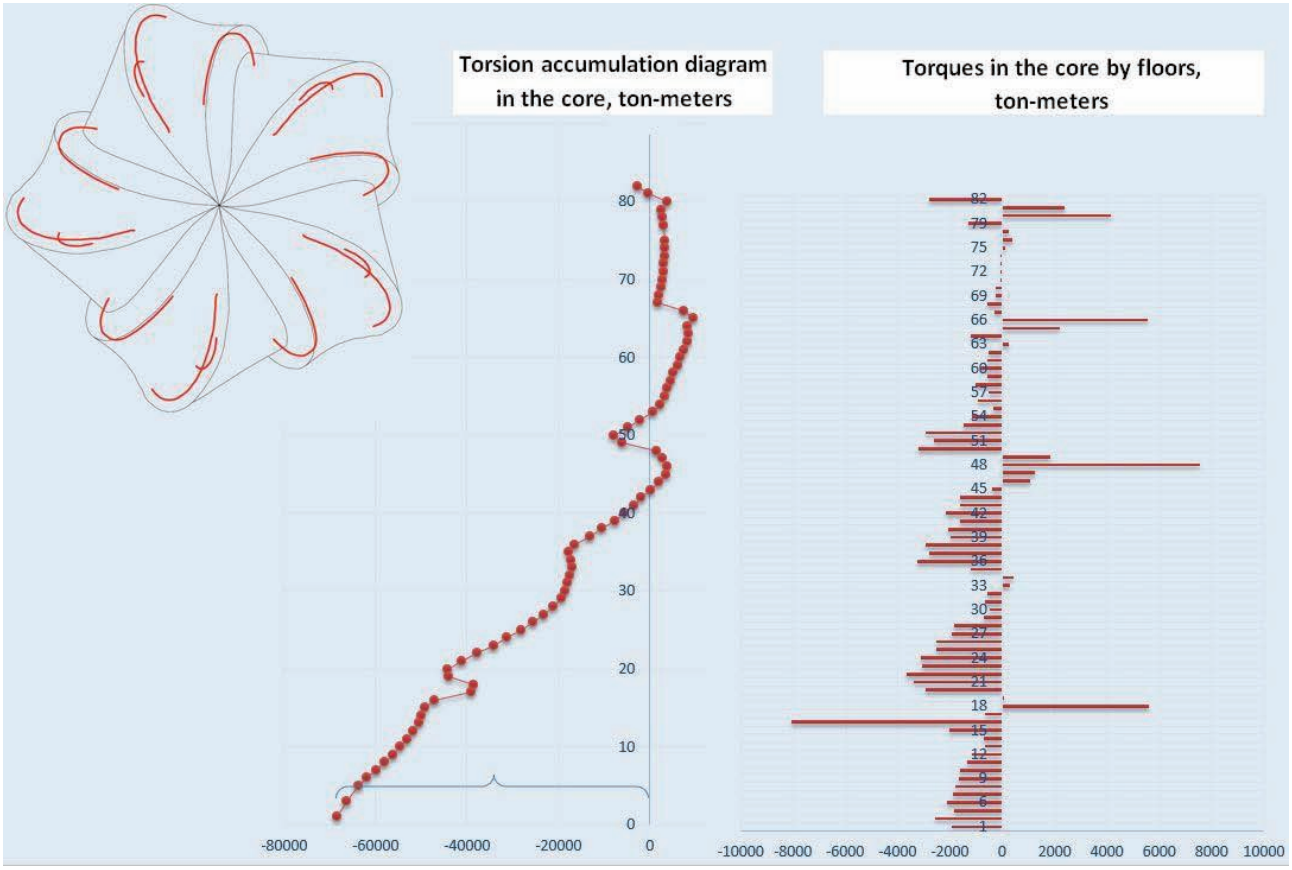

Figure 15. Torsion accumulation diagram in the core (left). Torques in the core by floors, ton-meters (right).

Outriggers are designed in the form of reinforced concrete beam walls, with steel trusses installed in the body of reinforced concrete. Steel trusses are designed for the perception of wind effects during the construction period of the building, before the inclusion of reinforced concrete outriggers.

As a result, the outrigger structures are an I-beam with the upper and lower shelves measuring 3.0x0.85 (h) meters and a wall of variable thickness (from 500 mm to 1500 mm in the adjoining zone to the core) 9.25 meters high. In order to strengthen the core at the level of adjacency of the upper and lower zones of the outrigger beam, annular monolithic reinforced concrete beams of size 2.5x1.2 (h) meters are made, in which openings are provided for passing vertical engineering communications.

Floor disks together with outrigger structures, provide joint spatial work of the main load-bearing structures of the building. In addition, due to the twisted shape of the building, the horizontal component of the forces from the fractures of the axes of the columns to the core of the building is transmitted through the floor disks. The structural design of the building leads to the accumulation of torque along the entire height of the central core. The maximum torque in the core at the level of its clamping in the upper plate of the box foundation is 770,000 kNm (Figure 15).

The walls of the central core of the tower were made of concrete of B80 compressive strength class.

6. DESIGN OF SLABS

The tower slabs outside the core are steel-reinforced concrete structures, made of in fixed formwork from a profiled steel sheets supported by metal beams.

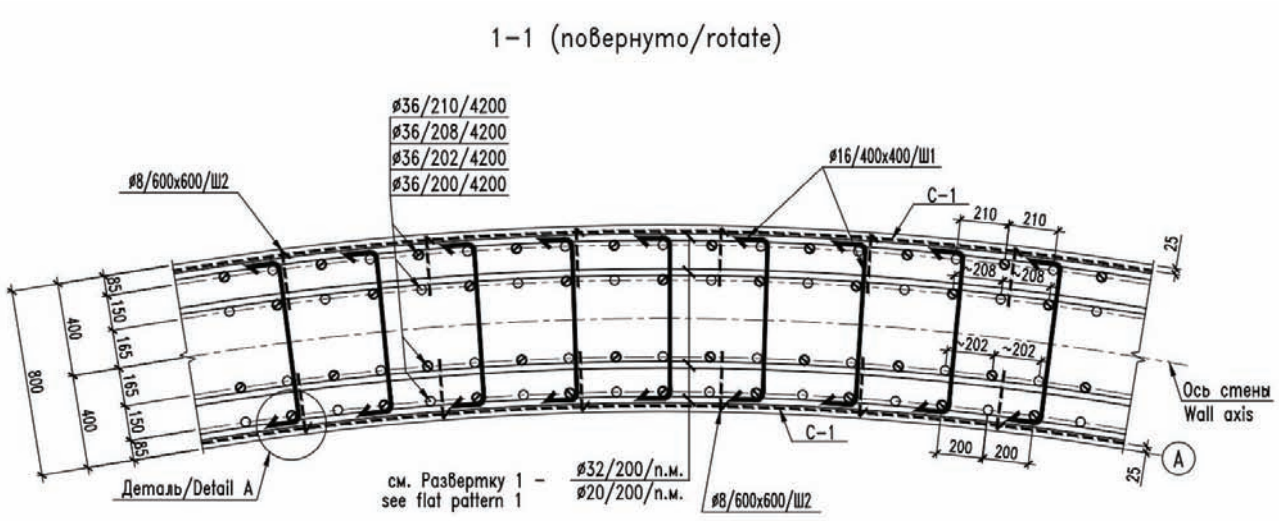

Figure 16. Fragment of reinforcing the wall of the central core.

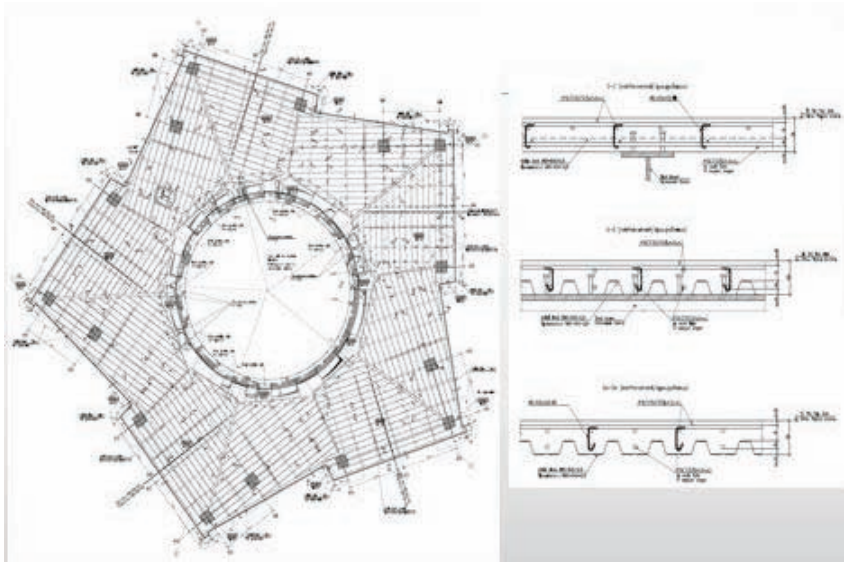

Figure 17. Floor slab design of a typical floor.

The thickness of such floor slabs is 150 mm, for which concrete of strength class B40 is used. Joint work of reinforced concrete floor slabs with metal floor beams is ensured by welding to the upper zones of the metal beams of flexible stops (studs) (Figure 17). The main I-beams located between the central core and the columns have a length of up to 17 m, they are made of welded, height from 750 to 1200 mm, secondary I-beams are made of rolled with sections up to 40B2 inclusive. The material of the metal beams is steel C345-3, C390. The nodes and mounting joints of the beams are frictional with high-strength bolts M24 of strength class 10.9 with controlled tension. The joining of the beams to the reinforced concrete structures of the central core is carried out using assembly welding to embedded parts.

Taking into account the architectural features of the building (a twisted spiral shape), each floor disk must perceive significant horizontal forces arising due to fractures in the axes of the columns and transmit constant general torsion forces to the core of the building. In this regard, it is provided:

- the use of intensified background reinforcement of a monolithic floor slab to transmit tensile and shear forces from inclined columns to the core of the building;
- the use of reinforcing cages and stud bolts, providing the transfer of global torsion efforts to the core of the building. The need for these frames is also caused by the presence of a large number of communication channels around the perimeter of the outer wall of the core.

The tower spire is functionally and constructively divided into two volumes:

- operated heated part, which is the completion of the volume of the tower and includes viewing platforms, elevators and ramps for lifting on them;
- the technical (unheated) part above the 87th floor mark, which has a front fence in the form of a steel mesh.
- The tower spire is designed in the form of a five-sided pyramid located around the central reinforced concrete core of the tower, and based on the overlapping of the 83rd floor at 344.400 m at the locations of the columns of the tower building. The height of the spire is about 118 meters, the width of the edge at the base of the spire pyramid is about 16.3 meters (Figure 18).

At the 87th floor mark (368.800 m) there is an overlap for the facade maintenance equipment, and at the 88th level mark (377.350 m) there is an overlap separating the lower exploited spire area from the upper technical one.

The spire is completed in the form of a steel pipe with a diameter of 1420 mm with a step-ladder located inside the spire to access the its top point.

The entrance block of the tower of 105 x 27m size is located in front of the building and is designed in the form of a front steel arch with a span of 105 m and has a coating made of steel supporting structures resting on the arch and on the main tower structures.

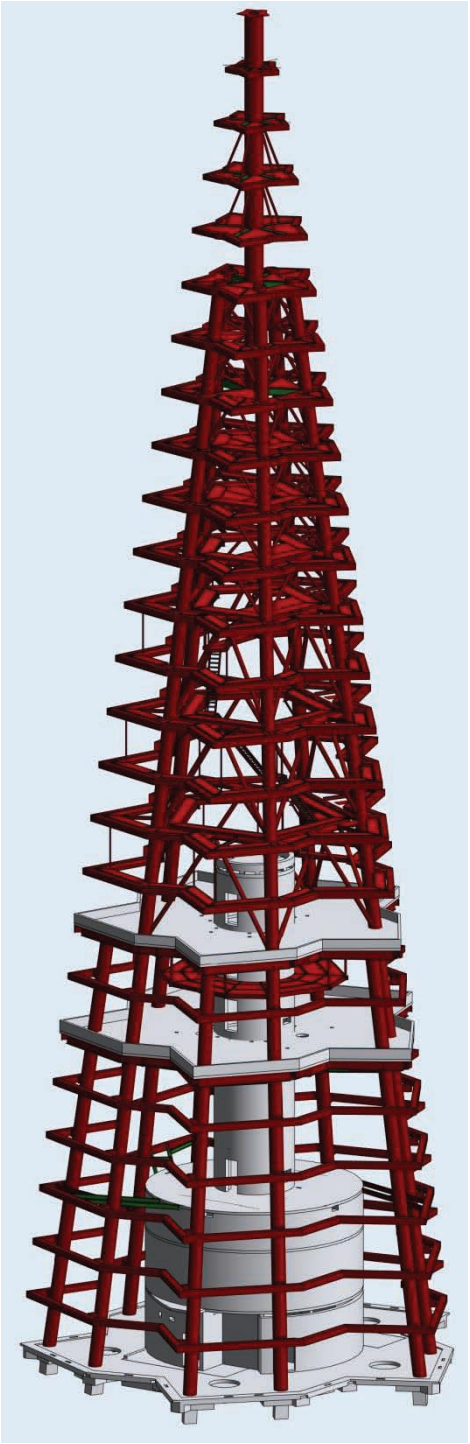

Figure 18. Spire pyramid.

The arch in its plane is glazed with the help of double-glazed windows, which are supported to the vertical load-bearing glass racks of variable height reaching 16.5 m and located along the arch with a step of 3.0 m. A section of the racks is 850 x 39.4 mm.

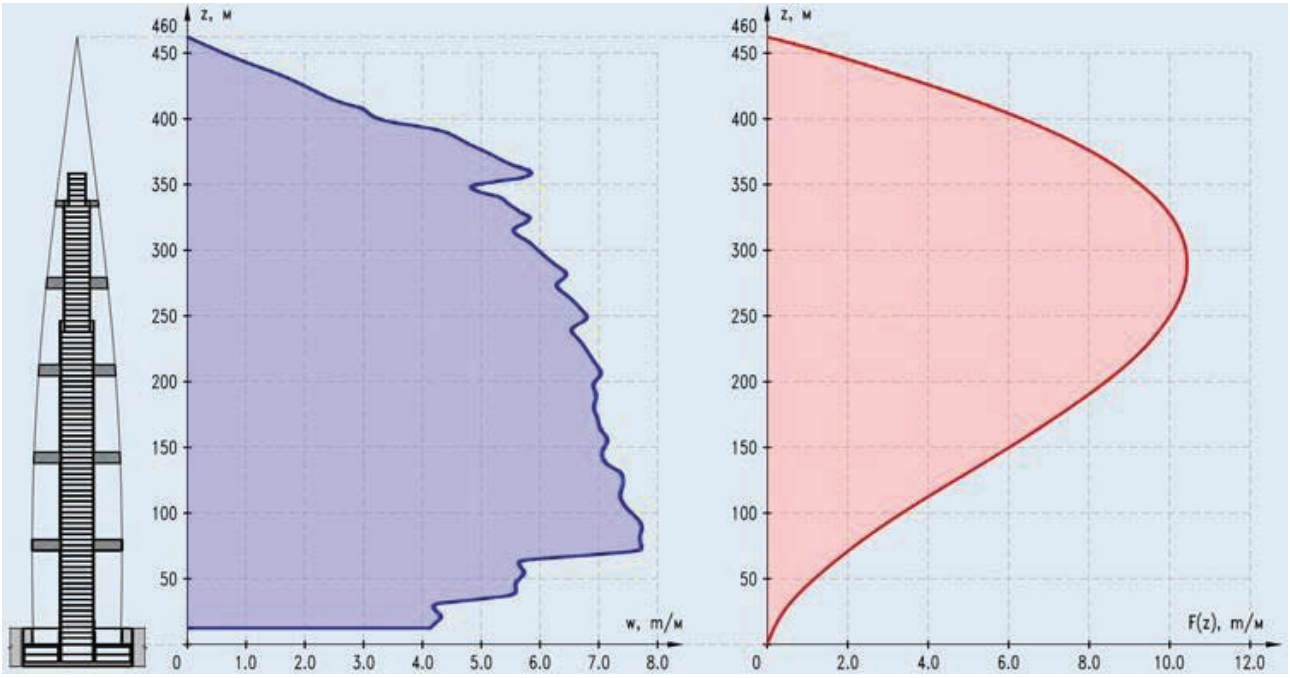

Figure 19. Wind loads.

They are glued from seven layers of heat-strengthened glass of 12 mm thick with a thickness of intermediate adhesive layers SG 0.89 mm.

7. STRUCTURAL ANALYSIS

In addition to gravitational loads, when conducting strutural analisys of the tower, wind loads were significant. The study of the model of the tower in the wind tunnel was performed by RWDI.

The aerodynamic coefficients of the total wind pressure *cp* as well as their distribution in plan in various sections along the height were determined.

The pulsation component of the wind load on the tower was determined on the basis of a dynamic calculation taking into account the value of the logarithmic decrement $\delta = 0.2$.

The maximum intensity values of wind loads, which must be taken into account when designing walling constructions and elements of their fastenings, were determined.

Special studies in the wind tunnel were carried out to determine the possible aerodynamically unstable oscillations of the tower. It turned out that with the accepted shape, size, rigidity and mass of the building, it did not undergo resonant vortex excitation or aerodynamic unstable vibrations such as galloping. In addition, the loss of aerodynamic stability such as divergence did not occur.

The surface ice loads acting on structural elements located at an altitude of 100 meters or more above the surface of the earth were also taken into account.

The sum of all horizontal forces from the action of the calculated wind load amounted to 48,360 kN, including the average component of the wind load - 30,790 kN and the pulsation component of the wind load - 17,580 kN (Figure 19). The value of the moment from the action of the full-calculated wind at the level of the top of the bottom plate of the box foundation is 9,379,000 kNm.

Modal analysis took into account about 100 modes of natural vibrations. The frequency in the first mode was 0.112 Hz. The total modal mass of the first eight modes of natural vibrations corresponds to approximately 75% of the total modal mass.

Figure 20 shows the first five modes of natural oscillations of the tower.

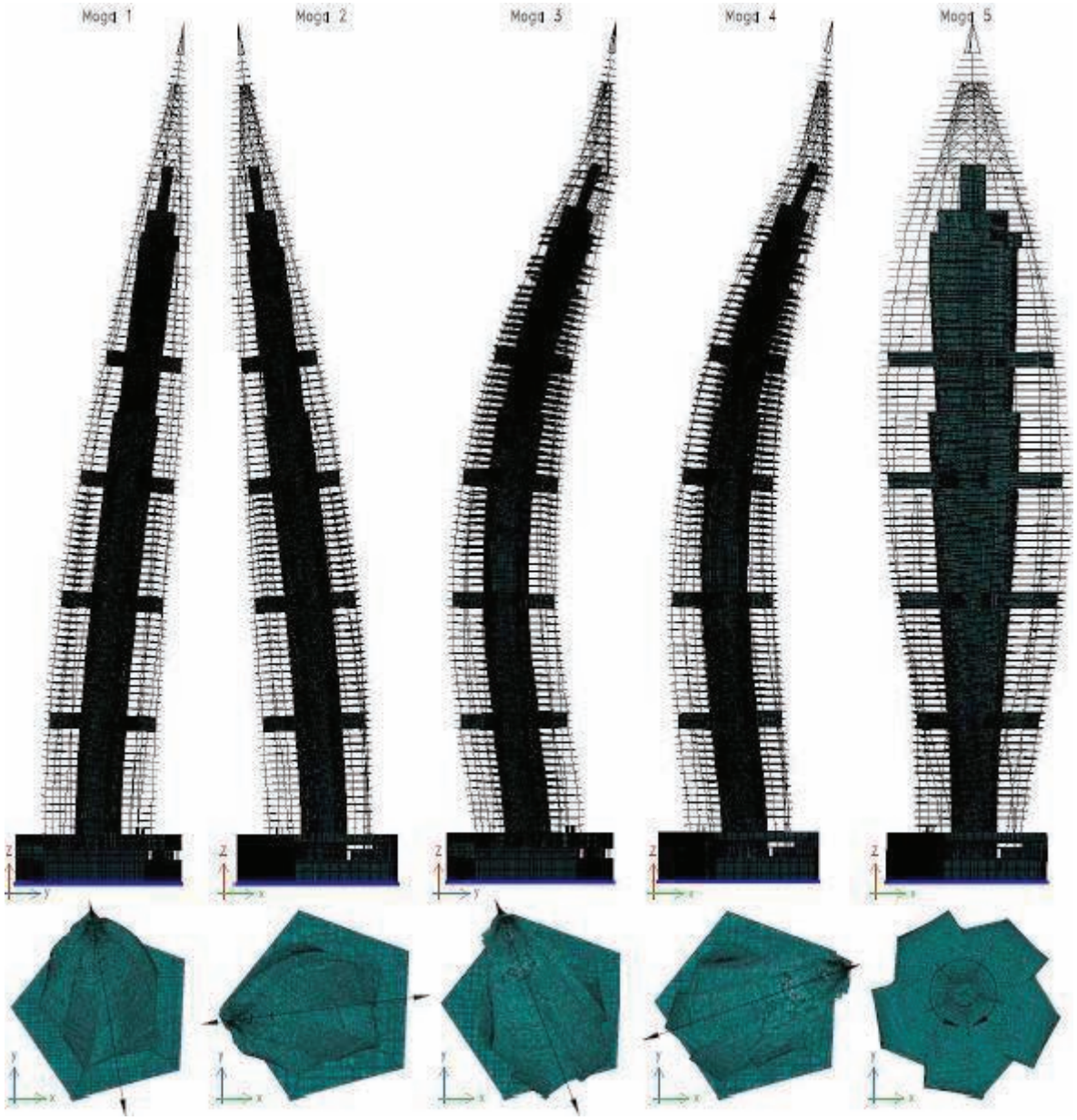

Figure 20. First five modes of natural oscillations of the tower.

The values of the horizontal displacement of the top and the acceleration of the vibrations of the top floors under wind pulsations are key indicators of the serviceability of a high-rise building.
Normative displacements under the components of the wind load at the level of the observation platform (mark 356.85 m) are 313 mm (1/1150 of the height of the building). The vibration acceleration, determined for the overlap of the upper office floor, was 0.0486 m / sec^2, which is 1.65 times lower than the maximum allowable vibration acceleration of the upper floors.

The design of such a unique building of a new architectural form, of great height, located on the coast of the Gulf of Finland in conditions of weak soils and unstable wind effects, with the development of new structural solutions using new construction materials, required a series of research works.
The test bases of TSNIISK named after V.A. Kucherenko, NIIZHB named after A.A. Gvozdev, NIIOSP named after N.M. Gersevanov, Perm National Research Polytechnic University, RWDI Laboratory (Canada) con-

ducted the following research studies of the Lakhta Center tower structures:

- The study of wind pressure and ice loads.
- Determination of soil properties.
- Tests of piles.
- Development of concrete compositions.
- Determination of the bearing capacity of steel-reinforced concrete columns.
- Tests of steel-reinforced concrete outriggers.
- Tests of glass load bearing columns.
- Development of the work technology.
- Monitoring.

We present the results of some of them.

8. AERODYNAMIC TESTS

The considering structure has a complex geometric shape, for which there are no values of the aerodynamic characteristics that need to assign the design wind loads acting on the load bearing and enclosing structures of the building and determine its aerodynamic stability. In order to determine the aerodynamic characteristics, the results of model aerodynamic tests conducted in the wind tunnel of RWDI (Canada) were used.

When designing the tower building, the following wind effects were found:

1. The average and pulsation components of the design wind load;
2. Peak values of the wind load acting on the structural elements of the fence;
3. The impact of wind on pedestrians in areas adjacent to the designed buildings.

Two design alternatives for the total wind load corresponding to the most unfavorable variants for loading the tower at wind acting angles of α = 190 ^{o} and 270 ^{o}, were considered.

The figure shows the sections of the plan on floors 76 - 84 of the structure for which aerodynamic coefficients were determined by blowing in the wind tunnel.

Resonant vortex excitation is associated with the regular breakaway of vortices from the side surfaces of structures in areas of the building with weak conicity within which the cross-sectional size varies slightly. Based on the experience of blowing models of high-rise buildings and structures of various shapes in wind tunnels, it was found that for conical structures with a taper ≥ 0.15, wind resonance phenomena are not observed. For the considering building at heights z < 200 m, the average conicity of the building is 0.15, and above the conicity increases.

Aerodynamically unstable vibrations such as galloping can occur if the wind speed V exceeds a certain critical value $V_{cr,g}$, i.e. if

$$V > V_{cr,g} \equiv 2\,Sc\,f_1\,d/(-a_g\,\gamma_{cr})$$

and

$$a_g \equiv \left(\frac{dc_y}{d\alpha} + c_x\right) k_s < 0$$

In the above relations

$$Sc = 2m_1\delta/(\rho_a d^2)$$

is Scruton number;

f_1 (Hz) is a frequency for i -th flexural natural vibration mode;

d (m) is a characteristic cross-section;

m_1 (kg/m) is an equivalent linear mass;

$\rho_a = 1.25$ kg/m^3 is density of air;

γ_{cr} = 1.25 is reliability coefficient;

$\delta = 0.07$ – logarithmic decrement for flexural vibrations of a building;

c_x and c_y are respectively, aerodynamic factors of frontal resistance and side force;

$k_s = 0.9$ is coefficient depending on vibration mode.

The results of tests in a wind tunnel showed that for the considering building, the coefficient $a_{g,max}$ = 0.92 is achieved at heights close to 300 m.

After calculation we obtained that critical value of wind speed, for which unstable vibrations similar to galloping can appear, significantly exceeds wind speed at height z = 300 m. Consequently, aerodynamically unstable vibrations of galloping type do not arise in the considering building.

Figure 21. View of the Lakhta Center model in the RWDI wind tunnel.

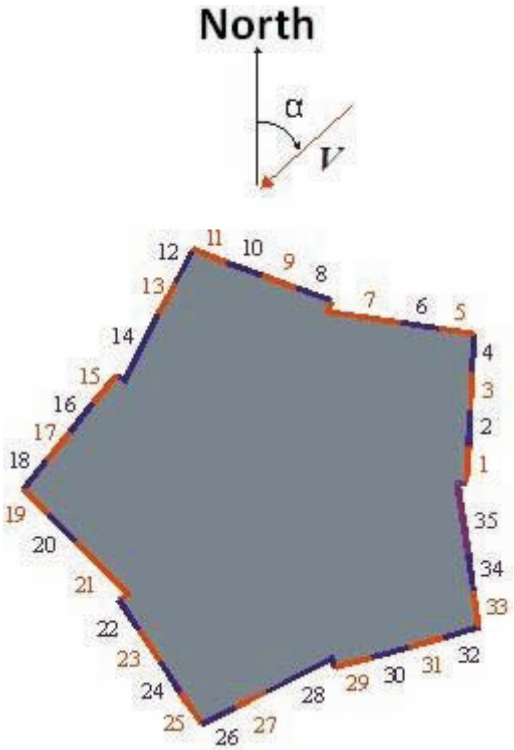

Figure 22. The scheme of locations of zones of the tower; floors 76-84.

Critical wind velocity, for which torsion unstable vibrations of divergence type arise, can be determined by the following formula

$$v_{div} = \sqrt{\frac{2G_t}{\rho d^2 dc_m / d\alpha}},$$

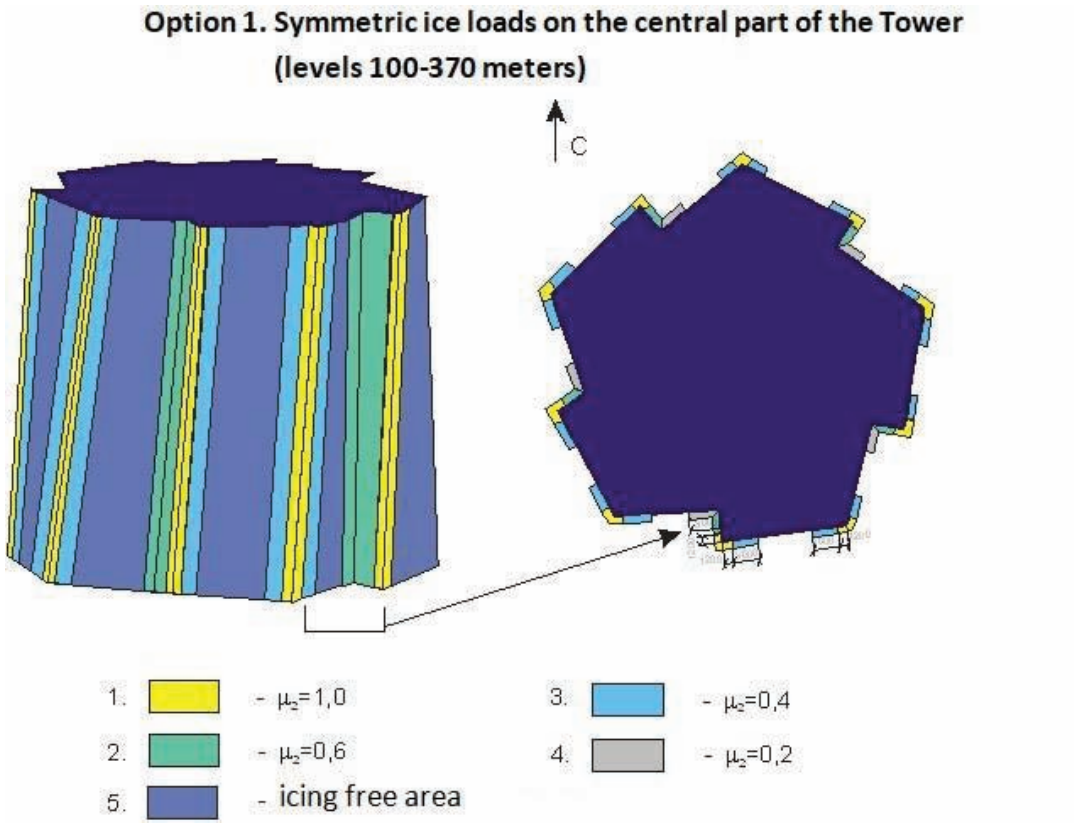

Figure 23. Ice loads (the first option).

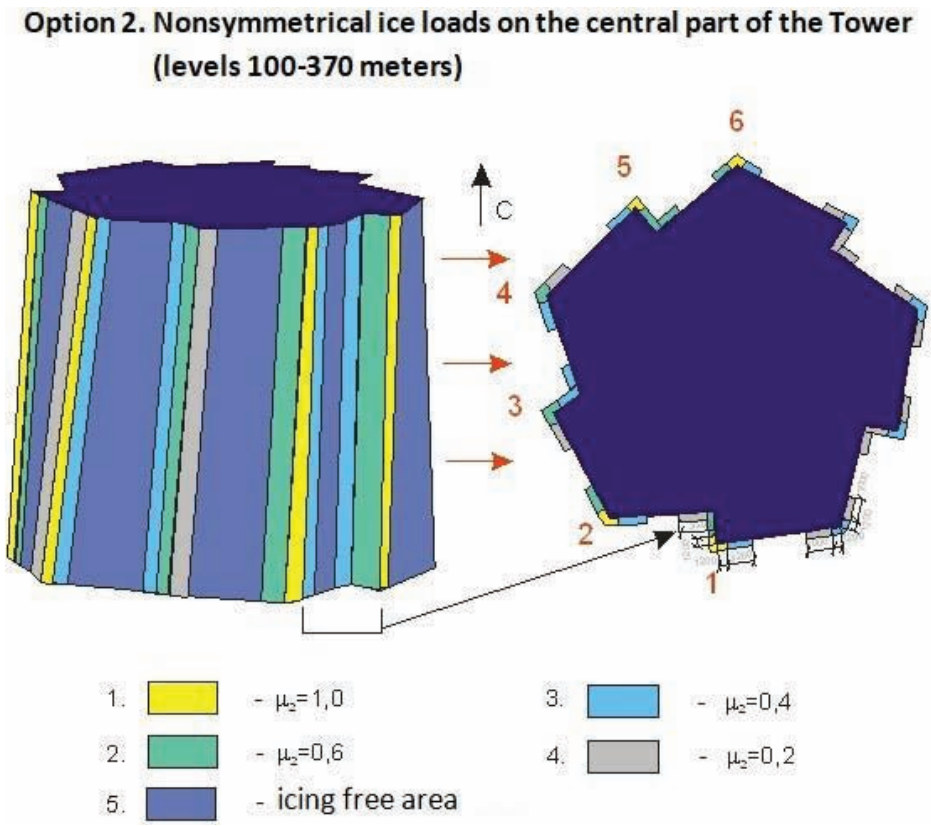

Figure 24. Ice loads (the second option).

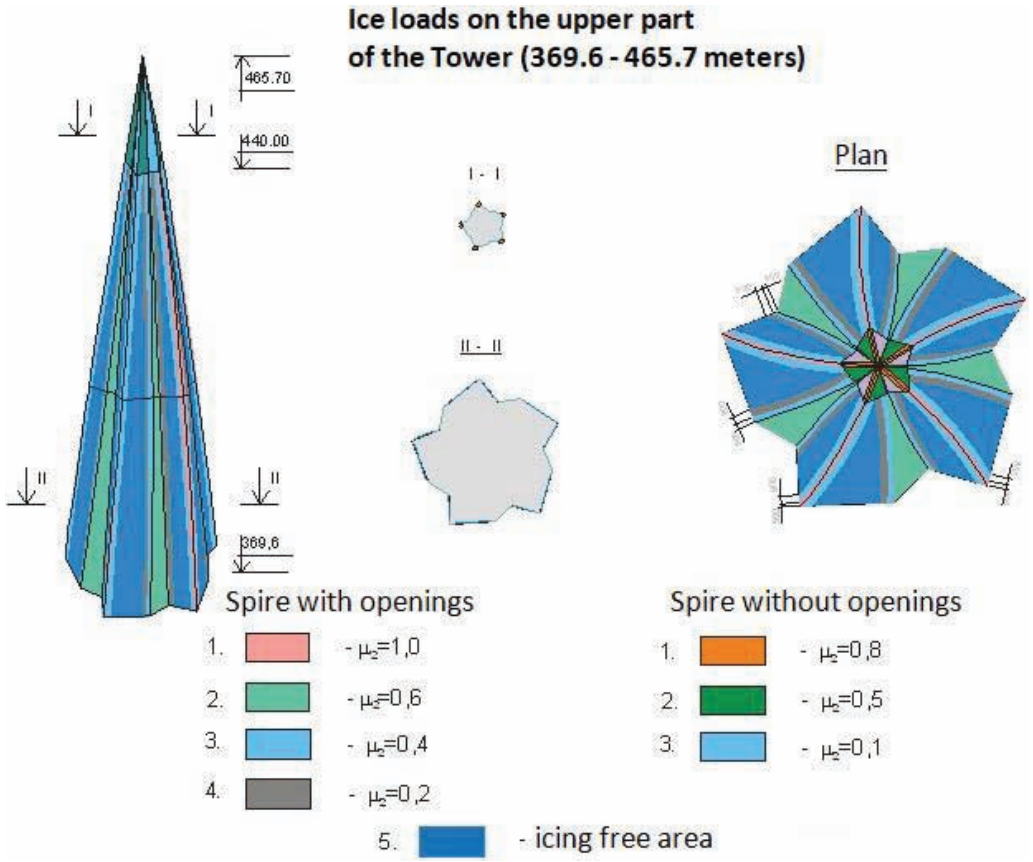

Figure 25. Ice loads.

where G_t is a torsion rigidity of a structure;
$dc_m/d\alpha$ is a gradient of moment coefficient c_m change in accordance with attack angle α.
The results of model tests in a wind tunnel showed that the coefficients c_m and $dc_m/d\alpha$ are close to zero, which eliminates the loss of aerodynamic stability such as divergence in the considering building.

9. ABOUT ICE LOAD

Since the tower building is located in low cloudy conditions when calculating it, the surface ice loads acting on structural elements located at an altitude of 100 or more meters above the ground were taken into account. The symmetric and asymmetric loading of the building surface of the tower was taken into account by the ice load.

10. ENGINEERING-GEOLOGICAL RESEARCH

In order to study the Vendian deposits, special researches were conducted, as a result of which it was established:

- the deformation modulus varies with depth;
- clays are over-compacted OCR = 2 ... 3;
- clay has a strongly expressed anisotropy
- clay has creep.

The highest values both in absolute value and in the rate of change with depth were obtained as a result of pressiometric tests, in which the deformation modulus changed from 100 MPa (at a depth of 35 m) to 560 MPa (95 m), i.e. 5.6 times. Studies of the effect of soil compaction on the foundation sediment showed that when the soil compaction coefficient (OCR) changes from 1 to 1.5, there is a sharp decrease of sediments for 25%, from 0.2 to 0.15 m, in the future it gradually decreases uniformly from 0,15 to 0.12 m when OCR changes from 1.5 to 4.

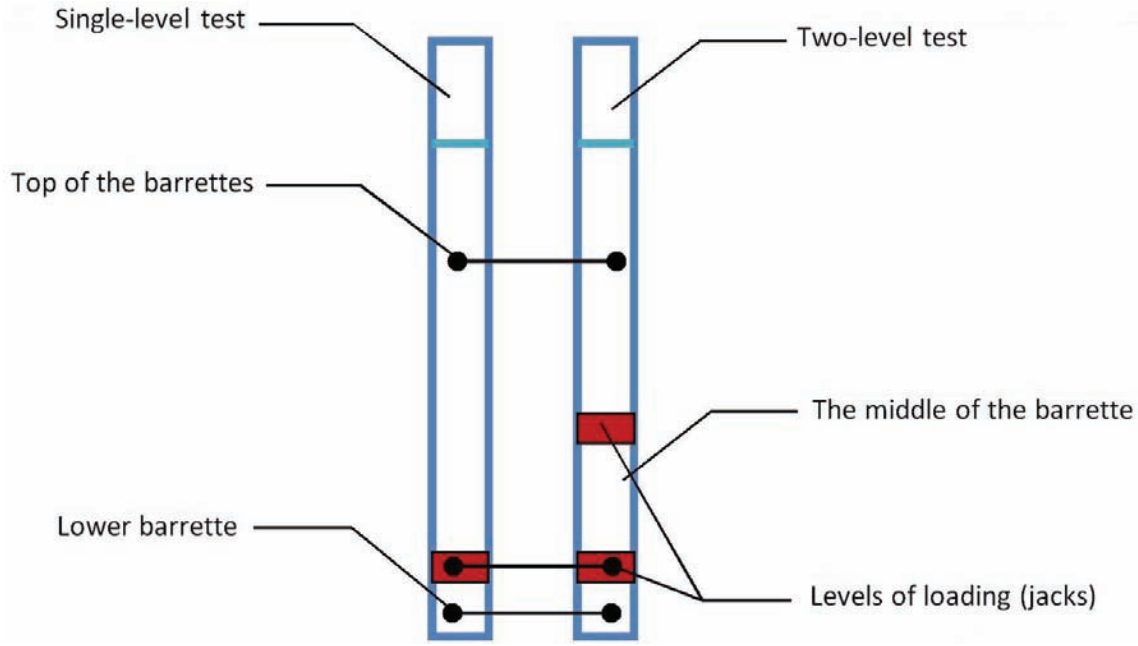

Figure 26. Scheme of barrettes.

In order to study the creep of the soil, corresponding laboratory tests were carried out. Such tests made it possible to reveal the dependence of the secondary consolidation coefficient on the load. The obtained values of creep were specified in the process of field stamp tests. The lower parts of piles and barrettes served as stamps. As a result of the studies, it was determined that additional sediment due to creep of the soil is 30%.

In order to study the interaction of the barrettes with each other and with the soil in a pile field, special geotechnical studies were carried out. It consisted of testing five barrettes with a working length of 65 m and a cross section of 1.5 × 2.8 m. Three of the five tested barrettes were subjected to a group test, in which loading was carried out simultaneously.

The submersible jacks were chosen for testing. Among the five tested barrettes, three were equipped with loading devices installed in two levels, and two barrettes had a single one, in one level. Schemes of one-level and two-level tests and the accepted names of the parts of the barrettes are shown in the Figure 26.

The study of the stress distribution along the length of the barrette during loading of the lower and upper level jacks showed that the greatest attenuation of the forces is along the length, and therefore the greatest resistance along the lateral surface was observed for the central barrette B2. A set of studies of weak soils for the possibility of building high-rise buildings on them allowed us to obtain a number of important results that can be used in similar cases, as well as included in the newly developed Building Codes.

11. TESTING OF STEEL-REINFORCED CONCRETE COLUMNS

When developing the project, it was initially intended to use reinforced concrete columns made of high-strength concrete. However, the cross-sectional dimensions turned out to be very large, which led to the loss of usable floor area. Therefore, it was proposed to use steel-reinforced concrete columns. The use of such columns made of high-strength concrete and new classes of high-strength steel allowed significantly increasing the useful area of the building. Due to the absence of design standards for such structures in the Russian Federation, experimental and theoretical studies of specimens of columns with rigid reinforcement in the form of

welded I-beams for central and eccentric compression, as well as for shear, were carried out.

Firstly, full-scale experiments on central and eccentric compression of column models were carried out. Totally, 44 specimens made of B80 concrete, fiber-reinforced concrete and C255 steel were tested.

As a result of tests under the compressive load, the dependences of stresses and strains in the steel core and concrete were obtained. The effect of the eccentricities of the load application and a large percentage of reinforcement from 10% to 18% when using high-strength concrete on the bearing capacity was studied.

The destruction of concrete prisms was characterized by a sharp loss of bearing capacity and brittle destruction with clapping. Fiber-reinforced concrete was characterized by a gradual decreasing the deformation modulus, a gradual accumulation of cracks.

The destruction of samples even with significant eccentricities occurred smoothly due to the plastic properties of steel.

When testing models made of concrete B80 and fiber-reinforced concrete, the actual ratio of the distribution of stresses, strains and forces between rigid reinforcement and concrete at each step of loading was established.

In order to detailed study of the process of deforming and fracture of the composite column structure and comparison with experimental results, numerical simulation of the tested specimens was performed using the finite element method by the ANSYS software.

The calculations were carried out in linear and nonlinear formulations.

The real characteristics of the materials obtained in the experiments were used. Rigid reinforcement and concrete were modeled by volumetric elements, flexible reinforcement simulated by rod elements.

The results of a linear calculation for central and eccentric compression showed that the stresses in concrete in certain zones exceed the limit values, which contributes to the appearance of cracks, and plastic deformations can appear in rigid reinforcement.

Therefore, a calculation that takes into account the nonlinear properties of concrete and steel was conducted.

Comparison of the experimental results with the calculation showed fairly close values, and the normative technique provides a large safety factor.

The presence of eccentricities under the action of the load on the column causes the appearance of bending moments in the structure and can cause a violation of the adhesion between concrete and rigid reinforcement.

Shear tests were performed to find out this fact. The main goal of such tests was to determine the parameters of the beginning of bond fracture, and the type of fracture in the steel-concrete contact zone when pressing rigid reinforcement into concrete, as well as the study of the possibility of increasing the adhesion strength in the contact zone.

The adhesion strength between the series of specimens differed slightly. For series of specimens made of concrete B80 and fiber-reinforced concrete, the following facts should be noted: concrete B80 was mainly characterized by a sharp breakdown of the contact surface, and fiber-reinforced concrete was characterized by a gradual decrease in its bearing capacity.

Fiber concrete collapsed with the formation of “ripped” and “hairy” cracks with exposure of steel fiber.

When the length of the steel-concrete contact zone was increased 1.5 times, the maximum load for separation of concrete from reinforcement increased almost proportionally.

Strengthening of rigid reinforcement with longitudinal re-bars in fiber reinforced concrete specimens practically did not lead to an increase in adhesion strength.

In order to justify the results of the experiments and to predict correctly the beginning of bond breaking in the contact zone, the boundary-value problem was solved taking into account the contact interaction of elements in the structure using the finite element method.

At the joint steel-concrete boundary, the normal and tangent components of the distributed contact force arise.

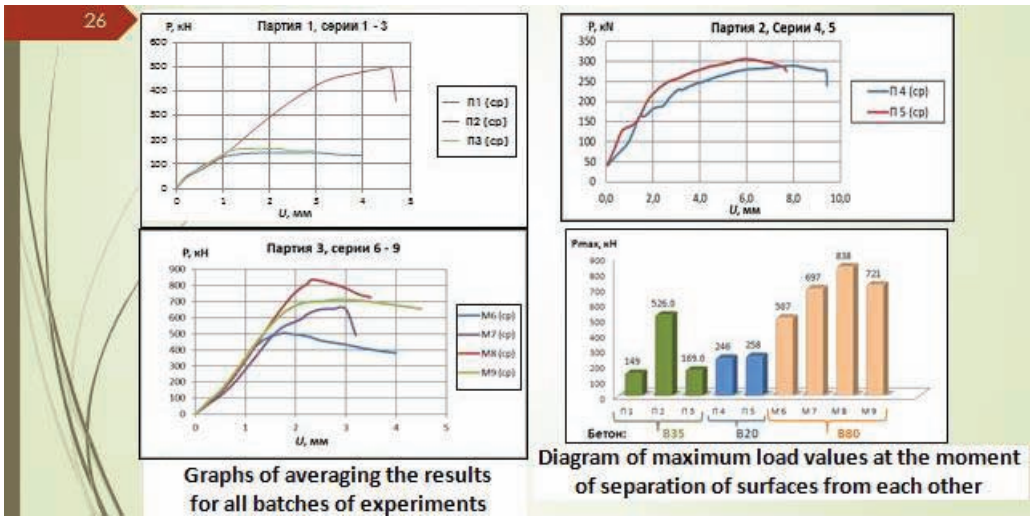

Figure 27. Shear Test Results.
Graphs of averaging the results for all batches of experiments (left).
Diagram of maximum load values at the moment of separation of surfaces from each other (right)).

While the bodies are glued together, the tangential forces do not depend on the normal contact forces, but when the bodies loss the contact, the shear begins.

The most important issue when modeling contact problems is the correct choice of a mathematical model for the interaction of contacting surfaces. The separation mechanism of bonded surfaces was modeled by contact elements. When constructing the finite element model, the symmetry of the computational domain was taken into account. The calculation was carried out on a quarter of the sample model. Different mesh options were considered. The problem was solved in linear and nonlinear formulations.

As a result, it was concluded that the geometric shape of rigid reinforcement affects the process of mechanical adhesion in the contact zone. The calculation results were in good agreement with the experimental results, and numerical modeling allowed us to determine the stress-strain state in the contact zone in an arbitrary point of rigid reinforcement, which changes during loading.

Taking into account the nonlinear properties of concrete made it possible to obtain a picture of crack formation with increasing load. Taking into account the nonlinear properties of steel showed the appearance and development of zones of plastic deformations in rigid reinforcement. The stresses in concrete and reinforcement for the given classes of concrete and reinforcement turned out to be lower than the calculated values, (with the exception of special points).

The influence of the geometry of the profile of rigid reinforcement on the load distribution between the elements of the steel-reinforced concrete column was also studied. Three versions of columns with the same cross-sectional area of concrete, flexible and rigid reinforcement were considered. A nonlinear calculation was performed, and the loads were determined when cracks in concrete and plastic deformations in the metal appeared. The calculation showed that rigid reinforcement made of two cross-mounted I-beams is able to provide a bearing capacity of up to 210,000 kN for the accepted section sizes, and it is the most rational among the considered variants.

12. GLASS RACKS

Tests on 18 samples of three groups of models of laminated heat-strengthened glass of rectangular cross-section were conducted. The first group of models was equivalent to full-scale facade racks in flexibility in both planes and was tested by central and eccentric compression with a given eccentricity.

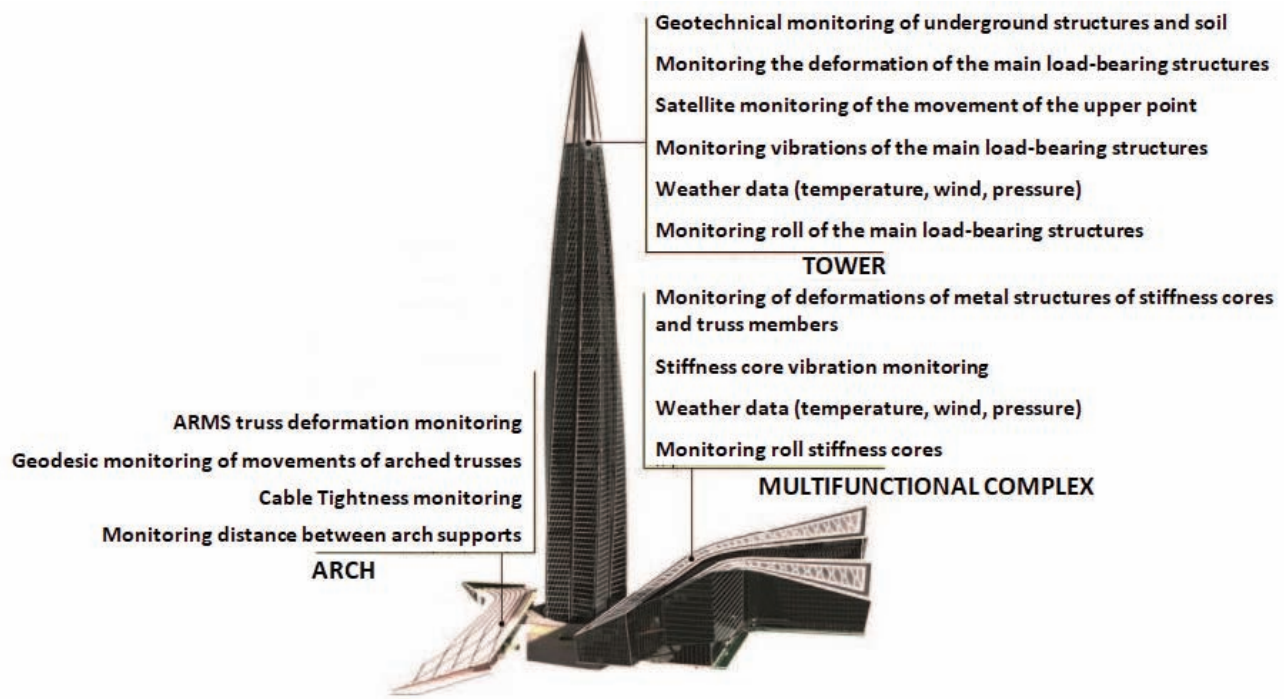

Figure 28. About structural health monitoring of the tower.

The second group of models was tested for pure bending. The third group of models was tested by central compression. Glasses for all models were heat-strengthened of 12 mm thick, adhesive layers of 0.89 mm thick. When testing models for compression, the hinge work of the upper and lower supports of the racks, the studied eccentricity, as well as the simple supporting for the beams were provided.

As a result of the tests, the values of breaking loads for the initial failure (by the appearance of the first crack) and complete destruction were obtained. Complete destruction of flexible rack specimens under normal loading occurred after loss of stability. When testing specimens of short beams, complete failure occurred immediately after the first cracks appeared. Centrally compressed prisms of low flexibility are characterized by a large difference between the initial and complete fracture stresses (1.4 ... 2.8 times).

The elastic modulus values of glass multilayer specimens differed for the main axes of the section and took the values: in the direction normal to the glass layers - 30,000 MPa; along the glass layers - 60,000 MPa. An elastic modulus of 12,500 MPa was accepted to calculate the deformations of glass structures.

13. STRUCTURAL HEALTH MONITORING

In accordance with the current regulatory documents, in order to ensure erection and operation safety of unique buildings as part of the scientific and technical support (STS) of construction, a set of measures was organized to continuously monitor the stress-strain state (SSS) of structures.

The main purpose of monitoring is minimizing of the possibility of emergencies caused by uncertainties in the work of the load bearing structures of a building and a soil of the foundation.

The development of the monitoring program for the foundations and the aboveground parts of the tower was carried out by specialists of SAMSUNG C&T, CJSC GORPROEKT, SODIS LAB, INFORSPROEKT, and NIIOSP named after N.M. Gersevanov in 2015 [4] (Figure 28 and Figure 29).

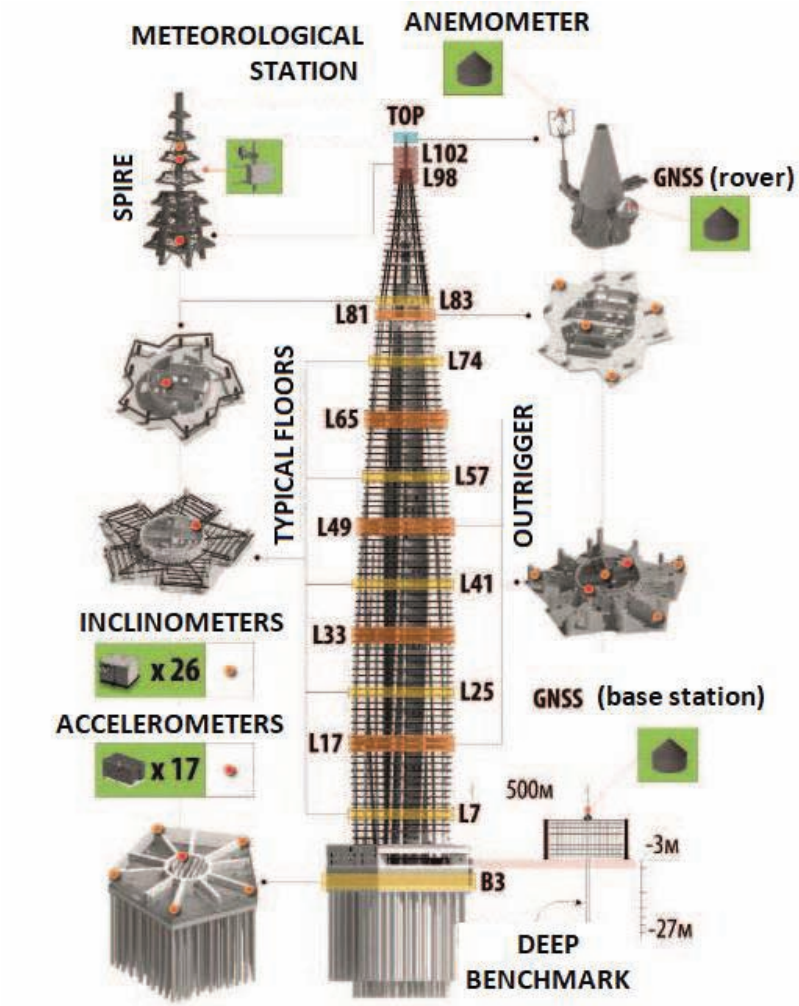

Figure 29. About structural health monitoring of the tower.

In order to control the stress-strain state, totally 1210 string strain gauges were installed in 196 targets on the rods of the working reinforcement of the lower plate, diaphragm walls and upper plate.

The aboveground part of the tower was equipped with an automated system for monitoring relative deformations. It consists of 1257 string strain gauges of various types. With their help, measurements are made of the axial deformations of composite columns on typical floors, vertical and horizontal deformations of the walls of the reinforced concrete core, comprehensive monitoring of the deformation of outrigger trusses and steel structures of the spire.

Real-time monitoring and post-processing planning of horizontal and vertical movements of the upper point of the building is carried out using a satellite geodetic monitoring system [5-10]. Satellite monitoring of the movement of the upper point, together with the results of monitoring of rolls and vibrations, provides comprehensive information about the deformation of the axis of the building.

Two weather stations allow conducting of a correlation analysis of the stress-strain state parameters and separating the changes in parameters associated with the degradation of building structures and seasonal and climatic changes.

REFERENCES

1. **Travush V.I., Shakhvorostov A.I.** Betonirovaniye nizhney plity korobchatogo fundamenta kompleksa «Lakhta tsentr» [Concreting of the bottom slab of the box-shaped

foundation of the Lakhta Center complex]. // *Vysotnyye zdaniya*, 2015, No. 1, pp. 92-101 (in Russian).
2. **Travush V.I., Konin D.V., Rozhkova L.S., Krylov A.S., Kaprielov S.S., Chilin I.A., Martirosyan A.S., Fim kin A.I.** Eksperimental'nyye issledovaniya stalezhelezobetonnykh konstruktsiy na vnetsentrennoye szhatiye [Experimental studies of steel-reinforced concrete structures for eccentric compression]. // *Academia. Arkhitektura i stroitel'stvo*, 2016, No 3, pp.127-135 (in Russian).
3. SP 63.13330.2012. Betonnyye i zhelezobetonnyye konstruktsii. Osnovnyye polozheniya [Concrete and reinforced concrete structures. The main provisions]. Design Code of the Russian Federation. Moscow, 2013 (in Russian).
4. **Travush V.I., Shakhraman'yan A.M., Kolotovichev YU.A., Shakhvorostov A.I., Desyatkin M.V., Shulyat'yev O.A., Shulyat'yev S.O.** "Lakhta tsentr" avtomatizirovannyy monitoring deformatsiy nesushchikh konstruktsiy i osnovaniya [Lakhta Center automated monitoring of deformations of load-bearing structures and foundations]. // *Academia. Arkhitektura i stroitel'stvo*, 2018, No. 4, pp. 94-108 (in Russian).
5. **Belostotsky A.M., Akimov P.A., Afanasyeva I.N., Kaytukov T.B.** Contemporary Problems of Numerical Modelling of Unique Structures and Buildings. // *International Journal for Computational Civil and Structural Engineering*, 2017, Volume 13, Issue 2, pp. 9-34.
6. **Belostotsky A.M., Akimov P.A.** Nauchnoissledovatelsky tsentr StaDyO. 25 let na fronte chislennogo modelirovaniys [25-th Anniversary of scientific research centre StaDyO]. // *International Journal for Computational Civil and Structural Engineering*, 2016, Volume 12, Issue 1, pp. 9-34 (in Russian).
7. **Belostotsky A.M., Akimov P.A.** O voprosakh avtomatizatsii system monitoring dlya otsenki tekuschego sostoyaniya stroitelnikh konstruktsiy zdaniy i sooruzheniy [About Automation of Structural Health Monitoring Systems]. // *International Journal for Computational Civil and Structural Engineering*, 2016, Volume 12, Issue 3, pp. 26-34 (in Russian).
8. **Ilyukhina E.A., Lahman S.I., Miller A.B., Travush V.I.** Konstruktivnye reshenija vysotnogo zdanija "Lahta Centr" v Sankt-Peterburge [Design Solutions of the High-Rise Building "Lakhta Center" in Saint-Petersburg]. // *Academia. Arkhitektura i stroitel'stvo*, 2019, No. 3, pp. 110-121 (in Russian).
9. **Travush V.I., Belostotsky A.M., Akimov P.A.** Contemporary Digital Technologies in Construction. Part 1: About Mathematical (Numerical) Modelling. // *IOP Conference Series: Materials Science and Engineering*, 2018, Volume 456, conference 1, 012029.
10. **Travush V.I., Belostotsky A.M., Akimov P.A.** Contemporary Digital Technologies in Construction. Part 2: About Experimental & Field Studies, Material Sciences, Construction Operations, BIM and "Smart" City. // *IOP Conference Series: Materials Science and Engineering*, 2018, Volume 456, conference 1, 012030.

СПИСОК ЛИТЕРАТУРЫ

1. **Травуш В.И., Шахворостов А.И.** Бетонирование нижней плиты коробчатого фундамента комплекса «Лахта центр». // Высотные здания, 2015, №1, с.92-101.
2. **Травуш В.И., Конин Д.В., Рожкова Л.С., Крылов А.С., Каприелов С.С., Чилин И.А., Мартиросян А.С., Фимкин А.И.** Экспериментальные исследования сталежелезобетонных конструкций на внецентренное сжатие. // *Academia. Архитектура и строительство*, 2016, №3, с. 127-135.
3. СП 63.13330.2012. Бетонные и железобетонные конструкции. Основные положения. – М., 2013.

4. **Травуш В.И., Шахраманьян А.М., Колотовичев Ю.А., Шахворостов А.И.. Десяткин М.В., Шулятьев О.А., Шулятьев С.О.** «Лахта центр» автоматизированный мониторинг деформаций несущих конструкций и основания. // *Academia. Архитектура и строительство*, 2018, №4, с. 94-108.
5. **Belostotsky A.M., Akimov P.A., Afanasyeva I.N., Kaytukov T.B.** Contemporary Problems of Numerical Modelling of Unique Structures and Buildings. // *International Journal for Computational Civil and Structural Engineering*, 2017, Volume 13, Issue 2, pp. 9-34.
6. **Белостоцкий А.М., Акимов П.А.** Научно-исследовательский центр СтаДиО. 25 лет на фронте численного моделирования. // *International Journal for Computational Civil and Structural Engineering*, 2016, Volume 12, Issue 1, pp. 9-34.
7. **Белостоцкий А.М., Акимов П.А.** О вопросах автоматизации систем мониторинга для оценки текущего состояния строительных конструкций, зданий и сооружений. // *International Journal for Computational Civil and Structural Engineering*, 2016, Volume 12, Issue 3, pp. 26-34.
8. **Илюхина Е.А., Лахман С.И., Миллер А.Б., Травуш В.И.** Конструктивные решения высотного здания «Лахта центр» в Санкт-Петербурге. // *Academia. Архитектура и строительство*, 2019, №3, с. 110-121.
9. **Travush V.I., Belostotsky A.M., Akimov P.A.** Contemporary Digital Technologies in Construction. Part 1: About Mathematical (Numerical) Modelling. // *IOP Conference Series: Materials Science and Engineering*, 2018, Volume 456, conference 1, 012029.
10. **Travush V.I., Belostotsky A.M., Akimov P.A.** Contemporary Digital Technologies in Construction. Part 2: About Experimental & Field Studies, Material Sciences, Construction Operations, BIM and “Smart” City. // *IOP Conference Series: Materials Science and Engineering*, 2018, Volume 456, conference 1, 012030.

Илюхина Елена Анатольевна, кандидат экономических наук; генеральный директор, Акционерное общество «Многофункциональный комплекс «Лахта центр»; 190000, Россия, г. Санкт-Петербург, ул. Почтамтская, д. 3-5, литер «А», ч.пом. 1Н, ком. 370;
тел. +7 (800) 700-31-52.

Лахман Сергей Ильич, кандидат экономических наук; генеральный директор, закрытое акционерное общество «Городской проектный институт жилых и общественных зданий»; 105064, Россия, г. Москва, Нижний Сусальный переулок, д.5, стр. 5А;
тел./факс +7 (495) 775-75-65;
E-mail: info@gorproject.ru.

Миллер Алексей Борисович, кандидат экономических наук; председатель правления, публичное акционерное общество «Газпром»; 117997, Россия, ГСП-7, г. Москва, ул. Наметкина, д. 16; тел. +7 (495) 719-21-09;
факсы: +7(495) 719-83-33, +7(812) 413-73-33;
E-mail: gazprom@gazprom.ru.

Травуш Владимир Ильич, академик РААСН, доктор технических наук, профессор; вице-президент Российской академии архитектуры и строительных наук; заместитель генерального директора, закрытое акционерное общество «Городской проектный институт жилых и общественных зданий»; 105064, Россия, г. Москва, Нижний Сусальный переулок, д.5, стр. 5А;
тел./факс: +7 (495) 775-75-65, +7(495) 909-39-39;
E-mail: travush@mail.ru.

Elena A. Ilyukhina, Ph.D., General Director, Joint Stock Company “Multifunctional complex Lakhta Center”; 3-5, ul. Pochtamtskaya, Saint-Petersburg, 190000, Russia; phone: +7(800) 700-31-52.

Sergey I. Lakhman, Ph.D., General Director of City Design Institute for Residential and Public Buildings; building 5A, 5, Nizhny Susalny pereulok, Moscow, 105064, Russia; phone/fax: +7 (495) 775-75-65;
E-mail: info@gorproject.ru.

Alexey B. Miller, Ph.D., Chairman of the Management Committee of public joint stock company “Gazprom”; 16, ul. Nametkina, Moscow, 117997, Russia;
fax: +7(495) 719-83-33, +7(812) 413-73-33;
E-mail: gazprom@gazprom.ru.

Vladimir I. Travush, Full Member of the Russian Academy of Architecture and Construction Sciences, Professor, Dr.Sc., Vice-President of the Russian Academy of Architecture and Construction Sciences; Vice-Director of City Design Institute for Residential and Public Buildings; building 5A, 5, Nizhny Susalny pereulok, Moscow, 105064, Russia; phone/fax: +7 (495) 775-75-65,
909-39-39; e-mail: travush@mail.ru.

DOI:10.22337/2587-9618-2019-15-3-40-54

"LAKHTA CENTER". MANAGEMENT CHALLENGES AND SOLUTIONS IN THE IMPLEMENTATION OF UNIQUE PROJECT DESIGNS

Elena A. Ilyukhina [1], Alexey B. Miller [2]

[1] Joint Stock Company "Multifunctional complex Lakhta Center", Saint-Petersburg, RUSSIA
[2] Public Joint Stock Company Gazprom, Saint-Petersburg, RUSSIA

Abstract: The "Lakhta Center" is the headquarters of public joint stock company "Gazprom", a key cultural and environmental project of Saint-Petersburg and the flagship object of the architectural, engineering and construction industries in Russia. The facility was completed for operating and became a precedent for the implementation of such a unique in scale and complexity project in Russia. It was realized on schedule and within the budget. The architectural dominant of the Lakhta Center is a tower with a height of 462 meters, which has become the tallest building in Europe. The following management challenges and solutions are under consideration in the distinctive paper: transfer of the object; land restrictions and related projects; the need to develop a regulatory documents; lack of relevant experience and competencies in Russia; building a flexible contracting system, separation of design and construction functions; a flexible approach to the preparation of project documentation, the main state expertise (Glavgosekspertiza) and the beginning of the zero cycle; building stages; package contracting system; managing by the global team; optimization of the project solutions; risk management system; global crisis; sanctions; changing the role of the customer / contractor during the project.

Keywords: high-rise building "Lakhta Center", building structures, management challenges and solutions, unique construction object

«ЛАХТА ЦЕНТР». УПРАВЛЕНЧЕСКИЕ ВЫЗОВЫ И РЕШЕНИЯ ПРИ РЕАЛИЗАЦИИ КОНСТРУКЦИЙ УНИКАЛЬНОГО ПРОЕКТА

Е.А. Илюхина [1], А.Б. Миллер [2]

[1] АО «Многофункциональный комплекс Лахта Центр», г. Санкт-Петербург, РОССИЯ
[2] ПАО «Газпром», г. Москва, РОССИЯ

Аннотация: «Лахта Центр» – штаб-квартира ПАО «Газпром», ключевой культурно-средовой проект Санкт-Петербурга и флагманский объект архитектурной, инженерной и строительной отраслей России. Данный объект, уже введенный в эксплуатацию и стал прецедентом реализации в России уникального по масштабу и сложности проекта в запланированные сроки и в рамках предусмотренного бюджета. Архитектурная доминанта «Лахта Центра» – башня высотой 462 метра – стала самым высоким зданием Европы. В настоящей статье рассматриваются следующие управленческие вызовы и решения: перенос объекта; ограничения участка и смежные проекты; необходимость разработки нормативной базы; отсутствие в России релевантного опыта и компетенций; выстраивание гибкой системы контрактования, разделение функций проектирования и СМР; гибкий подход в подготовке проектной документации, Главгосэкспертиза и начало нулевого цикла; этапы строительства; пакетное контрактование; управление глобальной командой; оптимизация проектных решений; система управления рисками; глобальный кризис; санкции; изменение роли заказчика/исполнителя в ходе реализации проекта.

Ключевые слова: высотное здание «Лахта Центр», строительные конструкции, управленческие вызовы и решения, уникальный строительный объект

1. GENERAL INFORMATION

Lakhta Center is the headquarters of PJSC Gazprom, a key cultural and environmental project of St. Petersburg and the flagship object of the architectural, engineering and construction industries in Russia [1-9]. It is located on the coast of the Gulf of Finland and has become a forming element of the new marine facade of the city. In future, comfortable embankments and infrastructure facilities will be created around the object. Due to this, a new modern center of attraction is being created in the north of St. Petersburg.

The complex consists of five buildings and structures, the construction of which is divided into two phases. The first phase is 4 objects with an area of 400 thousand square meters and a construction volume of more than 2 million cubic meters. Second stage is an object with an area of 150 thousand square meters with a implementation period of 3.5 years: from 2017 to 2021.

The construction of the multifunctional complex Lakhta Center (first phase), which was begun in October 2012, had been completed in October 2018. The facility was completed for operating and became a precedent for the implementation of such a unique in scale and complexity project in Russia. It was realized on schedule and within the budget.

The architectural dominant of the Lakhta Center is a tower with a height of 462 meters, which has become the tallest building in Europe.

About 600 Russian and foreign companies and more than 20,000 people from 18 countries participated in the project.

The general contractor of the project is Renaissance Construction. The RMJM team under the direction of Tony Kettle developed the architectural concept of the Lakhta Center. CJSC Gorproekt developed the project. Samsung C&T and CJSC Gorproekt (sub-designer) carried out detailed design.

2. OBJECTS OF COMPLEX

2.1. Skyscraper.

The aboveground part of the tower has 87 floors or 111 levels. At 360 m, the highest observation deck in Europe is located.

The supertall spins around for 90 degrees from the base to the top, expanding and narrowing as you climb. The floors of the tower, metal structures and facade elements are not repeated.

2.2. Multifunctional building.

A multifunctional building is the horizontal dominant of the complex, that is of 260 m long with a variable number of floors from 7 to 17 ones.

In terms of complexity of architectural and structural elements, the multifunctional building is not inferior to the tower building: its height differs from 22 to 85 meters; there are interior wide-span spaces, negative slopes of end facades.

The main pedestrian artery of the multifunctional building is the atrium, where the main public spaces of the Lakhta Center are concentrated: from a planetarium in the shape of a ball to a seven-story transformer hall.

2.3. Arch of the main entrance.

A separate building-entrance to the complex is a functionally unique solution that is made in the form of an asymmetric arch with a height difference from 18 to 24 m. At the vanishing points of the axes, the arch span reaches 98 meters.

2.4. Stylobate.

Stylobate is a two-level underground parking of the complex. All buildings of the first stage of the Lakhta Center are located on a single stylobate, which runs almost to the borders of the development spot. The roof is exploitable. In the future, landscaping will be done at the top.

2.5. Complex of buildings and structures.

The object of the second stage of the Lakhta Center for the location of Gazprom Group offices reminiscents the multifunctional building both in architectural appearance and in design solutions.

3. MANAGEMENT CHALLENGES AND SOLUTIONS

3.1. Transfer of the object.

The location of the facility in Lakhta is the result of a long dialogue with the conservative public of St. Petersburg. The initial concept of building of headquarters on the Okhtinsky cape, despite the obvious pluses for the development of the depressed Krasnogvardeisky district and the absence of a negative impact on the traditional postcard views of the city, was not accepted by the part of the urban urgency.

As a result, a location was determined. New location corresponded to the status of the project and was promising in terms of infrastructure development. The parameters of the site allowed significantly expanding the functionality of the project and making its architectural appearance more harmonious.

Overcoming the challenge was facilitated both by the fact of a bold and responsible decision to build an ambitious project in a conservative city, as well as by the unprecedented openness in its implementation, by effective non-standard information policy. As a result, the people unambiguously accepted the Lakhta Center project; it became a favorite attraction in the guise of a new futuristic ensemble on the coast.

3.2. Land restrictions and related projects.

The unique location of the building site in Lakhta on both sides limited by water and adjacent to the highway at the same time creates enormous difficulties at all stages. This is lacking of auxiliary sites for the deployment of construction camps, warehouses, heavy equipment, etc.; the need to synchronize plans and work with related projects (embankments, roads, and a yacht club), communication with city authorities on the timing of the introduction of engineering and road infrastructure.

Early planning and deep immersion in all the details of the organization of the construction process made it possible to prevent serious failures (for example, pouring the bottom plate of the box foundation [5] with coming of the concrete mixers on site every single minute).

In parallel, different types of work were carried out in each building. The next type of work started as soon as the site allowed and the documentation was ready. At peak moments, out by 12 thousand people simultaneously carried up to 3,000 types of work in a day. The work was carried out in three shifts 24/7. So, in 2017, building of core walls, installing columns, interfloor ceilings, facade glazing, laying engineering networks and architectural decoration went simultaneously at different levels of the tower.

In order to synchronize all types of work with the delivery of schedules up to minute plans, BIM technology was used. It allows you to visualize and synchronize schedules and logistics processes.

The construction of engineering infrastructure at the expense of the investor and solutions that were not obvious at first glance, for example, the construction of an autonomous gas boiler near the heating main, eliminated the dependence of the facility commissioning on third parties.

3.3. The need to develop a regulatory documents.

At the time of the start of design, practically there were not regulatory documents for high-rise and unique construction in Russia. So, for example, according to the "Technical Regulations for Fire Safety", all buildings above 50 meters are outside the regulation and should be designed according to specially developed Special Technical Condition (STU) with fire safety measures.

During the construction period, 3 “fire safety” STU for the Lakhta Center were issued. These documents covered totally about 20 points that were not regulated by standards.

There was also a need to develop and harmonize standards for new construction materials and technologies. In particular, it was necessary making a calculation proof, conducting tests and preparing STU to apply the composite structures in the tower (supporting perimeter columns).

The same situation arose with fachwerk pillar-columns made of laminated glass.

3.4. Lack of relevant experience and competencies in Russia.

The unique architecture and innovative technologies have another side. They are practically absent in Russia, and relevant experience and competencies are significantly limited even in the world. Even if there are ready-made solutions in the world experience, their scale, as a rule, differs from Lakhta Center (width and depth of piles [4], foundation box structures, area of facades, energy-efficient glass compounding, etc.).

This created significant difficulties not only in the formation of the project team, but also in the selection of contractors. Not many companies were announced to participate in the tender, many of which "fell off" when studying technical tasks and getting to know the requirements for quality and deadlines.

However, this challenge was overcome. As a result, people gathered in the team, were ready to think outside the box, quickly make complex and responsible decisions, and treat the project as a personal challenge. The key partners of the project were chosen by a similar principle.

On the other hand, specialists with rare competencies that have not been in demand in Russia in recent decades have found application in the project and gained unique experience during its implementation.

3.5. Building a flexible contracting system. Separation of design and construction functions.

The factors described above did not allow the project management to shift the responsibility for the implementation of the project to the general designer / general contractor by concluding one or two contracts for the whole range of works. The "design and build" scheme, which required many months to prepare the requirements specification and contract, was unacceptable.

In particular, the project went through several iterations from the architectural concept to the Project stage, with the subsequent development of working documentation, which went for several stages ahead of the construction.

The construction part was organized in a similar way. At the initial stage, Arabtec was involved as a general contractor for the underground part, and then Renaissance was involved for executing of the rest of the complex of work with a package contracting strategy.

3.6. A flexible approach to the preparation of project documentation. The main state expertise (Glavgosekspertiza) and the beginning of the zero cycle.

Project documentation was issued and approved by parts. The first projected object was the Lakhta Center tower. It passed the Glavgosexpertiza at the first time, which allowed us to begin work on the zero cycle (building a wall in the ground and creating a pile field under the box foundation of the future skyscraper). An early start of the zero-cycle construction and installation work was executed before the selection of the main general contractor, which the subsequently accept responsibility for previously completed work.

In parallel with the construction work, a package of documents was developed for the remaining facilities of the complex: Multifunctional building, Arch and Stylobate, after which the entire project was once again reviewed by the Main State Expertise (Glavgosekspertiza). Totally, there were six such examinations when adjustments were made or the degree of optimization and detailing of the Project increased. Therefore, for example, fachwerk pillar-columns made of laminated heat-strengthened glass, originally envisaged by the project, appeared in the Arch. However due to the lack of a regulatory base, it took time to develop requirements for such structures and include them in special technical specifications, conduct a series of tests for column specimens, develop a methodology of their calculation before defending the design decision in Glavgosekspertiza of Russia.

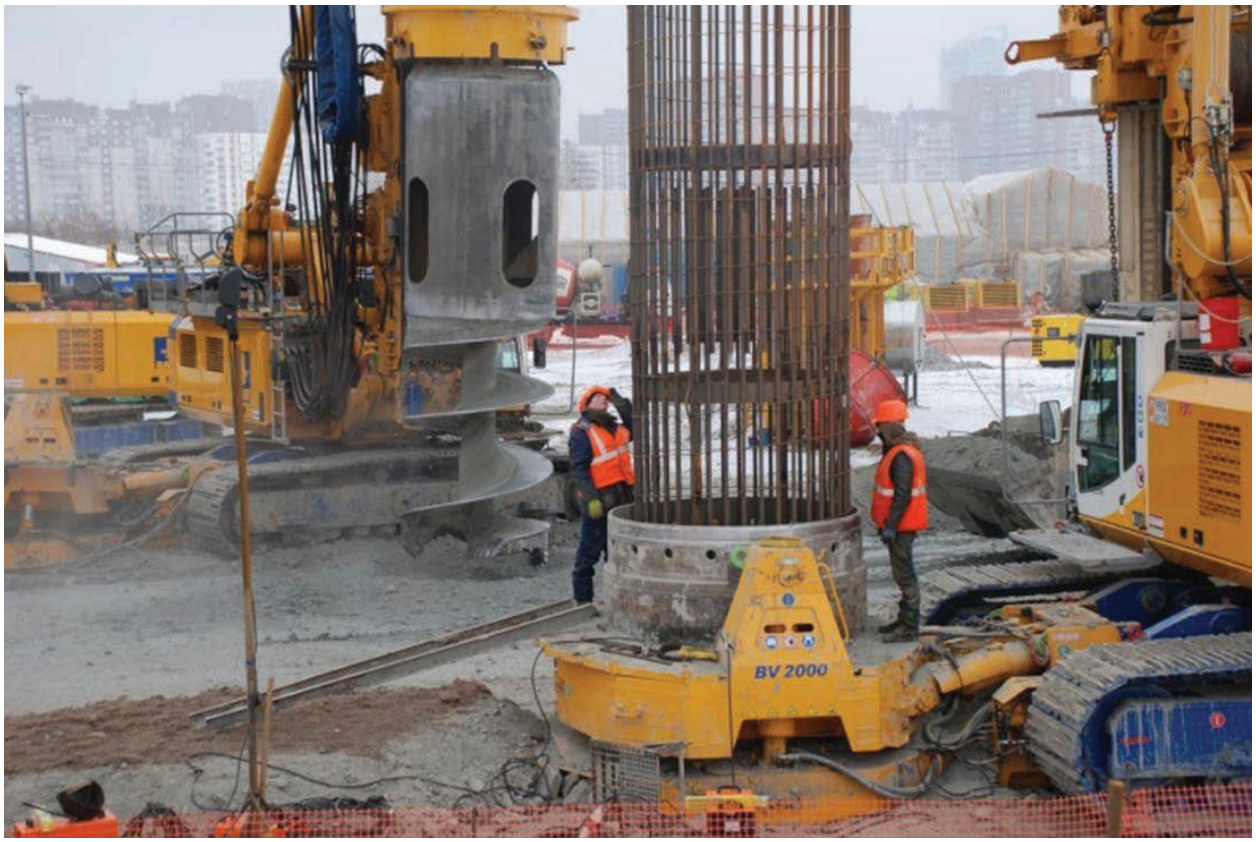

Figure 1. Installation of the frame of the bored pile.

Such a differentiated approach to coordination in the conditions of tight deadlines for the construction of the facility made it possible efficiently using the team's resources and to proceed as quickly as possible to the implementation of the project.

3.7. Building stages.

The construction of the Lakhta Center tower was launched in October 2012. At first, builders made 264 piles with a diameter of 2 meters with a length of 55 and 65 meters from ground level (or 72 and 82 meters, if we counted from the level of the surface of the earth). Then the foundation pit was fenced using the "wall in soil" and monolithic reinforced concrete disks around the perimeter using the "Semi-top-down" method.

In accordance with the design solution of the foundation, it was necessary to build a foundation pit with a depth of 18 m in the conditions of weak soils of St. Petersburg for placing the box foundation in the form of a pentagon inscribed in a circle with a diameter of 100 m.

Taking account the high level of groundwater, a wall in the ground, entering the Vendian clay, was chosen as the fence of the pit. In order to select a spacer structure, more than 10 variants were considered, including using anchor fasteners. The variant in the form of temporary 4 disk floor slabs of 600 mm thick in the form of a ring of minimum width of about 9 m was chosen as a result of the technical and economic comparison of the variants. The final variant of the enclosing and holding structures of the pit is shown in Figures 2, 3.

The next important stage was the construction of the box foundation structures, which includes two underground floors of the tower. The total volume of concrete in the box foundation is 46,000 m^3. The volume of concrete in the bottom slab of the box foundation with a thickness of 3.6 meters was 19,624 m^3.

In order to increase the reliability of the foundation, it was decided concreting the bottom plate of the box foundation without a time break, that avoided the installation of technological joints, which are additional stress concentrators.

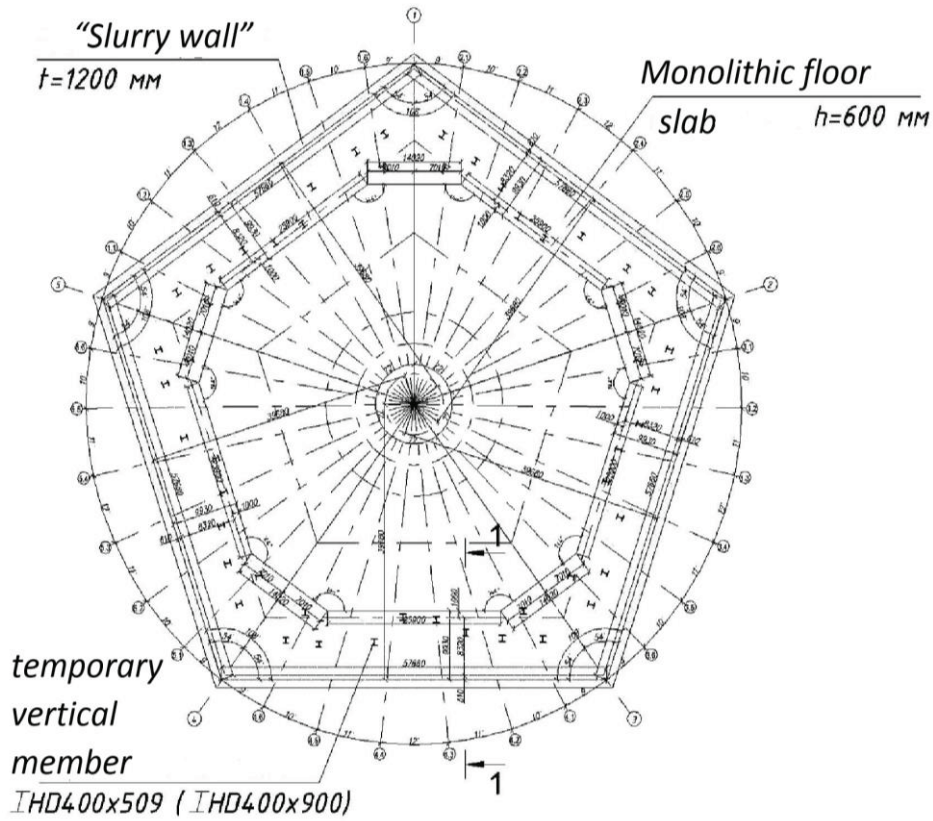

Figure 2. Plan of foundation pit fence for building of the tower.

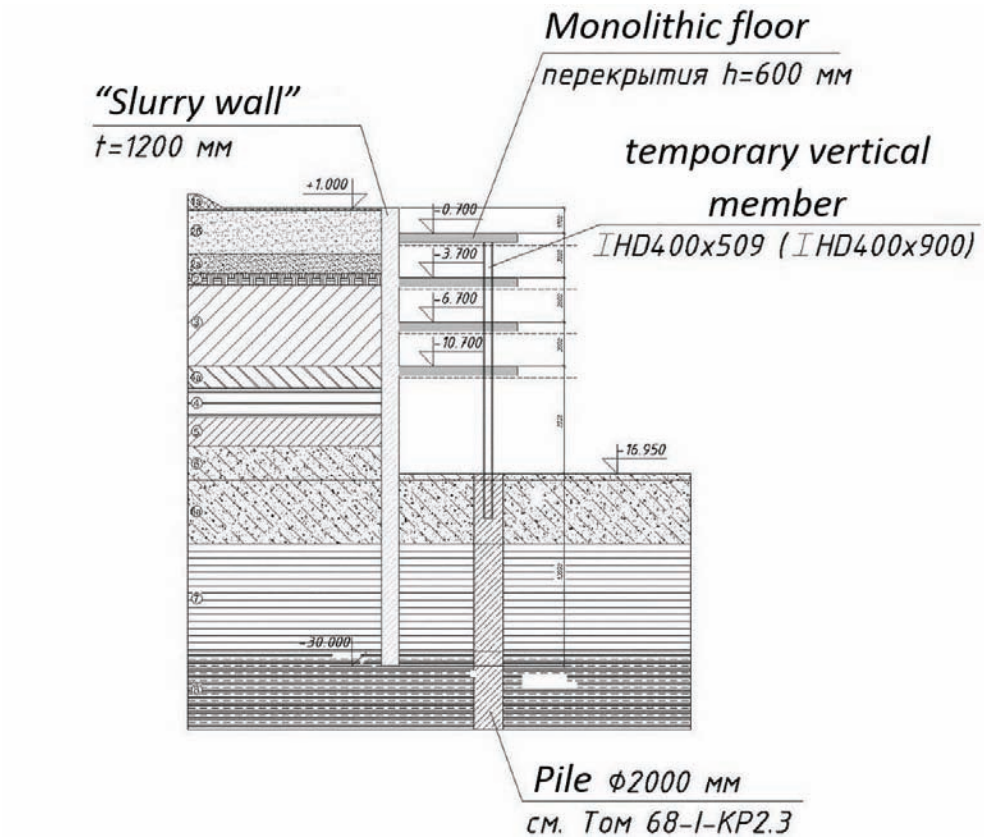

Figure 3. Section of the structure of the foundation pit fence for building of the tower.

Figure 4. General view of the pit after excavation until design mark and preparation for concreting.

Figure 5. Reinforcement of the bottom plate of the box foundation.

Figure 6. Certificate of Guinness Book of Records.

For this purpose, all reinforcement of the slab was previously connected in the foundation pit and the composition of special self-compacting concrete was developed. 18 points of concrete reception were organized on the edge of the foundation pit. 13 concrete working plants with an interval of 1-1.5 minutes delivered concrete. As a result, the bottom slab was concreted in 49.2 hours, and thereby it set the world record for continuous concreting, as recorded in the Guinness Book of Records.

In order to reduce the exothermy of concrete of class B60, it was stipulated that concrete mixtures should have a low energy potential and have a Portland cement consumption of not more than 360 kg / m3 in terms of clinker with a trialuminate content of not more than 8%. Concrete mixtures delivered to the construction site should have temperature in the range + 5 ... + 15 ° C. The densely reinforced structure of the lower foundation slab was concreted using a self-compacting concrete mixture with a mobility in the range from 60 to 65 cm. Particular attention was paid to the temperature regime when concrete mixture set the strength. Concrete should have minimal exotherm and hardening kinetics at an early age under normal temperature and humidity conditions. At the same time, the required compressive strength of concrete at least 1 day old is 0 MPa, at least 3 days old is 15 MPa, at least 7 days old is 40 MPa, and at least 28 days old is 65 MPa. The aging of concrete in the structure was carried out under conditions that prevent thermal shrinkage with the cooling rate of concrete in the core of the slab not more than 2.0–3.0 °C per day and the temperature difference between zones having a common border height of the slab of not more than 20 °C.

The concrete mixture was prepared according to the standard technological scheme taking into account the requirements of GOST 7473-2010 on the accuracy of dosing of materials and the features associated with the order of loading and mixing the main components of the mixture and powder additives. It was carried out in two stages: the stage of dosing, loading and mixing the components in a stationary concrete plant mixer; mixing stage in a concrete mixer during the transportation of mixtures to the construction site.

Builders mounted a protective tent in order to protect against atmospheric precipitation and ensure regulated requirements for the temperature regime of concrete curing, as well as for the comfortable organization of work on the entire front of concreting of the slab structure and to provide required temperature regime of heating the air under the tent.

Heat generators with adjustable power were used to control the temperature regime.

Figure 7. Building of the first floors of the tower.

Figure 8. Building of metal structures of outrigger level.

Figure 9. Overlaps.

The temperature control of the hardening of concrete in the lower foundation slab was carried out using an automated system based on the use of temperature sensors. Such sensors were installed in different zones of the concrete slab: in the core and on the periphery of the structure at three elevations, as well as in the upper zone of the slab in areas where are the walls of the box foundation.

During the construction of the aboveground part of the tower, advanced construction technologies were actively used. Initially, the reinforced concrete central core of the tower was made in average of 5-7 floors ahead of the other underlying structures. Then there was the installation of metal structures of the cores of steel-reinforced concrete columns [6-9], metal beams of floors. The final step of this technology for the construction of tower structures was the concreting of steel-reinforced concrete columns and floor slabs.

The spire of the tower with a height of 118 meters began to be mounted from the level of 83 floors at height mark 344,400. The top of the spire is located at height mark 462 meters. The installation of the spire was completed in early 2018.

The construction of the Lakhta Center skyscraper was launched in October 2012 and completed in 2018.

Key achivements are specified below.

- A world record fixed in the Guinness Book of Records was set. On March 1, 2015, a 49-hour non-stop pouring of concrete was completed. 19 624 m3 of concrete were laid in the bottom plate of the box foundation of the Lakhta Center tower.
- The Lakhta Center Tower has become the northernmost skyscraper in the world.
- For the first time, a Russian skyscraper received an international green certificate of the highest level - LEED Platinum.
- The largest volume of scientific support in the construction of civil buildings in Russia. Only at the zero cycle, 13 institutes and companies were involved.
- A world-class project gave an impetus to the development of the Russian construction industry in terms of developing a new regulatory documents for high-rise and unique construction.
- More than 100 technological innovations were applied, among which:
- The first in civil engineering applied composite supporting columns made of steel-reinforced concrete. The decision reduced the construction time of columns by 40% while reducing their cost by almost half.
- Implemented one of the largest volumes of facade glazing in the world – 130 thousand square meters of cold-formed glass.

Figure 10. Mounting the spire.

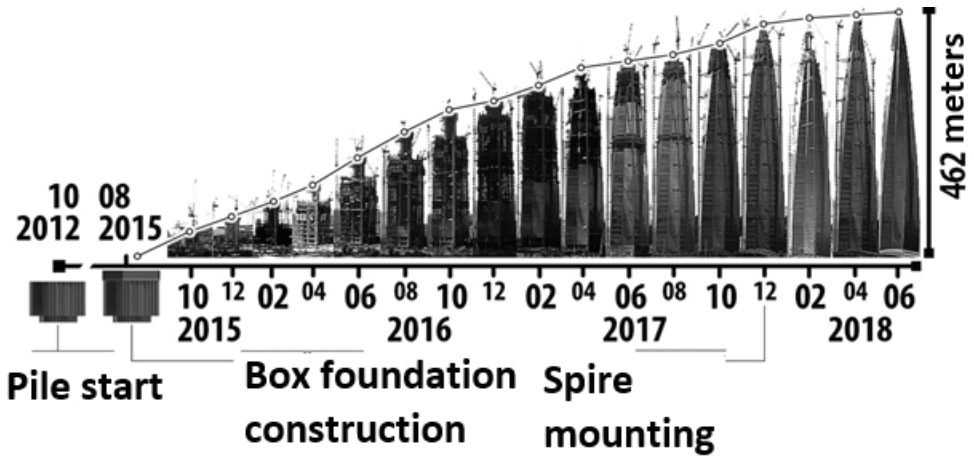

Figure 11. Building stages.

- For the first time in Russia, experience was gained in the construction of high-rise buildings on Vendian clay. About 40 km of exploratory wells were drilled until depth of 150 m on the Lakhta Center site; a scientific and practical base has been created for use in construction in Northwest Russia.
- Innovative techniques in the construction of a high-rise building made it possible to ensure absolute verticality. The maximum deviation during the construction of the core is up to 6 mm.
- A unique Russian development of a system for monitoring structural deformations, which in real time monitors the complex components according to hundreds of indicators [2, 3].

3.8. Package contracting system.

Lakhta Center specialists created their own package contracting system, which allowed not only staying within the budget, but also save up to 19% of the initial project budget at some stages. The essence of the approach is to divide the upcoming work front into large packages, the cost of which was calculated only after the appearance of working documentation. This allows us to determine the cost of the final list of works, taking into account real costs. With the traditional approach, such a cost would inevitably be approximate and overpriced. Such a strategy made it possible to reduce the terms of release and improve the quality of work due to cross-control between performers.

3.9. Managing by the global team.

Attracting the best world experience, the most experienced specialists and creating a competitive environment within the team by dividing the functions between large partners led to a unique result that is the creation of a huge global team. 18 countries, more than 600 companies and 20,000 people at the site became a challenge for the project management. The managing team of Russian specialists consists of 100 people in total.

Mental and cultural differences, language barriers as a result did not put to achieve the goal. On the contrary, the project strengthened the image as the global, gained international recognition in professional circles. This largely happened due to:

- flexibility in negotiations and the ability to interest potential partners in achieving the goal on mutually beneficial conditions;
- strategies for jointly with the construction manager and / or general contractor choosing contractors, attracting a wide range of contractors and suppliers, both foreign and Russian;
- the creation of a universal, flexible and mobile team of the Customer consisting of young, ambitious and highly qualified specialists, capable of solving issues of any complexity in all areas of activity (technical, financial, legal, administrative, commercial, communication and etc.);

- placing the Customer's team on the project site and direct interaction of the Customer with partners;
- deep involvement of the Customer team in the development of design and design solutions;
- the interest of all participants of the global team to implement non-standard tasks and advanced architectural and technological solutions;
- a flexible management system with a staff structure that varies depending on the stage of the project, the targeted involvement of leading experts and consultants.

3.10. Optimization of the project solutions.
A number of decisions were accepted that made it possible to maintain and even improve the quality of the project while reducing costs. So, the originally planned anchor spacer system was replaced with a disk spacer system, which significantly reduced the main costs and allowed to shorten the output period for the preparatory cycle of the Multifunctional building. The technology of glass supporting columns, successfully implemented in the facades of the multifunctional building, was subsequently applied on the facades of the arch, which is the main entrance to the complex. That makes the structure lighter and more transparent. Thanks to the optimization of engineering solutions, even in the smallest details, it was possible to achieve excellent indicators, for example, in water efficiency, which made it possible to achieve LEED Platinum.

3.11. Risk management system
Throughout the project implementation period, the project management team built a strategy and applied a risk management system. The risks included global country risks, including international sanctions; bankruptcy risk of large companies; risks of default on the part of related government agencies; risks of making significant changes to the project at the implementation stage and much more, up to the risks of small incidents during construction and weather conditions. In total, this is several thousand points.
Systematization, early diagnosis of the problems of contractors and suppliers, indifferent participation in resolving all issues up to going to production and offering technology and logistics allowed us to avoid significant delays even at certain stages, and in case of risks, allowed make changes to the sequence of work so that all resources are used as efficiently as possible.

3.12. Global crisis.
During the period from 2012 to 2018, there were a number of geopolitical shocks and a related currency crisis (2014-2015). This would seem that an increase in the costs of the project to be inevitable due to the revaluation of the cost of imported materials and services of foreign specialists. However, thanks to a non-trivial approach to the contracting process, agreements were reached with most counterparties on the separation of the ruble and currency components.
It was localized a number of foreign industries from the Italian Chimolai to the German Gartner, which allowed to reduce the long-term costs of the manufacturer and maintain the necessary level of product prices. Another resource is the use of domestic materials. Metal structures excepting the column cores, reinforcement, concrete and some other materials are completely Russian-made with the costs of the products in ruble value. In relation to hard currencies, such materials became cheaper and this offset the increase in costs of imported products. The situation with the cost of services is similar.

3.13. Sanctions.
The imposition of sanctions was a serious blow for many companies in a wide variety of industries working with foreign counterparties. In the case of Lakhta Center, this risk was not realized and did not affect the timing and cost of the facility. Global companies participated in the project in the form of their Russian divisions. For some, the condition for participation in the project was the localization of production. In addi-

tion, ceteris paribus during the competitive procedures, preference was given to Russian contractors and suppliers (metal structures).
Political risks during exacerbation of relations between the countries were offset by the presence of previously concluded contracts for all types of work.

3.14. Changing the role of the customer / contractor during the project.
Flexibility and adaptability allowed the project team to fulfill all the obligations and implement the project within the stated time, while maintaining the basic functionality and concept.
Therefore, the role of the Customer in the project has repeatedly changed. We acted as a developer realizing the task set by the Investor, as a management company that will operate the building, manage the leased space and represent the functional and program part of the project to the management company. Today, the company acts as a Seller, conducting the procedure of transferring the object to the new owner and as an Agent, completing a number of finishing work on the initiative of the owner.
However, as a result, despite the changing interaction format, the complex was put into operation and received an act of conformity with the project. In addition, a full-scale transfer to the owner is underway for subsequent operation.

REFERENCES

1. **Ilyukhina E.A., Lahman S.I., Miller A.B., Travush V.I.** Konstruktivnye reshenija vysotnogo zdanija «Lahta Centr» v Sankt-Peterburge [Design Solutions of the High-Rise Building "Lakhta Center" in Saint-Petersburg]. // *Academia. Arkhitektura i stroitel'stvo*, 2019, No. 3, pp. 110-121 (in Russian).
2. **Travush V.I., Shulyatev O.A., Shulyatev S.O., Shahramanyan A.M., Kolotovichev Yu.A.** Analiz rezul'tatov geotehnicheskogo monitoringa bashni "Lahta Centr" [Analysis of the results of geotechnical monitoring of the tower "Lakhta Center"]. // *Osnovanija, fundamenty i mehanika gruntov*, 2019, No. 2, pp. 15-21 (in Russian).
3. **Travush V.I., Shakhraman'yan A.M., Kolotovichev YU.A., Shakhvorostov A.I., Desyatkin M.V., Shulyat'yev O.A., Shulyat'yev S.O.** "Lakhta tsentr" avtomatizirovannyy monitoring deformatsiy nesushchikh konstruktsiy i osnovaniya [Lakhta Center automated monitoring of deformations of load-bearing structures and foundations]. // *Academia. Arkhitektura i stroitel'stvo*, 2018, No. 4, pp. 94-108 (in Russian).
4. **Travush V.I., Shulyatev S.O.** Adjusted pile foundation construction for skyscrapers. // *IOP Conference Series: Materials Science and Engineering*, 2018, Volume 456, conference 1, 012008.
5. **Travush V.I., Shakhvorostov A.I.** Betonirovaniye nizhney plity korobchatogo fundamenta kompleksa "Lakhta tsentr" [Concreting of the bottom slab of the box-shaped foundation of the Lakhta Center complex]. // *Vysotnyye zdaniya*, 2015, No. 1, pp. 92-101 (in Russian).
6. **Travush V.I., Konin D.V., Rozhkova L.S., Krylov A.S., Kaprielov S.S., Chilin I.A., Martirosyan A.S., Fimkin A.I.** Eksperimental'nyye issledovaniya stalezhelezobetonnykh konstruktsiy na vnetsentrennoye szhatiye [Experimental studies of steel-reinforced concrete structures for eccentric compression]. // *Academia. Arkhitektura i stroitel'stvo*, 2016, No 3, pp.127-135 (in Russian).
7. **Travush V.I., Konin D.V., Kaprielov S.S., Konin D.V., Krylov A.S., Chilin I.A.** Jeksperimental'nye issledovanija stalezhelezobetonnyh konstrukcij, rabotajushhih na izgib [Experimental studies of steel-reinforced concrete structures working on bending]. // *Stroitel'stvo i rekonstrukcija*, 2017, No. 4(72), pp. 63-71 (in Russian).
8. **Travush V.I., Kashevarova G.G., Martirosyan A.S.** Computer modelling as evaluation method of column base bearing ca-

pacity in tower building. // *Procedia Engineering*, 2016, Vol. 153, pp. 773-780.
9. **Travush V.I., Kashevarova G.G., Martirosyan A.S., Avhacheva I.A.** Experimental study of possible ways to increase cohesion strength in the "steel – concrete" contact zone under displacement conditions. // *Procedia Engineering*, 2016, Vol. 153, pp. 766-772.

СПИСОК ЛИТЕРАТУРЫ

1. **Илюхина Е.А., Лахман С.И., Миллер А.Б., Травуш В.И.** Конструктивные решения высотного здания «Лахта центр» в Санкт-Петербурге. // *Academia. Архитектура и строительство*, 2019, №3, с. 110-121.
2. **Травуш В.И., Шулятьев О.А., Шулятьев С.О., Шахраманьян А.М., Колотовичев Ю.А.** Анализ результатов геотехнического мониторинга башни «Лахта Центр». // *Основания, фундаменты и механика грунтов*, 2019, №2, с. 15-21.
3. **Травуш В.И., Шахраманьян А.М., Колотовичев Ю.А., Шахворостов А.И.. Десяткин М.В., Шулятьев О.А., Шулятьев С.О.** «Лахта центр» автоматизированный мониторинг деформаций несущих конструкций и основания. // *Academia. Архитектура и строительство*, 2018, №4, с. 94-108.
4. **Travush V.I., Shulyatev S.O.** Adjusted pile foundation construction for skyscrapers. // *IOP Conference Series: Materials Science and Engineering*, 2018, Volume 456, conference 1, 012008.
5. **Травуш В.И., Шахворостов А.И.** Бетонирование нижней плиты коробчатого фундамента комплекса «Лахта центр». // *Высотные здания*, 2015, №1, с. 92-101.
6. **Травуш В.И., Конин Д.В., Рожкова Л.С., Крылов А.С., Каприелов С.С., Чилин И.А., Мартиросян А.С., Фимкин А.И.** Экспериментальные исследования сталежелезобетонных конструкций на внецентренное сжатие. // *Academia. Архитектура и строительство*, 2016, №3, с. 127-135.
7. **Травуш В.И., Каприелов С.С., Конин Д.В., Крылов А.С., Чилин И.А.** Экспериментальные исследования сталежелезобетонных конструкций, работающих на изгиб. // *Строительство и реконструкция*, 2017, №4(72), с. 63-71.
8. **Travush V.I., Kashevarova G.G., Martirosyan A.S.** Computer modelling as evaluation method of column base bearing capacity in tower building. // *Procedia Engineering*, 2016, Vol. 153, pp. 773-780.
9. **Travush V.I., Kashevarova G.G., Martirosyan A.S., Avhacheva I.A.** Experimental study of possible ways to increase cohesion strength in the "steel – concrete" contact zone under displacement conditions. // *Procedia Engineering*, 2016, Vol. 153, pp. 766-772.

Илюхина Елена Анатольевна, кандидат экономических наук; генеральный директор, Акционерное общество «Многофункциональный комплекс «Лахта центр»; 190000, Россия, г. Санкт-Петербург, ул. Почтамтская, д. 3-5, литер «А», ч.пом. 1Н, ком. 370;
тел. +7 (800) 700-31-52.

Миллер Алексей Борисович, кандидат экономических наук; председатель правления, публичное акционерное общество «Газпром»; 117997, Россия, ГСП-7, г. Москва, ул. Наметкина, д. 16; тел. +7 (495) 719-21-09; факсы: +7(495) 719-83-33, +7(812) 413-73-33;
E-mail: gazprom@gazprom.ru.

Elena A. Ilyukhina, Ph.D., General Director, Joint Stock Company "Multifunctional complex Lakhta Center"; 3-5, ul. Pochtamtskaya, Saint-Petersburg, 190000, Russia; phone: +7(800) 700-31-52.

Alexey B. Miller, Ph.D., Chairman of the Management Committee of public joint stock company "Gazprom"; 16, ul. Nametkina, Moscow, 117997, Russia;
fax: +7(495) 719-83-33, +7(812) 413-73-33;
E-mail: gazprom@gazprom.ru.

DOI:10.22337/2587-9618-2019-15-3-55-76

SIMULATING THE BEHAVIOR OF SOFT COHESIVE SOILS USING THE GENERALIZED BOUNDING SURFACE MODEL

Victor N. Kaliakin [1], Andres Nieto-Leal [2]
[1] University of Delaware, Newark, USA
[2] Universidad Militar Nueva Granada, Cajica, COLOMBIA

Abstract: The Generalized Bounding Surface Model (GBSM) for saturated cohesive soils is a fully three-dimensional, time and temperature-dependent model that accounts for both inherent and stress induced anisotropy. To better simulate the behavior of cohesive soils exhibiting softening, the model employs a non-associative flow rule. The GBSM synthesizes many previous bounding surface constitutive models for saturated cohesive soils and improves upon their predictive capabilities. For those cases where the use of the more complex forms of the GBSM is not justified, the model can be adaptively changed to simpler forms, thus reducing the number of associated parameters, giving flexibility to the simulations and reducing the computational cost. Following a brief overview of the GBSM, the model's performance in simulating the response of soft, saturated cohesive soils is assessed under both axisymmetric and true triaxial conditions.

Keywords: bounding surface, elastoplasticity, viscoplasticity, cohesive soils, soft soils

МОДЕЛИРОВАНИЕ ПОВЕДЕНИЯ МЯГКИХ КОГЕТИЧЕСКИХ ПОЧВ С ИСПОЛЬЗОВАНИЕМ ОБОБЩЕННОЙ МОДЕЛИ ОБЪЕМНОЙ ПОВЕРХНОСТИ

В.Н. Калякин [1], Андрес Ньето-Лил [2]
[1] Университет штата Делавэр, г. Ньюарк, США
[2] Университет Милитара Нуэва, г. Кахика, КОЛУМБИЯ

Аннотация: Обобщенная модель ограничивающей поверхности (GBSM) для насыщенных связных почв является полностью трехмерной моделью, зависящей от времени и температуры, которая учитывает как собственную, так и вызванную напряжением анизотропию. Чтобы лучше моделировать поведение связных почв, проявляющих размягчение, модель использует неассоцированное правило потока. GBSM синтезирует многие предыдущие модели ограничивающей поверхности для насыщенных связных грунтов и улучшает их прогнозные возможности. Для тех случаев, когда использование более сложных форм GBSM неоправданно, модель может быть адаптивно изменена на более простые формы, тем самым уменьшая количество связанных параметров, обеспечивая гибкость моделирования и уменьшая вычислительные затраты. После краткого обзора GBSM эффективность модели при моделировании реакции мягких, насыщенных связных грунтов оценивается как в осесимметричных, так и в истинных трехосных условиях.

Ключевые слова: ограничивающая поверхность, упругопластичность, вязкопластичность, связные грунты, мягкие грунты

1. INTRODUCTION

The Generalized Bounding Surface Model (GBSM) synthesizes many previous bounding surface constitutive models for saturated cohesive soils and improves upon their simulative and predictive capabilities. In a recent paper [1], a detailed description of the GBSM was presented. Although some model simulations were also presented, they were, out of necessity, rather general in scope. As such, this paper supplements the earlier work [1]. Following a brief overview of the bounding surface concept and the GBSM, the model's performance in simulating the response of soft, saturated cohesive soils is assessed.

2. THE BOUNDING SURFACE CONCEPT IN STRESS SPACE

Some general aspects of the bounding surface concept in stress space are presented in this section. Additional details pertaining to theoretical aspects of this concept are given by Dafalias [2]; Kaliakin et al. [1] present a more specialized discussion of the concept as it applies to the GBSM. In the subsequent development tensorial quantities are presented in indicial form with the indices obeying the summation convention over repeated indices.

The material state is defined in terms of effective stresses σ'_{ij} and a set of proper internal variables q_n that embody the past loading history. In the subsequent development tensorial quantities are presented in indicial form with the indices obeying the summation convention over repeated indices. The single subscript on the q_n is not a tensorial index but denotes the plurality of these internal variables.

The existence of a smooth and convex bounding surface in effective stress space is assumed [2,3]. The surface always encloses the origin and is origin-convex; i.e., any radius emanating from the origin intersects the surface at only one point (Figure 1). Similar to a yield surface, the bounding surface is analytically given by

$$F\left(\bar{\sigma}'_{ij}, q_n\right) = 0 \tag{1}$$

where $\bar{\sigma}'_{ij}$ indicates an "image" point on the bounding surface. The actual stress point σ'_{ij} always lies within or on the surface. To each σ'_{ij} a unique $\bar{\sigma}'_{ij}$ is assigned by a properly defined "mapping" rule that becomes the identity mapping if σ'_{ij} lies on the bounding surface (i.e., if $\sigma'_{ij} = \bar{\sigma}'_{ij}$) [2].

Dafalias [4] introduced a very simple "radial mapping" form of the model that does not require an explicit definition of a yield surface.

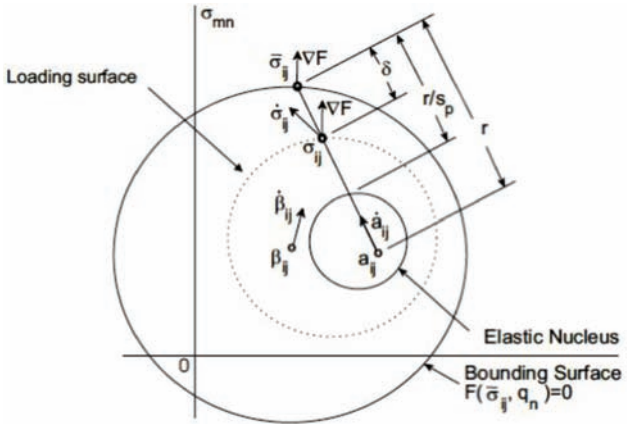

Figure 1. Schematic illustration of the bounding surface, a loading surface and radial mapping rule in multiaxial stress space.

In the radial mapping form of the model, shown schematically in Figure 1, it is assumed that the projection center a_{ij} lies always within the bounding surface and never crosses it. The a_{ij} evolves according to a proper rate equation, and is one of the q_n. It does not, however, enter into equation (1). Using a_{ij} as the projection center, the "image" stress is obtained by the radial projection of the actual stress (σ'_{ij}) onto the surface according to the following mapping rule:

$$\bar{\sigma}'_{ij} = b\left(\sigma'_{ij} - a_{ij}\right) + a_{ij} \tag{2}$$

which becomes the identity mapping if σ'_{ij} is on the surface (Figure 1). The dimensionless positive parameter b ($1 \leq b \leq \infty$) is determined in terms of the material state by substituting the "image" stress from equation (2) into an explicit form of equation (1), and solving the resulting expression for b.

The essence of the bounding surface concept is the hypothesis that inelastic deformations can occur for stress states either within or on a properly defined bounding surface. The extent of these deformations depends on the Euclidean distance δ between σ'_{ij} and an associated "image" stress that is defined using equation (2). Thus, unlike classical yield surface elastoplasticity, inelastic states are not restricted only to those lying on an outer loading or bounding surface [2].

To complete the formulation, a general state-dependent relation between the plastic modulus K_p (associated with the actual stress point) and the "bounding" plastic modulus $\bar{K}_p$ associated "image" stress points must be established as a function of the properly chosen distances δ and r shown in Figure 1 according to

$$K_p = \bar{K}_p + \hat{H}\left(\sigma'_{ij}, q_n\right) \frac{\delta}{\langle r - s_p\delta \rangle} \qquad (3)$$

where r can be related to b through the relation

$$r/\delta = b/(b - 1).$$

The "bounding" plastic modulus is obtained from the consistency condition; i.e., $\dot{F} = 0$. In equation (3), s_p (≥ 1.0) is a model parameter that defines the extent of the elastic nucleus (a region of purely elastic response), such that ($r - s_p\delta$) ≥ 0 (Figure 1), and the dimensionless parameter $b \geq 1.0$ is as previously defined. The quantity $\hat{H}$ denotes a proper scalar shape hardening function of the state that is independent of the explicit form of equation (1). The exact definition of $\hat{H}$ requires the identification and experimental determination of certain material parameters [5]. Finally, the symbols < > denote Macaulay brackets, which imply that, for some quantity d,

$$< d > = d \text{ if } d > 0 \text{ and } < d > = 0 \text{ if } d \leq 0.$$

Equation (3), which is by no means unique, embodies the meaning of the bounding surface concept. If $\delta < r$ and $\hat{H}$ is not approaching infinity, the concept allows for plastic deformations to occur for points either within or on the surface at a progressive pace that depends upon δ. The closer to the bounding surface is the actual stress point (σ'_{ij}), the smaller is K_p (it approaches the corresponding "bounding" plastic modulus), and the greater is the plastic strain increment for a given stress increment. Thus, $\hat{H}$ and its associated parameters are intimately related to the material response for states within the bounding surface (i.e., for $\delta > 0$). As such, they constitute important elements of the present formulation that differentiate it from ones based on classical yield surface elastoplasticity.

3. OVERVIEW OF THE GBSM

In its most general form, the GBSM for saturated cohesive soils is a fully three-dimensional, temperature and time-dependent model that accounts for both inherent and stress induced anisotropy. To better simulate the behavior of cohesive soils exhibiting softening, the model employs a non-associative flow rule. The microfabric-inspired rotational hardening rule associated with the model was developed after a thorough review of past modeling practice. In addition, the shape hardening function used in the GBSM was developed simplifying earlier versions without compromising the model's predictive capabilities. In both cases, the selected functional form simplified earlier versions without compromising the GBSM's predictive capabilities.

3.1. Definition of Invariants.

The GBSM accounts for both inherent and stress-induced anisotropy. The mathematical representation of the latter requires the use of rotational hardening [6]. Due to the fact that the GBSM employs either an associative or non-associative flow rule, the rotation of both the plastic potential surface (PPS) and the bounding surface (BS) must be quantified. The material state is thus determined by the state of effective stress and by a suitable measure of anisotropy [7]. The rotation of both surfaces is described by the symmetric second-order anisotropic tensors α_{ij} and β_{ij}, respectively [1].

In the GBSM, *reduced* invariants of the effective stress tensor are used, thus ensuring the proper analytical treatment of anisotropic forms of the model [8]. Decomposing σ'_{ij} into

the sum of the deviatoric stress tensor s_{ij} and the hydrostatic stress gives

$$s_{ij} = \sigma'_{ij} - \frac{1}{3}\delta_{ij}\sigma'_{kk} \tag{4}$$

where δ_{ij} is the Kronecker delta. The *reduced* deviatoric stress tensors associated with the PPS and BS are thus

$$s^{\alpha}_{ij} = s_{ij} - \frac{1}{3}\alpha_{ij}\sigma'_{kk}\ ;\ s^{\beta}_{ij} = s_{ij} - \frac{1}{3}\beta_{ij}\sigma'_{kk} \tag{5}$$

respectively. The PPS is thus analytically described by the following invariants:

$$I = \sigma'_{ij}\delta_{ij}\ ; \quad J^{\alpha} = \sqrt{\frac{1}{2}s^{\alpha}_{ij}s^{\alpha}_{ij}} \tag{6}$$

and

$$\theta^{\alpha} = \frac{1}{3}\sin^{-1}\left[\frac{\sqrt{3}}{2}\left(\frac{s^{\alpha}_{ij}s^{\alpha}_{jk}s^{\alpha}_{ki}}{(J^{\alpha})^3}\right)\right] \tag{7}$$

where I is the first invariant of the effective stress tensor, J^{α} is the square root of the second invariant of s^{α}_{ij}, and θ^{α} is the *reduced* Lode angle

$$(-\pi/6 \le \theta^{\alpha} \le \pi/6).$$

In a similar manner, the BS is analytically described by the following invariants:

$$I = \sigma'_{ij}\delta_{ij}\ ; \quad J^{\beta} = \sqrt{\frac{1}{2}s^{\beta}_{ij}s^{\beta}_{ij}} \tag{8}$$

$$\theta^{\beta} = \frac{1}{3}\sin^{-1}\left[\frac{\sqrt{3}}{2}\left(\frac{s^{\beta}_{ij}s^{\beta}_{jk}s^{\beta}_{ki}}{(J^{\beta})^3}\right)\right] \tag{9}$$

where I is as defined in equation (6), J^{β} is the square root of the second invariant of s^{β}_{ij}, and θ^{β} is the reduced Lode angle. For θ^{α} and θ^{β}, the values of $\pm\pi/6$ correspond to conditions of axisymmetric triaxial compression and extension, respectively.

In isotropic forms of the GBSM, both the PPS and BS are analytically defined by I, as given in equation (6) and (8), and by the following *isotropic* invariants:

$$J = \sqrt{\frac{1}{2}s_{ij}s_{ij}}\ ;\ \theta = \frac{1}{3}\sin^{-1}\left[\frac{\sqrt{3}}{2}\frac{s_{ij}s_{jk}s_{ki}}{(J)^3}\right] \tag{10}$$

where s_{ij} is as defined by equation (4), and $\pi/6 \le \theta \le \pi/6$.

In axisymmetric triaxial (p'-q) stress space, where $p' = I/3$ is the mean normal effective stress and $q = \pm\sqrt{3}\,J$ is the deviator stress, the measures of the anisotropic tensors α_{ij} and β_{ij} are defined by the scalar measures α and β, respectively, where

$$\alpha = \sqrt{\frac{3}{2}\,\alpha_{ij}\,\alpha_{ij}}\ ; \quad \beta = \sqrt{\frac{3}{2}\,\beta_{ij}\,\beta_{ij}} \tag{11}$$

These quantities characterize the rotation of the PPS and the BS, respectively.

The radial mapping rule given by equation (2) is next specialized by explicitly defining a_{ij}, as well as its evolution. For monotonic loading, a_{ij} must be an isotropic tensor with a principal value on the I-axis in invariant stress space. The radial mapping rule then becomes [1]

$$\bar{I} = b\,(I - CI_o) + CI_o\ ;\ \bar{J}^{\beta} = bJ^{\beta}\ ;\ \bar{\theta}^{\beta} = \theta^{\beta} \tag{12}$$

where b is as previously defined, C ($0 \le C < 1$) is the dimensionless projection center parameter, and I_o represents the point of intersection of the BS with the positive I-axis in invariant stress space (Figure 3). The inclusion of C into the formulation introduces the possibility of using a projection center $I_{PC} = CI_o$ different form the origin in stress space [9], thus allowing for the prediction of immediate negative (dilational) pore pressure development for heavily overconsolidated samples sheared under undrained conditions. With the projection

center at the origin (i.e., for C = 0), the older and generally more restrictive and inaccurate formulation is retrieved [10,11], with initially positive pore pressures always being predicted, even for highly overconsolidated samples.

3.2. The Plastic Potential and Bounding Surfaces.

In its most general form, the GBSM employs a non-associative flow rule. It thus requires that a PPS be defined in addition to the BS. Both surfaces must be smooth and convex [2,3]. The most general form of the PPS associated with the GBSM is given by

$$Q\left(\bar{I},\bar{J}^{\alpha},\theta^{\alpha},I_{\alpha},\alpha\right)=\left(\bar{J}^{\alpha}\right)^{2}(R-1)^{2}+\frac{\omega^{2}}{27}\left(\bar{I}+\frac{R-2}{R}I_{\alpha}\right)\left(\bar{I}-I_{\alpha}\right)=0 \quad (13)$$

where barred quantities are values of I and J^{α} associated with the "image" point on the PPS. The quantity I_{α} is the value of I at

where $$\bar{J}^{\alpha}=\tilde{\alpha}\bar{I},\qquad \tilde{\alpha}=\alpha/(3\sqrt{3}).$$

The value of I_{α} is adjusted so that equation (13) is satisfied for the current "image" stress point $\left(\bar{I},\bar{J}^{\beta}\right)$ on the PPS. Kaliakin and Nieto-Leal [13] give explicit expressions for I_{α} associated with the various forms of the GBSM. The dimensionless model parameter R ($\geq$ 2.0) controls the shape of the PPS [13]. Finally, ω is given by the following generalized expression:

$$\omega^{2}=\frac{M-\alpha}{2}\left[2\alpha(R-1)^{2}+M-\alpha+\sqrt{4\alpha(R-1)^{2}M+(M-\alpha)}\right] \quad (14)$$

where the dimensionless anisotropic variable α is as previous defined in equation (11).

The quantity M is the slope of the failure surface which, in a meridional section (i.e., for a specific value of θ^{α} in p' - q space, is assumed to be a straight line that coincides with the critical state line [14]. The counterpart of M in I - J^{α} space is

$$\tilde{M}=M/(3\sqrt{3}).$$

Both M and $\tilde{M}$ vary with θ^{α} according to

$$M\left(\theta^{\alpha},k_{M}\right)=g\left(\theta^{\alpha},k_{M}\right)M_{c}$$

and

$$\tilde{M}\left(\theta^{\alpha},k_{M}\right)=g\left(\theta^{\alpha},k_{M}\right)\tilde{M}_{c},$$

where the quantity

$$k_{M}=M_{e}/M_{c}=\tilde{M}_{e}/\tilde{M}_{c},$$

with

$$M_{e}=M(-\pi/6)\text{ and }M_{c}=M(\pi/6)$$

being the values of M associated with axisymmetric triaxial extension and compression, respectively. The dimensionless function $g = g(\theta^{\alpha}, k_{M})$ is given by [15]

$$g\left(\theta^{\alpha},k_{M}\right)=\left[\frac{2k_{M}^{4}}{1+k_{M}^{4}-(1-k_{M}^{4})\sin 3\theta^{\alpha}}\right]^{\frac{1}{4}} \quad (15)$$

which has been shown to be more robust than earlier functional forms of g [1]. Figure 2 shows the variation of the PPS and failure surface with Lode angle within the octahedral plane for *anisotropic* forms of the GBSM.

The PPS given by equation (13) must satisfy two fundamental requirements. For a given value of Lode angle (θ^{α}), it must pass through the "image" stress point $\left(\bar{I},\bar{J}^{\beta}\right)$. In addition, it must give

$$\partial Q/\partial\bar{I}=0$$

at its intersection with the critical state (failure) line, as defined by ω; the latter requirement is in keeping with the concept of a critical state [14].

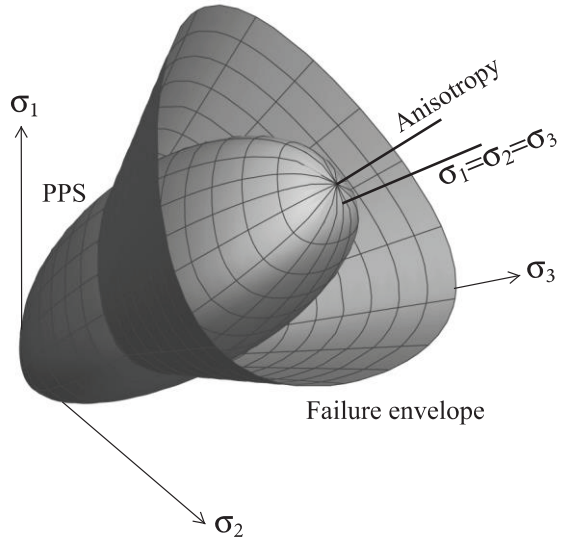

Figure 2. Plastic potential surface (PPS) and failure envelope for anisotropic form of the GBSM employing a non-associative flow rule.

Turning the attention to the definition of the BS, the results of an extensive study into suitable analytical expressions for bounding surfaces [3] showed that an elliptical form avoids potential difficulties associated with either previously used composite forms [9] or higher-order expressions. In light of this finding, the following elliptical BS is used in the GBSM model:

$$F\left(\bar{I},\bar{J}^{\beta},\theta^{\beta},I_o,\beta\right)=\left(\bar{J}^{\beta}\right)^2(R-1)^2 + \frac{N^2-\beta^2}{27}\left(\bar{I}+\frac{R-2}{R}I_o\right)\left(\bar{I}-I_o\right)=0 \tag{16}$$

where R is as previously defined, and barred quantities are values of I and J^{β} associated with the "image" point on the BS. The quantity I_o is as previously defined (Figure 3).
The parameter N defines the shape of the BS; its counterpart in stress invariant space is

$$\tilde{N}=N/(3\sqrt{3}).$$

Both N and $\tilde{N}$ vary with θ^{β} according to

$$N\left(\theta^{\alpha},k_N\right)=g\left(\theta^{\alpha},k_N\right)N_c$$

and

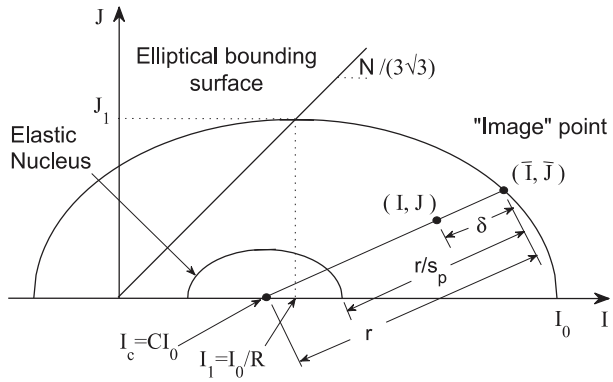

Figure 3. Schematic illustration of elliptical bounding surface and radial mapping rule in meridional section in stress invariant space for isotropic forms of the GBSM.

$$\tilde{N}\left(\theta^{\alpha},k_N\right)=g\left(\theta^{\alpha},k_N\right)\tilde{N}_c,$$

where the quantity

$$k_N=N_e/N_c=\tilde{N}_e/\tilde{N}_c,$$

with $N_e = N(-\pi/6)$ and $N_c = N(\pi/6)$ being the values of N associated with axisymmetric triaxial extension and compression, respectively. The dimensionless function g is given by equation (15), with θ^{β} and k_N replacing θ^{α} and k_M, respectively. Due to the fact that the GBSM is intended to be adaptive, specialization of equation (16) results in specific expressions appropriate for an associative flow rule and for the isotropic forms of the model [13].

3.3. Strain Decomposition.

The infinitesimal strain rate tensor is additively decomposed as

$$\dot{\varepsilon}_{ij}=\dot{\varepsilon}^e_{ij}+\dot{\varepsilon}^i_{ij}=\dot{\varepsilon}^e_{ij}+\dot{\varepsilon}^v_{ij}+\dot{\varepsilon}^p_{ij} \tag{17}$$

where the superscripts *e*, *i*, *v* and *p* denote its elastic, inelastic, viscoplastic (delayed) and plastic (instantaneous) components, respectively, and a superposed dot denotes a material time derivative or rate.
The internal variables (q_n) include proper measures of inelastic deformation that quantify the hardening of the bounding surface. An additive decomposition of $\dot{q}_n$ into a delayed or

viscoplastic part ($\dot{q}_n^v$) and an instantaneous or plastic part ($\dot{q}_n^p$) is assumed [16]; viz.,

$$\dot{q}_n = \dot{q}_n^v + \dot{q}_n^p \tag{18}$$

Both parts are, in general, incrementally irreversible. The $\dot{q}_n^v$, which accounts for the delayed deformation of the cohesive soil, depends only upon the state; it can, under certain conditions, be zero. The $\dot{q}_n^p$, on the other hand, depends upon the state and the rates $\dot{\sigma}'_{ij}$ and $\dot{q}_n^v$; it is non-zero only if the scalar loading (L) index is positive. This is done in order to emphasize the general *coupling* that exists between plastic and viscoplastic processes, whereby in addition to the $\dot{\sigma}'_{ij}$, the $\dot{q}_n^v$ may affect the plastic loading process [17].

Since it does not enter into equation (1), the projection center tensor a_{ij} (Figure 1) is one of the internal variables. It evolves according to the rate equation

$$\dot{a}_{ij} = \dot{a}_{ij}^v + \dot{a}_{ij}^p \tag{19}$$

where a_{ij}^v and a_{ij}^p being the viscoplastic (delayed) and plastic (instantaneous) parts of a_{ij}.

The elastic response is assumed to be independent of the rate of loading and to be unaltered by inelastic deformation. The elastic constitutive relations, in direct and inverse form, are

$$\dot{\varepsilon}_{ij}^e = B_{ijkl}\,\dot{\sigma}'_{kl} \quad \text{or} \quad \dot{\sigma}'_{ij} = D_{ijkl}\,\dot{\varepsilon}_{kl}^e \tag{20}$$

where B_{ijkl} and D_{ijkl} are the fourth-order tensors of elastic compliance and moduli, respectively. To date, bounding surface models for cohesive soils have exclusively assumed elastic isotropy. The explicit forms for B_{ijkl} and D_{ijkl} are thus typically written in terms of a non-linear elastic bulk modulus (K) and the shear modulus (G), with the latter often computed from K and a specified value of Poisson's ratio (ν).

The viscoplastic response is based upon a generalization of Perzyna's elastic/viscoplastic theory [18]. The associated rate equations are

$$\dot{\varepsilon}_{ij}^v = \langle\Phi\rangle\, R_{ij}\ ;\ \dot{q}_n^v = \langle\Phi\rangle\, r_n\ ;\ \dot{a}_{ij}^v = \langle\Phi\rangle\, r_{ij} \tag{21}$$

where R_{ij}, r_n and r_{ij} are proper tensorial functions of the state. The symbols < > again denote Macaulay brackets. In forms of the GBSM employing a non-associative flow rule, R_{ij} is the gradient of the PPS; i.e.,

$$R_{ij} = \partial Q / \partial \bar{\sigma}'_{ij}.$$

If an associative flow rule is assumed, then

$$F = Q.$$

In equation (21), Φ is a continuous scalar "overstress" function. Although several explicit functional forms for Φ(F) have been proposed [13}, perhaps the most commonly used form is the following "power" form:

$$\Phi = \frac{1}{V}\,(\Delta\hat{\sigma})^n = \frac{1}{V}\left[\frac{\hat{\delta}}{r\left(1-\frac{1}{s_v}\right)}\right]^n \tag{22}$$

where n and V are positive model parameters, and $\Delta\hat{\sigma}$ is a "normalized overstress" [16]. In equation (22) r is as defined in Figure 1, s_v (> 1) is a dimensionless model parameter, and $\hat{\delta}$ is the Euclidean distance between σ'_{ij} and a second "image" stress $\hat{\sigma}_{ij}$ on the boundary of a second elastic nucleus that is associated with the viscoplastic response and is homologous with the bounding surface. This elastic nucleus assumes the role of the "static" yield surface proposed by Perzyna [18]. Since the material is assumed to be inviscid in the elastic region, $\dot{\varepsilon}_{ij}^v$ becomes zero when $\Delta\hat{\sigma} \leq 0$; i.e., when σ'_{ij} is either on or within the second elastic nucleus.

The definition of the plastic response is predicated on *four* expressions associated with the bounding surface concept. First, the BS defines the direction of inelastic loading-unloading (L_{ij}). In particular, the expression for

L_{ij} at the actual stress point (σ'_{ij}) is defined as the gradient of F at the "image" point (Figure 1); viz.,

$$L_{ij} \equiv \nabla F = \partial F / \partial \bar{\sigma}'_{ij}.$$

Secondly, a scalar loading index (L) must be defined in terms of L_{ij}, the rate of the effective stress tensor, and the plastic moduli K_p; viz. [17],

$$L = \frac{1}{K_p}\left[L_{ij}\,\dot{\sigma}'_{ij} + \langle \Phi \rangle \frac{1}{b}\frac{\partial F}{\partial q_n} r_n - \langle \Phi \rangle \left(1 - \frac{1}{b}\right)\frac{\partial F}{\partial \bar{\sigma}'_{ij}} r_{ij} \right] \quad (23)$$

where L_{ij} and the dimensionless parameter b are as previously defined, and K_p is given by equation (3), which constitutes the third of the aforementioned expressions associated with the bounding surface concept. The presence of r_n and r_{ij} in equation (23) shows that L couples the plastic-viscoplastic hardening response for states on and within the bounding surface. Additional details pertaining to the terms appearing in this equation are given elsewhere [13,16].

When the stress point lies on the bounding surface, $\delta = 0$ (Figure 1),

$$K_p = \bar{K}_p, \; \dot{\sigma}'_{ij} = \dot{\bar{\sigma}}'_{ij}$$

and equation (23) simplifies accordingly. As noted in conjunction with equation (3), an explicit expression for $\bar{K}_p$, which is the fourth expression associated with the bounding surface concept, is determined from the consistency condition $\dot{F} = 0$. Additional details pertaining to the determination of $\bar{K}_p$ are given elsewhere [13].

The rate equations for plastic response are given by

$$\dot{\varepsilon}^p_{ij} = \langle L \rangle R_{ij} \; ; \; \dot{q}^p_n = \langle L \rangle r_n \; ; \; \dot{a}^p_{ij} = \langle L \rangle r_{ij} \quad (24)$$

where R_{ij}, r_n, and r_{ij} are as previously defined.

3.4. Hardening Rules.

In all forms of the GBSM, the BS hardens isotropically along the I-axis. The proper simulation of stress-induced anisotropy for anisotropic forms of the GBSM also requires that the BS and PPS undergo rotational hardening (RH) [7].

The isotropic hardening is controlled by a single scalar internal variable that measures the increment in inelastic volumetric strain; viz.,

$$\dot{\varepsilon}^i_{kk} = \dot{\varepsilon}^v_{kk} + \dot{\varepsilon}^p_{kk} = \left(\langle \Phi \rangle + \langle L \rangle\right) R_{kk} \quad (25)$$

where $R_{kk} = \partial Q / \partial \bar{I}$.

It is convenient to relate the evolution of the BS to the increment in inelastic volumetric strain through the value of I_o (recall Figure 3). The resulting analytical expression describing the isotropic hardening is [9,13]

$$\dot{I}_o = \frac{1 + e_{in}}{\lambda - \kappa}\left(\langle I_o - I_L \rangle + I_L\right)\dot{\varepsilon}^i_{kk} \quad (26)$$

where the critical state parameters λ and κ are equal to the negative of the slopes of the virgin consolidation and swell/recompression lines, respectively, in a plot of void ratio (e) versus the natural logarithm of I [14], and e_{in} represents the initial total void ratio corresponding to the reference configuration with respect to which engineering strains are measured; for natural strains, it represents the current total void ratio. The nonzero limiting "transitional" stress I_L is included in equation (26) so that for $I < I_L$ the relation between I and the elastic part of the void ratio (e^e) changes continuously from logarithmic to linear [9]. The singularity of the elastic stiffness near $I = 0$, resulting from excessive material softening, is thus removed. The quantity I_L is *not* a model parameter; its value is typically taken equal to one-third of the atmospheric pressure (P_a) [1].

The evolution of the stress-induced anisotropy during shearing is mathematically accounted for by RH of the BS (through the anisotropic tensor b_{ij}) and, if applicable, the PPS (through the anisotropic tensor a_{ij}). Recently [19], robust RH

rules for the BS and PPS, that were inspired by earlier formulations and by experimental observations of microfabric evolution of cohesive soils, were proposed. Nieto-Leal et al. [19] give additional details pertaining to these RH rules.

3.5. The Shape Hardening Function.

The positive hardening function $\hat{H}$ defines the shape of the response curves during inelastic hardening (or softening) for points *within* the BS [2]. It relates the plastic modulus K_p to its "bounding" value in the manner given by equation (3). For the GBSM,

$$\hat{H} = \frac{(1+e_{in})}{\lambda-\kappa} P_a \left[9\left(F_{,\bar{I}}\right)^2 + \frac{1}{3}\left(F_{,\bar{J}^\beta}\right)^2\right] \left[h\left(\theta^\beta\right) z^{0.02} + h_o\left(1-z^{0.02}\right)\right] f_n \qquad (27)$$

where e_{in}, λ, κ, and P_a are as previously defined. For brevity, the partial derivative with respect to an invariant is denoted with a comma followed by the symbol of the invariant as a subscript. The definition of the dimensionless variable z varies depending on the form of the GBSM used. For, example, for the *anisotropic* form of the GBSM employing a *non-associative* flow rule, z is given by

$$z = J^\beta / J_1^\beta = J^\beta / (\tilde{N} I_1) = 3\sqrt{3}\, J^\beta R / N I_o$$

(see Figure 3).

The dimensionless quantity $h\left(\theta^\beta\right)$ in equation (27) has the general form $h\left(\theta^\beta\right) = g\left(\theta^\beta, k_h\right) h_c$, where $k_h = h_e/h_c$, with $h_e = h(-\pi/6)$ and $h_c = h(\pi/6)$ being the values of h associated with axisymmetric triaxial extension and compression, respectively. The dimensionless function g is given by equation (15), with θ^β and k_h replacing θ^α and k_M, respectively.

Finally, the expression for f_n appearing in equation (27) is a generalization of the form given by Nieto-Leal and Kaliakin [5]; viz.,

$$f_n = \frac{1}{2}\left[a + \text{sign}\left(n_I\right)\left(|n_I|\right)^{\frac{1}{5}}\right]\left(\frac{I}{I_o}\right) \qquad (28)$$

where a (> 1.0) is a dimensionless model parameter [13], and n_I is the component, in the $\bar{I}$ direction, of the unit outward normal to the bounding surface in stress invariant space. For the *anisotropic* form of the GBSM with a *non-associative* flow rule,

$$n_I = \frac{F_{,\bar{I}}}{\sqrt{\left(F_{,\bar{I}}\right)^2 + \left(F_{,\bar{J}^\beta}\right)^2}} \qquad (29)$$

If an associative flow rule is used instead, $F_{,\bar{J}^\beta}$ is replaced by $F_{,\bar{J}^\alpha}$ in equations (27) and (29) and in the definition for z. Finally, if an isotropic form of the GBSM is used, $F_{,\bar{J}^\beta}$ is replaced by $F_{,\bar{J}}$ in the aforementioned equations.

4. THE INITIAL MATERIAL STATE

The definition of the initial state for all forms of the GBSM requires knowledge of the initial value (e_{in}) of the void ratio, which is one of the internal variables. In addition, the initial stress state is defined in terms of values of the total confining stresses, the total stresses associated with the maximum past preconsolidation pressure, and the initial excess pore fluid pressure.

Anisotropic forms of the GBSM require the specification of the inherent anisotropy. This is achieved by specifying the initial values of the anisotropic tensor, which is another type of internal variable. These values are commonly determined from the results of laboratory tests on anisotropically consolidated specimens. For the special case of a transversely anisotropic (or "cross-anisotropic") soil in which the x_1 direction is taken normal to the plane of isotropy, $\sigma_2' = \sigma_3'$. For this case, the stress ratio (η = q/p') in axisymmetric triaxial space is given by

$$\eta_{K_c} = 3\left(1-K_c\right)/\left(1+2K_c\right),$$

where

$$K_c = \sigma_3'/\sigma_1'$$

is the effective stress ratio. Recalling the definition of the scalar representation (α) of α_{ij}

in axismmetric triaxial space given by equation (11), it is relatively well established [20] that the value of α determined using an anisotropic constitutive model will be *less* than η. Thus,

$$\eta = \alpha/\mathrm{A}, \text{ where } A \leq 1.0.$$

For transversely anisotropic soils, the inherent (initial) values of α_{ij} are thus given by

$$\alpha_{11}^{in} = \frac{2A(1-K_{in})}{1+2K_{in}} \; ; \; \alpha_{22}^{in} = \alpha_{33}^{in} = -\frac{1}{2}\alpha_{11}^{in} \tag{30}$$

with

$$\alpha_{12}^{in} = \alpha_{21}^{in} = \alpha_{13}^{in} = \alpha_{31}^{in} = \alpha_{23}^{in} = \alpha_{32}^{in} = 0.$$

Here K_{in} denotes the constant initial effective stress ratio to which a soil has been subjected in a drained axisymmetric triaxial (isotropic) or oedometer (anisotropic) test.

In the anisotropic form of the GBSM employing a non-associative flow rule, α_{ij} represents the rotation of the PPS. The rotation of the BS is quantified through the symmetric anisotropic tensor β_{ij}. The measure of this tensor in axisymmetric triaxial stress space is defined by the scalar β, given by equation (11). Since the value of β associated with loading at a prescribed stress ratio η is purported to be equal to this ratio [20], the initial values of β_{ij}, corresponding to a transversely anisotropic stress, will be

$$\beta_{11}^{in} = \frac{2(1-K_{in})}{1+2K_{in}} \; ; \; \beta_{22}^{in} = \beta_{33}^{in} = -\frac{1}{2}\beta_{11}^{in} \tag{31}$$

with $\beta_{12}^{in} = \beta_{21}^{in} = \beta_{13}^{in} = \beta_{31}^{in} = \beta_{23}^{in} = \beta_{32}^{in} = 0$.

where K_{in} is as previously defined. The initial values of α_{ij} is again given by equation (30).

5. THE MODEL PARAMETERS

Since the GBSM includes both isotropic and anisotropic formulations, together with both associative and non-associative flow rules, the number of parameter values to be determined depends on the specific form of the model that is being used. To facilitate the subsequent discussion, the anisotropic forms of the GBSM employing non-associative and associative flow rules are referred to as GBSMan and GBSMaa, respectively; the isotropic forms of the model employing non-associative and associative flow rules are referred to as GBSMin and GBSMia, respectively.

The model parameters associated with all forms of the GBSM are grouped by their type as follows: The critical state parameters λ, κ, M_c and M_e; the elastic parameters G or ν; the surface configuration parameters R, N_c, and N_e, the projection center parameter C; the elastic nucleus parameter s_p; the shape hardening parameters h_c, h_e, and a; the rotational hardening parameters χ_η, ψ_1, and ψ_2, and the viscoplastic parameters s_v, V, and n. All of the above parameters are *positive*; with the exception of G and V, all parameters are dimensionless. Table 1 summarizes the model parameters associated with the *most general* forms of each of the forms of the GBSM.

With the exception of the viscoplastic parameters s_v, V, and n, values for all other (elastoplastic) parameters are determined from results of standard laboratory tests of short enough duration to ensure that time and rate effects are negligible. With some exceptions, the elastoplastic model parameters are identical to those used in conjunction with previous rate independent bounding surface formulations.

Most of the model parameter values are determined by curve-fitting; the availability of high-quality experimental data is thus requisite for obtaining accurate parameter calibrations. Although it would perhaps be desirable to determine the model parameter values from closed-form formulas, such expressions are rally available. Even when such expressions exist, the results they give are not always reliable. Thus, although curve fitting may be viewed as being somewhat simple-minded, with the proper guidelines it gives a safe and intuitive way in

which to determine values for the model parameters. The values typically selected for the model parameters either are fixed for most soils, or fall within fairly narrow ranges. Furthermore, the values of some of these parameters can be determined from standard soil test parameters.

Table 1. Parameters Associated with the GBSM.

GBSMan	GBSMaa	GBSMin	GBSMia
λ	λ	λ	λ
κ	κ	κ	κ
M_c	M_c	M_c	M_c
M_e	M_e	M_e	M_e
G or ν	G or ν	G or ν	G or ν
R	R	R	R
N_c	-	N_c	-
N_e	-	N_e	-
C	C	C	C
s_p	s_p	s_p	s_p
h_c	h_c	h_c	h_c
h_e	h_e	h_e	h_e
a	a	a	a
χ_η	χ_η	χ_η	χ_η
ψ_1	ψ_1	-	-
ψ_2	ψ_2	-	-
s_v	s_v	s_v	s_v
V	V	V	V
n	n	n	n

To establish the values of the necessary parameters associated with the *most general* form of the GBSM, a minimum of *eight* laboratory tests are required, namely: (a) A single isotropic or anisotropic (one-dimensional) consolidation or drained compression test with both loading and unloading phases, (b) Consolidated-undrained (preferable) or drained axisymmetric triaxial compression and extension tests (with pore pressure measurements) on anisotropically or isotropically consolidated specimens in the normally, lightly, and heavily overconsolidated regions (a total of six tests), and (c) At least one long term test such as undrained or drained triaxial creep or stress relaxation.

If a less general form of the bounding surface model is acceptable, both the number of model parameters involved and the number of laboratory tests required can be significantly reduced. For example, if only time independent analyses are to be considered, values of the three viscoplastic model parameters, as well as the long-term experiment(s) used in their determination, are no longer required. Furthermore, if the model is only to be used for the time-independent analysis of isotropically consolidated normally consolidated soils loaded in triaxial compression or extension, the number of required model parameters reduces to five, and only data from a consolidation test and a single triaxial test are required for the model calibration. Similar reductions in the number of required model parameters can be realized for overconsolidated soils by neglecting the difference between hardening parameters in compression and extension.

6. ASSESSMENT OF PERFORMANCE

To assess the simulative and predictive capabilities of the GBSM and to illustrate its flexibility, four soils were simulated using the model. All of the simulations and predictions shown in this section were generated using the CALBR8 computer program [21].

The simulative capabilities of the *simplest* (GBSMia) form of the GBSM, as applied to isotropically consolidated undrained compression (CIUC) test experimental results for normally consolidated Bangkok clay, were recently assessed [1]. Even though only five model parameters λ, κ, M_c, ν, and R) are active in such applications, the agreement between GBSMia simulations and experimental results was excellent.

6.1 Simulation of Taipei Silty Clay.

In light of the aforementioned simulation effort, the ability of the GBSM to simulate the more complex anisotropic, softening response is thus first assessed herein. Since the proper

simulation of softening requires the use of a non-associative flow rule [20], the present simulations require the use of the most complex form of the model; i.e., the anisotropic non-associative version (GBSMan).

The soil considered is Taipei silty clay (TSC). The data set used in the present assessment of the GBSMan form of the model was generated by Chin and Liu [22], who performed a set of axisymmetric triaxial CK_0UC and CK_0UE tests on samples with OCRs of 1.0, 2.0, and 4.0. The TSC tested had a liquid limit (w_L) of 40% and a plasticity index (I_p) of 22%.

The following values for the critical state parameters were obtained directly from the data of Chin and Liu [22]: λ = 0.17, κ = 0.02, M_c = 1.05, and M_e = 0.95. The Poisson's ratio equal to 0.29 was assumed. A value of R = 2.50 was determined by matching the experimental undrained stress paths for the normally consolidated samples. A value of 0.65 for the projection center parameter (C) was determined from a best fit of the undrained stress paths for OCRs of 2.0 and 4.0. Values for the shape hardening parameters h_c = 5.0, h_e = 25.0, and a = 1.5 were determined from a best fit of the deviator stress versus axial strain response for these same OCR values. A value of 1.0 for the elastic nucleus parameter s_p, which reduces the nucleus to a point, was found to be adequate. Values of the configuration parameters N_c and N_e equal to 0.90 and 1.13, respectively, were determined by matching the response in compression and extension for the normally consolidated sample. Finally, the rotational hardening parameters were assigned values of χ_η = 1.5, ψ_1 = 200.0 and ψ_2 = 50.0.

The time-independent model simulations were obtained using the aforementioned parameter values. Figure 4 compares the simulations of anisotropically consolidated samples with experimental values. From this figure, it is evident that the agreement between the simulated and experimental normalized undrained stress paths is quite good. The normalized deviator stress versus axial strain simulations are somewhat less accurate than the undrained stress paths. Chin and Liu [22] did not report any experimental values for excess pore pressure.

6.2. Simulation of Grundite Clay.

Since the GBSM is formulated in terms of three stress invariants, its predictive capabilities under true triaxial (TT) states of stress are next investigated. In TT tests, the values of the three principal stresses can be varied independently. The relative magnitude of the intermediate principal stress (σ_2) is typically expressed by means of the following ratio between principal stress differences: $b_{TT} = (\sigma_2 - \sigma_3)/(\sigma_1 - \sigma_3)$, where it is assumed that $\sigma_1 \geq \sigma_2 \geq \sigma_3$. The ratio b_{TT} is zero (0.0) for axisymmetric triaxial compression, where $\sigma_2 = \sigma_3$; it is equal to unity (1.0) for axisymmetric triaxial extension, where $\sigma_1 = \sigma_2$. Based on the results of past TT tests [23-30], the relative magnitude of the intermediate principal stress has a significant influence on the three-dimensional stress-strain, strength, and volume change or pore pressure characteristics of cohesive soils.

Lade and Musante [25] experimentally studied the influence of the intermediate principal stress on the stress-strain, pore pressure and strength characteristics of a remolded clay under undrained conditions. In this study, consolidated-undrained axisymmetric triaxial compression tests and TT tests with independent control of all three principal stresses on cubical specimens were performed.

The soil used in all tests performed by Lade and Musante [25] was called “Grundite” clay, which is a trade name used by the Illinois Clay Products Company. Grundite is composed primarily of the clay mineral illite, and is mined in the Goose Lake area of Illinois [31]. The particle size distribution indicated that the clay consisted of about equal amounts of silt and clay size particles. The w_L and I_P of the soil were equal to 54.8% and 30.1%, respectively. Lade and Musante did not report the specific gravity of solids (G_s) for Grundite clay.

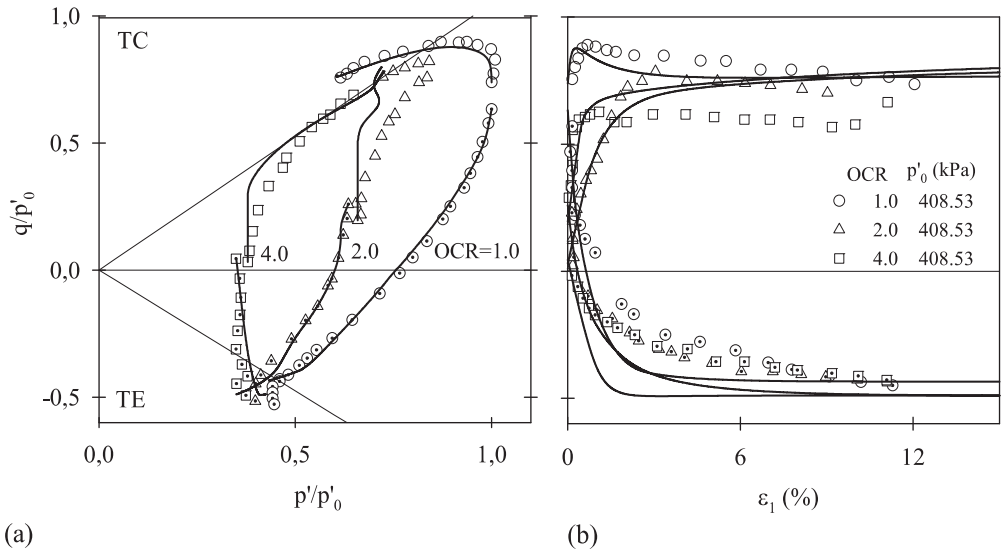

Figure 4. Comparison of simulated and experimental undrained response of anisotropically consolidated samples of TSC for data of Chin and Liu [22].

However, in their experimental study of the same soil, Perloff and Osterberg [32] and Kondner and Horner [33] reported a value of G_s equal to 2.74 (they also reported w_L and I_P values equal to 54.5% and 28.5%, respectively, which are very close to the values reported by Lade and Musante). Consequently, a value of G_s equal to 2.74 was used to compute initial values of void ratio (described below) for all numerical simulations reported herein.

All specimens of Grundite clay used in Lade and Musante's study were produced from a slurry with a water content of 90%. The uniform slurry was consolidated in a double draining consolidometer at a vertical pressure smaller than the final isotropic consolidation pressure to be used in the subsequent tests. After consolidation, specimens were thoroughly remolded to eliminate the inherent anisotropy due to the initial K_0 consolidation. Specimens with the respective shapes were next trimmed, installed in the testing apparatus, and consolidated isotropically at 98.0 kPa, 147.0 kPa, and 196.0 kPa, corresponding to water contents of 34.4, 31.9 and 30.1%, respectively. For a value of G_s equal to 2.74, the associated values of initial void ratio (e_{in}) are 0.943, 0.874 and 0.825. With the exception of triaxial compression, Lade and Musante [25] presented experimental results only for a confining stress of 147.0 kPa.

Following the above preliminary tests, three series of consolidated-undrained tests were performed in a cubical triaxial apparatus similar to that described by Lade and Duncan [34]. This apparatus was designed to permit application of three unequal principal stresses to a cubical specimen. The side dimensions of the specimen were 76 mm. Each test in the series was conducted with constant confining pressure σ_3. The horizontal and vertical deviator stresses were increased proportionally until the specimen failed. The ratio: b_{TT} between the deviator stresses was maintained constant in each test. For each consolidation pressure, the values of: b_{TT} used in the tests were chosen so that the failure surface, the stress-strain relations, and the pore pressure response could be determined over the full range of the intermediate principal stress. Lade and Musante [25] noted that the response of specimens of remolded Grundite clay was essentially isotropic. The strengths of test specimens with b_{TT} values equal to 0.95 (i.e., near triaxial extension) were approximately the same whether they failed horizontally or vertically.

Lade and Musante [25] did not show consolidation data for Grundite clay. However,

based on laboratory data [35] for two isotropic compression tests and one K_0 consolidation test performed on Grundite clay, an average value of λ equal to 0.152 was determined. Since no rebound data was available, the aforementioned work of Perloff and Osterberg [32] and Kondner and Horner [33] was consulted. Perloff and Osterberg [32] performed isotropic compression tests with loading and rebound phases on 23 specimens of Grundite clay. The average values of λ and κ associated with these tests were 0.152 and 0.076, respectively. Consequently, these values were used in the present simulations of Grundite clay.

The determination of the slope of the critical state line in triaxial compression (M_c) and extension (M_e) requires the values of the effective friction angle for both states. In the case of triaxial compression (b_{TT} = 0.0) of cubical samples, Lade and Musante [25] computed effective friction angles ϕ'_c of 30.6, 28.2 and 27.4^o for consolidation stresses of 98.0 kPa, 147.0 kPa, and 196.0 kPa, respectively. In axisymmetric triaxial tests performed on the same soil [35], ϕ'_c values equal to 29.6, 30.1 and 30.1^o were computed for tests with a consolidation stress of 98.0 kPa. In two tests with a consolidation stress of 147.0 kPa, ϕ'_c values of 29.3 and 28.7^o were computed. Finally, in two tests with a consolidation stress of 196.0 kPa, ϕ'_c values of 27.9 and 28.2^o were computed. The overall average of these values is 29.1^o. Using this friction angle gives

$$M_c = \frac{6 \sin \phi'_c}{3 - \sin \phi'_c} = 1.163 \tag{32}$$

In two true triaxial tests near extension (b_{TT} = 0.95), Lade and Musante [25] obtained effective friction angles of 30.6 and 31.2^o for a consolidation stress of 147.0 kPa. The results of additional true triaxial tests at consolidation stresses of 98.0 kPa and 196.0 kPa yielded ϕ'_e values of 35.1 and 31.0^o, respectively. The overall average of these values is 31.0^o. Using this friction angle gives

$$M_e = \frac{6 \sin \phi'_e}{3 + \sin \phi'_e} = 0.900 \tag{33}$$

The ratio M_e/M_c is thus equal to 0.774. For the similar illitic clay tested by France and Sangrey [36] this ratio was equal to 0.76.

A value of Poisson's ratio ν equal to 0.27 was assumed. This is consistent with the empirical relation presented by Lade [37] for an I_p of approximately 30%.

Since the Grundite clay specimens were purported to be normally consolidated, the bounding surface shape parameter R would normally be determined from the three undrained triaxial compression tests (i.e., for b_{TT} = 0.00) at consolidation stresses of 98.0 kPa, 147.0 kPa, and 196.0 kPa. However, a plot of the associated undrained stress paths showed that these more closely resembled ones for lightly overconsolidated specimens. While this is likely due to the fact that the soil was repeatedly remolded, it nonetheless requires that these tests be modeled as slightly overconsolidated. As such, the overconsolidation ratio was numerically estimated to be approximately 1.5. This ratio was maintained in all of the numerical simulations of Grundite clay. Since the specimens are lightly overconsolidated, the magnitude of the projection center parameter C influences the simulations. From the shape of the undrained stress paths for the three tests at b_{TT} = 0.00, it was determined that a value of C equal to 0.20 was appropriate.

A value for the shape hardening parameter associated with triaxial compression (h_c) was determined by best matching the experimental results for b_{TT} = 0.21 and 0.40. The value for the shape hardening parameter associated with triaxial compression (h_e) was determined by matching the experimental results for b_{TT} = 0.95. As in the case of many other soils, the remaining shape hardening parameter (a) was taken equal to 1.2. Finally, values of the configuration parameters N_c and N_e equal to 1.125 and 0.870, respectively, were determined

by matching the experimental results for b_{TT} = 0.00 and 0.95.

Using the aforementioned parameter values in conjunction with the GBSMin form of the GBSM, the TT tests performed by Lade and Musante [25] were simulated numerically. Following the actual experimental procedure, in each simulation the minor principal total stress (σ_3) was maintained constant. The major and intermediate total stress were increased in such a manner so as to maintain the experimental values of b_{TT} (i.e., 0.00, 0.21, 0.40, 0.70, and 0.95) constant. Figures 5 to 8 summarize the results of these time-independent simulations and compare them to the experimental results. In these figures, experimental results are depicted by discrete symbols. The simulated results are depicted by continuous curves; in the legends these results are denoted by the "(sim)".

Figure 5 compares the simulated principal effective stress difference $(\sigma_1' - \sigma_3')$ versus major principal strain (ε_1) response with experimental values. Although the experimental results for b_{TT} = 0.40 are somewhat under predicted, the overall agreement between simulated and experimental results is quite good.

Figure 6 compares the simulated excess pore pressure versus ε_1 response with experimental values. Although the ε_1 response for b_{TT} = 0.21 is under predicted, the overall agreement between simulated and experimental results is quite good.

In Figures 7 and 8 are shown the comparisons between the simulated and experimental principal strain response. From Figure 7 it is evident that the simulated ε_2 versus ε_1 response is somewhat under predicted for b_{TT} = 0.21. The agreement between the simulated and experimental response for the other values of b_{TT} is, however, much better. Similar conclusions are drawn in the case of the major (ε_1) versus minor principal strain (ε_3) response (Figure 8).

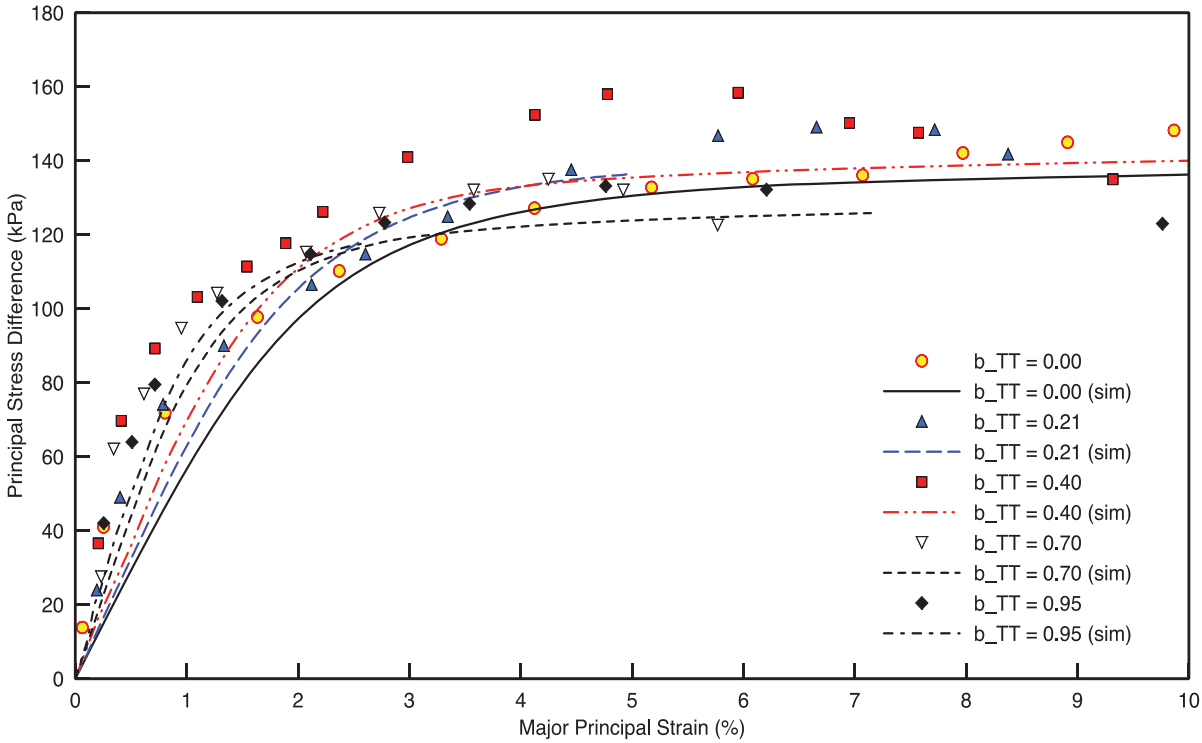

Figure 5. Comparison of simulated and experimental principal stress difference vs. major principal strain response of TT tests on samples of undrained Grundite clay [37].

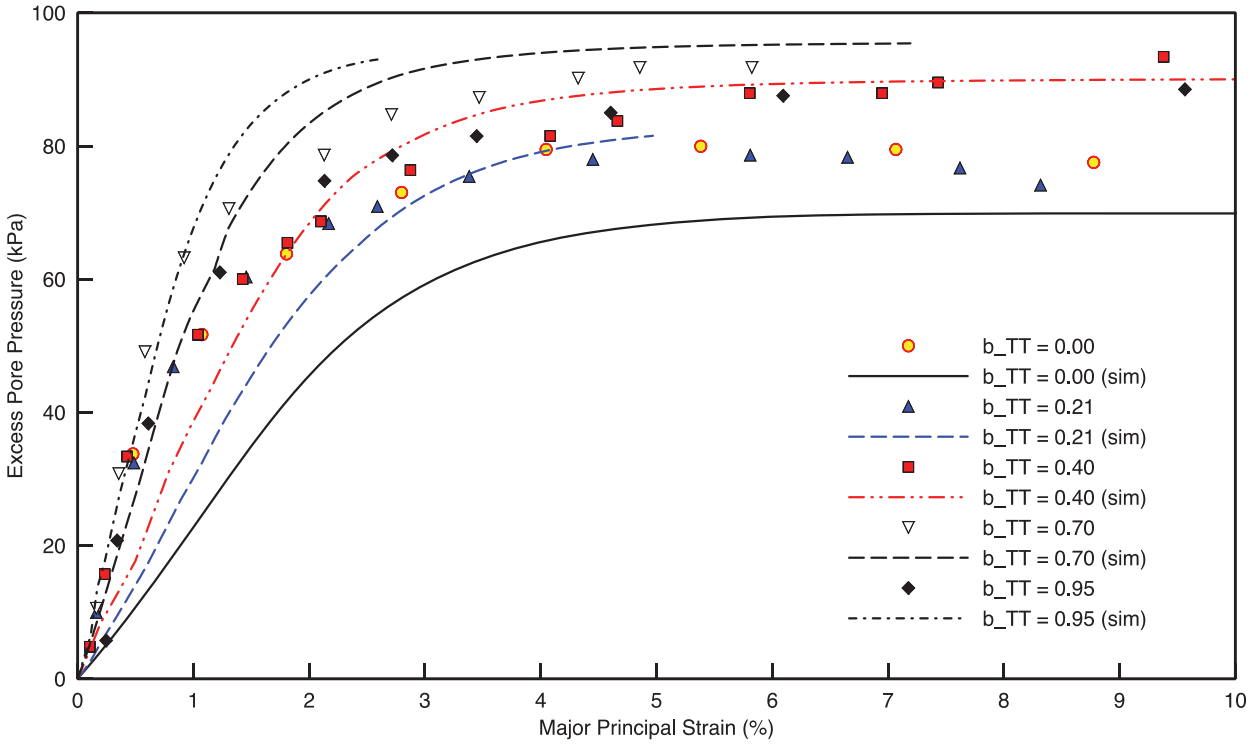

Figure 6. Comparison of simulated and experimental excess pore pressure vs. major principal strain response of TT tests on samples of undrained Grundite clay [37].

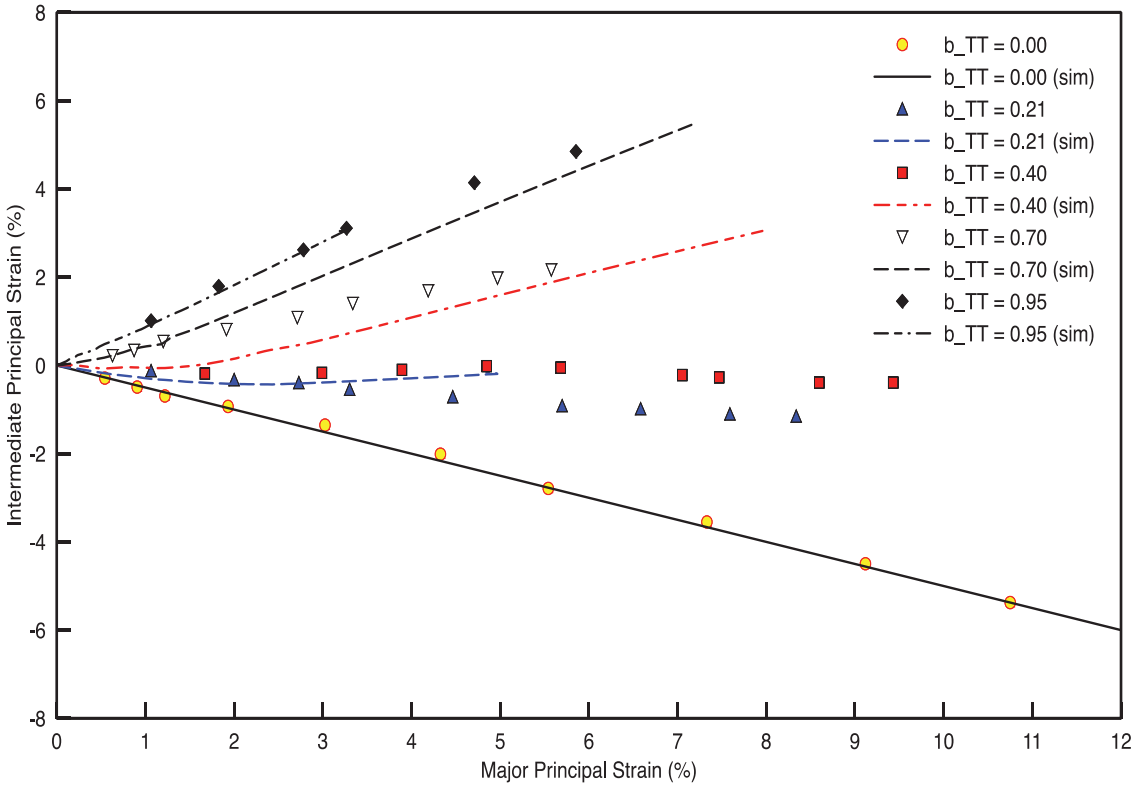

Figure 7. Comparison of simulated and experimental intermediate vs. major principal strain response of TT tests on samples of undrained Grundite clay [37].

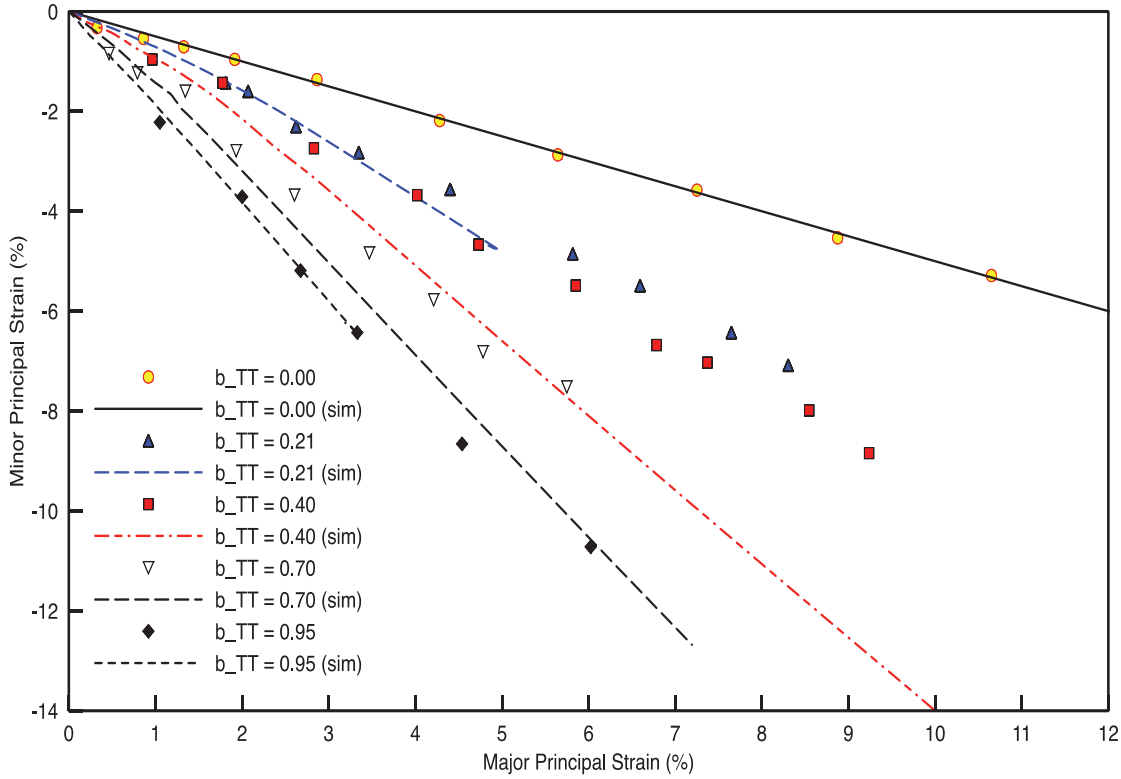

Figure 8. Comparison of simulated and experimental minor vs. major principal strain response of TT tests on samples of undrained Grundite clay [37].

7. CONCLUSIONS

The Generalized Bounding Surface Model (GBSM) synthesizes many previous forms of the bounding surface model for cohesive soils and improves upon many aspects of these models. The GBSM is a fully three-dimensional, time-dependent model that accounts for both inherent and stress induced anisotropy through a suitable rotational hardening laws. In addition, the model employs either an associative or non-associative flow rule. This paper assessed the model's performance in simulating the response of *soft*, saturated cohesive soils. Based on comparisons with experimental results for two different saturated cohesive soils, the GBSMan and GBSMin forms of the GBSM were shown to realistically simulate the time-independent, isothermal response of such soils when subjected to monotonic loading.

REFERENCES

1. **Kaliakin V.N., Leal A.N., Mashayekhi M.** Modeling the Time- and Temperature-Dependent Response of Cohesive Soils in a Generalized Bounding Surface Framework. // *Transportation Infrastructure Geotechnology*, 2018, Vol. 5, No. 3, pp. 250-286.
2. **Dafalias Y.F.** Bounding Surface Plasticity. I: Mathematical Foundation and the Concept of Hypoplasticity. // *Journal of Engineering Mechanics*, ASCE, Vol. 112, No. 90, 1986, pp. 966-987.
3. **Nieto-Leal A., Kaliakin V.N.** On Soil Yielding and Suitable Choices for Yield and Bounding Surfaces. Report, Department of Civil and Environmental Engineering, University of Delaware, DE, 2013.
4. **Dafalias Y.F.** The Concept and Application of the Bounding Surface in Plasticity Theory. // *IUTAM Symposium on Physical Non-Linearities in Structural Analysis*, Hult

J. and Lemaitre J. (Eds.). Springer-Verlag, Berlin, 1981, pp. 56-63.

5. **Nieto-Leal A., Kaliakin V.N.** Improved Shape Hardening Function for Bounding Surface Model for Cohesive Soils // *Journal of Rock Mechanics and Geotechnical Engineering*, 2014, Vol. 6. No. 3, pp. 327-337.
6. **Dafalias Y.F.** An Anisotropic Critical State Soil Plasticity Model. // *Mechanics Research Communications*, 1986, Vol. 13, No. 6, pp. 341-347.
7. **Baker R., Desai C.S**. Induced Anisotropy During Plastic Straining. // *International Journal for Numerical and Analytical Methods in Geomechanics*, 1984, Vol. 8, No. 2, pp. 167-185.
8. **Crouch R.S., Wolf J.P.** On a Three-dimensional Anisotropic Plastic Model for Soil. // *Geotechnique*, 1995, Vol. 45, No. 2, pp. 301-305.
9. **Dafalias Y.F., Herrmann L.R.** Bounding Surface Plasticity II: Application to Isotropic Cohesive Soils. // *Journal of Engineering Mechanics*, ASCE, 1986, Vol. 112, No. 12, pp. 1263-1291.
10. **Dafalias Y.F., Herrmann L.R.** A Bounding Surface Soil Plasticity Model. // *Proceedings of the International Symposium on Soils Under Cyclic and Transient Loading*, Pande G.N. and Zienkiewicz O.C. (Eds.), A.A. Balkema, Rotterdam, 1980, pp. 335-345.
11. **Dafalias Y.F., Herrmann L.R.** Bounding Surface Formulation of Soil Plasticity. // *Soil Mechanics – Transient and Cyclic Loads*, Pande G.N. and Zienkiewicz O.C. (Eds.), John Wiley and Sons, Chichester, UK, Chapter 10, 1982, pp. 253-282.
12. **Kaliakin V.N., Nieto-Leal A.** Details Pertaining to the Generalized Bounding Surface Model for Cohesive Soils. Revised & Expanded, Report, Department of Civil and Environmental Engineering, University of Delaware, DE, 2017.
13. **Kaliakin V.N., Dafalias Y.F.** Simplifications to the Bounding Surface Model for Cohesive Soils. // *International Journal for Numerical and Analytical Methods in Geomechanics*, 1989, Vol. 13, No. 1, pp. 91-100.
14. **Schofield A.N., Wroth C.P.** Critical State Soil Mechanics. McGraw-Hill Book Co., Inc., London, UK, 1968, 310 pages.
15. **Sheng D., Sloan S.W., Yu H.S.** Aspects of finite element implementation of critical state models. // *Computational Mechanics*, 2000, Vol. 26, pp. 185-196.
16. **Kaliakin V.N., Dafalias Y.F.** Theoretical Aspects of the Elastoplastic-Viscoplastic Bounding Surface Model for Cohesive Soils. // *Soils and Foundations*, 1990, Vol. 30, No. 3, pp. 11-14.
17. **Dafalias Y.F.** Bounding Surface Elastoplasticity-Viscoplasticity for Particulate Cohesive Media. // *Deformation and Failure of Granular Materials, IUTAM Symposium on Deformation and Failure of Granular Materials*, Vermeer P.A. and Luger H.J. (Eds.), A.A. Balkema, Rotterdam, 1982, pp. 97-107.
18. **Perzyna P.** Fundamental Problems in Viscoplasticity. // *Advances in Applied Mechanics*, 1966, Vol. 9, pp. 243-377.
19. **Nieto-Leal A.N., Kaliakin V.N., Mashayekhi M.** Improved RH rule for cohesive soils and inherent anisotropy. // *International Journal for Numerical and Analytical Methods in Geomechanics*, 2018, Vol. 42, No. 3, pp. 469-487.
20. **Dafalias Y.F., Manzari M.T., Papadimitriou A.G.** SANICLAY: simple anisotropic clay plasticity model. // *International Journal for Numerical and Analytical Methods in Geomechanics*, 2006, Vol. 30, No. 12, pp. 1231-1257.
21. **Kaliakin V.N.** CALBR8, A Simple Computer Program for Assessing the Idiosyncrasies of Various Constitutive Models Used to Characterize Soils. Report 92-1, Department of Civil and Environmental Engineering, University of Delaware, DE, 1992.

22. **Chin C.T., Liu C.C.** Volumetric and undrained behaviors of Taipei silty clay. // *Journal of the Chinese Institute of Civil and Hydraulic Engineering*, 1997, Vol. 9, No. 4, pp. 665-678.
23. **Shibata T., Karube D.** Influence of the Variation of the Intermediate Principal Stress on the Mechanical Properties of Normally Consolidated Clays. // *Proceedings of the 6th International Conference on Soil Mechanics and Foundation Engineering*, Montreal, Canada, 1965, Vol. 1, pp. 359-363.
24. **Yong R.N., McKyes E.** Yield and Failure of a Clay Under Triaxial Stresses. // *Journal of the Soil Mechanics and Foundation Division*, ASCE, 1971, Vol. 97, No. SM1, pp. 159-176.
25. **Lade P.V., Musante H.M.** Three-Dimensional Behavior of Remolded Clay. // *Journal of the Geotechnical Engineering Division*, 1978, ASCE, Vol. 104, No. GT2, pp. 193-209.
26. **Nakai T., Matsuoka H., Okuno N., Tsuzuki K.** True Triaxial Tests on Normally Consolidated Clay and Analysis of The Observed Shear Behavior Using Elastoplastic Constitutive Models. // *Soils and Foundations*, 1986, Vol. 26, No. 4, pp. 67-78.
27. **Lade P.V.** Single-Hardening Model with Application to NC Clay. // *Journal of Geotechnical Engineering*, ASCE, 1990, Vol. 116, No. 3, pp. 394-414.
28. **Kirkgard M.M., Lade P.V**. Anisotropic Three-Dimensional Behavior of a Normally Consolidated Clay. // *Canadian Geotechnical Journal*, 1993, Vol. 30, No. 5, pp. 848-858.
29. **Prashant A., Penumadu D.** Effect of Intermediate Principal Stress on Overconsolidated Kaolin Clay. // *Journal of Geotechnical and Geoenvironmental Engineering*, ASCE, 2004, Vol. 130, No. 3, pp. 284-292.
30. **Anantanasakul P., Yamamuro J., Lade P.V.** Three-dimensional drained behavior of normally consolidated anisotropic kaolin clay. // *Soils and Foundations*, 2012, Vol. 52, No. 1, pp. 146-159.
31. **Grim R.E., Bradley R.F.** A Unique Clay form Goose Lake, Illinois Area. // *Journal of the American Ceramic Society*, 1939, Vol. 22, No. 5, pp. 157-164.
32. **Perloff W.H., Osterberg J.O.** The Effect of Strain Rate on the Undrained Shear Strength of Cohesive Soils. // *Proceedings of the Second Pan American Conference on Soil Mechanics and Foundation Engineering*, Sao Paulo, Brasil, 1963, Vol. 1, pp. 103-128.
33. **Kondner R.L., Horner J.M.** Triaxial Compression of a Cohesive Soil with Effective Octahedral Normal Stress Control. // *Canadian Geotechnical Journal*, 1965, Vol. 2, No. 1, pp. 40-52.
34. **Lade P.V., Duncan J.M.** Cubical Triaxial Tests on Cohesionless Soil. // *Journal of the Soil Mechanics and Foundation Division*, ASCE, 1973, Vol. 99, No. SM10, pp. 793-812.
35. **Lade P.V.** Experimental Data for Grundite Clay. Personal communication, 2003.
36. **France J., Sangrey D.A.** Effects of Drainage in Repeated Loading of Clays. // *Journal of Geotechnical Engineering Division*, ASCE, 1977, Vol. 103, No. GT7, pp. 769-785.
37. **Lade P.V.** Stress-Strain Theory for Normally Consolidated Clay. // *Proceedings of the 3rd International Conference on Numerical Methods in Geomechanics*, Aachen, West Germany, 1979, Vol. 1, pp. 1325-1337.

СПИСОК ЛИТЕРАТУРЫ

1. **Kaliakin V.N., Leal A.N., Mashayekhi M.** Modeling the Time- and Temperature-Dependent Response of Cohesive Soils in a Generalized Bounding Surface Framework. // *Transportation Infrastructure Geotechnology*, 2018, Vol. 5, No. 3, pp. 250-286.

2. **Dafalias Y.F.** Bounding Surface Plasticity. I: Mathematical Foundation and the Concept of Hypoplasticity. // *Journal of Engineering Mechanics*, ASCE, Vol. 112, No. 90, 1986, pp. 966-987.
3. **Nieto-Leal A., Kaliakin V.N.** On Soil Yielding and Suitable Choices for Yield and Bounding Surfaces. Report, Department of Civil and Environmental Engineering, University of Delaware, DE, 2013.
4. **Dafalias Y.F.** The Concept and Application of the Bounding Surface in Plasticity Theory. // *IUTAM Symposium on Physical Non-Linearities in Structural Analysis*, Hult J. and Lemaitre J. (Eds.). Springer-Verlag, Berlin, 1981, pp. 56-63.
5. **Nieto-Leal A., Kaliakin V.N.** Improved Shape Hardening Function for Bounding Surface Model for Cohesive Soils // *Journal of Rock Mechanics and Geotechnical Engineering*, 2014, Vol. 6. No. 3, pp. 327-337.
6. **Dafalias Y.F.** An Anisotropic Critical State Soil Plasticity Model. // *Mechanics Research Communications*, 1986, Vol. 13, No. 6, pp. 341-347.
7. **Baker R., Desai C.S**. Induced Anisotropy During Plastic Straining. // *International Journal for Numerical and Analytical Methods in Geomechanics*, 1984, Vol. 8, No. 2, pp. 167-185.
8. **Crouch R.S., Wolf J.P.** On a Three-dimensional Anisotropic Plastic Model for Soil. // *Geotechnique*, 1995, Vol. 45, No. 2, pp. 301-305.
9. **Dafalias Y.F., Herrmann L.R.** Bounding Surface Plasticity II: Application to Isotropic Cohesive Soils. // *Journal of Engineering Mechanics*, ASCE, 1986, Vol. 112, No. 12, pp. 1263-1291.
10. **Dafalias Y.F., Herrmann L.R.** A Bounding Surface Soil Plasticity Model. // *Proceedings of the International Symposium on Soils Under Cyclic and Transient Loading*, Pande G.N. and Zienkiewicz O.C. (Eds.), A.A. Balkema, Rotterdam, 1980, pp. 335-345.
11. **Dafalias Y.F., Herrmann L.R.** Bounding Surface Formulation of Soil Plasticity. // *Soil Mechanics – Transient and Cyclic Loads*, Pande G.N. and Zienkiewicz O.C. (Eds.), John Wiley and Sons, Chichester, UK, Chapter 10, 1982, pp. 253-282.
12. **Kaliakin V.N., Nieto-Leal A.** Details Pertaining to the Generalized Bounding Surface Model for Cohesive Soils. Revised & Expanded, Report, Department of Civil and Environmental Engineering, University of Delaware, DE, 2017.
13. **Kaliakin V.N., Dafalias Y.F.** Simplifications to the Bounding Surface Model for Cohesive Soils. // *International Journal for Numerical and Analytical Methods in Geomechanics*, 1989, Vol. 13, No. 1, pp. 91-100.
14. **Schofield A.N., Wroth C.P.** Critical State Soil Mechanics. McGraw-Hill Book Co., Inc., London, UK, 1968, 310 pages.
15. **Sheng D., Sloan S.W., Yu H.S.** Aspects of finite element implementation of critical state models. // *Computational Mechanics*, 2000, Vol. 26, pp. 185-196.
16. **Kaliakin V.N., Dafalias Y.F.** Theoretical Aspects of the Elastoplastic-Viscoplastic Bounding Surface Model for Cohesive Soils. // *Soils and Foundations*, 1990, Vol. 30, No. 3, pp. 11-14.
17. **Dafalias Y.F.** Bounding Surface Elastoplasticity-Viscoplasticity for Particulate Cohesive Media. // *Deformation and Failure of Granular Materials, IUTAM Symposium on Deformation and Failure of Granular Materials*, Vermeer P.A. and Luger H.J. (Eds.), A.A. Balkema, Rotterdam, 1982, pp. 97-107.
18. **Perzyna P.** Fundamental Problems in Viscoplasticity. // *Advances in Applied Mechanics*, 1966, Vol. 9, pp. 243-377.
19. **Nieto-Leal A.N., Kaliakin V.N., Mashayekhi M.** Improved RH rule for cohesive soils and inherent anisotropy. // *International Journal for Numerical and*

Analytical Methods in Geomechanics, 2018, Vol. 42, No. 3, pp. 469-487.

20. **Dafalias Y.F., Manzari M.T., Papadimitriou A.G.** SANICLAY: simple anisotropic clay plasticity model. // *International Journal for Numerical and Analytical Methods in Geomechanics*, 2006, Vol. 30, No. 12, pp. 1231-1257.
21. **Kaliakin V.N.** CALBR8, A Simple Computer Program for Assessing the Idiosyncrasies of Various Constitutive Models Used to Characterize Soils. Report 92-1, Department of Civil and Environmental Engineering, University of Delaware, DE, 1992.
22. **Chin C.T., Liu C.C.** Volumetric and undrained behaviors of Taipei silty clay. // *Journal of the Chinese Institute of Civil and Hydraulic Engineering*, 1997, Vol. 9, No. 4, pp. 665-678.
23. **Shibata T., Karube D.** Influence of the Variation of the Intermediate Principal Stress on the Mechanical Properties of Normally Consolidated Clays. // *Proceedings of the 6th International Conference on Soil Mechanics and Foundation Engineering*, Montreal, Canada, 1965, Vol. 1, pp. 359-363.
24. **Yong R.N., McKyes E.** Yield and Failure of a Clay Under Triaxial Stresses. // *Journal of the Soil Mechanics and Foundation Division*, ASCE, 1971, Vol. 97, No. SM1, pp. 159-176.
25. **Lade P.V., Musante H.M.** Three-Dimensional Behavior of Remolded Clay. // *Journal of the Geotechnical Engineering Division*, 1978, ASCE, Vol. 104, No. GT2, pp. 193-209.
26. **Nakai T., Matsuoka H., Okuno N., Tsuzuki K.** True Triaxial Tests on Normally Consolidated Clay and Analysis of The Observed Shear Behavior Using Elastoplastic Constitutive Models. // *Soils and Foundations*, 1986, Vol. 26, No. 4, pp. 67-78.
27. **Lade P.V.** Single-Hardening Model with Application to NC Clay. // *Journal of Geotechnical Engineering*, ASCE, 1990, Vol. 116, No. 3, pp. 394-414.
28. **Kirkgard M.M., Lade P.V**. Anisotropic Three-Dimensional Behavior of a Normally Consolidated Clay. // *Canadian Geotechnical Journal*, 1993, Vol. 30, No. 5, pp. 848-858.
29. **Prashant A., Penumadu D.** Effect of Intermediate Principal Stress on Overconsolidated Kaolin Clay. // *Journal of Geotechnical and Geoenvironmental Engineering*, ASCE, 2004, Vol. 130, No. 3, pp. 284-292.
30. **Anantanasakul P., Yamamuro J., Lade P.V.** Three-dimensional drained behavior of normally consolidated anisotropic kaolin clay. // *Soils and Foundations*, 2012, Vol. 52, No. 1, pp. 146-159.
31. **Grim R.E., Bradley R.F.** A Unique Clay form Goose Lake, Illinois Area. // *Journal of the American Ceramic Society*, 1939, Vol. 22, No. 5, pp. 157-164.
32. **Perloff W.H., Osterberg J.O.** The Effect of Strain Rate on the Undrained Shear Strength of Cohesive Soils. // *Proceedings of the Second Pan American Conference on Soil Mechanics and Foundation Engineering*, Sao Paulo, Brasil, 1963, Vol. 1, pp. 103-128.
33. **Kondner R.L., Horner J.M.** Triaxial Compression of a Cohesive Soil with Effective Octahedral Normal Stress Control. // *Canadian Geotechnical Journal*, 1965, Vol. 2, No. 1, pp. 40-52.
34. **Lade P.V., Duncan J.M.** Cubical Triaxial Tests on Cohesionless Soil. // *Journal of the Soil Mechanics and Foundation Division*, ASCE, 1973, Vol. 99, No. SM10, pp. 793-812.
35. **Lade P.V.** Experimental Data for Grundite Clay. Personal communication, 2003.
36. **France J., Sangrey D.A.** Effects of Drainage in Repeated Loading of Clays. // *Journal of Geotechnical Engineering Division*, ASCE, 1977, Vol. 103, No. GT7, pp. 769-785.

37. **Lade P.V.** Stress-Strain Theory for Normally Consolidated Clay. // *Proceedings of the 3rd International Conference on Numerical Methods in Geomechanics*, Aachen, West Germany, 1979, Vol. 1, pp. 1325-1337.

Victor N. Kaliakin, Professor, Ph.D., Department of Civil & Environmental Engineering, University of Delaware, 19716, USA; phone +1(302)831-2409 (office); fax +1(302)831-3640;
E-mail: kaliakin@udel.edu.

Andres Nieto-Leal, Assistant Professor, Ph.D., Chairman, Department of Civil Engineering, Universidad Militar Nueva Granada, Cajica, 250247, Colombia; e-mail: andres.nieto@unimilitar.edu.co.

Калякин Виктор Н., профессор, доктор наук; Департамент гражданского и экологического инжиниринга, Университет штата Делавэр, г. Ньюарк, США; тел. +1(302) 831-2409;
факс +1(302)831-3640; e-mail: kaliakin@udel.edu.

Андрес Ньето-Лил, доцент, доктор наук, Департамент гражданского строительства, Университет Милитара Нуэва, Гранада, Кахика, 250247, Колумбия;
E-mail: andres.nieto@unimilitar.edu.co.

DOI:10.22337/2587-9618-2019-15-3-77-83

FORCED VIBRATIONS OF ANISOTROPIC ELASTIC SOLIDS SUBJECTED TO AN ACTION OF COMPLICATED LOADS

Elena B. Koreneva [1], ***Valery R. Grosman*** [2]

[1] Moscow Higher Combined-Arms Command Academy, Moscow, RUSSIA

[2] Moscow State Academy for River Transport, branch of Admiral Makarov State University of Maritime and Inland Shipping, Moscow, RUSSIA

Abstract: The work studies the forced vibrations of anisotropic elastic circular plates caused by dynamic loads uniformly distributed along concentric circumferences and over ring surfaces. The method of compensating loads (MCL) is used to solve the formulated problems. A new technique is used to construct basic and compensating solutions. The Nielsen's equation is taken into consideration. The solutions are obtained in closed form in terms of Bessel functions. Formulae of addition of cylindrical functions are used.

Keywords: anisotropy, circular plates, forced vibrations, Bessel functions

ВЫНУЖДЕННЫЕ КОЛЕБАНИЯ АНИЗОТРОПНЫХ УПРУГИХ ТЕЛ ПРИ СЛОЖНЫХ НАГРУЗКАХ

Е.Б. Коренева [1], ***В.Р. Гросман*** [2]

[1] Московское высшее общевойсковое командное орденов Жукова, Ленина и Октябрьской Революции Краснознаменное училище, г. Москва, РОССИЯ

[2] Московская государственная академия водного транспорта – филиал Государственного университета морского и речного флота имени адмирала С.О. Макарова, г. Москва, РОССИЯ

Аннотация: В работе изучаются вынужденные колебания анизотропных упругих круглых пластин, вызванные действием нагрузок, распределенных вдоль концентрических окружностей и по площадям колец. Для решения поставленных задач используется метод компенсирующих нагрузок (МКН). Для построения базовых решений – основного и компенсирующего, используется новый прием, берется в рассмотрение уравнение Нильсена. Решения получены в замкнутом виде и выражены в функциях Бесселя. Используются формулы сложения цилиндрических функций.

Ключевые слова: анизотропия, круглые пластины, вынужденные колебания, функции Бесселя

1. INTRODUCTION

In literature, for example in [1], the questions concerning analytical methods application to the solution of problems of statics and oscillations of elastic isotropic circular plates are covered. However, if the mentioned constructions are made from anisotropic material the application of analytical methods in the same ways as for isotropic ones causes considerable difficulties. For the cases of isotropic plates the resolving differential equation of the fourth order with variable coefficients is decomposed into two conjugate differential equations of the second order. The solutions are expressed in terms of Bessel functions. When solving the problems of anisotropic plates, the corresponding differential equation of the fourth order with variable coefficients does not decompose into two conjugate equations for any parameter values. This work applies the new approach for solving certain dynamic problems.

Nielsen's equation is used. First the similar approach was proposed for consideration of static problems of anisotropic circular plates resting on Winkler's foundation [2].

Let us assume that the plate material has cylindrical anisotropy and is orthotropic. The construction under study is subjected to an action of dynamic loads uniformly distributed along the lengths of concentric circles and over ring surfaces.

2. THE RESOLVING EQUATION

We present a differential equation describing the natural axisymmetric oscillation of a circular orthotropic plate [3], [4]:

$$r^4\frac{\partial^4 w}{\partial r^4}+2r^3\frac{\partial^3 w}{\partial r^3}-n^2r^2\frac{\partial^2 w}{\partial r^2}+n^2r\frac{\partial w}{\partial r}+ +\frac{\gamma h}{gn_2D}\frac{\partial^2 w}{\partial t^2}=0, \quad (1)$$

where D – cylindrical rigidity,

$$E_r=\frac{E}{n_1},\ E_\theta=En_2,\ \sigma_r=\frac{\sigma}{n^2},\ \sigma_\theta=\sigma,$$

$$n^2=n_1n_2.$$

When considering axisymmetric vibrations the solution of the equation (1) has the form:

$$w=\sum_{S=0}^{\infty}(A_S\cos p_St+B_S\sin p_St)W_S, \quad (2)$$

here p_S - circular frequency of natural vibrations, W_S - a function of only the coordinate r, constants A_S and B_S are determined from initial conditions, S is the number of nodal diameters.

As it was mentioned above, the studies have shown that for a plate made from orthotropic material, the initial fourth-order differential equation for any parameter values does not decay into two mutually adjoint second order equations as in the case for isotropic plates. Therefore, here to obtain an accurate analytical solution in terms of Bessel functions and for the application of the method of compensating loads (MCL) [2], [3], another technique was used. Nielsen's equation was introduced into consideration. As a result the following solutions were obtained.

When the parameter $\mu=0$, the general solution of the differential equation (2) has the form:

$$W_S=C_1J_0(br)+C_2Y_0(br)+C_3I_0(br)+ +C_4K_0(br); \quad (3)$$

for the parameter values $\mu=\pm2$ the general solution of (2) is determined from the expression:

$$W_S=B_1u_\mu(br)+B_2\upsilon_\mu(br)+B_3f_\mu(br)+ +B_4g_\mu(br), \quad (4)$$

where

$$b=\sqrt[4]{\frac{\gamma h}{gn_2D}p_S^2}.$$

3. THE METHOD OF COMPENSATING LOADS

In [3], forced oscillations of a circular orthotropic plate subjected to an action of a concentrated force in the center were studied. MCL was used for this purpose.

Below we will consider the forced vibrations of such plates under the action of much more complicated loads distributed along circumferences that do not coincide with the contour and loads distributed over areas of rings. MCL will also be used to build the solution. We introduce a dimensionless coordinate $x=br$. Let us assume that the plate under study is clamped along the contour.

First we will examine an action on the plate of the concentrated force $P\sin pt$ applied in the center.

Then the basic solution, which should contain a feature of the type of concentrated force, should be written in the form:

$$W_0=C_0Y_0(x)+D_0K_0(x). \quad (5)$$

The compensating solution is determined by the formula:

$$W_k=A_0J_0(x)+B_0I_0(x). \quad (6)$$

In the expression (5) the functions $Y_0(x)$ and $K_0(x)$ are tend to infinity as $\ln x$. On the basis of the theory of Bessel functions we put

$$D_0 = \frac{2}{\pi} C_0.$$

The coefficient C_0 is determined from equilibrium conditions. Let us draw a circle of small radius x/b with the center in the point $x = 0$. We calculate the sum of the transverse forces acting on the circle of the mentioned radius and passage to the limit when $x \to 0$.
Performing all calculations [3], we get:

$$C_0 = -\frac{P}{8Dn_2b^2}. \tag{7}$$

As a result, (5) will take the form:

$$W_0 = -\frac{P}{8Dn_2b^2}\left[Y_0(x) + \frac{2}{\pi}K_0(x)\right]. \tag{8}$$

Summing up the basic and the compensating solutions, we define:

$$W = A_0J_0(x) + B_0I_0(x) - \frac{P}{8Dn_2b^2} \times \left[Y_0(x) + \frac{2}{\pi}K_0(x)\right]. \tag{9}$$

The constants A_0 and B_0 are determined from boundary conditions. We set in our case that when $x = \beta$ the outer boundary is clamped. When

$$x = \beta,\ w = 0,\ \frac{dw}{dx} = 0.$$

As a result of a number of transformations and using certain dependencies from Bessel's functions theory, we obtain the following expressions for A_0 and B_0:

$$A_0 = \frac{P}{8D_0n_2b^2} \times \frac{I_1(\beta)Y_0(\beta) + I_0(\beta)Y_1(\beta) + \frac{2}{\pi\beta}}{J_0(\beta)I_1(\beta) + J_1(\beta)I_0(\beta)},$$
$$B_0 = \frac{P}{8D_0n_2b^2} \times \frac{\frac{2}{\pi}[J_1(\beta)K_0(\beta) - J_0(\beta)K_1(\beta)] + \frac{2}{\pi\beta}}{J_0(\beta)I_1(\beta) + J_1(\beta)I_0(\beta)}. \tag{10}$$

In the case of another boundary conditions on the contour, the basic solutions will remain unchanged and the general form of the compensating solution will also remain. Due to the change of boundary conditions only the formulae for determining of the constants A_0 and B_0 will be different.

4. THE CALCULATION OF THE EFFECT OF LOAD DISTRIBUTED ALONG CIRCLES

We proceed to the study of the problem of forced oscillation of an anisotropic circular plate clamped along the contour caused by a load uniformly distributed around the circumference concentric with the contour and having a radius a_1. Denote the amplitude of the load $q\sin pt$ as q.
As it was shown above, we present the form of oscillation as the sum of the basic solution W_0 and the compensating solution W_k.
First we will define the basic solution. For this aim, mentally divide the loads acting along the circumference on the number of elementary loads. Next we sum-up the result of these loads. Take on the circle, on which the load is applied, a point with the coordinates (a_1, x). Elementary load acting on the section of arc with the length $a_1d\theta$ is determined by the expression

$$\frac{qa_1d\theta}{b}. \tag{11}$$

Find the deflection in the point with the reduced coordinates x,φ. To do this we use the formula (8). Substituting instead P the expression (11) and instead x the distance from the point of the elementary force application to the considered point of the plate, which is as follows:

$$z = \sqrt{a_1^2 + x^2 - 2a_1 x\cos(\theta - \varphi)}.$$

We make integration. Calculation of integrals should use the formulae of cylindrical functions addition, which in the studied case are of the form:

when $x \le a_1$

$$Y_0\left(\sqrt{a_1^2 + x^2 - 2a_1 x\cos(\theta - \varphi)}\right) = 2\sum_0^{\infty}{}' J_n(x)Y_n(a_1)\cos n(\theta - \varphi), \quad (12)$$

$$K_0\left(\sqrt{a_1^2 + x^2 - 2a_1 x\cos(\theta - \varphi)}\right) = 2\sum_0^{\infty}{}' I_n(x)K_n(a_1)\cos n(\theta - \varphi), \quad (13)$$

when $x \ge a_1$

$$Y_0\left(\sqrt{a_1^2 + x^2 - 2a_1 x\cos(\theta - \varphi)}\right) = 2\sum_0^{\infty}{}' J_n(a_1)Y_n(x)\cos n(\theta - \varphi), \quad (14)$$

$$K_0\left(\sqrt{a_1^2 + x^2 - 2a_1 x\cos(\theta - \varphi)}\right) = 2\sum_0^{\infty}{}' I_n(a_1)K_n(x)\cos n(\theta - \varphi). \quad (15)$$

In this formulae the sign ' means that for $n = 0$ an additional factor $1/2$ is introduced.
Write down:

$$w_0 = -\int_0^{2\pi} \frac{qa_1}{8Dn_2b^3}\left[Y_0(z) + \frac{2}{\pi}K_0(z)\right]d\theta = -\frac{qa_1}{8Dn_1b^3} \times \left[\int_0^{2\pi} Y_0\left(\sqrt{a_1^2 + x^2 - 2a_1 x\cos(\theta - \varphi)}\right)d\theta + \frac{2}{\pi}\int_0^{2\pi} K_0\left(\sqrt{a_1^2 + x^2 - 2a_1 x\cos(\theta - \varphi)}\right)d\theta\right]. \quad (16)$$

Substituting (12), (13), (14) and (15) in (16) and performing the integration; we note that all the series members when $n \ge 0$ at integration give zero. Therefore the solution will include only the result of integration of the zero term.
We have when $x \le a_1$

$$w_0 = -\frac{\pi qa_1}{4Dn_2b^3} \times \left[J_0(x)Y_0(a_1) + \frac{2}{\pi}I_0(x)K_0(a_1)\right], \quad (17)$$

when $x > a_1$

$$w_0 = -\frac{\pi qa_1}{4Dn_2b^3} \times \left[J_0(a_1)Y_0(x) + \frac{2}{\pi}I_0(a_1)K_0(x)\right]. \quad (18)$$

We receive the solution of the problem adding to the basic solution the compensating one:

$$w = w_0 + A_0J_0(x) + B_0I_0(x). \quad (19)$$

The coefficients A_0 and B_0 are determined from the boundary conditions. Here it was assumed that the outer contour of the plate when $x = \beta$ is clamped. Determining the mentioned coefficients A_0 and B_0 and using the expression for Wronskian, we get:

$$A_0 = \frac{\pi q a_1}{4Dn_2 b^3} \frac{J_0(a_1)[I_1(\beta)Y_0(\beta) + I_0(\beta)Y_1(\beta)] + \frac{2}{\pi\beta} I_0(a_1)}{I_0(\beta)J_1(\beta) + I_1(\beta)J_0(\beta)}, \tag{20}$$

$$B_0 = \frac{\pi q a_1}{4Dn_2 b^3} \frac{\frac{1}{\beta} J_0(a_1) + I_0(a_1)[I_1(\beta)K_0(\beta) - J_0(\beta)K_1(\beta)]}{I_0(\beta)J_1(\beta) + I_1(\beta)J_0(\beta)}. \tag{21}$$

For the cases of other boundary conditions only the equations for determining the constants A_0 and B_0 in the corresponding compensating solution will change.

5. THE LOADS DISTRIBUTED OVER RING SURFACES

We proceed to the study of forced oscillations caused by the load $q_1 \sin pt$, uniformly distributed over the area of the ring with the inner radius a_2 and the outer one a_3 $(a_2 < a_1 < a_3)$.

Let's define the basic solution. To do this the specified ring is divided into elementary concentric rings. The reduced inner radius of the elementary ring is denote by a_1, the outer one as $a_1 + da_1$. The load acting on the unit length of the ring is equal to

$$q = q_1 \frac{da_1}{b}.$$

The solution corresponding to the action of the elementary load is determined by the expressions (17) and (18) in which q should be replaced by

$$q_1 \frac{da_1}{b}.$$

Integrating these expressions in the range a_1 from a_2 to a_3, we obtain a solution of the problem under study. If the cross-section is in the inner circle when $x \le a_2$ which is free from external load, the expression (17) is to be integrated, that is

$$w_0 = -\frac{\pi q_1}{4Db^4} \times \\ \times \int_{a_2}^{a_3} \left[J_0(x)Y_0(a_1) + \frac{2}{\pi} I_0(x)K_0(a_1) \right] a_1 da_1. \tag{22}$$

From the theory of Bessel functions, for example from [1], the following relations are known:

$$\frac{d}{dx}\left[x^n Y_n(x)\right] = x^n Y_{n-1}(x), \tag{23}$$

$$\frac{d}{dx}\left[x^n K_n(x)\right] = -x^n K_{n-1}(x). \tag{24}$$

Assuming $n = 1$ we get:

$$\int x Y_0(x)dx = x Y_1(x), \tag{25}$$

$$\int x K_0(x)dx = -x K_1(x). \tag{26}$$

Taking into account (25) and (26) the expression for w_0 when $x \le a_2$ will take the following form:

$$w_0 = -\frac{\pi q_1}{4Dn_2 b^4} \{[a_3 Y_1(a_3) - a_2 Y_1(a_2)]J_0(x) - \\ -\frac{2}{\pi}[a_3 K_1(a_3) - a_2 K_1(a_2)]I_0(x)\}. \tag{27}$$

When considering a part $x \ge a_3$ the expression (18) must be integrated. To do this we should take into account the ratio [1]:

$$\frac{d}{dx}\left[x^n J_n(x)\right] = x^n J_{n-1}(x), \tag{28}$$

$$\frac{d}{dx}\left[x^n I_n(x)\right] = x^n I_{n-1}(x); \tag{29}$$

hence for $n=1$ we get:

$$\int xJ_0(x)dx = xJ_1(x), \tag{30}$$

$$\int xI_0(x)dx = xI_1(x). \tag{31}$$

Thus when $x \geq a_3$ we get:

$$w_0 = -\frac{\pi q_1}{4Dn_2b^4}\{[a_3J_1(a_3) - a_2J_1(a_2)]Y_0(x) + \\ + \frac{2}{\pi}[a_3I_1(a_3) - a_2I_1(a_2)]K_0(x)\}. \tag{32}$$

When considering the area under the load when $a_2 \leq x \leq a_3$ to determine the solution of the problem we should integrate (18) when $a_2 \leq a_1 \leq x$ and when $a_1 \leq x \leq a_3$ we should integrate (17), replacing q on

$$q_1\frac{da_1}{b}$$

as elsewhere. At the same time, using the formulae (25), (26), (30) and (31), we get the following result when $a_2 \leq x \leq a_1$:

$$w_0 = -\frac{\pi q_1}{4Dn_2b^4}\{[xJ_1(x) - a_3J_1(a_2)] - \\ - Y_0(x) + \frac{2}{\pi}[xI_1(x) - a_2I_1(a_2)]K_0(x) + \\ + [a_3Y_1(a_3) - xY_1(x)]J_0(x) - \\ - \frac{2}{\pi}[a_3K_1(a_3) - xK_1(x)]I_0(x)\}. \tag{33}$$

By regrouping we obtain:

$$w_0 = -\frac{\pi q_1}{4Dn_2b^4}\{x[J_1(x)Y_0(x) - Y_1(x)J_0(x)] + \\ + \frac{2x}{\pi}[I_1(x)K_0(x) + I_0(x)K_1(x)] - \\ - a_2J_1(a_2)Y_0(x) - \frac{2}{\pi}a_2I_1(a_2)K_0(x) + \\ + a_3Y_1(a_3)J_0(x) - \frac{2}{\pi}a_3K_1(a_3)I_0(x)\}. \tag{34}$$

Using the expression for Wronskian we get:

$$w_0 = -\frac{\pi q_1}{4Dn_2b^4}\left[\frac{4}{\pi} - a_2J_1(a_2)Y_0(x) - \right. \\ - \frac{2}{\pi}a_2I_1(a_2)K_0(x) + a_3Y_1(a_3)J_0(x) - \\ \left. - \frac{2}{\pi}a_3K_1(a_3)I_0(x)\right]. \tag{35}$$

Summing the basic and compensating solutions we obtain the expression which is similar to (19) where the constants A_0 and B_0 are determined from the boundary conditions.

6. CONCLUSION

The present work for the first time receives the exact analytical solutions of the problems of forced vibrations of circular plates which are made from material having cylindrical anisotropy. The constructions under study are subjected to an action of dynamic loads uniformly distributed along the lengths of concentric circumferences and over areas of ring surfaces. Method of compensating loads for determination of the solutions is used. The solutions are obtained in terms of Bessel functions.

REFERENCES

1. **Korenev B.G.** Nekotoryye Zadachi Teorii Uprugosti i Teploprovodnosti, Reshayemyye v Besselevykh Funktsiyakh. [Some Problems of the Theory of Elasticity and Heat Conductivity, Solved in Terms of Bessel Functions]. Moscow, Fizmatgiz, 1960, 458 pages (in Russian).
2. **Koreneva E.B.** Method of Compensating Loads for Solving of Anisotropic Medium Problems // *International Journal for Computational Civil and Structural Engineering*, 2018, Volume 14, Issue 1, pp. 71-77.
3. **Koreneva E.B.** Analiticheskiy Metod dlya Resheniya Zadach o Kolebaniyah Anizotropnych Uprugich Tel. [Analytical Method for Solving of Anisotropic Elastic

Solids Vibration Problems] // *Stroitelnaya Mekhanika i Raschet Sooruzheniy*, 2018, No. 5, pp. 47-51 (in Russian).
4. **Koreneva E.B.** Analiticheskoje Modelirovanije Nekotorych Zadach Statiki i Kolebanij Anizotropnych Uprugich Tel. [Analytical Simulation of Certain Statics and Vibration Problems of Anisotropic Solids] // VII International Symposium APCSCE, July, 1-8, 2018, Novosibirsk, p. 478 (in Russian).

СПИСОК ЛИТЕРАТУРЫ

1. **Коренев Б.Г.** Некоторые задачи теории упругости и теплопроводности, решаемые в бесселевых функциях. – М.: Физматгиз, 1960. – 458 с.
2. **Коренева Е.Б.** Метод компенсирующих нагрузок для решения задач об анизотропных средах. // *International Journal for Computational Civil and Structural Engineering*, 2018, Volume 14, Issue 1, с. 71-77.
3. **Коренева Е.Б.** Аналитический метод для решения задач о колебаниях анизотропных упругих тел. // *Строительная механика и расчет сооружений*, 2018, №5, с. 47-51.
4. **Коренева Е.Б.** Аналитическое моделирование некоторых задач статики и колебаний анизотропных упругих тел. // VII International Symposium APCSCE, July, 1-8, 2018, Novosibirsk, с. 478.

Elena B. Koreneva, Dr.Sc., Professor; Moscow Higher Combined-Arms Command Academy; ul. Golovacheva, 2, 109380, Moscow, Russia; phone: +7(499)175-82-45;
E-mail: elena.koreneva2010@yandex.ru.

Valery R. Grosman, Associate Professor, Moscow State Academy for River Transport, branch of Admiral Makarov State University of Maritime and Inland Shipping; Novodanilovskaya nab., 2, k.1, 117105, Moscow, Russia, phone: +7(499)618-52-56;
E-mail: elena.koreneva2010@yandex.ru.

Коренева Елена Борисовна, профессор, доктор технических наук; Московское высшее общевойсковое командное орденов Жукова, Ленина и Октябрьской Революции Краснознаменное училище, 109380, Россия, г. Москва, ул. Головачева, д.2; тел.: +7(499)175-82-45,
E-mail: elena.koreneva2010@yandex.ru.

Гросман Валерий Романович, старший преподаватель, Московская государственная академия водного транспорта – филиал Государственного университета морского и речного флота имени адмирала С.О. Макарова; 117105, Россия, г. Москва, Новоданиловская наб., д.2, корп.1, тел.: +7(499)618-52-56;
E-mail: elena.koreneva2010@yandex.ru.

DOI:10.22337/2587-9618-2019-15-3-84-95

NUMERICAL ANALYSIS OF THE ACCOUNT OF THE STAGES IN THE CALCULATION OF THE SHELL TOGETHER WITH THE SOIL MASSIF

Sergey B. Kosytsyn, Vladimir Y. Akulich
Russian University of Transport (MIIT), Moscow, RUSSIA

Abstract: The distinctive paper discusses the stress-strain state of a cylindrical shell with and without taking into account changes in the design model in time. The volumetric design model of the cylindrical shell and the soil massif is made. The calculation consists of several stages from the beginning of the tunnel shell construction to the end of the work. The authors analyzed the results and made appropriate recommendations.

Keywords: construction stages, soil massif, shell, finite elements, contact elements

ЧИСЛЕННЫЙ АНАЛИЗ УЧЕТА СТАДИЙНОСТИ В РАСЧЕТАХ ОБОЛОЧКИ СОВМЕСТНО С МАССИВОМ ГРУНТА

С.Б. Косицын, В.Ю. Акулич
Российский университет транспорта (МИИТ), г. Москва, РОССИЯ

Аннотация: в работе исследовано напряженно-деформированное состояние цилиндрической оболочки с учетом и без учета изменения расчетной модели во времени. Поставлена наследственная пространственно-временная задача с ее последовательным решением по стадиям от начала работ до окончания для цилиндрической оболочки и окружающего основания. Полученные результаты проанализированы, даны соответствующие рекомендации.

Ключевые слова: стадии строительства, грунтовый массив, оболочка, плоские и пространственные конечные элементы, контактные конечные элементы

1. INTRODACTION

The technology of civil, industrial and other purposes objects construction, as a rule, consists of several stages. After each stage, the stress-strain state is created in the structures, which is the initial state for the next stage and has a significant impact on the final stress-strain state of the structure. In strength calculations of structures by numerical methods, this factor is important.

Engineering calculations of building structures by numerical methods, as a rule, are performed without taking into account the initial state, the structure model is taken free from stresses and strains. However, most of the construction objects have initial and residual stress-strain state caused by each stage of their construction. As examples of such objects can be towers and masts, in the elements of which there are significant installation forces, reinforced concrete bridges with stepped concreting of the added sections, or transport tunnels, the rings of which are formed in several stages. Taking into account the initial and residual stress-strain state is important not only for new construction, but also for the repair and restoration of existing facilities. In these cases, the importance of taking into account the stress-strain state at each stage of structure construction is obvious.

In this paper, the authors consider how the construction stages affect the stress-strain state of the tunnel shell and the soil massif using numerical methods. The volumetric design model of

the tunnel shell and the soil massif is made. The calculation consists of several stages from the beginning of the tunnel shell construction to the end of the work. The authors analyzed the results and made appropriate recommendations

2. DETERMINATION THE STRESS-STRAIN STATE OF THE CYLINDRICAL SHELL AND THE SOIL MASSIF TAKING INTO ACCOUNT CHANGES DESIGN MODEL IN TIME

ANSYS software package allows creating a volumetric design model taking into account the construction stages from the beginning of the tunnel shell construction to the end of the work. ANSYS software package verified by the Russian Academy of Architecture and Construction Sciences (RAACS). Option "Birth and Death Element" of this software package allow modeling the construction stages of the considered structures. This option defines the finite elements that are to be activated or deactivated during the calculation based on some criterion: the stress state, the position in the model, etc. Deactivation, or "death", of the finite element, occurs by multiplying the stiffness of the element by a small value. The loads applied to the deactivated element are equal to zero. In addition, all load transfer mechanisms through this element are temporarily reset. When the finite element is activated, its mass, loads and stiffness return to their original values [1,2].

When modeling the construction stages in the ANSYS software package, the following features should be taken into account: it is necessary to fix the displacements or other degrees of freedom of deactivated finite elements to avoid excessive distortion. With the possible activation of these finite elements, the artificial fixation must be removed; activation and deactivation of the elements occur instantaneously, which is a step nonlinearity (similar to the status of the contact zones) that can cause problems with the numerical convergence of the solution. This problem can be overcome by reducing the number of finite elements to be activated and deactivated at one stage of the solution; when viewing the results, deactivated elements must be excluded to avoid non-physical values [3].

The compiled volumetric design model includes a cylindrical shell and a soil massif. The diameter of the shell D = 3 m, the thickness of the shell t = 0.3 m, the distance between the shell and the left and right sides of the soil massif is $W = 5D$, the distance between the shell and the upper and lower sides of the soil massif is $H = 5D$. The shell consists of 32 separate rings with a width of 1 m, the soil massif at the installation site of the rings is also divided into 32 parts – the activated ring replaces part of the soil massif.

The soil massif is modeled by volumetric elements. Volumetric elements consist of twenty nodes. The shell is modeled by flat elements. Flat elements consist of 4 nodes. Local coordinate systems of shell elements are co-directed for a correct display of results [4,5]. The volumetric design model is shown in Figure 1.

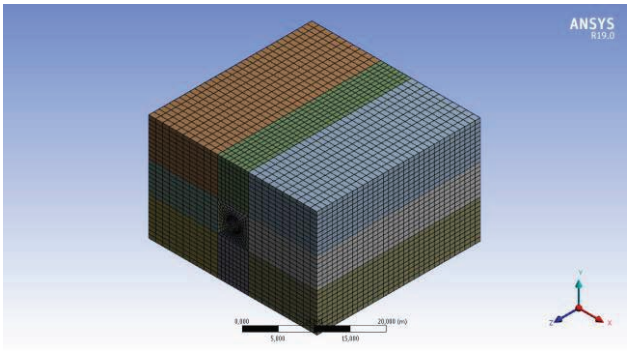

Figure 1. Volumetric design model in ANSYS Mechanical.

The material of the soil massif is presented by an elastic-plastic model of Mohr–Coulomb with the following characteristics: density ρ - 2000 kg/m^3, deformation modulus E_{def} - 10 MPa, Poisson's ratio μ - 0.30, cohesion C_u - 10 kPa, friction angle φ - 25°. The material of the cylindrical shell is presented by a linear-elastic model with the following characteristics: density ρ - 2300 kg/m3, elastic modulus E – 30000 MPa,

Poisson's ratio μ - 0.20. These material models require a physically nonlinear calculation.

The soil massif has constraint on the side faces and on the bottom face. The load consists of the own weight of the soil massif and the shell.

In addition, there is a gap between the shell and the soil massif in the design model, which takes into account the influence of a slurry shield during the construction of the cylindrical shell. Special contact elements CONTAxxx and TARGExxx provide contact interaction between the shell and the soil massif. These elements are located on the surface of the soil massif and the cylindrical shell.

The type of contact nonlinearity is a status change. The contact status (open or closed) determines the stiffness of the system. Contact interaction occurs when the nodes of the bodies come close to a certain distance, which is called “Pinball Radius”. Modeling contact interaction begins with search nodes of bodies that are close to each other. The search can be carried out through the element integration points to ensure increased accuracy [6,7]. The search algorithm for contacting nodes causes high computational complexity, so the search area can be limited. To do this, on the required surface create a contact interface of two types: contact and target.

The next algorithm stage uses the contact and the target areas to calculate the interaction forces of the bodies. The contact forces are usually determined using a method called "Penalty method". This method uses the possibility of surface nodes interpenetration by a small value. The interaction forces $F_{contact}$ depend on the penetration value and the contact stiffness. These forces are applied only to the contact surface and cause its deformation, which reduces the penetration of the surfaces [8,9]. In addition, when determining the penetration value, the thickness of the cylindrical shell is taken into account.

The calculation was done geometrically, structurally and physically nonlinear statement. Constructive nonlinearity appears as a result of changes in the model during its deformation, for example, changing the status of the elements constraints, the "birth" and "death" elements and so on. Constructive nonlinearity should be taken into account when modeling objects in the process of installation and dismantling, when new connections are created; when changing the loading mode or when constraints are turned off [10,11].

There are six design cases in the research work that allows determining the effect of taking into account changes in the design model in time on the stress-strain state of the cylindrical shell. The first design case consists of 33 stages of determining the stress-strain state of the cylindrical shell and the soil massif: the first (zero) stage calculates the natural state of the soil massif without the shell, the next 32 stages calculate the stress-strain state of the model after activating each individual ring of the shell and deactivating part of the soil massif. The second design case consists of 17 stages, as not one, but two rings of the shell are activated in one stage. Thus, the number of rings activated in one stage doubled in each case. There are design cases with 32, 16, 8, 4, 2 and 1 stages of calculation (first stage (zero) calculated the natural state of the soil massif in each design case).

According to the obtained results, the authors carried out a comparative analysis of the equivalent stresses according to the IV strength theory (von Mises) of the cylindrical shell for 1, 4, 8, 12, 16, 20, 24, 28 and 32 rings of cylindrical shell. The stress curves of the cylindrical shell rings depending on the number of stages in the design case are shown in Figures 2 – 10.

It can be seen from the chart that the maximum stresses values of the six design cases are markedly different. Note that in the interval from 4 to 28 ring, starting with the design case, which has 8 stages, a further increase in the number of stages did not lead to significant changes in the maximum stresses values. It is also seen from the chart that the stresses in the first ring of the shell grow significantly in going from the 8-stage design case to the 16 and 32-stage design cases. The stresses in the last ring of the shell reduces significantly in going from the 8-stage design case to the 16 and 32-stage design cases.

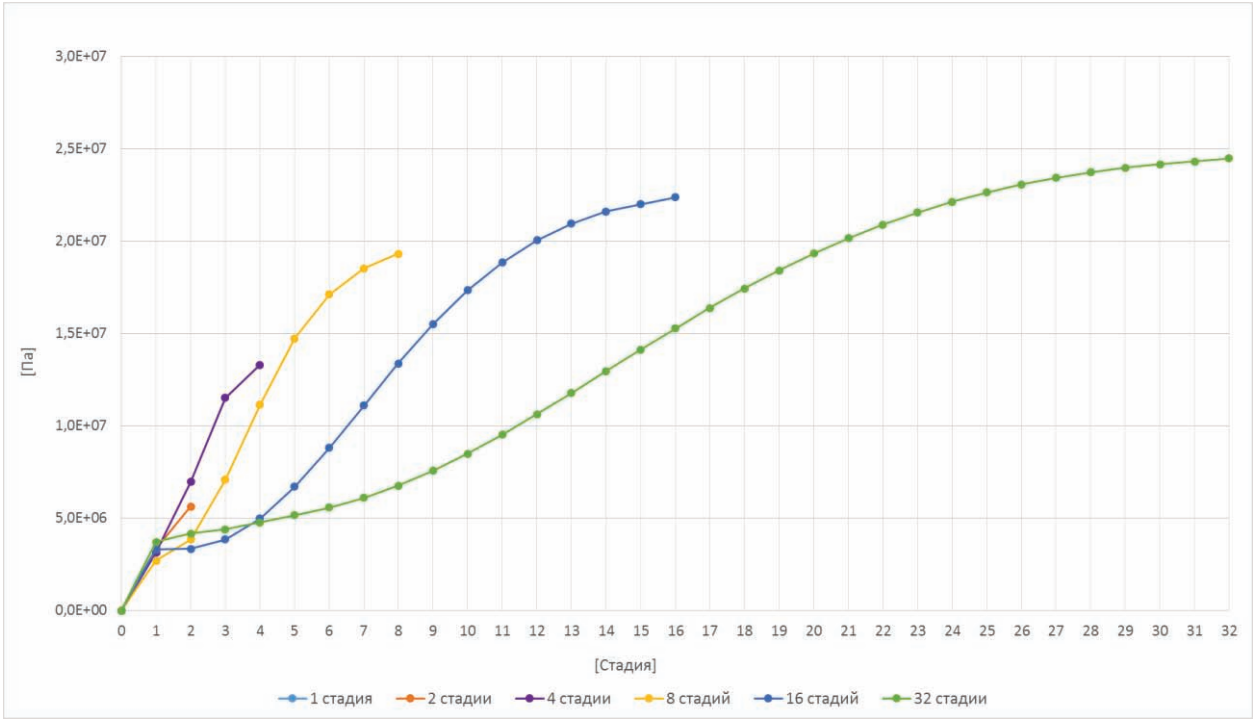

Figure 2. The maximum equivalent stresses according to the IV strength theory (von Mises) of 01 ring of the shell.

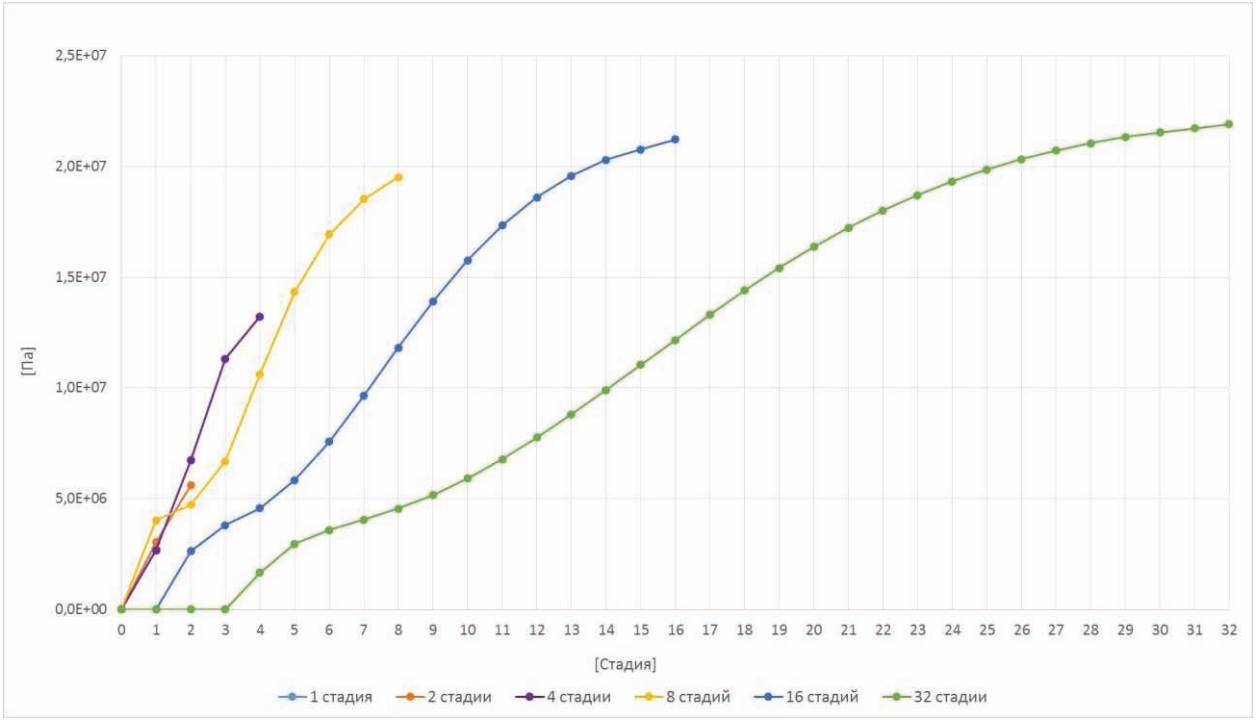

Figure 3. The maximum equivalent stresses according to the IV strength theory (von Mises) of 04 ring of the shell.

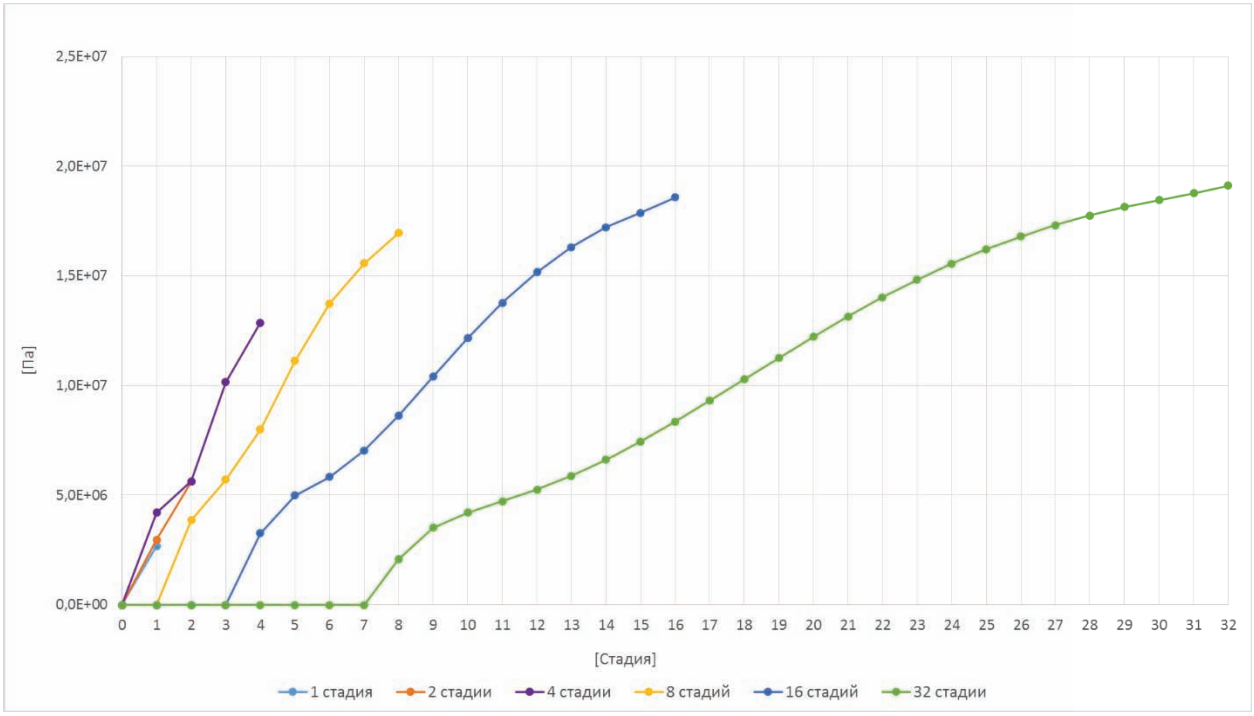

Figure 4. The maximum equivalent stresses according to the IV strength theory (von Mises) of 08 ring of the shell.

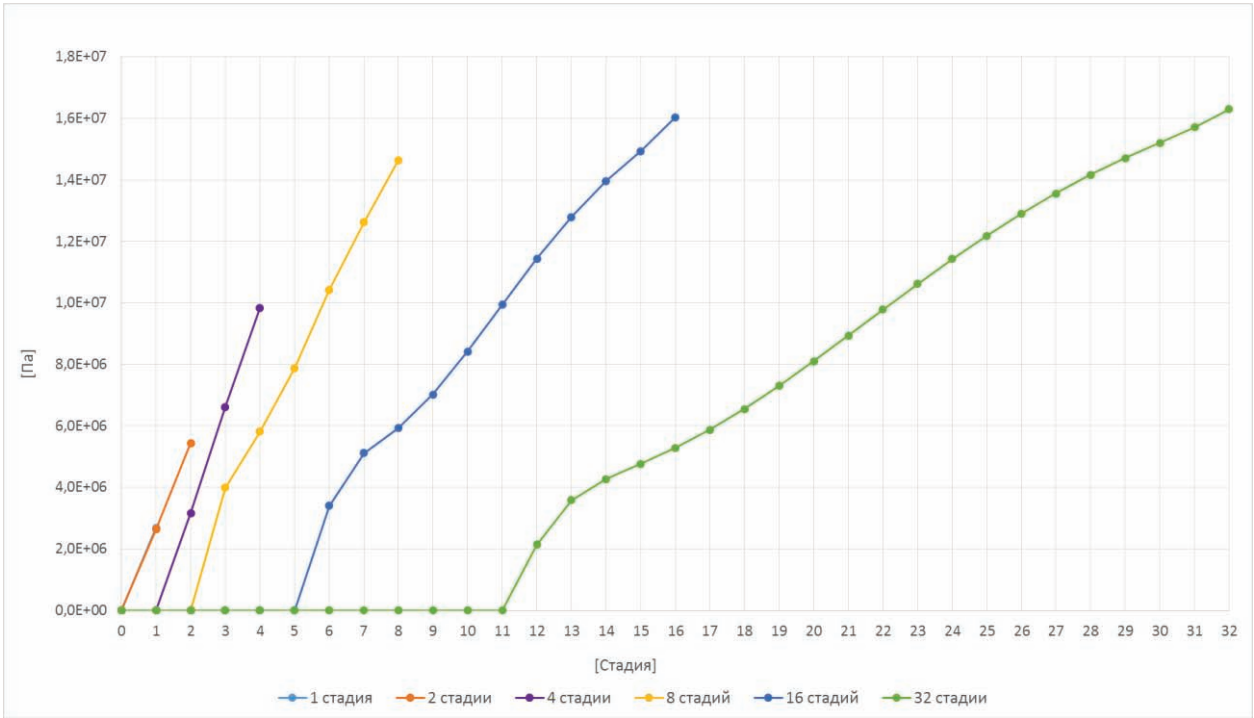

Figure 5. The maximum equivalent stresses according to the IV strength theory (von Mises) of 12 ring of the shell.

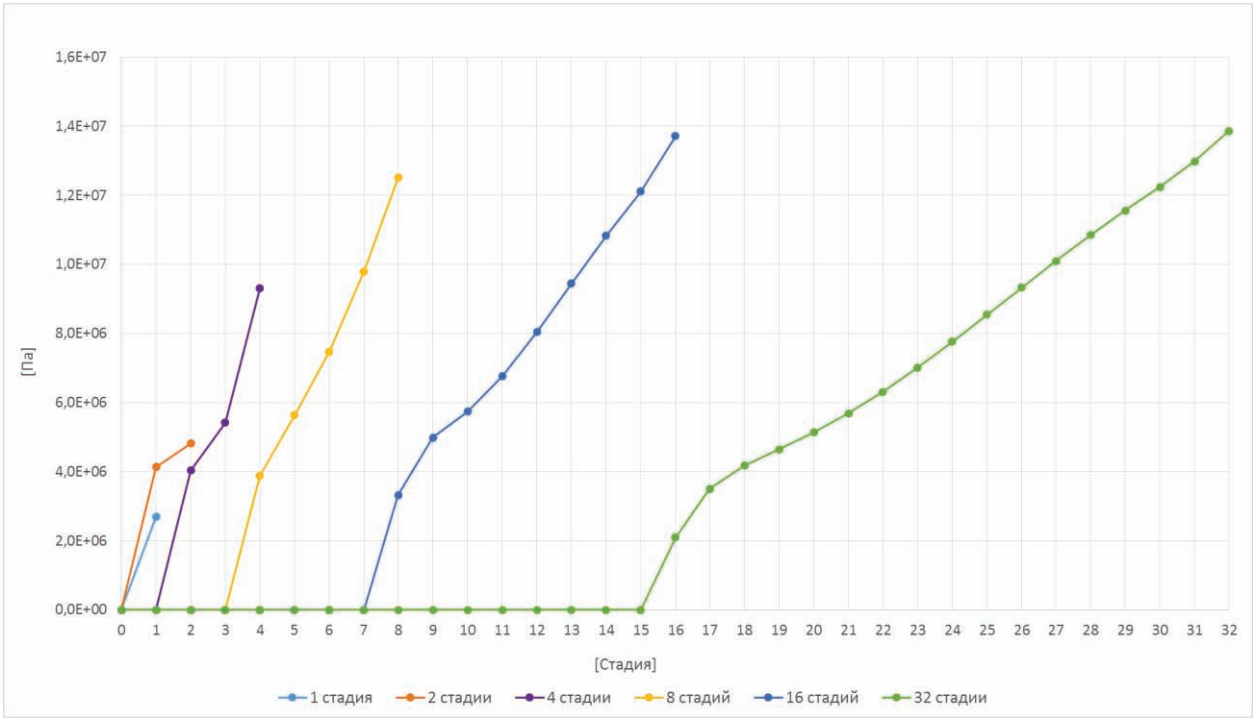

Figure 6. The maximum equivalent stresses according to the IV strength theory (von Mises) of 16 ring of the shell.

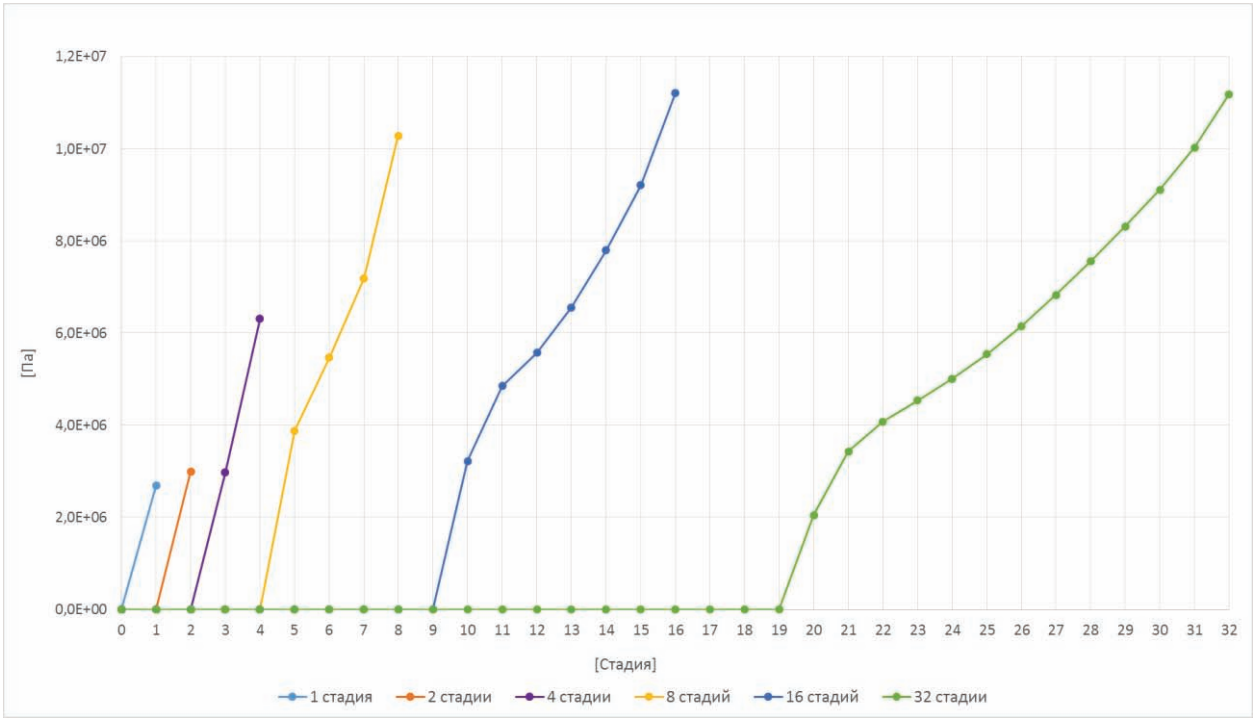

Figure 7. The maximum equivalent stresses according to the IV strength theory (von Mises) of 20 ring of the shell.

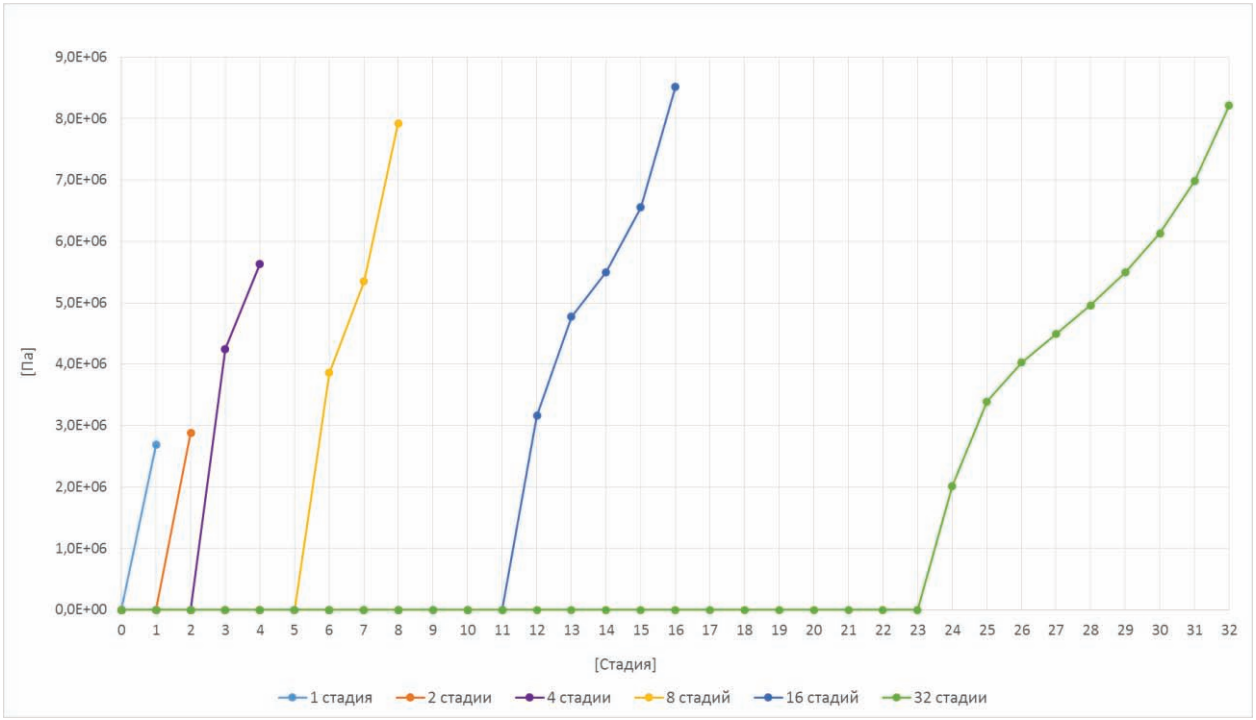

Figure 8. The maximum equivalent stresses according to the IV strength theory (von Mises) of 24 ring of the shell.

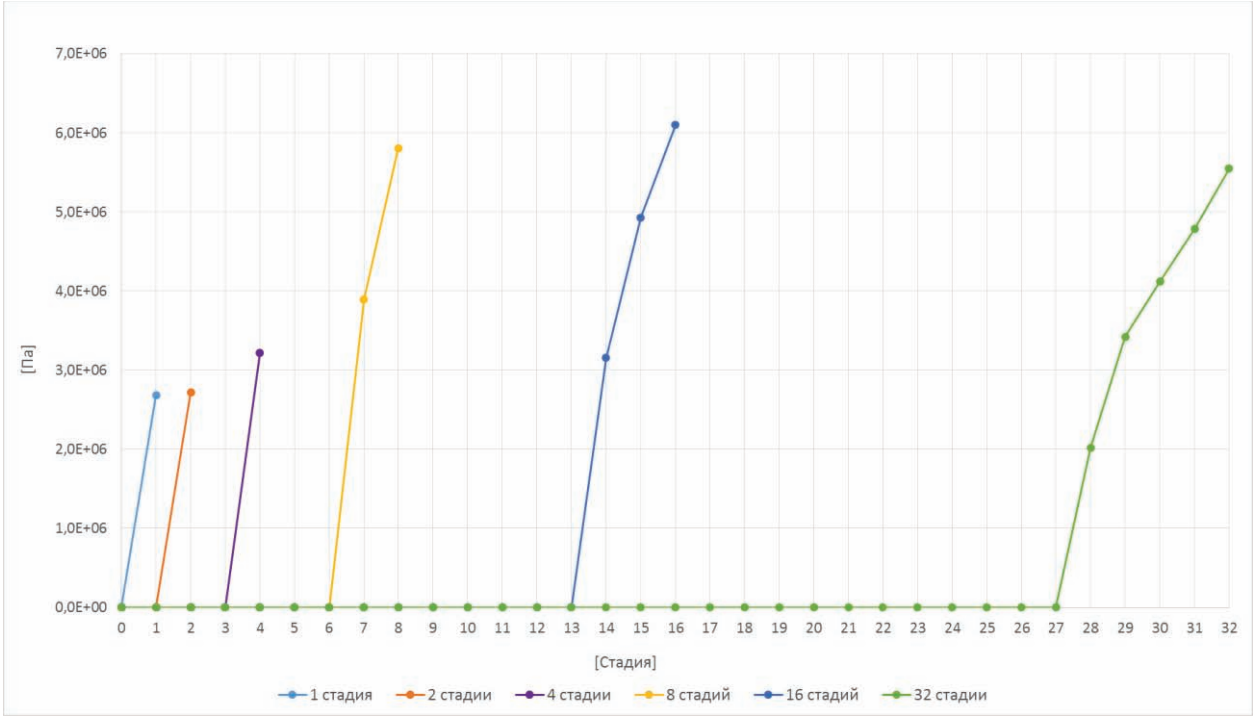

Figure 9. The maximum equivalent stresses according to the IV strength theory (von Mises) of 28 ring of the shell.

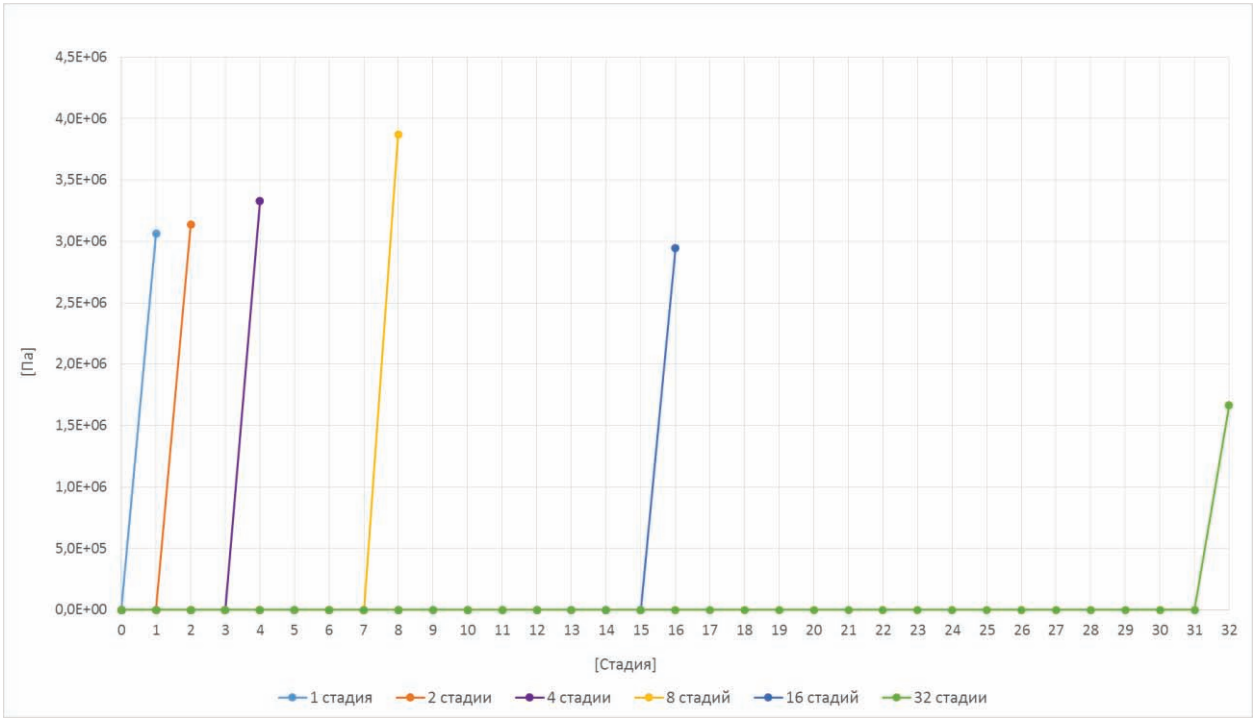

Figure 10. The maximum equivalent stresses according to the IV strength theory (von Mises) of 32 ring of the shell.

This is due to the first ring of the shell (or the first two or the first four rings, depending on the design case) starts to work before the others. The first ring takes most of the loads from the soil massif and the added rings. In the case of the last ring of the shell, conversely, a significant part of the soil massif loads is already redistributed to the activated rings of the shell, so the last ring takes a smaller part of the loads.

It should also be noted that all considered shell rings, except the last one, have significantly underestimated stresses in the design cases, which have less than 8 stages. This is due to the fact that in these cases all the shell rings or a large number of rings are activated in one stage. Therefore, the load from the soil massif is redistributed evenly and there are no residual stresses in the shell rings from the previous stages of calculation.

In Figure 11 are shown the distribution of the maximum equivalent stresses according to the IV strength theory (von Mises) in the shell rings of the design case with 32 stages. The maximum stress values are at the bottom of the shell ring, the minimum stress values are at the sides of the shell.

In table 1 is shown the difference in the percentage of the maximum equivalent stresses according to the IV strength theory (von Mises) [12,13] in the shell rings of all design cases compared to the stresses obtained in the design case with 32 stages.

3. CONCLUSION

The authors consider how the construction stages affect the stress-strain state of the tunnel shell and the soil massif using numerical methods. The volumetric design model of the tunnel shell and the soil massif is made. The calculation consists of several stages from the beginning of the tunnel shell construction to the end of the work.

The results showed that the account of the construction stages in the design model significantly affects the stress-strain state of the shell and the soil massif. In design cases, which have less than 8 stages, the maximum equivalent stresses according to the IV strength theory (von Mises) in the vast majority of shell rings are significantly underestimated.

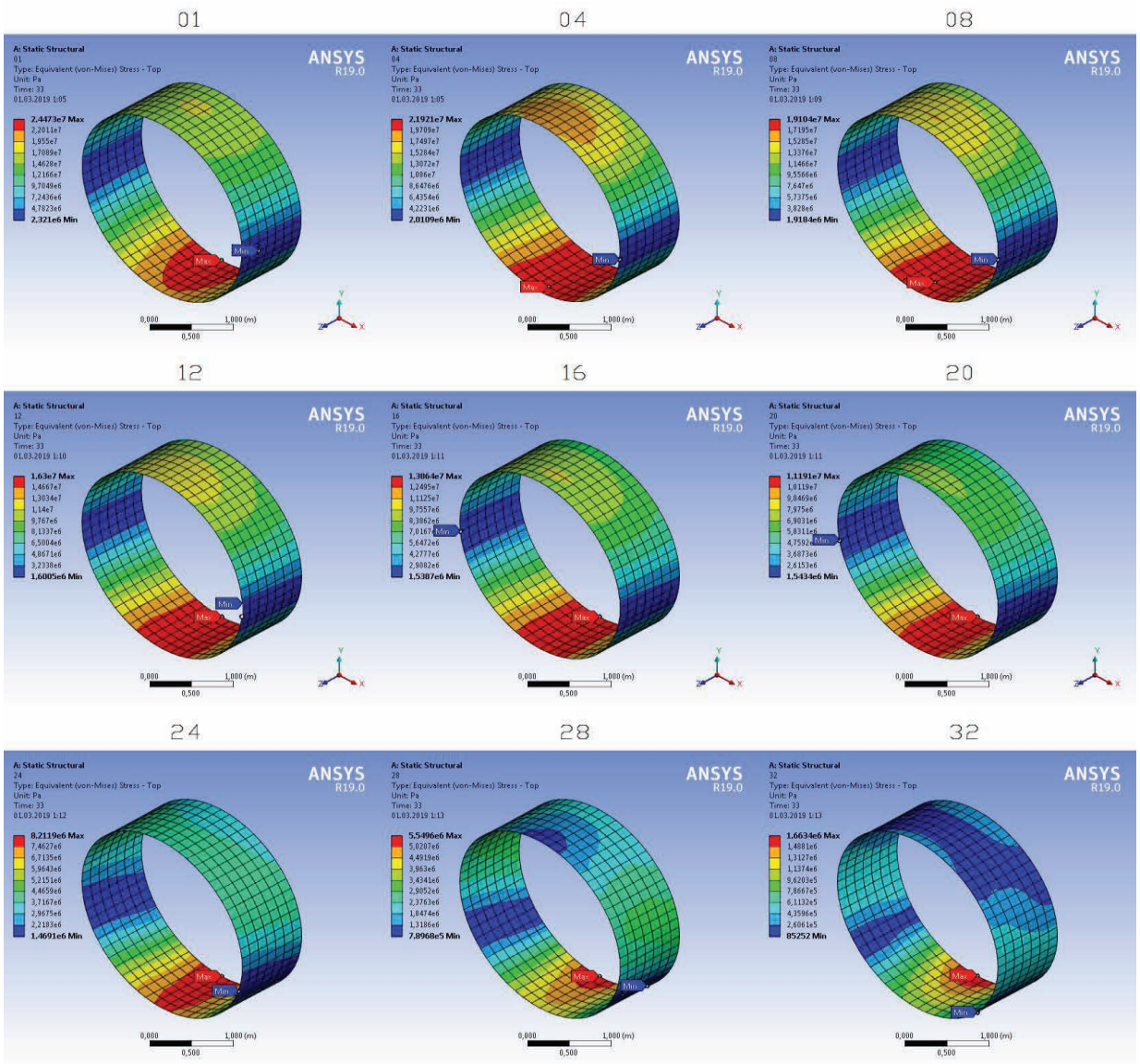

Figure 11. The distribution of the maximum equivalent stresses according to the IV strength theory (von Mises) in the shell rings of the design case with 32 stages.

Table 1. The difference in the percentage of the maximum equivalent stresses according to the IV strength theory (von Mises).

Shell ring	1 stage	2 stages	4 stages	8 stages	16 stages
1	682,2 %	334,6 %	84,0 %	26,7 %	9,4 %
4	713,9 %	291,6 %	65,7 %	12,3 %	3,3 %
8	610,7 %	240,5 %	48,6 %	12,7 %	2,8 %
12	506,5 %	199,8 %	65,7 %	11,4 %	1,6 %
16	415,8 %	187,6 %	48,8 %	10,8 %	1,1 %
20	316,3 %	273,5 %	77,4 %	8,8 %	- 0,3 %
24	205,6 %	184,9 %	45,7 %	3,7 %	-3,6 %
28	106,7 %	104,0 %	72,3 %	-4,4 %	-9,0 %
32	-45,7 %	-46,9 %	-50,0 %	-57,0 %	-43,6 %

This is due to the fact that in these cases all the shell rings or a large number of rings are activated in one stage. Therefore, the load from the soil massif is redistributed evenly and there are no residual stresses in the shell rings from the previous stages of calculation.

Therefore, on account of the results obtained from the six design cases of the volumetric model taking into account the construction stages, the authors recommend in practical calculations to take 8 or more stages of the shell construction. It is permissible to take no more than 8 stages due to the complexity and time costs of calculations. However, it is worth noting that in the first and last rings of the shell the maximum equivalent stresses will be underestimated and overstated respectively.

The results showed that the account of the construction stages in the design model significantly affects the stress-strain state of the shell and the soil massif. In design cases, which have less than 8 stages, the maximum equivalent stresses according to the IV strength theory (von Mises) in the vast majority of shell rings are significantly underestimated. This is due to the fact that in these cases all the shell rings or a large number of rings are activated in one stage. Therefore, the load from the soil massif is redistributed evenly and there are no residual stresses in the shell rings from the previous stages of calculation.

Therefore, on account of the results obtained from the six design cases of the volumetric model taking into account the construction stages, the authors recommend in practical calculations to take 8 or more stages of the shell construction. It is permissible to take no more than 8 stages due to the complexity and time costs of calculations. However, it is worth noting that in the first and last rings of the shell the maximum equivalent stresses will be underestimated and overstated respectively.

REFERENCES

1. **Alexandrov A.V., Potapov V.D.** Osnovy teorii uprugosti i plastichnosti [Foundations of the theory of elasticity and plasticity]. Moscow, High school, 1990, 400 pages (in Russian).
2. **Bate K., Wilson E.** Chislennye metody analiza i metod konechnyh jelementov [Numerical analysis methods and finite element method]. Moscow, Stroizdat, 1982, 446 pages (in Russian).
3. **Gallagher R.** Metod konechnyh jelementov. Osnovy [The finite element method. Basics]. Moscow, Mir, 1984. 429 pages (in Russian).
4. **Kositsyn S.B., Dolotkazin D.B.** Raschet sterzhnevyh sistem, vzaimodejstvujushhih s uprugim osnovaniem, metodom konechnyh jelementov s ispol'zovaniem programmnogo kompleksa MSC/NASTRAN FOR WINDOWS [Calculation of beam systems interacting with an elastic foundation by finite element method using the software complex MSC/NASTRAN FOR WINDOWS]. Moscow, MIIT, 2004, 116 pages (in Russian).
5. **Kositsyn S.B., Tran Xuan Linh.** Chislennyj analiz naprjazhenno-deformirovannogo sostojanija ortogonal'no peresekajushhihsja cilindricheskih obolochek bez ucheta i s uchetom ih odnostoronnego vzaimodejstvija s okruzhajushhim massivom grunta [Numerical analysis of stress – strain state of orthogonal intersecting cylindrical shells with and without taking into account their unilateral interaction with the surrounding soil]. // *International Journal for Computational Civil and Structural Engineering*, 2014, Volume 10, Issue 1, pp. 72-78 (in Russian).
6. **Perelmuter A.V., Slivker V.I.** Raschetnye modeli sooruzhenij i vozmozhnosti ih analiza [Design models of structures and possibilities of their analysis]. Kiev, Steel, 2002, 445 pages (in Russian).
7. **Prevo R.** Raschet na prochnost' truboprovodov zalozhennyh v grunt [Strength calculation of pipelines laid in the

ground]. Moscow, Stroyizdat, 1964, 123 pages (in Russian).
8. **Strang G., Fix J.** Teorija metoda konechnyh jelementov [Theory of the finite element method]. Moscow, Mir, 1977, 349 pages (in Russian).
9. **Shaposhnikov N.N.** Raschet krugovyh tonnel'nyh obdelok na uprugom osnovanii, harakterizuemom dvumja kojefficientami posteli [Calculation of circular tunnel linings in elastic foundation characterized by the two coefficients of elastic foundation]. // *Scientific Proc. of Moscow state university of railway engineering*, 1961, Issue 131, pp. 296-305 (in Russian).
10. **Attewell P.B.** Ground movements caused by tunnelling in soil. Large ground movements and structures. London, Pentech Press, 1978, pp. 120-140.
11. **Attewell P.B., Woodman J.P.** Predicting the dynamics of ground settlement and its derivatives caused by tunneling in soil. // *Ground Engineering*, 1982, pp. 75-83.
12. **Broms B.B., Bennermark H.** Stability of clay in vertical openings. // *Journal of Soil Mechanics and Foundations*, ASCE, 1967, 193 pages.
13. **Zienkiewicz O.C., Taylor R.L.** The finite element method. Volume 2: Solid mechanics. Butterworth-Heinemann, 2000, 479 pages.

СПИСОК ЛИТЕРАТУРЫ

1. **Александров А.В., Потапов В.Д.** Основы теории упругости и пластичности. – М.: Высшая школа, 1990. – 400 с.
2. **Бате К., Вилсон Е.** Численные методы анализа и метод конечных элементов. – М.: Стройиздат, 1982. – 446 с.
3. **Галлагер Р.** Метод конечных элементов. Основы. – М.: Мир, 1984. – 429 с.
4. **Косицын С.Б., Долотказин Д.Б.** Расчет стержневых систем, взаимодействующих с упругим основанием, методом конечных элементов с использованием программного комплекса MSC/NASTRAN FOR WINDOWS. – М.: МИИТ, 2004 – 116 с.
5. **Косицын С.Б., Чан Суан Линь.** Численный анализ напряженно-деформированного состояния ортогонально пересекающихся цилиндрических оболочек без учета и с учетом их одностороннего взаимодействия с окружающим массивом грунта. // *International Journal for Computational Civil and Structural Engineering*, 2014, Volume 10, Issue 1, pp. 72-78.
6. **Перельмутер А.В., Сливкер В.И.** Расчетные модели сооружений и возможности их анализа. – Киев: Сталь, 2002. – 445 с.
7. **Прево Р.** Расчет на прочность трубопроводов заложенных в грунт. – М.: Стройиздат, 1964. – 123 с.
8. **Стренг Г., Фикс Дж.** Теория метода конечных элементов. – М.: Мир, 1977, 349 с.
9. **Шапошников Н.Н.** Расчет круговых тоннельных обделок на упругом основании, характеризуемом двумя коэффициентами постели. // Научн. тр. Московского института инженеров железнодорожного транспорта, 1961, Вып. 131, с. 296-305.
10. **Attewell P.B.** Ground movements caused by tunnelling in soil. Large ground movements and structures. London, Pentech Press, 1978, pp. 120-140.
11. **Attewell P.B., Woodman J.P.** Predicting the dynamics of ground settlement and its derivatives caused by tunneling in soil. // *Ground Engineering*, 1982, pp. 75-83.
12. **Broms B.B., Bennermark H.** Stability of clay in vertical openings. // *Journal of Soil Mechanics and Foundations*, ASCE, 1967, 193 pages.
13. **Zienkiewicz O.C., Taylor R.L.** The finite element method. Volume 2: Solid

mechanics. Butterworth-Heinemann, 2000, 479 pages.

Sergey B. Kosytsyn, Advisor of the Russian Academy of Architecture and Construction Sciences (RAASN), Dr. Sc., Professor, Head of Department of Theoretical Mechanics, Russian University of Transport (MIIT); 9b9, Obrazcova Street, Moscow, 127994, Russia;
phone/fax: +7(499) 978-16-73;
E-mail: kositsyn-s@yandex.ru, kositsyn-s@mail.ru.

Vladimir Y. Akulich, PhD student of Department of Theoretical Mechanics, Russian University of Transport (MIIT); 9b9, Obrazcova Street, Moscow, 127994, Russia;
phone/fax: +7(499) 978-16-73;
E-mail: 79859670635@yandex.ru.

Косицын Сергей Борисович, советник РААСН, доктор технических наук, профессор; заведующий кафедрой «Теоретическая механика», Российский университет транспорта (МИИТ); 127994, Россия, г. Москва, ул. Образцова, 9, стр. 9; тел./факс +7(499) 978-16-73;
E-mail: kositsyn-s@yandex.ru, kositsyn-s@mail.ru

Акулич Владимир Юрьевич, аспирант кафедры «Теоретическая механика», Российский университет транспорта (МИИТ); 127994, Россия, г. Москва, ул. Образцова, 9, стр. 9; тел./факс +7(499) 978-16-73;
E-mail: 79859670635@yandex.ru.

DOI:10.22337/2587-9618-2019-15-3-96-108

WAVELET-BASED DISCRETE-CONTINUAL FINITE ELEMENT PLATE ANALYSIS WITH THE USE OF DAUBECHIES SCALING FUNCTIONS

Marina L. Mozgaleva [1]***, Pavel A. Akimov*** [2, 3, 4, 5]***, Taymuraz B. Kaytukov*** [2, 6]

[1] National Research Moscow State University of Civil Engineering, Moscow, RUSSIA
[2] Russian Academy of Architecture and Building Sciences, Moscow, RUSSIA
[3] Scientific Research Center "StaDyO", Moscow, RUSSIA
[4] Tomsk State University of Architecture and Civil Engineering, Tomsk, RUSSIA
[5] Peoples' Friendship University of Russia, Moscow, RUSSIA
[6] Central Institute for Research and Design of the Ministry of Construction and Housing and Communal Services of the Russian Federation, Moscow, RUSSIA

Abstract: The distinctive paper is detoded to special version of wavelet-based discrete-continual finite element method of plate analysis. Daubechies scaling functions are used within this version. Its field of application comprises plates with constant (generally piecewise constant) physical and geometrical parameters along one direction (so-called "basic" direction). Modified continual operational formulation of the problem with the use of the method of extended domain (proposed by A.B. Zolotov) is presented. Corresponding discrete-continual formulation is given as well. Brief information about computer implementation of the method with the use of MATLAB software is provided. Besides numerical sample of analysis of thin plate is considered.

Keywords: boundary problem, structural analysis, plate analysis, thin plate, numerical solution, wavelet-based discrete-continual finite element method, wavelet analysis, Daubechies scaling function, Daubechies wavelet

ВЕЙВЛЕТ-РЕАЛИЗАЦИЯ ДИСКРЕТНО-КОНТИНУАЛЬНОГО МЕТОДА КОНЕЧНЫХ ЭЛЕМЕНТОВ ДЛЯ РАСЧЕТА ПЛИТ С ИСПОЛЬЗОВАНИЕМ МАСШТАБИРУЮЩИХ ФУНКЦИЙ ДОБЕШИ

М.Л. Мозгалева [1]***, П.А. Акимов*** [2, 3, 4, 5]***, Т.Б. Кайтуков*** [2, 6]

[1] Национальный исследовательский Московский государственный строительный университет, г. Москва, РОССИЯ
[2] Российская академия архитектуры и строительных наук, г. Москва, РОССИЯ
[3] Научно-исследовательский центр СтаДиО, г. Москва, РОССИЯ
[4] Томский государственный архитектурно-строительный университет, г. Томск, РОССИЯ
[5] Российский университет дружбы народов, г. Москва, РОССИЯ
[6] Центральный научно-исследовательский и проектный институт Министерства строительства и жилищно-коммунального хозяйства, г. Москва, РОССИЯ

Аннотация: Настоящая статья посвящена одной специальной версии вейвлет-реализации дискретно-континуального метода конечных элементов для расчета плитных конструкций. В рамках указанной версии используются масштабирующие функции Добеши. Область применения данного метода составляют пластины с постоянными (в общем случае кусочно-постоянными) физико-геометрическими параметрами по одному из направлений (это так называемое «основное» направление). В статье приведена преобразованная континуальная постановка задачи с использованием аппарата метода расширенной области, предложенного А.Б. Золотовым. Кроме того, здесь представлены соответствующая дискретно-контиунальная постановка, краткие сведения о компьютерной реализации метода с использованием системы MATLAB, а также пример расчета.

Ключевые слова: краевая задача, расчеты строительных конструкций, расчет пластин, тонкая пластина, численное решение, вейвлет-реализация дискретно-континуального метода конечных элементов, вейвлет-анализ, масштабирующая функция Добеши, вейвлет Добеши

As is known wavelet analysis has the desirable advantages of multi-resolution properties and various basis functions, which fulfill an enormous potential fo rsolving partial differential equations. The distinctive paper is devoted to further development of wavelet-based discrete-continual finite element method of structural analysis. Particularly problems of plate analysis with the use of Daubechies scaling functions [1-29] are under consideration.

1. CONTINUAL FORMULATION OF PROBLEM

Let x_1, x_2 are cartesian coordinates. Besides, let x_2 be coordimate corresponding to "basic" direction of plate (i.e. direction along which physical and geometrical parameters of plate are constant). It is is necessary to note that physical and geometrical parameters of plate can be changed arbitrarily along x_1. Let us consider the following domain occupied by plate:

$$\Omega = \{ (x_1, x_1) : \ 0 < x_1 < \ell_1, \ \ 0 < x_2 < \ell_2 \}. \quad (1.1)$$

Operational formulation of coorresponding boundary problem of plate analysis (Kirghoff model) at extended domain [30], embordering considering structure has the form:

$$L\, y = \widetilde{F}, \quad 0 \le x_1 \le \ell_1, \quad 0 \le x_2 \le \ell_2, \quad (1.2)$$

where y is plate deflection in domain Ω; L is the operator of the considering problem; $\widetilde{F}$ is the corresponding right-side function;

$$L = -L_4\, \partial_2^4 + L_2\, \partial_2^2 + L_0; \quad (1.3)$$

$$L_4 = \theta D; \quad (1.4)$$

$$L_2 = -[\partial_1^2 \theta D \nu + 2\partial_1 D(1-\nu)\partial_1 + \theta D \nu \partial_1^2]; \quad (1.5)$$

$$L_0 = -\partial_1^2 \theta D \partial_1^2; \quad (1.6)$$

$$\widetilde{F} = \theta F + \delta_\Gamma f; \quad (1.7)$$

$$\partial_j = \partial / \partial x_j, \ \ \partial_j^* = -\partial / \partial x_j, \ \ j = 1, 2; \quad (1.8)$$

$\overline{F}$ is the force in domain Ω; $\bar{f}_k$ is the boundary force at $\Gamma = \partial\Omega$; D, ν are plate modulus and Poison's ratio in domain Ω;

$$D = Eh^3 / [12(1-\nu^2)]; \quad (1.9)$$

h is plate thickness in domain Ω;

$$\theta = \theta(x_1, x_2) = \begin{cases} 1, & (x_1, x_2) \in \Omega \\ 0, & (x_1, x_2) \notin \Omega; \end{cases} \quad (1.10)$$

is the characteristic function of domain Ω [30];

$$\delta_\Gamma = \delta_\Gamma(x_1, x_2) = \frac{\partial \theta}{\partial \overline{n}}; \quad (1.11)$$

is the delta-function of border $\Gamma = \partial\Omega_k$; $\overline{n} = [\, n_1 \ \ n_2 \,]^T$ is unit normal vector of domain boundary $\Gamma = \partial\Omega$ [30];
Let us introduce the following notation [4,7-15]:

$$y_1 = y, \quad y_2 = \partial_2 y = y_1', \quad y_3 = \partial_2^2 y = y_2', \quad y_4 = \partial_2^3 y = y_3'. \quad (1.12)$$

Therefor we can rewrite (1.2) in the form

$$-L_4 y_4' + L_2 y_3 + L_0 y_1 = \widetilde{F}. \quad (1.13)$$

Taking into account (1.12) and (1.13), we get

$$\begin{Vmatrix} y_1' \\ y_2' \\ y_3' \\ y_4' \end{Vmatrix} = \begin{Vmatrix} 0 & 1 & 0 & 0 \\ 0 & 0 & 1 & 0 \\ 0 & 0 & 0 & 1 \\ L_4^{-1} L_0 & 0 & L_4^{-1} L_2 & 0 \end{Vmatrix} \begin{Vmatrix} y_1 \\ y_2 \\ y_3 \\ y_4 \end{Vmatrix} = \begin{Vmatrix} 0 \\ 0 \\ 0 \\ -L_4^{-1} \widetilde{F} \end{Vmatrix}. \quad (1.14)$$

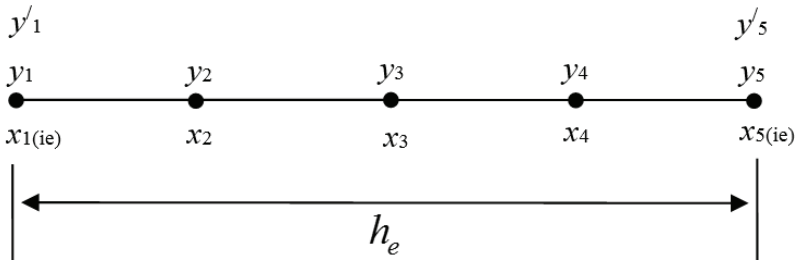

Figure 1. Approximation on the element.

We can also rewrite (1.14) in matrix form

$$\overline{U}' = \widetilde{L}\overline{U} + \overline{\overline{F}}, \qquad (1.15)$$

where

$$\widetilde{L} = \begin{bmatrix} 0 & 1 & 0 & 0 \\ 0 & 0 & 1 & 0 \\ 0 & 0 & 0 & 1 \\ L_4^{-1}L_0 & 0 & L_4^{-1}L_2 & 0 \end{bmatrix}; \qquad (1.16)$$

$$\overline{\overline{F}} = \begin{bmatrix} 0 \\ 0 \\ 0 \\ -L_4^{-1}\widetilde{F} \end{bmatrix}; \quad \overline{U} = \begin{bmatrix} y_1 \\ y_2 \\ y_3 \\ y_4 \end{bmatrix}; \qquad (1.17)$$

Besides, the system of equations (1.15) is supplemented by the boundary conditions that are specified in sections with coordinates (coordinates of boundary points)

$$x_{2,1}^b = 0, \quad x_{2,2}^b = \ell_2. \qquad (1.18)$$

2. DISCRETE-CONTINUAL FORMULATION OF PROBLEM

The discrete component of the numerical solution is represented by the direction along the axis x_1. Fulfillment on an element (interval) for all components of the vector-function $\overline{U}$ is the same. Therefore, for simplicity let us denote locally in this paragraph

$$x = x_1, \quad \ell = \ell_1, \quad y = y_j \qquad (2.1)$$

for all $j = 1,2,3,4$. We can divide the interval $[0, \ell]$ into N_e parts (elements) and $h_e = \ell / N_e$ is the length of each element. Besides, we can divide each element into N_k parts (for instance, sample with $N_k = 4$ is presented in Fig. 1. Let us use the following notation: i_e is the number of the element; $x_1(i_e)$ is the coordinate of the starting point; $x_5(i_e)$ is the coordinate of the end point of the ith element. Let y_i and $y_i' = \partial_1 y(x_i)$ be unknowns at boundary points ($i = 1,5$). Let y_i be unknown internal points ($i = 2,3,4$). Thus, the total number of unknowns on an element with such discretization is equal to $N = N_k - 1 + 2 \cdot 2 = N_k + 3 = 7$.

Let us introduce the local coordinate within the element:

$$t = \frac{x - x_{1(i_e)}}{h_e}, \quad x_{1(i_e)} \le x \le x_{5(i_e)}. \qquad (2.2)$$

Thus, we have the following formulas:

$$\begin{cases} x = x_{1(i_e)} \Rightarrow t = 0 \\ x = x_2 \Rightarrow t = 0.25 \\ x = x_3 \Rightarrow t = 0.5 \\ x = x_4 \Rightarrow t = 0.75 \\ x = x_{5(i_e)} \Rightarrow t = 1; \end{cases} \qquad (2.3)$$

$$\frac{d}{dx} = \frac{d}{dt} \cdot \frac{dt}{dx} = \frac{1}{h_e}\frac{d}{dt}; \quad \frac{d^p}{dx^p} = \frac{1}{h_e^p}\frac{d^p}{dt^p}; \qquad (2.4)$$

$$dx = h_e \cdot dt. \tag{2.5}$$

In order to construct local stiffness matrices corresponding to continual operators (1.6), (1.5) and (1.4) let us consider bilinear forms taking into account relations (2.3)-(2.5):

$$\begin{aligned} B_0(y,z) &= < L_0 y, z > = \\ &= -\int_{x_{1(i_e)}}^{x_{5(i_e)}} \frac{d^2}{dx^2}\theta D \frac{d^2 y}{dx^2}\cdot z\, dx = \\ &= -\theta_{i_e} D_{i_e} \int_{x_{1(i_e)}}^{x_{5(i_e)}} \frac{d^2 y}{dx^2}\cdot\frac{d^2 z}{dx^2} dx = \\ &= -\frac{1}{h_e^3}\theta_{i_e} D_{i_e} \int_0^1 \frac{d^2 w}{dt^2}\cdot\frac{d^2 v}{dt^2} dt = \\ &= B_0(w,v); \end{aligned} \tag{2.6}$$

$$\begin{aligned} B_4(y,z) &= < L_4 y, z > = \\ &= \theta_{i_e} D_{i_e} \int_{x_{1(i_e)}}^{x_{5(i_e)}} y\cdot z\, dx = \\ &= h_e \theta_{i_e} D_{i_e} \int_0^1 w\cdot v\, dt = B_4(w,v); \end{aligned} \tag{2.7}$$

$$\begin{aligned} B_2(y,z) &= < L_2 y, z > = \\ &= < L_{21} y, z > + < L_{22} y, z > + \\ &+ < L_{23} y, z >, \end{aligned} \tag{2.8}$$

where

$$\begin{aligned} < L_{21} y, z > &= -\theta_{i_e} D_{i_e} \nu_{i_e} \int_{x_{1(i_e)}}^{x_{5(i_e)}} \frac{d^2 y}{dx^2} z\, dx = \\ &= -\frac{1}{h_e}\theta_{i_e} D_{i_e} \nu_{i_e} \int_0^1 \frac{d^2 w}{dt^2}\cdot v\, dt = \\ &= B_{21}(w,v); \end{aligned} \tag{2.9}$$

$$\begin{aligned} < L_{23} y, z > &= -\theta_{i_e} D_{i_e} \nu_{i_e} \int_{x_{1(i_e)}}^{x_{5(i_e)}} y\cdot\frac{d^2 z}{dx^2} dx = \\ &= -\frac{1}{h_e}\theta_{i_e} D_{i_e} \nu_{i_e} \int_0^1 w\cdot\frac{d^2 v}{dt^2} dt = \\ &= B_{23}(w,v); \end{aligned} \tag{2.10}$$

$$\begin{aligned} < L_{22} y, z > &= -2\int_{x_{1(i_e)}}^{x_{5(i_e)}} \frac{d}{dx}\theta D(1-\nu)\frac{dy}{dx}\cdot z\, dx = \\ &= 2\theta_{i_e} D_{i_e}(1-\nu_{i_e}) \int_{x_{1(i_e)}}^{x_{5(i_e)}} \frac{dy}{dx}\cdot\frac{dz}{dx} dx = \\ &= \frac{1}{h_e} 2\theta_{i_e} D_{i_e}(1-\nu_{i_e}) \int_0^1 \frac{dw}{dt}\cdot\frac{dv}{dt} dt = \\ &= B_{22}(w,v) \end{aligned} \tag{2.11}$$

$$y(x) = w(t) = \sum_{k=0}^{N-1} \alpha_k \varphi(t+k),$$

$$x_{1(i_e)} \le x \le x_{5(i_e)}, \quad 0 \le t \le 1; \tag{2.12}$$

$$z(x) = v(t) = \sum_{k=0}^{N-1} \beta_k \varphi(t+k),$$

$$x_{1(i_e)} \le x \le x_{5(i_e)}, \quad 0 \le t \le 1; \tag{2.13}$$

$\varphi(s)$ is Daubechies scaling function,

$$[0,\ N] \subseteq \operatorname{sup\,p}\varphi.$$

Thus, we can substitute (2.12), (2.13) sequentially in (2.6)-(2.11):

$$\begin{aligned} B_0(w,v) &= -\frac{1}{h_e^3}\theta_{i_e} D_{i_e} \int_0^1 \frac{d^2 w}{dt^2}\cdot\frac{d^2 v}{dt^2} dt = \\ &-\frac{\theta_{i_e} D_{i_e}}{h_e^3} \sum_{i=0}^{N-1}\sum_{j=0}^{N-1} \alpha_i \beta_j \int_0^1 \varphi''(t+i)\varphi''(t+j)\, dt = \\ &= -\frac{\theta_{i_e} D_{i_e}}{h_e^3}(K^0_{\alpha\beta}\overline{\alpha}, \overline{\beta}), \end{aligned} \tag{2.14}$$

where

$$K^0_{\alpha\beta}(i,j) = \int_0^1 \varphi''(t+i)\varphi''(t+j)\, dt, \quad \varphi'' = \frac{d^2\varphi}{dt^2}; \tag{2.15}$$

$$\begin{aligned} B_4(w,v) &= h_e\theta_{i_e} D_{i_e} \int_0^1 w\cdot v\, dt = \\ &= \theta_{i_e} D_{i_e} h_e \sum_{i=0}^{N-1}\sum_{j=0}^{N-1} \alpha_i \beta_j \int_0^1 \varphi(t+i)\varphi(t+j)\, dt = \\ &= h_e\theta_{i_e} D_{i_e}(K^4_{\alpha\beta}\overline{\alpha}, \overline{\beta}); \end{aligned} \tag{2.16}$$

$$\theta_{i_e} D_{i_e} h_e \sum_{i=0}^{N-1}\sum_{j=0}^{N-1}\alpha_i\beta_j\int_0^1 \varphi(t+i)\varphi(t+j)\,dt = \\ = h_e\theta_{i_e} D_{i_e}(K^4_{\alpha\beta}\overline{\alpha},\overline{\beta}), \tag{2.17}$$

where

$$K^4_{\alpha\beta}(i,j) = K^4_{\alpha\beta}(i,j) = \int_0^1 \varphi(t+i)\varphi(t+j)\,dt; \tag{2.18}$$

$$B_{21}(w,v) = -\frac{1}{h_e}\theta_{i_e} D_{i_e}\nu_{i_e}\int_0^1 \frac{d^2w}{dt^2}\cdot v\,dt = \\ = -\frac{\theta_{i_e} D_{i_e}\nu_{i_e}}{h_e}\sum_{i=0}^{N-1}\sum_{j=0}^{N-1}\alpha_i\beta_j\int_0^1 \varphi''(t+i)\varphi(t+j)\,dt = \\ = -\frac{\theta_{i_e} D_{i_e}\nu_{i_e}}{h_e}(K^{21}_{\alpha\beta}\overline{\alpha},\overline{\beta}), \tag{2.19}$$

where

$$K^{21}_{\alpha\beta}(i,j) = \int_0^1 \varphi''(t+i)\varphi(t+j)\,dt; \tag{2.20}$$

$$B_{23}(w,v) = -\frac{1}{h_e}\theta_{i_e} D_{i_e}\nu_{i_e}\int_0^1 w\cdot\frac{d^2v}{dt^2}\,dt = \\ = -\frac{\theta_{i_e} D_{i_e}\nu_{i_e}}{h_e}\sum_{i=0}^{N-1}\sum_{j=0}^{N-1}\alpha_i\beta_j\int_0^1 \varphi(t+i)\varphi''(t+j)\,dt = \\ = -\frac{\theta_{i_e} D_{i_e}\nu_{i_e}}{h_e}(K^{23}_{\alpha\beta}\overline{\alpha},\overline{\beta}), \tag{2.21}$$

where

$$K^{23}_{\alpha\beta}(i,j) = \int_0^1 \varphi(t+i)\varphi''(t+j)\,dt = K^{21}_{\alpha\beta}(j,i); \tag{2.22}$$

$$B_{22}(w,v) = \frac{1}{h_e}2\theta_{i_e} D_{i_e}(1-\nu_{i_e})\int_0^1 \frac{dw}{dt}\cdot\frac{dv}{dt}\,dt = \\ = 2\frac{\theta_{i_e} D_{i_e}(1-\nu_{i_e})}{h_e}\times \\ \times\sum_{i=0}^{N-1}\sum_{j=0}^{N-1}\alpha_i\beta_j\int_0^1 \varphi'(t+i)\varphi'(t+j)\,dt = \\ = 2\frac{\theta_{i_e} D_{i_e}(1-\nu_{i_e})}{h_e}(K^{22}_{\alpha\beta}\overline{\alpha},\overline{\beta}); \tag{2.23}$$

$$K^{22}_{\alpha\beta}(i,j) = \int_0^1 \varphi'(t+i)\varphi'(t+j)\,dt, \quad \varphi' = \frac{d\varphi}{dt}. \tag{2.24}$$

We define the parameters α_k and β_k through the node unknowns on the element:

$$\begin{cases} y_1 = w(0) = \sum_{k=0}^{N-1}\alpha_k\varphi(k) \\ \frac{dy_1}{dx} = \frac{1}{h_e}w'(0) = \frac{1}{h_e}\sum_{k=0}^{N-1}\alpha_k\varphi'(k) \\ y_2 = w(0.25) = \sum_{k=0}^{N-1}\alpha_k\varphi(k+0.25) \\ y_3 = w(0.5) = \sum_{k=0}^{N-1}\alpha_k\varphi(k+0.5) \\ y_4 = w(0.75) = \sum_{k=0}^{N-1}\alpha_k\varphi(k+0.75) \\ y_5 = w(1) = \sum_{k=0}^{N-1}\alpha_k\varphi(k+1) \\ \frac{dy_5}{dx} = \frac{1}{h_e}w'(1) = \frac{1}{h_e}\sum_{k=0}^{N-1}\alpha_k\varphi'(k+1) \end{cases} \tag{2.25}$$

Therefor we have

$$\overline{y}^{i_e} = T\overline{\alpha}, \tag{2.26}$$

where

$$\overline{y}^{i_e} = [y_1 \ \ \frac{dy_1}{dx} \ \ y_2 \ \ y_3 \ \ y_4 \ \ y_5 \ \ \frac{dy_5}{dx}]^T; \tag{2.27}$$

$$\overline{\alpha} = [\alpha_0 \ \ \alpha_1 \ \ \alpha_2 \ \ \alpha_3 \ \ \alpha_4 \ \ \alpha_5 \ \ \alpha_6]^T; \tag{2.28}$$

$$T = D\begin{vmatrix} \varphi(0) & \varphi(1) & \varphi(2) & \varphi(3) & \varphi(4) & \varphi(5) & \varphi(6) \\ \varphi'(0) & \varphi'(1) & \varphi'(2) & \varphi'(3) & \varphi'(4) & \varphi'(5) & \varphi'(6) \\ \varphi(0.25) & \varphi(1.25) & \varphi(2.25) & \varphi(3.25) & \varphi(4.25) & \varphi(5.25) & \varphi(6.25) \\ \varphi(0.5) & \varphi(1.5) & \varphi(2.5) & \varphi(3.5) & \varphi(4.5) & \varphi(5.5) & \varphi(6.5) \\ \varphi(0.75) & \varphi(1.75) & \varphi(2.75) & \varphi(3.75) & \varphi(4.75) & \varphi(5.75) & \varphi(6.75) \\ \varphi(1) & \varphi(2) & \varphi(3) & \varphi(4) & \varphi(5) & \varphi(6) & \varphi(7) \\ \varphi'(1) & \varphi'(2) & \varphi'(3) & \varphi'(4) & \varphi'(5) & \varphi'(6) & \varphi'(7) \end{vmatrix}; \quad (2.29)$$

$$D = diag(1 \quad 1/h_e \quad 1 \quad 1 \quad 1 \quad 1 \quad 1/h_e). \quad (2.30)$$

Similarly, we get

$$\bar{z}^{i_e} = T\bar{\beta}. \quad (2.31)$$

Taking into account (2.26) and (2.31) we get

$$\bar{\alpha} = T^{-1}\bar{y}^{i_e}; \quad \bar{\beta} = T^{-1}\bar{z}^{i_e}. \quad (2.32)$$

In the general case, the following chain of equalities holds:

$$\begin{aligned}(K_{\alpha\beta}\bar{\alpha}, \bar{\beta}) &= (K_{\alpha\beta}T^{-1}\bar{y}^{i_e}, T^{-1}\bar{z}^{i_e}) = \\ &= ((T^{-1})^{\mathrm{T}} K_{\alpha\beta}T^{-1}\bar{y}^{i_e}, \bar{z}^{i_e}).\end{aligned} \quad (2.33)$$

Therefore, substituting (2.32) sequentially into (2.14), (2.16), (2.19), (2.21), (2.23), we obtain local stiffness matrices $K_0^{i_e}$, $K_4^{i_e}$, $K_{21}^{i_e}$, $K_{23}^{i_e}$, $K_{22}^{i_e}$, $K_2^{i_e}$, corresponding to the operators L_0, L_4, L_{21}, L_{23}, L_{22}, L_2,

$$K_0^{i_e} = -\frac{\theta_{i_e} D_{i_e}}{h_e^3}(T^{-1})^{\mathrm{T}} K_{\alpha\beta}^0 T^{-1}; \quad (2.34)$$

$$K_4^{i_e} = h_e \theta_{i_e} D_{i_e}(T^{-1})^{\mathrm{T}} K_{\alpha\beta}^4 T^{-1}; \quad (2.35)$$

$$K_{21}^{i_e} = -\frac{\theta_{i_e} D_{i_e} \nu_{i_e}}{h_e}(T^{-1})^{\mathrm{T}} K_{\alpha\beta}^{21} T^{-1}; \quad (2.36)$$

$$K_{23}^{i_e} = -\frac{\theta_{i_e} D_{i_e} \nu_{i_e}}{h_e}(T^{-1})^{\mathrm{T}} K_{\alpha\beta}^{23} T^{-1} = (K_{21}^{i_e})^T; \quad (2.37)$$

$$K_{22}^{i_e} = 2\frac{\theta_{i_e} D_{i_e}(1-\nu_{i_e})}{h_e}(T^{-1})^{\mathrm{T}} K_{\alpha\beta}^{22} T^{-1}. \quad (2.38)$$

Due to the fact that

$$L_2 = L_{21} + L_{22} + L_{23}, \quad (2.39)$$

we have the following local stiffness matrix

$$K_2^{i_e} = K_{21}^{i_e} + K_{22}^{i_e} + K_{23}^{i_e}. \quad (2.40)$$

3. NUMERICAL IMPLEMENTATION

The presented algorithm can be implemented using the tools of MATLAB. In particular, the reference to the standard function

```
wavefun('db14',0)
```

allows researcher to get the values of the scaling Daubeshi function φ on the interval $[0, 27] = \mathrm{supp}(\varphi)$ with steps $h_t = 1/256 = 2^{-8}$. Let us denote $N_t = 256 = 2^8$. For the considering value $N = 7$ we can use the first $N_l = N_t \cdot N + 1$ values of φ, defined on the segment $[0, N] = [0, 7]$. With such a small step, it will be natural to compute the derivatives in the form of finite differences:

$$\varphi'(t_k) \approx d\varphi_k = \frac{\varphi_{k+1} - \varphi_{k-1}}{2h_t}, \quad k = 1, 2, ..., N_l; \quad (3.1)$$

$$\varphi''(t_k) \approx d2\varphi_k = \frac{\varphi_{k+1} - 2\varphi_k + \varphi_{k-1}}{h_t^2}, \quad k = 1, 2, ..., N_l, \quad (3.2)$$

where $\varphi_k = \varphi(t_k); \quad t_k = k \cdot h_t.$ (3.3)

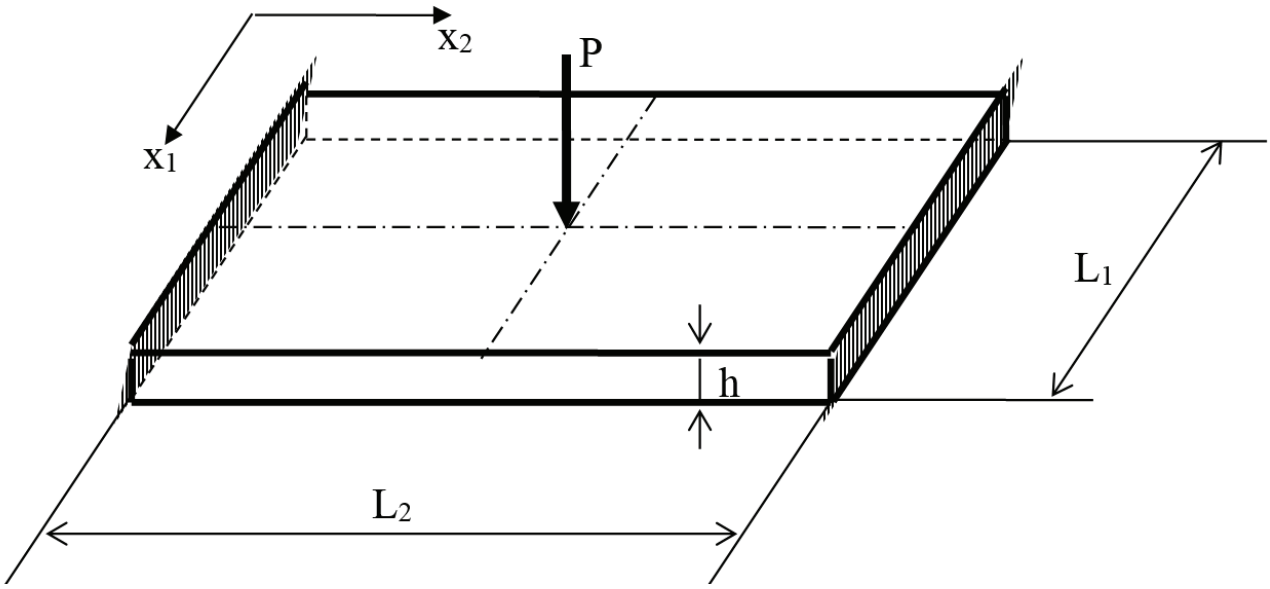

Figure 2. About formulation of the problem.

If $t_k \notin [0,27]$ then $\varphi_k = \varphi(t_k) = 0$.

When computing the coefficients of the local stiffness matrix (formulas (2.14), (2.16), (2.19), (2.21), (2.23)), one can use the simplest quadrature formulas for numerical integration, in particular, midpoint quadrature rule with step $2h_t$.

As an example, we consider the problem of bending a thin plate rigidly fixed along the lateral faces under the influence of a load concentrated in the center (Figure 2).

Geometric parameters: $L_1 = 0.9\,\text{m}$, $L_2 = 1.0\,\text{m}$, $h = 0.05\,\text{m}$ (thickness). The calculated parameters of the plate material: coefficient of elasticity $E = 3000 \cdot 10^4\,\text{kN/m}^2$, $\nu = 0.16$ is Poisson's ratio. External load parameter: $P = 1\,\text{kN}$.

Let $N_e = 3$ be the number of elements.

The length of the element

$$h_e = L_1 / N_e = 0.9/3 = 0.3.$$

Distance between coordinates of nodes

$$h_p = h_e / 4 = 0.3/4 = 0.075\ .$$

The number of nodal unknowns for each component of the vector function y_j, $j = 1,2,3,4$:

$$N_g = N_p + 2N_b = 3 \cdot 3 + 2 \cdot (3+1) = 17\ ,$$

where $N_p = N_e(N_k - 1)$ is the total number of internal nodes for all elements; $N_b = N_e + 1$ is the total number of boundary nodes for all elements. Total number of unknowns is equal to

$$N_U = 4N_g = 4 \cdot 17 = 68\ .$$

For comparison, we use the traditional finite element method, where unknown functions on an element are represented as a cubic parabola and in the node each unknown function is represented by two unknown nodal quantities: the nodal value of the unknown function itself and its first derivative in the discrete direction.

The total number of nodal points in a discrete direction x_1 is equal to

$$N_1 = L_1 / h_p + 1 = 0.9/0.075 + 1 = 13\ .$$

The number of nodal unknowns for each component of the vector function y_j, $j = 1,2,3,4$:

$$N_g = 2N_1 = 26.$$

Total number of unknowns is equal to

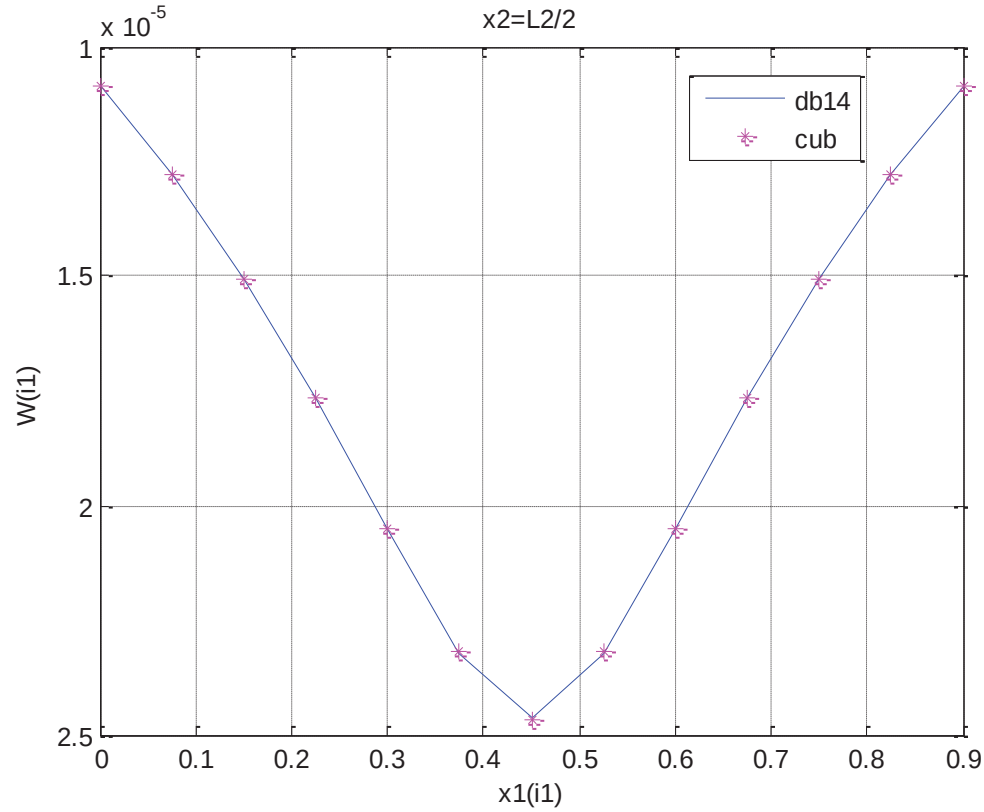

a)

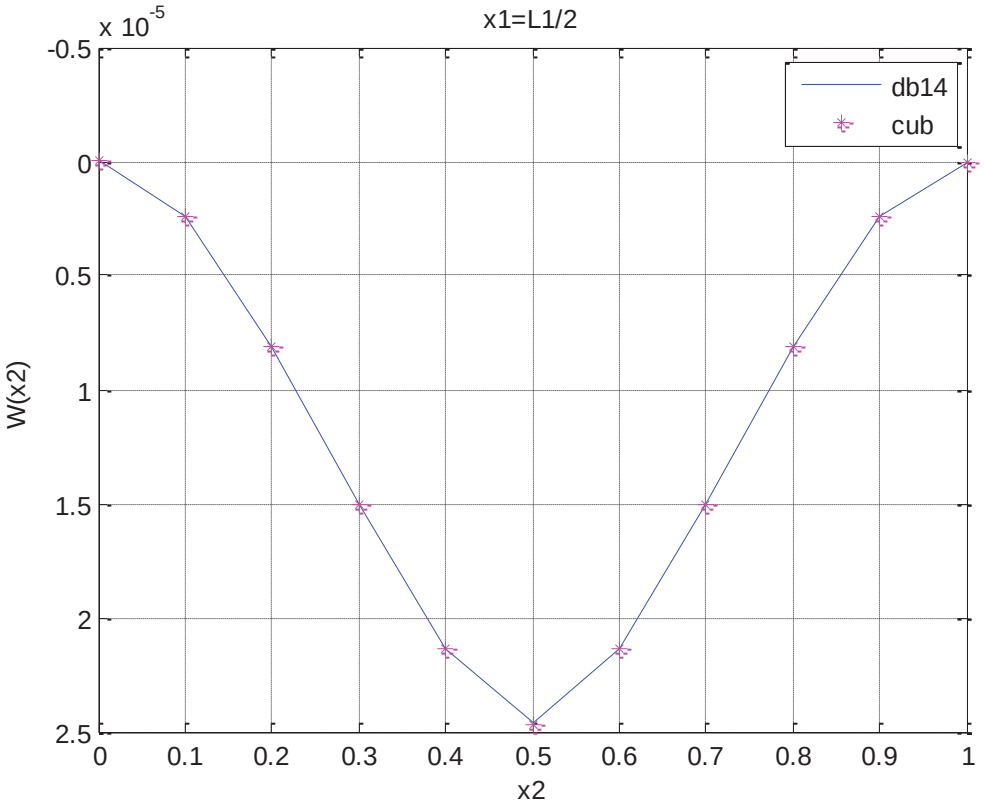

b)

Figure 3. Comparison of results in mid sections in each direction.

$$N_U = 4N_g = 4 \cdot 26 = 104 .$$

Graphical comparison of the results of analysis is presented at Figure 3 (`db14` is deflection values obtained using the Daubechies scaling function; `cub` is deflection values obtained, obtained on the basis of the traditional finite element method; $h_1 = 0.075$, $h_2 = 0.1$ are steps of issuing results in the directions x_1 and x_2, respectively.

As can be seen, the results obtained practically coincide. Moreover, the finite element method algorithm based on the Daubechies scaling function leads to a significant decrease in the number of unknowns. The difference is equal to $4N_p$.

REFERENCES

1. **Daubechies I.** Orthonormal bases of compactly supported wavelets. // Commun. Pure Appl. Math., 1988, vol. 41, pp. 909-996.
2. **Akimov P.A., Aslami M.** About Verification of Correct Wavelet-Based Approach to Local Static Analysis of Bernoulli Beam. // *Applied Mechanics and Materials*, 2014, Vols. 580-583, pp. 3013-3016.
3. **Akimov P.A., Aslami M.** Theoretical Foundations of Correct Wavelet-Based Approach to Local Static Analysis of Bernoulli Beam. // *Applied Mechanics and Materials*, 2014, Vols. 580-583, pp. 2924-2927.
4. **Akimov P.A., Belostotsky A.M., Kaytukov T.B., Mozgaleva M.L., Aslami M.** About several numerical and semianalytical methods of local structural analysis. // *International Journal for Computational Civil and Structural Engineering*, 2018, Vol. 14, Issue 4, pp. 59-69.
5. **Akimov P.A., Mozgaleva M.L.** Correct Wavelet-based Multilevel Numerical Method of Local Solution of Boundary Problems of Structural Analysis. // *Applied Mechanics and Materials*, 2012, Vols. 166-169, pp. 3155-3158.
6. **Aslami M., Akimov P.A.** Wavelet-based finite element method for multilevel local plate analysis. // *Thin-Walled Structures*, 2015-2016, Vol. 98, Part B, pp. 392-402.
7. **Akimov P.A., Belostotsky A.M., Mozgaleva M.L., Aslami M., Negrozov O.A.** Correct Multilevel Discrete-Continual Finite Element Method of Structural Analysis. // *Advanced Materials Research*, 2014, Vol. 1040, pp. 664-669.
8. **Akimov P.A., Belostotsky A.M., Sidorov V.N., Mozgaleva M.L., Negrozov O.A.** Application of discrete-continual finite element method for global and local analysis of multilevel systems. // *Applied Mechanics and Materials; AIP Conference Proceedings*, 2014, Vol. 1623(3), pp. 3-6.
9. **Akimov P.A., Mozgaleva M.L.** Correct Wavelet-based Multilevel Discrete-Continual Methods for Local Solution of Boundary Problems of Structural Analysis. // *Applied Mechanics and Materials*, 2013, Vols. 353-356, pp. 3224-3227.
10. **Akimov P.A., Mozgaleva M.L.** Wavelet-based Multilevel Discrete-Continual Finite Element Method for Local Deep Beam Analysis. // *Applied Mechanics and Materials*, 2013, Vols. 405-408, pp. 3165-3168.
11. **Akimov P.A., Mozgaleva M.L.** Wavelet-based Multilevel Discrete-Continual Finite Element Method for Local Plate Analysis. // *Applied Mechanics and Materials*, 2013, Vols. 351-352, pp. 13-16.
12. **Akimov P.A., Mozgaleva M.L., Aslami M., Negrozov O.A.** Modified Wavelet-based Multilevel Discrete-Continual Finite Element. Part 1: Continual and Discrete-Continual Formulations of the Problems Method for Local Structural Analysis. // *Applied Mechanics and Materials*, 2014, Vols. 670-671, pp. 720-723.
13. **Akimov P.A., Mozgaleva M.L., Aslami M., Negrozov O.A.** Modified Wavelet-based Multilevel Discrete-Continual Finite Element. Part 2: Reduced Formulations of the Problems in Haar Basis Method for Local Structural Analysis. // *Applied Mechan-*

ics and Materials, 2014, Vols. 670-671, pp. 724-727.

14. **Mozgaleva M.L., Akimov P.A.** About Verification of Wavelet-Based Discrete-Continual Finite Element Method for Three-Dimensional Problems. Part 1: Structures with Constant Physical and Geometrical of Structural Analysis Parameters Along Basic Direction. // *Applied Mechanics & Materials*, 2015, Vol. 709, pp. 105-108.
15. **Mozgaleva M.L., Akimov P.A.** About Verification of Wavelet-Based Discrete-Continual Finite Element Method for Three-Dimensional Problems. Part 2: Structures with Piecewise Constant Physical and Geometrical Parameters Along Basic Direction of Structural Analysis. // *Applied Mechanics & Materials*, 2015, Vol. 709, pp. 109-112.
16. **Mozgaleva M.L., Akimov P.A., Kaytukov T.B.** About wavelet-based multigrid numerical method of structural analysis with the use of discrete Haar basis. // *International Journal for Computational Civil and Structural Engineering*, 2018, Vol. 14, Issue 3, pp. 83-102.
17. **Li B., Chen X.** Wavelet-based numerical analysis: A review and classification. // *Finite Elements in Analysis and Design*, 2014, vol. 81, pp. 14-31.
18. **Ko J., Kurdila A.J., Pilant M.S.** A class of finite element methods based on orthonormal, compactly supported wavelets. // *Comput. Mech.*, 1995, Vol. 16, pp. 235-244.
19. **Patton R.D., Marks P.C.** One-dimensional finite elements based on the Daubechies family of wavelets. // *AIAAJ*, 1996, Vol. 34, pp. 1696-1698.
20. **Ma J.X., Xue J.J.** A study of the construction and application of a Daubechies wavelet-based beam element. // *Finite Elem. Anal. Des.*, 2003, vol. 39, pp. 965-975.
21. **Chen X.F., Yang S.J., Ma J.X.** The construction of wavelet finite element and its application. // *Finite Elem. Anal. Des.*, 2004, vol. 40, pp. 541-554.
22. **Li B., Cao H.R., He Z.J.** The construction of one-dimensional Daubechies wavelet-based finite elements for structural response analysis. // *J. Vibroeng*, 2011, vol. 13, pp. 729-738.
23. **Jin J.M., Xue P.X., Xu Y.X., Zhu Y.L.** Compactly supported non-tensor product form two-dimension wavelet finite element. // *Appl. Math. Mech.*, 2006, Vol. 27, pp. 1673-1686.
24. **Zhou Y.H., Zhou J.** A modified wavelet approximation of deflections for solving PDEs of beams and square thin plates. // *Finite Elements in Analysis and Design*, 2008, vol. 44, pp. 773-783.
25. **Mitra M., Gopalakrishnan S.** Extraction of wave characteristics from wavelet-based spectral finite element formulation. // Mech. Syst. Signal Process, 2006, vol. 20, pp. 2046–2079.
26. **Mitra M., Gopalakrishnan S.** Wavelet Spectral element for wave propagation studies in pressure loaded axisymmetric cylinders. // J. Mech. Mater. Struct., 2007, vol. 4, pp. 753-772.
27. **Mitra M., Gopalakrishnan S.** Wave propagationan alysis in anisotropic plate using wavelet spectral element approach. // J. Appl. Mech., 2008, vol. 75, pp. 1-6.
28. **Mitra M., Gopalakrishnan S.** Wavelet-based spectral finite element modelling and detection of delamination in composite beams. // *Proceed. R. Soc. A*, 2006, vol. 462, pp. 1721-1740.
29. **Aslami M., Akimov P.A.** Analytical solution for beams with multipoint boundary conditions on two-parameter elastic foundations. // *Archives of Civil and Mechanical Engineering*, 2016, Vol. 16, Issue 4, pp. 668-677.
30. **Akimov P.A., Mozgaleva M.L.** Method of Extended Domain and General Principles of Mesh Approximation for Boundary Problems of Structural Analysis. // Applied Mechanics and Materials, Vols. 580-583 (2014) pp. 2898-2902.

СПИСОК ЛИТЕРАТУРЫ

1. **Daubechies I.** Orthonormal bases of compactly supported wavelets. // Commun. Pure Appl. Math., 1988, vol. 41, pp. 909-996.
2. **Akimov P.A., Aslami M.** About Verification of Correct Wavelet-Based Approach to Local Static Analysis of Bernoulli Beam. // *Applied Mechanics and Materials*, 2014, Vols. 580-583, pp. 3013-3016.
3. **Akimov P.A., Aslami M.** Theoretical Foundations of Correct Wavelet-Based Approach to Local Static Analysis of Bernoulli Beam. // *Applied Mechanics and Materials*, 2014, Vols. 580-583, pp. 2924-2927.
4. **Akimov P.A., Belostotsky A.M., Kaytukov T.B., Mozgaleva M.L., Aslami M.** About several numerical and semianalytical methods of local structural analysis. // *International Journal for Computational Civil and Structural Engineering*, 2018, Vol. 14, Issue 4, pp. 59-69.
5. **Akimov P.A., Mozgaleva M.L.** Correct Wavelet-based Multilevel Numerical Method of Local Solution of Boundary Problems of Structural Analysis. // *Applied Mechanics and Materials*, 2012, Vols. 166-169, pp. 3155-3158.
6. **Aslami M., Akimov P.A.** Wavelet-based finite element method for multilevel local plate analysis. // *Thin-Walled Structures*, 2015-2016, Vol. 98, Part B, pp. 392-402.
7. **Akimov P.A., Belostotsky A.M., Mozgaleva M.L., Aslami M., Negrozov O.A.** Correct Multilevel Discrete-Continual Finite Element Method of Structural Analysis. // *Advanced Materials Research*, 2014, Vol. 1040, pp. 664-669.
8. **Akimov P.A., Belostotsky A.M., Sidorov V.N., Mozgaleva M.L., Negrozov O.A.** Application of discrete-continual finite element method for global and local analysis of multilevel systems. // *Applied Mechanics and Materials; AIP Conference Proceedings*, 2014, Vol. 1623(3), pp. 3-6.
9. **Akimov P.A., Mozgaleva M.L.** Correct Wavelet-based Multilevel Discrete-Continual Methods for Local Solution of Boundary Problems of Structural Analysis. // *Applied Mechanics and Materials*, 2013, Vols. 353-356, pp. 3224-3227.
10. **Akimov P.A., Mozgaleva M.L.** Wavelet-based Multilevel Discrete-Continual Finite Element Method for Local Deep Beam Analysis. // *Applied Mechanics and Materials*, 2013, Vols. 405-408, pp. 3165-3168.
11. **Akimov P.A., Mozgaleva M.L.** Wavelet-based Multilevel Discrete-Continual Finite Element Method for Local Plate Analysis. // *Applied Mechanics and Materials*, 2013, Vols. 351-352, pp. 13-16.
12. **Akimov P.A., Mozgaleva M.L., Aslami M., Negrozov O.A.** Modified Wavelet-based Multilevel Discrete-Continual Finite Element. Part 1: Continual and Discrete-Continual Formulations of the Problems Method for Local Structural Analysis. // *Applied Mechanics and Materials*, 2014, Vols. 670-671, pp. 720-723.
13. **Akimov P.A., Mozgaleva M.L., Aslami M., Negrozov O.A.** Modified Wavelet-based Multilevel Discrete-Continual Finite Element. Part 2: Reduced Formulations of the Problems in Haar Basis Method for Local Structural Analysis. // *Applied Mechanics and Materials*, 2014, Vols. 670-671, pp. 724-727.
14. **Mozgaleva M.L., Akimov P.A.** About Verification of Wavelet-Based Discrete-Continual Finite Element Method for Three-Dimensional Problems. Part 1: Structures with Constant Physical and Geometrical of Structural Analysis Parameters Along Basic Direction. // *Applied Mechanics & Materials*, 2015, Vol. 709, pp. 105-108.
15. **Mozgaleva M.L., Akimov P.A.** About Verification of Wavelet-Based Discrete-Continual Finite Element Method for Three-Dimensional Problems. Part 2: Structures with Piecewise Constant Physical and Geometrical Parameters Along Basic Direc-

tion of Structural Analysis. // *Applied Mechanics & Materials,* 2015, Vol. 709, pp. 109-112.
16. **Mozgaleva M.L., Akimov P.A., Kaytukov T.B.** About wavelet-based multigrid numerical method of structural analysis with the use of discrete Haar basis. // *International Journal for Computational Civil and Structural Engineering*, 2018, Vol. 14, Issue 3, pp. 83-102.
17. **Li B., Chen X.** Wavelet-based numerical analysis: A review and classification. // *Finite Elements in Analysis and Design*, 2014, vol. 81, pp. 14-31.
18. **Ko J., Kurdila A.J., Pilant M.S.** A class of finite element methods based on orthonormal, compactly supported wavelets. // *Comput. Mech.*, 1995, Vol. 16, pp. 235-244.
19. **Patton R.D., Marks P.C.** One-dimensional finite elements based on the Daubechies family of wavelets. // *AIAAJ*, 1996, Vol. 34, pp. 1696-1698.
20. **Ma J.X., Xue J.J.** A study of the construction and application of a Daubechies wavelet-based beam element. // *Finite Elements in Analysis and Design*, 2003, vol. 39, pp. 965-975.
21. **Chen X.F., Yang S.J., Ma J.X.** The construction of wavelet finite element and its application. // *Finite Elements in Analysis and Design*, 2004, vol. 40, pp. 541-554.
22. **Li B., Cao H.R., He Z.J.** The construction of one-dimensional Daubechies wavelet-based finite elements for structural response analysis. // *J. Vibroeng*, 2011, vol. 13, pp. 729-738.
23. **Jin J.M., Xue P.X., Xu Y.X., Zhu Y.L.** Compactly supported non-tensor product form two-dimension wavelet finite element. // *Appl. Math. Mech.*, 2006, Vol. 27, pp. 1673-1686.
24. **Zhou Y.H., Zhou J.** A modified wavelet approximation of deflections for solving PDEs of beams and square thin plates. // *Finite Elements in Analysis and Design*, 2008, vol. 44, pp. 773-783.
25. **Mitra M., Gopalakrishnan S.** Extraction of wave characteristics from wavelet-based spectral finite element formulation. // Mech. Syst. Signal Process, 2006, vol. 20, pp. 2046–2079.
26. **Mitra M., Gopalakrishnan S.** Wavelet Spectral element for wave propagation studies in pressure loaded axisymmetric cylinders. // J. Mech. Mater. Struct., 2007, vol. 4, pp. 753-772.
27. **Mitra M., Gopalakrishnan S.** Wave propagationan alysis in anisotropic plate using wavelet spectral element approach. // J. Appl. Mech., 2008, vol. 75, pp. 1-6.
28. **Mitra M., Gopalakrishnan S.** Wavelet-based spectral finite element modelling and detection of delamination in composite beams. // *Proceed. R. Soc. A*, 2006, vol. 462, pp. 1721-1740.
29. **Aslami M., Akimov P.A.** Analytical solution for beams with multipoint boundary conditions on two-parameter elastic foundations. // *Archives of Civil and Mechanical Engineering*, 2016, Vol. 16, Issue 4, pp. 668-677.
30. **Akimov P.A., Mozgaleva M.L.** Method of Extended Domain and General Principles of Mesh Approximation for Boundary Problems of Structural Analysis. // Applied Mechanics and Materials, Vols. 580-583 (2014) pp. 2898-2902.

Marina L. Mozgaleva, Dr.Sc., Professor, Department of Applied Mathematics, National Research Moscow State University of Civil Engineering, 26, Yaroslavskoe Shosse, Moscow, 129337, Russia;
phone/fax: +7(499) 183-59-94;
E-mail: marina.mozgaleva@gmail.com.

Pavel A. Akimov, Full Member of the Russian Academy of Architecture and Construction Sciences (RAACS), Professor, Dr.Sc.; Executive Scientific Secretary of Russian Academy of Architecture and Construction Sciences; Vice-Director for Science Activities, Scientific Research Center "StaDyO"; Professor of Department of Architecture and Construction, Peoples' Friendship University of Russia; Professor of Department of Structural Mechanics, Tomsk State University of Architecture and Building; 24, Ul. Bolshaya Dmitrovka, 107031, Moscow, Russia;

phone +7(495) 625-71-63; fax: +7 (495) 650-27-31;
E-mail: akimov@raasn.ru, pavel.akimov@gmail.com.

Taymuraz B. Kaytukov, Advisor of the Russian Academy of Architecture and Construction Sciences, Associated Professor, Ph.D.; Deputy Executive Scientific Secretary of Russian Academy of Architecture and Construction Sciences; Central Institute for Research and Design of the Ministry of Construction and Housing and Communal Services of the Russian Federation; 24, Ul. Bolshaya Dmitrovka, 107031, Moscow, Russia;
phone +7(495) 625-81-53; fax: +7 (495) 650-27-31;
E-mail: kaytukov@raasn.ru, tkaytukov@gmail.com.

Мозгалева Марина Леонидовна, доцент, доктор технических наук, профессор кафедры прикладной математики, Национальный исследовательский Московский государственный строительный университет (НИУ МГСУ), Россия, 129337, Москва, Ярославское шоссе, д.26, тел./факс: +7(499) 183-59-94,
E-mail: marina.mozgaleva@gmail.com.

Акимов Павел Алексеевич, академик Российской академии архитектуры и строительных наук (РААСН), профессор, доктор технических наук; главный ученый секретарь Российской академии архитектуры и строительных наук; заместитель генерального директора по науке ЗАО «Научно-исследовательский центр СтаДиО»; профессор Департамента архитектуры и строительства Российского университета дружбы народов; профессор кафедры строительной механики Томского государственного архитектурно-строительного университета; 107031, г. Москва, ул. Большая Дмитровка, д. 24, стр. 1; тел. +7(495) 625-71-63;
факс +7 (495) 650-27-31; E-mail: akimov@raasn.ru, pavel.akimov@gmail.com.

Кайтуков Таймураз Батразович, советник РААСН, доцент, кандидат технических наук, заместитель главного ученого секретаря Российской академии архитектуры и строительных наук; Центральный научно-исследовательский и проектный институт Министерства строительства и жилищно-коммунального хозяйства Российской Федерации; 107031, г. Москва, ул. Большая Дмитровка, д. 24, стр. 1;
тел. +7(495) 625-81-53; факс +7 (495) 650-27-31;
E-mail: kaytukov@raasn.ru, tkaytukov@gmail.com.

DOI:10.22337/2587-9618-2019-15-3-109-119

DETERMINATION OF THE ELEMENTS SIGNIFICANCE IN THE RELIABILITY OF REDUNDANT FRAMES

Sergii F. Pichugin, Viktor P. Chichulin, Ksenia V. Chichulina
Poltava National Technical Yuri Kondratyuk University, Poltava, UKRAINE

Abstract: The paper attacks the problem of steel redundant structures reliability. In calculations the probabilistic method of limit equilibrium is applied. All possible mechanisms of structural failure are considered. The influence of each section on the work of the frame as a whole is taken into account. Stochastic strength and load characteristics are used in the calculations. The proposed method of calculation allows to obtain structures with a given reliability. The calculation provides an opportunity to take into account the existing reserves of frames. The numerical example uses the logic of probabilistic transformations. The graphs of specific contributions of individual sections and the most probable mechanisms of destruction are presented. The probabilistic method takes into account the correlation between the individual mechanisms of destruction. The developed method determines the limiting moments, but it is allowed to take into account the action of the longitudinal force. In this example, the task was to align the impact of the frame sections without reducing the specified reliability, but it is possible to obtain a design with the same specific contributions, which is most economically justified. Specific contributions are increased or decreased as necessary to obtain a design with equal probability of failure. In the design, the influence of destruction individual mechanisms is used, because the cross sections of the beam span or floor column do not change from the design conditions. The method provides an opportunity to obtain more optimal designs and the use of modern software systems for static calculation. Recommendations for the design of these structures have been developed. It is proposed to use the reliability coefficient of redundant steel structures.

Keywords: cross section of destruction,, mechanism of destruction, specific contribution, significance, probabilistic method, correlation, steel frame, reliability coefficient

ОПРЕДЕЛЕНИЕ ЗНАЧИМОСТИ ОТДЕЛЬНЫХ ЭЛЕМЕНТОВ В НАДЁЖНОСТИ СТАТИЧЕСКИ НЕОПРЕДЕЛИМЫХ РАМ

С.Ф. Пичугин, В.П. Чичулин, К.В. Чичулина
Полтавский национальный технический университет имени Юрия Кондратюка, г. Полтава, УКРАИНА

Аннотация: Публикация посвящена проблеме избыточной надежности стальных статически неопределимых конструкций. В вычислениях используется вероятностный метод предельного равновесия. Рассматриваются все возможные механизмы разрушения конструкции. Учитывается влияние каждого сечения на работу рамы в целом. В вычислениях используются стохастические характеристики прочности и нагрузки. Предложенный метод вычисления позволяет получать сооружения с заданной надежностью. Расчет даёт возможность учесть существующие резервы рам. В числовом примере используются логико-вероятностные преобразования. Представлены графики удельных вкладов как отдельных сечений, так и наиболее вероятных механизмов разрушения. Вероятностный метод учитывает корреляционные связи между отдельными механизмами разрушения. Разработанный метод определяет предельные моменты, но можно учитывать и действие продольной силы. В этом примере, задачей было сравнять влияние сечений рамы без снижения заданной надежности, но возможно получить конструкцию с одинаковыми удельными вкладами, что наиболее эффективно. Удельные вклады возрастают или уменьшаются по мере необходимости, чтобы получить конструкцию с равной вероятностью отказа. При проектировании, используется влияние отдельных механизмов разрушения, потому что сечения балки пролёта или колонны этажа не изменяются по условиям конструирования. Метод позволяет получить более оптимальные конструкции при использовании современных программных комплексов статического расчета. Разработаны рекомендации для непосредственного проектирования данного типа конструкций. Предлагается использовать коэффициент надежности стальных статически неопределимых конструкций.

Ключевые слова: опасное сечение, механизм разрушения, удельный вклад, значимость, вероятностный метод, корреляционная связь, стальная рама, коэффициент надёжности

1. INTRODUCTION

The article is devoted to probabilistic estimation of steel redundant structures. Some beams and simple frames, as well as multistory and multi-span structures of industrial and residential buildings present this type of structures. The failures of these systems are various. This article attacks the problem which concern is only steel structures with the loss of carrying load capacity. Redundant structure failures occur after some member failures in the form of transmission to different workable states. These states match different designing schemes with various probabilistic parameters. Thus, the redundant structure failure estimation is a very complicated problem as depends upon the system complexity. For redundant systems in the design with a given reliability, an important step is to obtain the economic characteristics of the sections. The search for the optimum and minimum weight redundant systems dedicated a lot of research. These studies make it possible to obtain optimal frames on the bearing capacity.

2. MAIN BODY

2.1. Review of the issue status.

Evaluation of the building structures reliability is presented in a large number of works. Calculations of steel frames reliability are devoted to the work [1-10]. Consider some of these works. In particular in [1] design-by-analysis methods for steel structures are receiving considerable attention from professional engineers, researchers and standard-writing groups. Designing by analysis, termed as the Direct Design Method (DDM), is premised on the use of geometric nonlinear inelastic finite element analysis to determine the ultimate strength of steel structural frames and subsequently incorporating a system resistance factor to account for the effects of uncertainties in geometric parameters, stiffness and strength. This paper outlines the DDM in the context of cold-formed compact Hollow Steel Sections (HSS), including the reliability analysis framework at system level underpinning the Method. The system resistance factors for a series of representative 3D frames with hollow locally stable cross-sections are derived. In [2] several steel design specifications worldwide have incorporated provisions for designing through inelastic analysis of overall system behaviour. However, requirements for minimum system reliability have been implemented in such design-by-inelastic analysis methods through a simple adaptation of resistance factors originally developed from member reliability considerations. This paper [2] examines system resistance factors through a system reliability analysis of two steel moment frames subjected to combined gravity and wind loads. The frames are designed using second-order inelastic analysis and their strength and serviceability reliabilities are evaluated. The effects on the system reliabilities of system resistance factor and wind-to-gravity load ratio are examined. The paper also identifies some research issues that should be addressed prior to implementing a system reliability-based design methodology. In paper [3] a method to efficiently evaluate the reliability of elastic-perfectly plastic structures is proposed. The method is based on combining dynamic shakedown theory with Subset Simulation. In particular, focus is on describing the shakedown behaviour of uncertain elastic-plastic systems driven by stochastic wind loads. The ability of the structure to shakedown is assumed as a limit state separating plastic collapse from a safe, if not elastic, state of the structure. The limit state is therefore evaluated in terms of a probabilistic load multiplier estimated through solving a series of linear programming problems posed in terms of the responses of the underlying linear elastic model and self-stress distribution. The efficiency of the proposed procedure is guaranteed by the simplicity of the mathematical programming

problem, the underlying structural model solved at each iteration, and the efficiency of Subset Simulation. The rigor of the approach is assured by the dynamic shakedown theory. The applicability of the framework is illustrated on a steel frame example. The work [4] proposes a novel data-driven optimization strategy that can efficiently handle system-level first excursion performance constraints posed on large-scale uncertain structures subject to general stochastic wind excitation. The framework is centred on defining and solving a limited sequence of decoupled optimization sub-problems. In particular, each problem is formulated in terms of information obtained from a single simulation carried out in the solution of the previous sub-problem. Two examples involving the optimal design of uncertain systems subject to stochastic wind loads are presented to demonstrate the effectiveness, efficiency, and scalability of the proposed framework. The paper [5] describes an inter-story drift reliability-based optimization method of frames subjected to stochastic earthquake loads. First, the formulas for eigenvalue and eigenvector, drift PSD functions, drift spectral moments, drift reliabilities, their first and second derivatives are derived based on random vibration theory. The computational procedure of drift reliabilities, their first and second derivatives are given in detail. Second, optimal problem of drift reliability-based optimization design is formulated in a dimensionless way. Optimal mathematic model is converted into unconstrained mathematic model using penalty function method. Gradient and Hessian matrix of penalty function are derived using drift reliabilities and structural mass, their first and second derivatives. Third, solution step of optimal problem is constructed using conjugate gradient method. Finally, optimization designs of two planar frames are demonstrated. Sensitivity analysis of optimum design indicates the drift reliability-based optimization method can obtain local optimum design. The paper [6] is focused on the development of an efficient reliability-based design optimization algorithm for solving problems posed on redundant linear dynamic systems characterized by large design variable vectors and driven by non-stationary stochastic excitation. The interest in such problems lies in the desire to define a new generation of tools that can efficiently solve practical problems, such as the design of high-rise buildings in seismic zones, characterized by numerous free parameters in a rigorously probabilistic setting. To this end a novel decoupling approach is developed based on defining and solving a limited sequence of deterministic optimization sub-problems. In particular, each sub-problem is formulated from information pertaining to a single simulation carried out exclusively in the current design point. This characteristic drastically limits the number of simulations necessary to find a solution to the original problem while making the proposed approach practically insensitive to the size of the design variable vector. To demonstrate the efficiency and strong convergence properties of the proposed approach, the structural system of a high-rise building defined by over three hundred free parameters is optimized under non-stationary stochastic earthquake excitation. The influence of different load sequences on the deterministic resistance of steel structures (in the inelastic range) is a well-understood phenomenon. However, the impact of different load sequences on the reliability of members and frames made of steel has not been specifically studied in the past. Design rules for the stability and strength checks of such elements and structures are found, e.g., in Eurocode 3 [7]. The published background shows that load sequences and amplification patterns were not systematically included in the analysis of the reliability of the design rules for steel structures in Eurocode 3. In the paper [8], the impact of different load sequences on the reliability of three design rules or procedures (the resistance of plastic cross sections, of beam columns and of portal frame structures) is studied and illustrated by means of representative examples. The results show the significance of the load sequence at the level of

scatter and non-exceedance probability of resistances. The paper finally discusses the implications of the study's findings for code-making, as well as the potential of accounting for the load sequence in the reliability assessment of, e.g., existing structures. Large amounts of energy and carbon are embodied in the frames of buildings, making efficient structural design a key aspect of reducing the carbon footprint of buildings [9]. The unused mass of steel framed building could amount to nearly 46% of the total mass due to over-specification of the sections, we find a value of 36%. This value correlates with the design method, with software-aided design bringing significant improvements and with the design stage, where most of the optimization seems to occur between the preliminary and tender stage. Authors [9] find that neither the regularity of the structure nor the cost, independent of the measure used, correlate with the mean utilization ratio (ur). Conversely, we observe an apparent reluctance to design beams above a 0.8 capacity ur. This reluctance explains most of the unused mass in buildings. The rest of unused mass consists in cores, trimmers and ties (6%), some of which bear loads not captured in this analysis but are otherwise necessary for stability reasons, and in edge secondary beams (3%) which design is constrained, and should not necessarily be considered as ‘unused’ mass. Recently developed steel self-centering moment-resisting frames (SC-MRFs) have been analytically and experimentally validated as having the potential to eliminate structural damage under a design basis earthquake and restore their original vertical position following a major earthquake. Using Monte Carlo simulation, subjected three nonlinear models of prototype SC-MRFs to thousands of synthetic ground motions, and recorded peak demand responses such as story drift and beam-column relative rotation. Used this data to examine the sensitivity of SC-MRF behavior to structural properties and geometry, seeking to generate recommendations to improve the existing design procedure. A reliability-based methodology was used to assess the likelihood of reaching the limit state of post-tensioned strand yielding. The [10] study proposes modifications to the existing design procedure and illustrates a reliability-based methodology for developing improved seismic design recommendations.

2.2. General approach to solving the problem.

In the course of the study, many publications on the reliability of redundant systems were identified. But some do not include the issues of linking structural reliability calculations of steel frames with their optimization. That is, these issues remain insufficiently developed for today.

In order to obtain economic redundant steel frames with a given reliability, taking into account the plastic work of the material, the random characteristics of the material and the load, it is necessary to calculate the importance of each element in the system with respect to the reliability of the frames. It is necessary to obtain the value of the importance of the elements. Then you can adjust the existing reserves of the frame by changing the cross sections of the elements while maintaining the overall level of reliability of the structure. For existing structures, the definition of significance makes it possible to identify "weak links". During the reconstruction, this allows you to rationally influence the carrying capacity of a complex system.

The significance of the element x_i in the system $y(x_1,...x_n)$ is a partial derivative of the probability of failure-free operation of the system R_s in terms of the probability of failure-free operation of the element R_i:

$$\xi_i = \frac{dR_s}{dR_i} = \frac{R_{s1} - R_s}{R_i} = \frac{Q_s - Q_{s1}}{R_i}, \qquad (1)$$

where R_{s1}, Q_{s1} – the probability of the system failure-free operation (the probability of failure with absolute reliability of the i - th structural element); R_s, Q_s – the probability of the system failure-free operation (the probability of system

failure); R_i – the failure-free operation probability of the i-th structural element.

The criterion "significance of the element ξ_i" characterizes not only the location of this element x_i in the system structure $y(x_1,...x_n)$, but also the dependence on the probability of all system elements failure.

Consider such a characteristic as "the contribution of an element x_i" to the system $y(x_1,...x_n)$, which is equal to the product of the failure-free operation probability R_i on its significance:

$$B_i = R_i \cdot \xi_i = R_i \cdot \frac{dR_s}{dR_i} = Q_s - Q_{s1}. \qquad (2)$$

The criterion of contribution B_i characterizes the increment of the system reliability after the element restoration x_i with the actual probability of its failure-free operation, equal R_i. The contribution determines the location of the element in the system structure, the conditions of its functioning and the relationship with the probability of the system elements failure. The specific contribution of the *i*-th element to the reliability of the system can be expressed as:

$$b_i = \frac{B_i}{\sum_{i=1}^{n} B_i}. \qquad (3)$$

When calculating the failure probability of redundant systems, calculations are carried out in the region of low probability, and it is safe to assume that the failure probability of the system linearly depends on the failure probability of the element R_i. Then the increase in the reliability of the system can be determined:

$$\Delta R_s = \frac{dR_s}{dR_i} \cdot \Delta R_s = \frac{Q_s - Q_{s1}}{R_i} \cdot \Delta R_s. \qquad (4)$$

Using the formula (4), it is possible to influence the system. You can change the cross sections of elements by iteration according to significance This makes it possible to save material without reducing the overall level of reliability.

Consider the importance of elements that affect the system reliability. It is necessary to divide the structure into groups of sections. That is, you need to change the sections of the elements. So get a design with a smooth reliability of the elements. In particular, considering the work of the crossbar, the characteristics of the destruction beam mechanism are taken into account. This mechanism is based on one element. The cross section of this element is often constant along the entire length. Therefore, the change in the cross section should be done for the entire crossbar completely. Consider the surface mechanism of destruction, that is, several elements (columns). It can be assumed that the step of changing the cross sections of these elements is the same for the main mechanism as a whole.

2.3. Practical calculation.

Consider a practical example of frame calculation (Figure 1). We analyse the impact of the significance of individual elementary mechanisms (Table 1) on the system failure probability as a whole. The coefficient μ stiffness ratio was also calculated.

Calculations are performed by the probabilistic method of limiting equilibrium [11]. The significance of the elements is estimated only for the main floor and beam mechanisms of destruction. In the system of equations it will be mechanisms for No 7-12 (Table 1) number them respectively No 1-6 (Table 2).

According to the above formulas, we determine the significance, contribution and specific contribution of the frame destruction mechanisms (Table 2).

Figure 2 shows a significant difference in the specific contributions of the frame destruction mechanisms. Beam mechanisms are distinguished from them. Try to align the contributions of the elementary mechanisms in the reliability of the frame as a whole. To do this, change the ratio of stiffness in the structural elements. We will take into account the specific contribution to the reliability of the system.

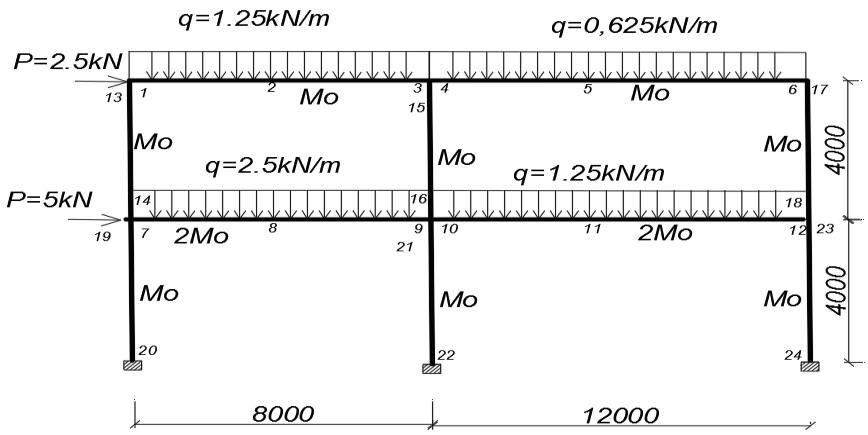

Figure 1. Scheme of the frame.

Table 1. The matrix of equilibrium conditions for elementary mechanisms.

	No sections																								
No equation	1	2	3	4	5	6	7	8	9	10	11	12	13	14	15	16	17	18	19	20	21	22	23	24	The right side of the equation
1	1	0	0	0	0	0	0	0	0	0	0	0	1	0	0	0	0	0	0	0	0	0	0	0	0
2	0	0	1	1	0	0	0	0	0	0	0	0	0	0	1	0	0	0	0	0	0	0	0	0	0
3	0	0	0	0	0	1	0	0	0	0	0	0	0	0	0	0	1	0	0	0	0	0	0	0	0
4	0	0	0	0	0	0	1	0	0	0	0	0	0	1	0	0	0	0	1	0	0	0	0	0	0
5	0	0	0	0	0	0	0	0	1	1	0	0	0	0	0	1	0	0	0	0	0	0	0	0	0
6	0	0	0	0	0	0	0	0	0	0	0	1	0	0	0	0	0	1	0	0	0	0	0	0	0
7	0	0	0	0	0	0	0	0	0	0	0	0	-1	-1	-1	-1	-1	-1	0	0	0	0	0	0	5
8	0	0	0	0	0	0	0	0	0	0	0	0	0	0	0	0	0	0	-1	-1	-1	-1	-1	-1	15
9	-1	2	1	0	0	0	0	0	0	0	0	0	0	0	0	0	0	0	0	0	0	0	0	0	10
10	0	0	0	-1	2	1	0	0	0	0	0	0	0	0	0	0	0	0	0	0	0	0	0	0	11,5
11	0	0	0	0	0		-1	2	1	0	0	0	0	0	0	0	0	0	0	0	0	0	0	0	20
12										-1	2	1	0	0	0	0	0	0	0	0	0	0	0	0	22,5
μ	1	1	1	1	1	1	2	2	2	2	2	2	1	1	1	1	1	1	1	1	1	1	1	1	

The rigidity of the frame will change according to Table 3.

When analyzing the specific contributions, we note that for the floor mechanisms 1 and 2 the specific contribution is less than in the beam 3-6. The reserve is 15-20 % by the moment. It remains as a reserve for the effect of longitudinal force in determining the bearing capacity of compressed curved rods. The application of this calculating method the significance of the elements and contributions of each elementary mechanism to the reliability of the system as a whole will have a significant economic effect. That is, it is possible to obtain more economical designs of redundant steel frames. Let's show it on an example and estimate economy on values of the bending moment (Table 5).

Let us analyze the results of table 5. It should be noted that the savings on the values of the limiting moment reaches 10-55 %. This can be taken into account when solving new design problems. In addition, when reconstructing existing buildings, it is often necessary to determine whether the frame structure will withstand a given load. In this situation, it may be necessary to strengthen the structure. If we strengthen the most important element (for the frame bolt 4, 5, 6), you can get smoothly reliable design with significantly greater load-bearing capacity and a given reliability.

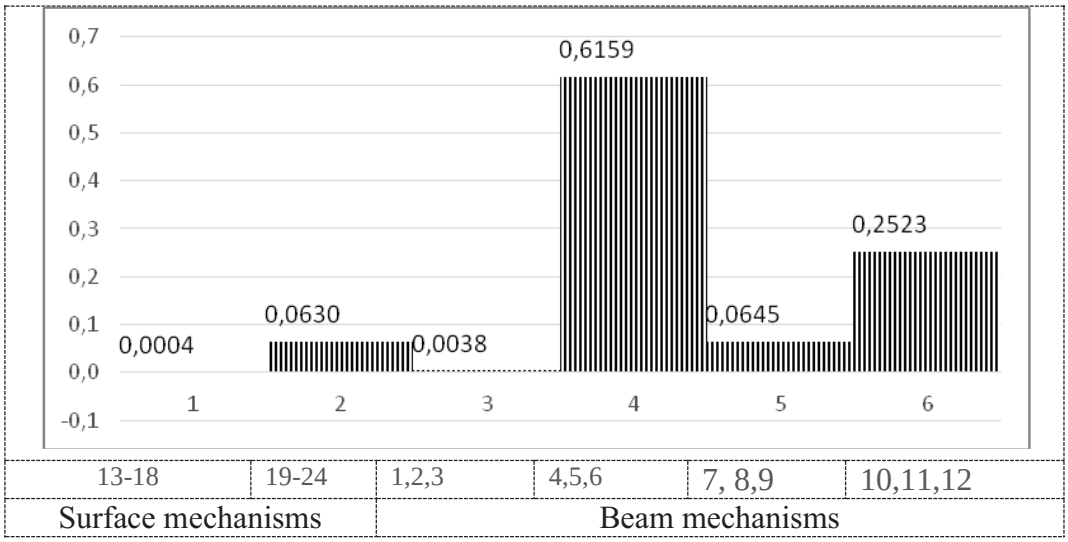

Figure 2. Unit contribution scheme for the main mechanisms.

Table 3. The ratio of the stiffness of the elements.

Mechanism	Initial	Final
1	1	0,5
2	1	1
3	1	0,87
4	1	1
5	2	1,59
6	2	1,78

Table 4. The calculating results of the individual basic significance mechanisms of destruction.

No.	The probability of the elementary mechanism failure	Significance ξ_i	Contribution B_i	The specific contribution b_i
1	4.393E-42	0.358951E-8	00.358951E-8	0.0761850
2	2.157E-20	0.331310E-8	0.331310E-8	0.0703184
3	8.953E-12	0.856663E-8	0.856663E-8	0.181821
4	6.763E-12	0.149853E-7	0.149853E-7	0.318053
5	6.446E-10	0.822502E-8	0.822502E-8	0.174571
6	8.1577E-10	0.843618E-8	0.843618E-8	0.179052

Table 5. The values of the limiting moments at the beginning of the calculation and after the alignment.

Mechanism	Initial value	Value after alignment	Percentage savings
1	8.89	3.99	55.1
2	8.89	7.98	10.2
3	8.89	6.94	21.9
4	8.89	7.98	10.2
5	17.78	12.69	28.6
6	17.78	14.2	20.1

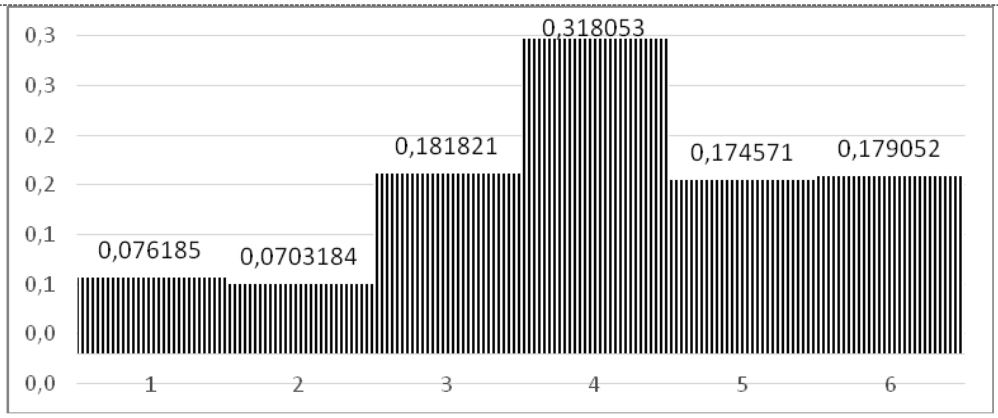

	13-18	19-24	1,2,3	4,5,6	7, 8,9	10,11,12	
	floor mechanisms		Beam mechanisms				

Figure 3. A diagram of specific payments is for basic mechanisms after the change of inflexibilities of elements.

Table 6. The significance and contributions of the frame sections.

No	1	2	3	4	5	6	7	8	9	10	11	12	13	14	15	16	17	18	19	20	21	22	23	24
Significance	.178154E-09	.325983E-09	.325983E-09	.521380E-07	.521735E-07	.521016E-07	.766320E-10	.54€278E-08	.546278E-08	.213737E-07	.213737E-107	.197929E-07	.112223E-09	.535054E-08	.127898E-12	.356266E-10	.107526E-09	.161539E-08	.887752 E-10	.533849E-08	.533B49E-08	.533849E-08	.691925E-08	.533849E-08
Conditional contribution	.668823E-03	.122380E-02	.122380E-02	.195735E-00	.195868E-00	.195598E-00	.287690E-03	.205082E-01	.205082E-01	.802406E-01	.802406E-01	.743062 E-01	.421305E-03	.200869E-01	.480150E-06	.133749E-03	.403673E-03	.606822E-02	.333278E-03	.200415E-01	.200416E-01	.200416E-01	.259761E-01	.200416E-01

In order to achieve this goal, the contributions of the elementary mechanisms to the reliability of the system as a whole are equalized in the calculations. To do this, change the ratio of stiffness in the structural elements, respectively, the specific contribution of each mechanism to the reliability of the system. Close to the optimum ratio of rigidity is very important for the normal static calculations of frames.

Perform the analysis of the calculation results of the contribution and value of individual cross-sections in the frame reliability. These values are calculated by the probabilistic method of limiting equilibrium [11]. The calculation results are given in Table 6, the specific contribution dependence diagram for each section is shown in Figure 4.

The diagram shows that the individual sections (1-24) contribute differently to the reliability of the system as a whole. Won give a different contribution even within the same basic mechanism. Deviations of specific contributions of sections within the main mechanisms are insignificant (the numbers of the main mechanisms are shown in the diagram in the bottom line). Therefore, it is sufficient to reliably generalize the finding of contributions for the main mechanisms, which include the elements as a whole, or a group of unified elements.

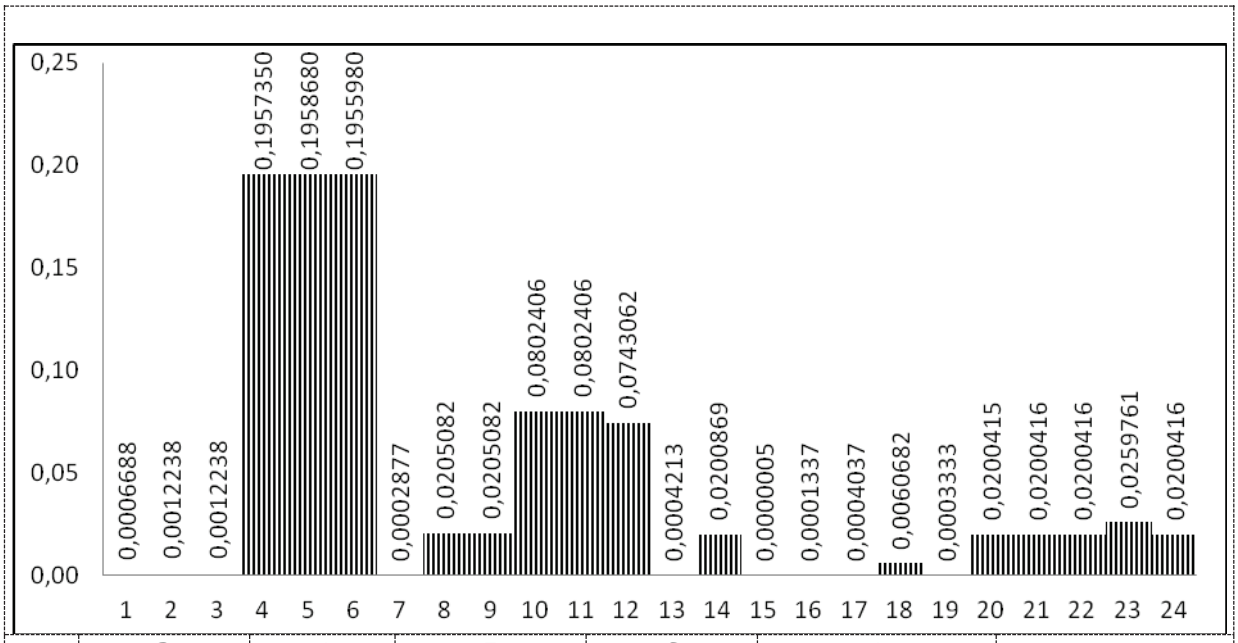

Figure 4. Diagram of the specific contribution for each section of the frame.

As you can see in the diagram (Figure 4), for the most likely mechanism "4" the specific contribution and significance of all sections are the same and equal respectively 0.196 and 0.521 E-7. Therefore, it is advisable to determine the significance and contribution for this beam mechanism as a single element.

The diagram shows that the individual sections (1-24) contribute differently to the reliability of the system. They give different contributions even within the same basic mechanism. Deviations of specific contributions of sections within the main mechanisms are insignificant (the numbers of the main mechanisms are shown in the bottom line). Therefore, quite accurate to summarize the finding of the contributions for the basic mechanisms. They include either whole elements or groups of unified elements. For the most probable mechanism "4" the specific contribution and significance of all sections are the same and equal respectively 0.196 and 0.521 E-7 (Figure 4). Therefore, it is advisable to determine the significance and contribution for this beam mechanism as a single element.

In fact, the most likely mechanisms of destruction may include only part of the dangerous sections relative to the main mechanism. These sections are more important for the reliability of the system as a whole than the sections that are not included in these mechanisms. The significance of individual sections can be taken into account in the state method. Thus, the work of the section is considered separately, and not in the work of the mechanisms as a whole.

According to the calculation of the probabilistic method of the limit equilibrium at the initial limiting moment is

$$M_o = 10.71kNm.$$

After the calculation we find a new value of the limiting moment (M_o = 7.978kNm). The probability of failure (for this example) is

$$Q_s=0.305028E\text{-}07.$$

The safety factor is

$$\gamma_s = 10.71/7.978 = 1.342 .$$

3. CONCLUSION

A method for regulating the reliability of redundant frames with a given standard probability of failure-free operation is proposed. This method is obtained by changing the value of the limiting moment and the alignment of the reliability parameters of individual elements. The ratio of the initial and the resulting limiting moment of the frames is recommended to call the coefficient of circuit reliability of steel statically uncertain frames. Its minimum value is 1.1. In the calculation of the contributions of individual elements, it is possible to obtain significantly higher values in the range of 1.1 to 1.4. This provides a significant saving of materials.

REFERENCES

1. **Wenyu L.W., Zhang H., Rasmussen K.** System reliability-based Direct Design Method for space frames with cold–formed steel hollow sections. // *Engineering Structures*, 2018, Vol. 166, pp. 79-92.
2. **Zhang H., Ellingwood R.B., Rasmussen K.** System reliabilities in steel structural frame design by inelastic analysis. // *Engineering Structures*, 2014, Vol. 181, pp. 341-348
3. **Tabbuso P., Spence S., Palizzolo L., Pirrotta A., Kareem A.** 2016 An efficient framework for the elasto-plastic reliability assessment of uncertain wind excited systems. // *Structural Safety*, 2016, Vol. 58, pp. 69-78.
4. **Suksuwan A., Spence M.J.S.** Optimization of uncertain structures subject to stochastic wind loads under system-level first excursion constraints: A data-driven approach. // *Computers & Structures*, 2018, Vol. 210, pp. 58-68.
5. **Liu Q., Paavola J.** 2015 Drift reliability-based optimization method of frames subjected to stochastic earthquake ground motion. // *Applied Mathematical Modelling*, 2015, Vol. 39, pp. 982-999.
6. **Spence M.J.S., Gioffre M., Kareem A.** An efficient framework for the reliability-based design optimization of large-scale uncertain and stochastic linear systems. // *Probabilistic Engineering Mechanics*, 2016, Vol. 44, pp. 174-182
7. **EN 1993-1-1 2010** Eurocode 3: Design of steel structures–part 1–1: general rules and rules for buildings (Brussels: CEN).
8. **Taras A, Huemer S** 2015 On the influence of the load sequence on the structural reliability of steel members and frames. // *Structures*, 2015, Vol. 4, pp. 91-104.
9. **Dunant F.C., Drewniok P.M., Eleftheriadis S., Cullen V.J., Allwood M.J.** 2018 Regularity and optimisation practice in steel structural frames in real design cases. // *Resources, Conservation and Recycling*, 2018, Vol. 134, pp. 294-302.
10. **Herning G., Garlock E.M.M., Vanmarcke E.** Reliability-based evaluation of design and performance of steel self-centering moment frames. // *Journal of Constructional Steel Research*, 2011, Vol. 67, pp. 1495-1505.
11. **Chichulina K., Chichulin V.** Steel statically uncertain transverse frames probabilistic calculation. // *International Journal of Engineering & Technology*, 2018, Vol. 7, No 3.2, pp. 79-85.

REFERENCES

1. **Wenyu L.W., Zhang H., Rasmussen K.** System reliability-based Direct Design Method for space frames with cold–formed steel hollow sections. // *Engineering Structures*, 2018, Vol. 166, pp. 79-92.
2. **Zhang H., Ellingwood R.B., Rasmussen K.** System reliabilities in steel structural frame design by inelastic analysis. // *Engineering Structures*, 2014, Vol. 181, pp. 341-348
3. **Tabbuso P., Spence S., Palizzolo L.,**

Pirrotta A., Kareem A. 2016 An efficient framework for the elasto-plastic reliability assessment of uncertain wind excited systems. // *Structural Safety,* 2016, Vol. 58, pp. 69-78.

4. **Suksuwan A., Spence M.J.S.** Optimization of uncertain structures subject to stochastic wind loads under system-level first excursion constraints: A data-driven approach. // *Computers & Structures,* 2018, Vol. 210, pp. 58-68.
5. **Liu Q., Paavola J.** 2015 Drift reliability-based optimization method of frames subjected to stochastic earthquake ground motion. // *Applied Mathematical Modelling,* 2015, Vol. 39, pp. 982-999.
6. **Spence M.J.S., Gioffre M., Kareem A.** An efficient framework for the reliability-based design optimization of large-scale uncertain and stochastic linear systems. // *Probabilistic Engineering Mechanics,* 2016, Vol. 44, pp. 174-182
7. **EN 1993-1-1 2010** Eurocode 3: Design of steel structures–part 1–1: general rules and rules for buildings (Brussels: CEN).
8. **Taras A, Huemer S** 2015 On the influence of the load sequence on the structural reliability of steel members and frames. // *Structures*, 2015, Vol. 4, pp. 91-104.
9. **Dunant F.C., Drewniok P.M., Eleftheriadis S., Cullen V.J., Allwood M.J.** 2018 Regularity and optimisation practice in steel structural frames in real design cases. // *Resources, Conservation and Recycling*, 2018, Vol. 134, pp. 294-302.
10. **Herning G., Garlock E.M.M., Vanmarcke E.** Reliability-based evaluation of design and performance of steel self-centering moment frames. // *Journal of Constructional Steel Research*, 2011, Vol. 67, pp. 1495-1505.
11. **Chichulina K., Chichulin V.** Steel statically uncertain transverse frames probabilistic calculation. // *International Journal of Engineering & Technology*, 2018, Vol. 7, No 3.2, pp. 79-85.

Sergii F. Pichugin, Dr.Sc., Professor, Head of the Department of Metal, Wooden and Plastic Structures; Poltava National Technical Yuri Kondratyuk University; 24, Pershotravneviy Ave., Poltava, 36011, Ukraine;
phone: +38 (050) 591 77 28;
E-mail: pichugin.sf@gmail.com.

Viktor P. Chichulin, Candidate of Technical Sciences, Associated Professor, Department of Metal, Wooden and Plastic Structures; Poltava National Technical Yuri Kondratyuk University; 24, Pershotravneviy Ave., Poltava, 36011, Ukraine; phone: +38 (050) 230 00 93;
E-mail: chichulinvp@gmail.com.

Ksenia V. Chichulina, Candidate of Technical Sciences, Associated Professor, Department of Entreprise Economics and Personal Management; Poltava National Technical Yuri Kondratyuk University; 24, Pershotravneviy Ave., Poltava, 36011, Ukraine;
phone: +38 (050) 013 72 82;
E-mail: chichulinak@rambler.com.

Пичугин Сергей Федорович, доктор технических наук, профессор, заведующий кафедрой конструкций из металла, дерева и пластмасс; Полтавский национальный технический университет имени Юрия Кондратюка; 36011, Украина, г. Полтава, Первомайский пр., 24; тел.: +38 (050) 591 77 28;
E-mail: pichugin.sf@gmail.com.

Чичулин Виктор Петрович, кандидат технических наук, доцент кафедры конструкций из металла, дерева и пластмасс; Полтавский национальный технический университет имени Юрия Кондратюка; 36011, Украина, г. Полтава, Первомайский пр., 24;
тел.: +38 (050) 230 00 93;
E-mail: chichulinvp@gmail.com.

Чичулина Ксения Викторовна, кандидат технических наук, доцент кафедры экономики предприятия и управления персоналом; Полтавский национальный технический университет имени Юрия Кондратюка; 36011, Украина, г. Полтава, Первомайский пр., 24;
тел.: +38 (050) 013 72 82;
E-mail: chichulinak@rambler.com.

DOI:10.22337/2587-9618-2019-15-3-120-130

THE ELASTOPLASTIC CALCULATION OF FRAMES USING THE DISPLACEMENT METHOD

Alexander N. Potapov
South Ural State University (national research university), Chelyabinsk, RUSSIA

Abstract: We proposed a method for calculating statical indeterminacy frames taking into account plastic deformations, which is based on the use of a schematized diagram of material with hardening. Two types of standard beams with supports are used during the implementation of the displacement method (DM) and the elastic solution of the problem: “fixed” - “pinned” and “fixed” – “fixed”, but unlike the elastic solution, standard beams contain plastic zones (PZs). So as the stresses in these zones did not exceed the limit of yielding in the nonlinear frame calculation, we took measures to transform the PZs into equal strength plastic zones (ESPZ). The calculations were made for both types of beams for all single and load impacts. The frame calculation consists of two stages (elastic and plastic). At the elastic stage, we determine an elastic moment diagram and the corresponding load. For a practical use of the DM in a nonlinear frame calculation, we introduced a simplifying prerequisite supplementing the well-known hypotheses of the classical version of the method, and formulated a Statement of the limiting load. According to the Statement, each length of the PZ can correspond to the lower boundary of the limiting load. The plastic stage of the calculation is performed at a given length of the PZ using the method of sequential loadings. At each loading stage, incremental equations are written using the DM equations, which establish relations between incremental moments and the incremental load, that allows you to get the resulting moment diagram. This diagram represents a sum of the elastic diagram and the diagrams of incremental moments at all previous loading stages. According to the resulting diagram, we calculate the length of the PZ, together with the limiting load. The calculation is considered complete if the length of the PZ does not exceed the specified value within the margin of error.

Keywords: displacement method, limit of yielding, stress, plastic zone, bending moment, stiffness

УПРУГОПЛАСТИЧЕСКИЙ РАСЧЕТ РАМ МЕТОДОМ ПЕРЕМЕЩЕНИЙ

А.Н. Потапов
Южно-Уральский государственный университет (национальный исследовательский университет), г. Челябинск, РОССИЯ

Аннотация: Предложен метод расчета статически неопределимых рам с учетом пластических деформаций, основанный на использовании схематизированной диаграммы материала с упрочнением. При реализации метода перемещений (МП), как и при упругом решении задачи, используются два типа стандартных балок с закреплениями: «заделка» – «шарнир» и «заделка» – «заделка», но в отличие от упругого решения стандартные балки содержат пластические зоны (ПЗ). Для того, чтобы в нелинейном расчете рамы напряжения в этих зонах не превышали предел текучести, проведены мероприятия по преобразованию ПЗ в пластические зоны равного сопротивления (ПЗРС). Для обоих типов балок выполнены расчеты на все единичные и грузовые воздействия. Расчет рамы состоит из двух этапов (упругого и пластического). На упругом этапе определяются предельно-упругая эпюра моментов и соответствующая ей нагрузка. Для практического использования МП в нелинейном расчете рамы введена упрощающая предпосылка, дополняющая известные гипотезы классического варианта метода, и сформулировано утверждение о предельной нагрузке. Согласно утверждению, каждой длине ПЗ можно поставить в соответствие нижнюю границу предельной нагрузки. Пластический этап расчета выполняется при заданной длине ПЗ по методу последовательных нагружений. На каждой ступени нагружения с помощью уравнений МП записываются инкрементальные уравнения, устанавливающие связи между приращением изгибающих моментов и приращением нагрузки, что позволяет построить результирующую эпюру моментов. Эта эпюра представляет собой сумму предельно упругой эпюры и эпюр приращений моментов на всех предыдущих ступенях нагружения. По результирующей эпюре вычисляется длина ПЗ и соответствующая ей предельная

нагрузка. Расчет считается законченным, если длина ПЗ не превышает заданную величину в пределах погрешности.

Ключевые слова: метод перемещений, предел текучести, напряжение, пластическая зона, изгибающий момент, жесткость

INTRODUCTION

Elastic-plastic deformations are generally accounted within the framework of the limiting equilibrium theory (LET), which is based on the representation of an ideal elastic-plastic behavior of the material described by Prandtl diagram. The theory was developed by Soviet scientist Gvozdev A.A., who in 1938 formulated three basic limiting equilibrium theorems (static, kinematic and duality theorems) [1]. The creation of this theory allowed to developed effective methods for calculating and designing many structures, especially reinforced concrete (RC) structures. The provisions of the LET are included in the main regulatory documents [2, 3] on the calculation and design of modern structures.

In scientific literature, the concept of PZs is used mainly in seismic construction. For the first time, this concept was introduced by Paulay T. and Bull I.N. [5] in the calculation of RC earthquake-resistant frames. Experts are long familiar with the fact that plastic deformations have the ability to absorb seismic energy, transforming it into thermal energy and then dissipating it into the environment. The ability of loaded structural elements to absorb and dissipate energy generally ensures a decrease in the seismic impact on the frame. Thus, the structure, apart from its main designation, also works as an energy absorber. However, the operation of the structure beyond the limit of elasticity often leads to material degradation and destruction in these zones [6].

These developments aroused considerable interest among experts; they were consolidated in regulatory documents (codes) of the United States and other countries [7–9]. Studies related to determining the length of the PZ, its location in the structure, the number of PZs, etc. In most cases, we are talking about the features of the design of the PZs in RC [10–14] and metal [15–18] structures under cyclic loads associated with seismic action.

In [10], a numerical analysis of the behavior of plastic hinges using the DIANA computing software, a calibrated FEM model was studied. On the extent of the rebar yielding zone, concrete crush zone and the real plastic hinge length a series of studies was conducted.

In [11–15] discuss issues of studying the plastic hinge length of RC columns. Moreover, in [11] for 4- and 7-story flat RC frames, studies were carried out in the SAP2000 8 program with the default (based on ATC-40 document [7]) hinges properties at both ends of beams and columns. In [12], based on the use of 3D FEM, it was shown that the PZ length for cyclically loaded columns is longer than for monotonic loading. An empirical model of the equivalent PZ length is proposed, which takes into account the effect of changes in this length on changes in the number of load cycles. In [13], the same ideas were applied to a fiber reinforced polymer. In [14], under the cyclic action of lateral force, the problem of assigning the PZ length in a RC column was studied and the role of the main reinforcement during its deformation beyond the limit of yielding into the hardening range was noted.

The design features of PZs in metal structures were considered in [15, 16], where a two-node super-element was developed for taking into account plastic deformations in steel frame structures in the analysis of static, cyclic [15] and impact [16] loads. In this case, in the super-element uses a model with two generalized (concentrated) plastic hinges located at the ends of the elastic beam element. When analyzing steel frames fabricated according to the «strong columns – weak beams» design concept [17], the authors proposed a composite beam-to-column connection, including a friction damper.

In [18], experimental and analytical studies of seismic characteristics of the device proposed in [17] were continued, where its resistance to damage was noted when the length of the PZ at the ends of the beam was lp = 12 cm.
In Russia and in the post-Soviet space, this problem is also reflected in [19–21]. It should be noted that both abroad and in Russian practice, the concept of PZs is considered as an equal strength zone [20], since its based on LET. Therefore, the stresses inside these zones should not exceed the limit of yielding σ_{yl}.

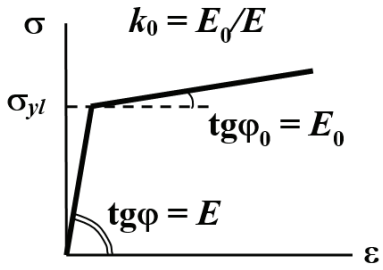

Figure 1. Diagram of the linearly hardening material deformation.

This article proposes a new approach to the calculation of statical indeterminacy frames using the DM, based on a physically nonlinear material deformation according to a hardening diagram (Figure 1). According to this diagram, when a limiting state appears in any section of the structure, a further load increase will lead to an increase in internal forces and stresses exceeding the limit yielding σ_{yl} (Figure 2, *a*). As a result, a PZ of some length l_p will appear in the vicinity of the considered section, the stresses on the right boundary of which correspond to the limiting plastic stress (section 1, Figure 2, *b*). This boundary is determined by the level of the plastic moment $M_0 = W_0\sigma_{yl}$, where W_0 is the plastic section modulus [4]. Normal stresses $\sigma_{max} > \sigma_{yl}$ are inside this zone and in section 2 (Figure 2, *c*).
In order to ensure that the stresses in the PZ section do not exceed the yield strength and correspond to the plastic zone of equal strength (ESPZ), it is necessary to increase the stiffness of the element, requiring that the law of change in the stiffness of the element in this section be consistent with the law of change in bending moment.

BASIC IDEA OF THE METHOD

The solution of the problem of tranforming the area with nonlinear deformations into an equal strength plastic zone (ESPZ) should be integrated into the calculation algorithm of the method and performed in parallel with the nonlinear process of determining the limiting load for a given length of the PZ.

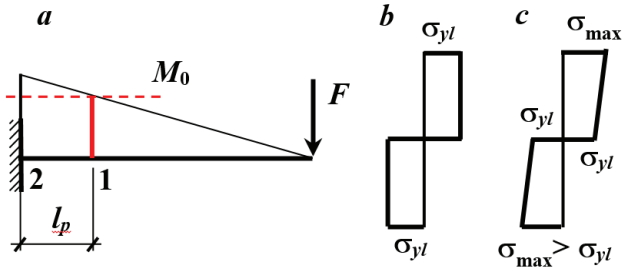

Figure 2. Yielding state in the beam:
a – PZ with the length of l_p;
b – stress in section 1;
c – stress in section 2.

In case of a nonlinear calculation of statical indeterminacy frames by the DM, as well as in the classical version of this method, standard elements are used – beams with two types of supports: “fixed” – “pinned” and “fixed” – “fixed”, which should be designed for different types of unit and load impacts. However, in these calculations, a number of additional parameters should be taken into account related to the presence ESPZ. This is the relative length of the zone, its location in the span of the beam, the modulus of hardening of the material, the law of variation of the area moment of inertia within the length of the zone. Then, in addition to the known coefficients, the calculated characteristics will include additional dimensionless functions $f_j(\alpha)$,where $\alpha = l_p/l$, l – beam length, characterizing the nonlinear operation of the standard element.
To simplify the nonlinear calculation, we introduce a new prerequisite for the modulus of elas-

ticity of the elastoplastic section located between the elastic and plastic stress diagrams, hereinafter referred to as the *intermediate section* (IS). This prerequisite supplements the known hypotheses of the classical DM version, allowing us to control the deformed state of the frame model at the IS.

Prerequisite. For all the fibers of the intermediate section of the frame design model, the modulus of elasticity is assumed to be *kE*, where the coefficient k is within $k \in [1, k_0]$.

Specifying the values of k within $k \in [1, k_0]$, we can obtain estimates for various levels of the stress-strain state and limiting loads. At $k = 1$, the IS is in a purely elastic state, which corresponds to the lower boundary of the limiting load. The deformed state at $k < 1$ can be considered as a consequence of an increase in the potential energy of the system spent on the development of plastic deformations in the IS and, as a result, leads to an increase in the ultimate load compared to its level in the elastic state of the IS.

Statement: *For a given length of the PZ, the limiting load of the design model will be lower than the actual value of the limiting load, provided that the prerequisite condition is satisfied at k = 1.*

Since at k = 1 the stiffness of the rod in the IS is higher than the real stiffness of this section, the potential energy will be spent only on the creation of elastic deformations. They will be lower than the costs for the deformation of the elastoplastic section at k < 1. Therefore, these levels will determine the lower limits of ultimate loads.

The Statement is realized for the value of the plastic moment

$$M_0 = W_0\sigma_{yl},$$

where W_0 is the plastic section modulus. The frame calculation consists of two independent stages (elastic and plastic). The elastic stage of the calculation includes determining of a bending moment diagram M and finding of a critical section with the maximum moment $M_{\max}$ and the ratio

$$m = M_0 / M_{\max}. \quad (1)$$

By coefficient (1) is the ultimate elastic diagram of moments and ultimate load

$$M_e = mM,\ F_0 = mF. \quad (2)$$

It should be noted that the diagram M_e is *conditionally elastic*, since, alongside with the elastic values of the moments, it contains the maximum moment equal to M_0.

The plastic stage of the calculation is performed at a given length l_p using the method of sequential loadings. For each loading stage dF_0, we use incremental ratios connecting the diagrams of incremental moments and incremental loads. When determining the diagram of increments of moments, the basic system of the DM is used. For the first loading stage, the initial length l_{p1} can be taken based on the linear nature of the distribution of forces, for example, for the diagram M_e multiplied by the coefficient

$$n = 1 + dF_0 / F_0.$$

Based on the calculated correction (nonlinear) functions $f_j(\alpha_1)$ we form the coefficients (reactive forces) of the system of canonical equations and the right sides of the equations from incremental loads dF_0. After solving the system and obtaining the diagram of increments of moments dMp1, the resulting diagram is determined:

$$M_{p1} = M_e + dM_{p1},$$

from which we calculate the length l_{p2} for the next iteration step by the maximum value of the moment ($> M_0$). We simultaneously determine the current limiting load:

$$F_{p1} = F_0 + dF_0.$$

The obtained length is used to determine nonlinear functions $f_j(\alpha_2)$ for the second loading stage. In each i-th iteration, the following are calculated: the incremental moment diagram dM_{pi}, the resulting diagram M_{pi}, the limiting load:

$$M_{pi} = M_{p,i-1} + dM_{pi},\ \ F_{pi} = F_{p,i-1} + dF_0 \quad (3)$$

and the PZ length $l_{p,i}$. The loading process continues until the obtained value does not reach the specified length l_p according to the inequality:

$$(l_p - l_{p,i+1}) \le \text{eps}. \quad (4)$$

EQUAL STRENGTH PLASTIC ZONES

As it follows from the review, during frame deformations caused by the seismic action, PZs can occur in the end parts of both horizontal (beams) or vertical (columns) frame elements. The procedure of design an ESPZ for horizontal frame elements is shown below (Figure 3).

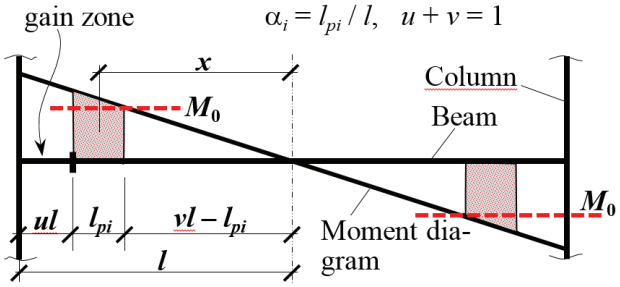

Figure 3. PZ in a beam of a seismic-resistant frame.

So that plastic deformations do not penetrate into the nodes of structural elements, according to the regulatory documents, the PZs are designed at a certain distance from the column. In this area (gain zone), the load-bearing capacity of the beam is ensured by increased rigidity. This is a mandatory requirement for both steel and RC structures [20, 21].

Taking into account the shape of the moment diagram (Figure 3), we accept the linear law of variation of the area moment of inertia

$$I_x = I\frac{x}{l(v-\alpha_i)}, \quad (5)$$

which ensures, within the limits of length l_p, an equal carrying capacity with stresses σ_{yl}.

For a standard beam supported according to the "fixed – pinned" scheme, shows all power characteristics from unit angle of rotation φ = 1 are given (Figure 4). The correction nonlinear function f_1 has the form:

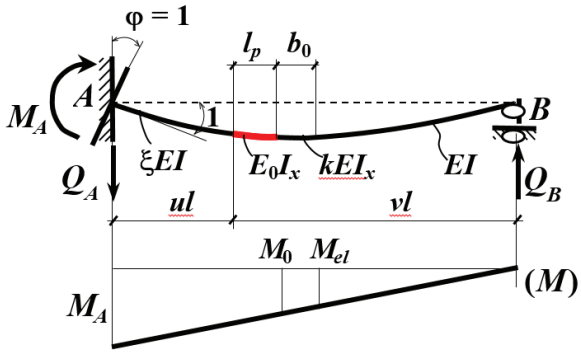

$$M_A = \frac{3EI}{l}\cdot\frac{1}{f_1} \qquad Q_B = -Q_A = \frac{3EI}{l^2}\cdot\frac{1}{f_1}$$

Figure 4. Beam with ESPZ ("fixed" – "pinned") at a unit angle of rotation.

$$f_1 = (1 - v^3) / \xi + 3\alpha_i b_i(v - \alpha_i / 2) / k_0, + \\ + [b_i^3 - (b_i - b_0)^3/k] + (b_i - b_0)^3, \quad (6)$$

where

$$b_i = (v - \alpha_i), \quad b_0 = v(1 - M_{el} / M_0)\ , \quad (7)$$
$$\alpha_i = l_{pi} / l,\ k_0 = E_0 / E,$$

ξ is the stiffness coefficient of the support (gain) zone; b_0 is the IS length.

The dimensionless function (6) contains four terms, each of which takes into account the contribution made to the overall ductility by the corresponding bar section, including the gain zone (1st term), the PZ (2nd term), and the IS (3 term). In the IS length formula (7), the elastic moment M_{el} is determined on the right IS boundary.

The second term in (6) was obtained for a section of the length l_{pi} taking into account the variable stiffness (5):

$$\delta_{pi} = \int_{vl-l_{pi}}^{vl} \frac{x^2 dx}{E_0 I_x} = \int_{vl-l_{pi}}^{vl} \frac{xl(v-\alpha_i)dx}{E_0 I} =$$

$$= \frac{l^3}{3EI} 3\alpha_i (v - \alpha_i)(v - \alpha_I / 2) / k_0.$$

The proposed approach is illustrated by an example of a static calculation of a two-story frame on the action of horizontal forces simulating the seismic impact.

EXAMPLE

The design scheme of a two-story steel frame is shown in Figure 5, *a* (F = 40 kN, $F_1 = -0{,}3F$, $F_2 = F$, l = 300 cm, $h_1 = 1{,}9l$, $h_2 = 1.6l$). The frame material is C345 steel. The crossbar of the lower story is made of a wended I-beam № 27 (shelf – sheet 0,65x7,0 cm; wall – sheet 0,5x25,7 cm: I_x = 2287,2 cm^4; W_x = 169,4 cm^3); the crossbar of the top floor and the vertical elements are made of twin channels № 20 (GOST 8240-72).

The strength characteristics are limits of yielding and strength, respectively: σ_{el} = 345 MPa, σ_B = 490 MPa. The modulus of elasticity is $E = 2{,}1\cdot10^5$ MPa, the modulus of hardening is E_0 = 647,33 MPa. The elastic moment and the plastic moment are, respectively: $M_{el} = W_x\sigma_{yl}$ = 58,45 kN·m, $M_0 = W_0\sigma_{yl}$ = 70,14 kN·m, where $W_0 = 1{,}2W_x$; flexural stiffnesses of the bars – EI = 4803,08 kN·m^2, E_0I = 15,92 kN·m^2; the coefficient k_0 = 0,0033.

The preliminary calculation shows that the maximum bending moments occur in the end parts of the crossbar of the 1st floor. The PZ is designed at u = 0,05 and ξ = 1,5 (Figure 5, *a*).

The purpose of the example is to show how the lower (at k = 1) boundaries of the limiting loads F_p are determined for the given ESPZ lengths l_p using the DM. We consider the PZ lengths from 2 cm to 14 cm, which are multiple to the pitch of 2 cm.

Due to the frame symmetry, the main DM system has four unknowns Z_k (Figure 5, *b*). The numbering of additional bonds is shown by the numbers in small squares. The relative length α_i of the ESPZ is formed in a nonlinear process at each i-th loading stage.

The pattern of solving the problem according to Statement at k = 1 is shown below. From the preliminary frame calculation (at F = 40 kN), we obtain the highest stresses in section 6 (Fig. 5*a*) with a bending moment M_6 = 63,43 kN

According to the elastic calculation results (at (1) m = 1,106), we will obtain a moment diagram (2)M_e containing the moment M_0 in section 6 and the limiting load F_0 = 44,229 kN (at l_p = 0). The diagram M_e is shown on the right half of the frame (Fig. 6, blue, the values are given in brackets).

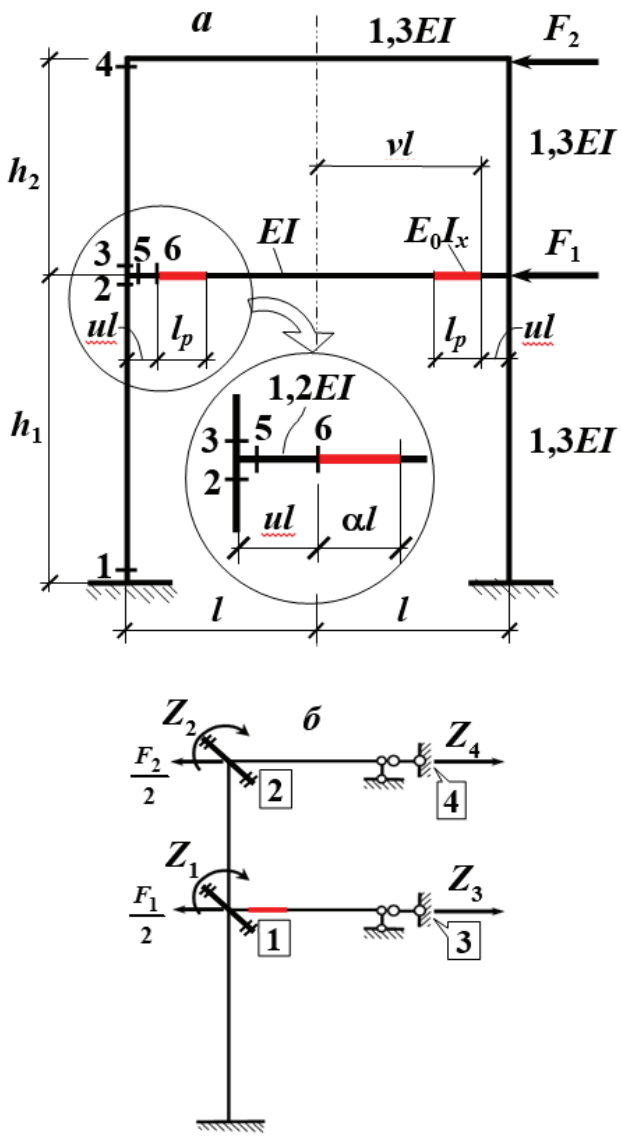

Figure 5. Design scheme of a two-story frame with PZs in the first-story crossbar (a); b – main system of the DM.

In the nonlinear calculation, the system of incremental canonical equations at the i-th loading stage has the form:

$$KdZ + R_{dF} = 0 \Leftrightarrow$$

$$\begin{bmatrix} r_{11} & r_{12} & r_{13} & r_{14} \\ r_{21} & r_{22} & r_{23} & r_{24} \\ r_{31} & r_{32} & r_{33} & r_{34} \\ r_{41} & r_{42} & r_{43} & r_{44} \end{bmatrix} \cdot \begin{bmatrix} dZ_1 \\ dZ_2 \\ dZ_3 \\ dZ_4 \end{bmatrix} + \begin{bmatrix} R_{1dF} \\ R_{2dF} \\ R_{3dF} \\ R_{4dF} \end{bmatrix} = 0,$$

where: $r_{11} = (6{,}121 + 3\frac{1}{f_1})\frac{EI}{l}$, $r_{12} = 1{,}661\frac{EI}{l}$,

$r_{13} = 0{,}906\frac{EI}{l^2}$, $r_{14} = -3{,}115\frac{EI}{l^2}$, $r_{22} = 7{,}31\frac{EI}{l}$,

$r_{23} = -r_{14}$, $r_{24} = r_{14}$, $r_{33} = 6{,}219\frac{EI}{l^2}$,

$r_{34} = -3{,}894\frac{EI}{l^3}$, $r_{44} = -r_{34}$;

$R_{1dF} = R_{2dF} = 0$, $R_{3dF} = -0{,}15dF$, $R_{4dF} = 0{,}5dF$.

A diagram of incremental bending moments for the 1st loading stage

$$dF = 0{,}0016\ F_0 = 0{,}0708 \text{ kN}$$

is shown on the left half of the frame (Figure 6).

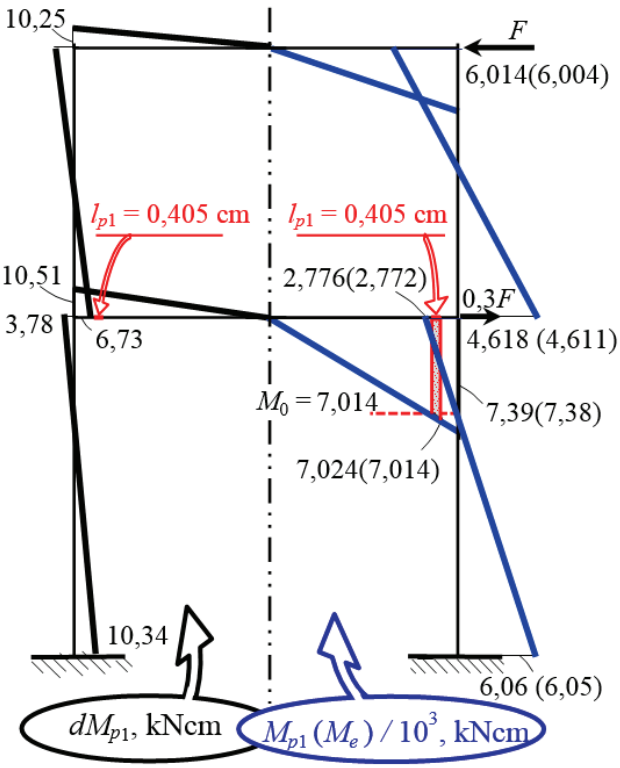

Figure 6. Bending moment diagrams at the 1st loading step at l_{p1} = 0.405 cm: to the left – incremental dM_{p1}; to the right – resulting M_{p1} (elastic M_e).

At the initial stage:

$$l_{p1} = vl(1 - M_0/M_6) = 0{,}145 \text{ cm},$$

where

$$M_6 = 1{,}0005M_0,$$

we form the correction function (6) $f_1 = 1{,}399$. After solving the system of the canonical equations of the DM, we obtain the diagram of incremental moments dM_{p1} (shown on the left half of the frame, Figure 6) and the resulting diagram

$$M_{p1} = M_e + dM_{p1}$$

(shown on the right half of the frame, Figure 6). According to the results of the 1st iteration, the ESPZ length was $l_{p2} = 0{,}405$ cm, the load was

$$F_{p1} = F_0 + dF = 44{,}3 \text{ kN}.$$

At the next loading steps for a given length l_p = 2 cm, the following results were obtained: l_{pi} = 2,002 cm, F_{pi} = 44,79 kN. The final nonlinear moment diagram M_p is shown on the left half of the frame (Figure 7).

The bending moment at the left end of the ESPZ (section 6) was

$$M_6 = 70{,}64 \text{ kNm} > M_0 = 70{,}14 \text{ kNm}.$$

The stresses were:

$\sigma_1 = -202{,}3$ MPa, $\sigma_4 = 200{,}6$ MPa;

$\sigma_5 = 243{,}8$ MPa $< \sigma_{yl} = 345$ MPa.

The moment diagram M_p for the length l_p = 14 cm obtained at the limiting load F_p = 59,8 (65,18) kN is shown on the right half of the frame (Figure 7). The results in brackets were obtained at the IS stiffness corresponding to the coefficient k = 0,5. The stresses were:

$\sigma_1 = 306{,}5$ (344,7) MPa,
$\sigma_4 = 303{,}7$ (342,4) MPa,
$\sigma_5 = 305{,}5$ (305,5) MPa.

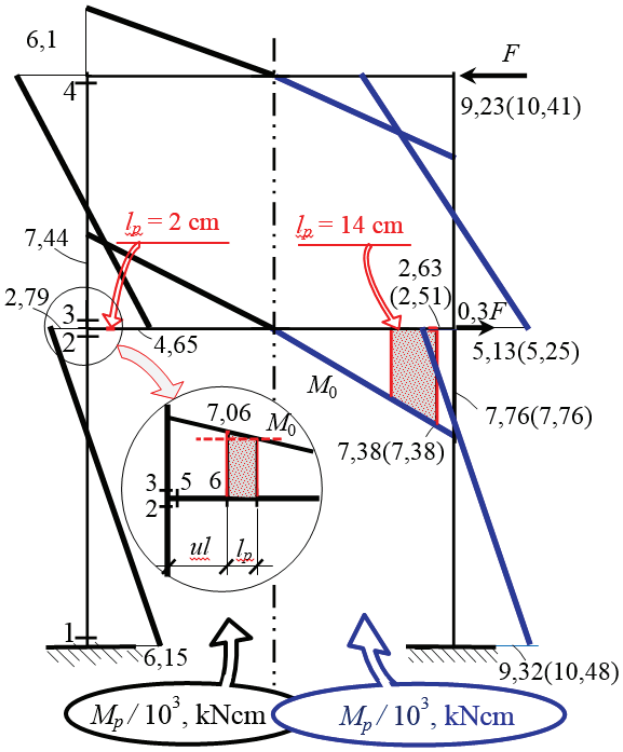

Figure 7. Bending moment diagrams M_p at the ESPZ length: l_p = 2 cm (to the left); l_p = 14 cm (to the right; in brackets the results are at k = 0,5).

Figure 8 gives a general picture of the change in the lower boundary of the limiting loads depending on the ESPZ lengths obtained for the perfect elastic state of the IS (at k = 1).

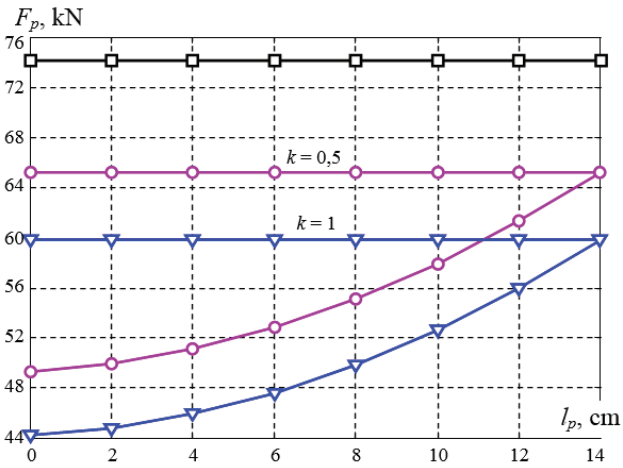

Figure 8. Limiting loads for the corresponding ESPZ: lower boundary (k = 1); limiting load boundary at the intermediate section stiffness coefficient k = 0,5.

When the IS stiffness decreases (at k = 0,5), the boundary of the limiting loads increases. The failure load P_0 = 74,07 kN calculated by the limiting equilibrium method is presented as a black horizontal straight line.

Thus, when designing an ESPZ of a given length, we proposed an approach to the nonlinear calculation of statical indeterminacy frames based on the DM, using a one-sided assessment in the analysis of the stress-strain state of the design models. In addition to the limiting equilibrium method, this approach can be used in the design of structural systems in regions of an increased seismic activity.

CONCLUSIONS

1. An algorithm is proposed for the elastoplastic calculation of statical indeterminacy frames using the DM based on Statement 1, which allows us to determine the lower boundary of the limiting load for a given ESPZ length;
2. The calculations according to the proposed methodology allow us to estimate more effectively the limiting loads for the specified zones of yielding and, thereby, to create more cost-effective and reliable structures;
3. The calculation method when creating a PZ of equal resistance can be recommended when designing earthquake-resistant frames;
4. The proposed methodology can be used in the educational process when studying the discipline “Nonlinear Problems of Structural Mechanics”.

REFERENCES

1. **Gvozdev A.A.** Raschet nesushhej sposobnosti konstrukcij po metodu predel'nogo ravnovesija [The Calculation of the Load-Bearing Capacity of Structures by the Limiting Equilibrium Method]. Moscow, Stroyizdat, 1949, 280 pages (in Russian).
2. SP 63.13330.2012 (SNiP 52-01-2003) Betonnye i zhelezobetonnye konstrukcii. Osnov-

nye polozhenija. Aktualizirovannaja redakcija SNiP 52-01-2003 [Concrete and Reinforced Concrete Structures. The Main Provisions (Updated version of SNiP 52-01-2003)]. Moscow, SUE Center for Design Products in Construction, 2012, 128 pages (in Russian).
3. SP 16.13330.2017 Stal'nye konstrukcii. Aktualizirovannaja redakcija SNiP II-23-81* [Steel Structures. Updated edition of SNiP II-23-81*]. Moscow, Ministry of Construction of Russia, 2017, 148 pages (in Russian).
4. **Birger I.A., Shorr B.F., Iosilevich G.B.** Raschet na prochnost' detalej mashin [Strength Analysis of Machine Parts]. Moscow, Mashinostroyenie (Mechanical Engineering), 1993, 640 pages (in Russian).
5. **Paulay T., Bull I.N.** Shear Effect on Plastic Hinges of Earthquake Resisting Reinforced Concrete Frames, Structural Concrete under Seismic Actions. // Bulletin D. Information. Comite Euro-International du Beton. Paris, 1979, No. 132, pp. 165-172.
6. **Travush V.I., Krylov S.B., Konin D.V., Krylov A.S.** Ultimate state of the support zone of reinforced concrete beams. // *Magazine of Civil Engineering*, 2018, No. 7, pp. 165-174.
7. ATC-40 Seismic Evaluation and Retrofit of Concrete Buildings, California, USA, 1996. 334 pages.
8. NZS 3101. Part 2. 2. 2006 Code of Design Practice for the Design of Concrete Structures, New Zealand Standards Association, Wellington, 17 pages.
9. Eurocode 8 (EUR 25204 EN – 2012): Seismic Design of Buildings. Worked examples, 522 pages.
10. **Zhao X., Wu Y.-F., Leung A.Yt., Lam H.F.** Plastic Length in Reinforced Concrete Flexural Members. // *Procedia Engineering*, 2011, Volume 14, pp. 1266-1274.
11. **Inel M., Ozmen H.B.** Effects of Plastic Hinge Properties in Nonlinear Analysis Reinforced Concrete Buildings. // *Journal of Engineering Structures*, 2006, Vol. 28, pp. 1494-1502.
12. **Yuan F., Wu Y.-F.** Effect of load cycling on plastic hinge length in RC columns. // *Journal of Engineering Structures*, 2017, Vol. 147, pp. 90-102.
13. **Yuan F., Wu Y.-F., Li C.-Q.** Modelling plastic hinge of FRP-confined RC columns. // *Journal of Engineering Structures*, 2017, Vol. 131, pp. 651-668.
14. **Megalooikonomou K.G., Tastani S.P., Pantazopoulou S.J.** Effect of yield penetration on column plastic hinge length. // *Journal of Engineering Structures*, 2018, Vol. 156, pp. 161-174.
15. **Alhasawi A., Heng P., Hjiaj M., Guezouli S., Battini J.-M.** Co-rotational planar beam element with generalized elasto-plastic hinges. // *Journal of Engineering Structures*, 2017, Vol. 151, pp. 188-205.
16. **Heng P., Alhasawi A., Battini J.-M., Hjiaj M.** Co-rotating rigid beam with generalized plastic hinges for the nonlinear dynamic analysis of planar framed structures subjected to impact loading. // *Finite Elements in Analysis and Design*, 2019, Vol. 157, pp. 38-49.
17. **Deng K., Wang T., Kurata M., Zhao C., Wang K.** Numerical study on a fully-prefabricated damage-tolerant beam to column connection for an earthquake-resilient frame. // *Journal of Engineering Structures*, 2018, Vol. 159, pp. 320-331.
18. **Deng K., Zheng D., Yang C., Xu T.** Experimental and Analytical Study of Fully Prefabricated Damage-Tolerant Beam to Column Connection for Earthquake-Resilient Frame. // *ASCE Journal of Structural Engineering*, 2019, Vol. 145, No. 3.
19. SNiP II-7-81*. Stroitel'stvo v sejsmicheskih rajonah [SNiP II-7-81*. Construction in Seismic Regions]. Gosstroy of Russia. Moscow: SUE Center for Design Products in Construction, 2002, 44 pages (in Russian).
20. Manual for the calculation and design of steel earthquake-resistant frames of multistory buildings (in the development of SNiP RK 2.03-04-2001). Part I., Ministry of Industry and Trade of the Republic of Kazakhstan (MIT of the RK). 2003, 52 pages

(in Russian).
21. **Sosnin A.V.** Metodika dvuhstadijnogo rascheta armirovanija jelementov zhelezobetonnyh karkasnyh zdanij i sooruzhenij na dejstvie sejsmicheskih sil s primeneniem koncepcii nelinejnogo staticheskogo analiza. Chast' 1: Postanovka zadachi, struktura metodiki, informacionnaja baza issledovanija i strategija opredelenija parametrov zon plastichnosti [The Methodology of a Two-Stage Calculation of Reinforcing Elements of Reinforced Concrete Frame Buildings and Structures on the Action of Seismic Forces Using the Concept of a Nonlinear Static Analysis. Part 1: Problem Statement, Methodology Structure, Research Information Base and Strategy for Determining the Parameters of Plasticity Zones]. // *Bulletin of SUSU. Series "Construction and Architecture"*, 2018, Vol. 18, No. 1, pp. 5-31 (in Russian).

СПИСОК ЛИТЕРАТУРЫ

1. **Гвоздев А.А.** Расчет несущей способности конструкций по методу предельного равновесия. – М.: Стройиздат, 1949. – 280 с.
2. СП 63.13330.2012 Бетонные и железобетонные конструкции. Основные положения. Актуализированная редакция СНиП 52-01-2003 (с Изменениями №1, 2, 3). – М.: АО «Кодекс», 2012. – 128 с.
3. СП 16.13330.2017 Стальные конструкции. Актуализированная редакция СНиП II-23-81* (с Поправкой, с Изменением №1). – М.: АО «Кодекс», 2017. – 148 с.
4. **Биргер И.А., Шорр Б.Ф., Иосилевич Г.Б.** Расчет на прочность деталей машин. – М.: Машиностроение, 1993. – 640 с.
5. **Paulay T., Bull I.N.** Shear Effect on Plastic Hinges of Earthquake Resisting Reinforced Concrete Frames, Structural Concrete under Seismic Actions. // Bulletin D. Information. Comite Euro-International du Beton. Paris, 1979, No. 132, pp. 165-172.
6. **Travush V.I., Krylov S.B., Konin D.V., Krylov A.S.** Ultimate state of the support zone of reinforced concrete beams. // *Magazine of Civil Engineering*, 2018, No. 7, pp. 165-174.
7. ATC-40 Seismic Evaluation and Retrofit of Concrete Buildings, California, USA, 1996. 334 pages.
8. NZS 3101. Part 2. 2. 2006 Code of Design Practice for the Design of Concrete Structures, New Zealand Standards Association, Wellington, 17 pages.
9. Eurocode 8 (EUR 25204 EN – 2012): Seismic Design of Buildings. Worked examples, 522 pages.
10. **Zhao X., Wu Y.-F., Leung A.Yt., Lam H.F.** Plastic Length in Reinforced Concrete Flexural Members. // *Procedia Engineering*, 2011, Volume 14, pp. 1266-1274.
11. **Inel M., Ozmen H.B.** Effects of Plastic Hinge Properties in Nonlinear Analysis Reinforced Concrete Buildings. // *Journal of Engineering Structures*, 2006, Vol. 28, pp. 1494-1502.
12. **Yuan F., Wu Y.-F.** Effect of load cycling on plastic hinge length in RC columns. // *Journal of Engineering Structures*, 2017, Vol. 147, pp. 90-102.
13. **Yuan F., Wu Y.-F., Li C.-Q.** Modelling plastic hinge of FRP-confined RC columns. // *Journal of Engineering Structures*, 2017, Vol. 131, pp. 651-668.
14. **Megalooikonomou K.G., Tastani S.P., Pantazopoulou S.J.** Effect of yield penetration on column plastic hinge length. // *Journal of Engineering Structures*, 2018, Vol. 156, pp. 161-174.
15. **Alhasawi A., Heng P., Hjiaj M., Guezouli S., Battini J.-M.** Co-rotational planar beam element with generalized elasto-plastic hinges. // *Journal of Engineering Structures*, 2017, Vol. 151, pp. 188-205.
16. **Heng P., Alhasawi A., Battini J.-M., Hjiaj M.** Co-rotating rigid beam with generalized plastic hinges for the nonlinear dynamic analysis of planar framed structures subjected to impact loading. // *Finite Elements in Analysis and Design*, 2019, Vol. 157, pp. 38-49.

17. **Deng K., Wang T., Kurata M., Zhao C., Wang K.** Numerical study on a fully-prefabricated damage-tolerant beam to column connection for an earthquake-resilient frame. // *Journal of Engineering Structures*, 2018, Vol. 159, pp. 320-331.
18. **Deng K., Zheng D., Yang C., Xu T.** Experimental and Analytical Study of Fully Prefabricated Damage-Tolerant Beam to Column Connection for Earthquake-Resilient Frame. // *ASCE Journal of Structural Engineering*, 2019, Vol. 145, No. 3.
19. СНиП II-7-81*. Строительство в сейсмических районах (с Изменениями и дополнениями). – М.: ГУП ЦПП, 2002. – 44 с.
20. Manual for the calculation and design of steel earthquake-resistant frames of multi-story buildings (in the development of SNiP RK 2.03-04-2001). Part I., Ministry of Industry and Trade of the Republic of Kazakhstan (MIT of the RK). 2003, 52 pages.
21. **Соснин А.В.** Методика двухстадийного расчета армирования элементов железобетонных каркасных зданий и сооружений на действие сейсмических сил с применением концепции нелинейного статического анализа. Часть 1: Постановка задачи, структура методики, информационная база исследования и стратегия определения параметров зон пластичности. // *Вестник Южно-Уральского государственного университета. Серия: «Строительство и архитектура»*, 2018, том 18, №1, с. 5-31.

Потапов Александр Николаевич, профессор, доктор технических наук; профессор кафедры «Строительное производство и теория сооружений», Южно-Уральский государственный университет (национальный исследовательский университет); 454080, Россия, г. Челябинск, пр. Ленина, дом 76;
тел.: +7(351) 267-91-83, +7(919) 343-71-29;
E-mail: potapov.alni@gmail.com.

Alexander N. Potapov, Dr.Sc., Professor; Professor of Department “Construction production and theory of structures”, South-Ural State University (national research university); 76, Lenin Prospect, Chelyabinsk, 454080, Russia; phone: +7(351) 267-91-83, +7(919) 343-71-29;
E-mail: potapov.alni@gmail.com.

DOI:10.22337/2587-9618-2019-15-3-131-148

ANALYSIS OF FORCED VIBRATIONS OF NONLINEAR PLATES IN A VISCOELASTIC MEDIUM UNDER THE CONDITIONS OF THE DIFFERENT COMBINATIONAL INTERNAL RESONANCES

Marina V. Shitikova, Vladimir V. Kandu
Voronezh State Technical University, Voronezh, RUSSIA

Abstract: In the present paper, the force driven dynamic response of a nonlinear plate embedded in a viscoelastic medium, damping features of which are described by the Kelvin-Voigt fractional derivative model, is studied. The motion of the plate is described by three coupled nonlinear differential equations with due account for the fact that the plate is being under the conditions of the internal combinational resonance accompanied by the external resonance, resulting in the interaction of three modes corresponding to the mutually orthogonal displacements. A comparative analysis of numerical calculations for the cases of free and forced vibrations has been carried out.

Keywords: Nonlinear vibrations of thin plates, interaction of internal and external resonances, fractional derivative viscoelastic surrounding medium, combinational internal resonance

ЧИСЛЕННЫЙ АНАЛИЗ ВЫНУЖДЕННЫХ НЕЛИНЕЙНЫХ КОЛЕБАНИЙ ПЛАСТИНОК В ВЯЗКОУПРУГОЙ СРЕДЕ ПРИ НАЛИЧИИ КОМБИНАЦИОННОГО РЕЗОНАНСА

М.В. Шитикова, В.В. Канду
Воронежский государственный технический университет, г. Воронеж, РОССИЯ

Аннотация: Исследованы нелинейные вынужденные колебания тонких пластинок в вязкоупругой среде, демпфирующие свойства которой задаются с помощью модели Кельвина-Фойгта с дробной производной. Колебания пластинки в вязкоупругой среде описываются в декартовской системе координат тремя дифференциальными уравнениями, с учетом того, что пластинка находится в условиях внутреннего комбинационного резонанса, сопровождаемого внешним резонансом. Приведен сравнительный анализ численных исследований свободных и вынужденных колебаний при наличии различных комбинационных внутренних резонансов для различных геометрических параметров пластинки.

Ключевые слова: нелинейные колебания пластинок, сочетание внутреннего и внешнего резонансов, дробная производная, комбинационный резонанс

1. INTRODUCTION

Recently the interest to nonlinear dynamic response of viscoelastic plates or elastic plates vibrating in a viscoelastic surrounding medium has been greatly renewed due to the appearance of advanced materials exhibiting nonlinear behaviour, and a comprehensive review in the field, including experimental results, could be found in [1-6]. In so doing the damping forces are usually taken into account via the Rayleigh's hypothesis [1,7], resulting in the modal damping [8], i.e. it is assumed that each natural mode of vibrations possesses its own damping coefficient dependent on its natural frequency. For describing the viscoelastic features of plates, the Kelvin-Voigt model [4] or standard linear solid model [5] are of

frequent use in engineering practice considering either linear or nonlinear springs in viscoelastic elements [9].

The analysis of free undamped [10] and damped [4] vibrations of nonlinear systems is of great importance for defining the dynamic system's characteristics dependent on the amplitude-phase relationships and modes of vibration. Moreover, nonlinear vibrations could be accompanied by such a phenomenon as the internal resonance, resulting in strong coupling between the modes of vibrations involved [10-15] and hence in the energy exchange between the interacting modes.

The internal resonance could be observed in the case of some combination of natural frequencies of one and the same type of vibrations. Thus, nonlinear vibrations of rectangular plates, dynamic behaviour of which is described by von Karman equations in terms of the plate's deflection and stress function, have been considered in [12] by reducing the governing equations to a set of two modal equations applying the Galerkin procedure. The case of the one-to-one internal resonance (when frequencies of two modes of flexural vibration are equal to each other) accompanied by the external resonance (when the frequency of the harmonic force is close to one of the natural frequency) has been studied.

The one-to-one internal resonance has been investigated also in [13] and [14] for nonlinear vertical vibrations of rectangular plates under the action of harmonic forces acting in the plate's plane [13] and out of the plate's plane [13,14], in so doing a set of three equations in terms of two in-plane displacements and deflection and a set of five equations considering the shear deformations have been used in [13] and [14], respectively. However, considering the inertia forces only for vertical vibrations and utilizing the Galerkin procedure, in both papers a set of two nonlinear equations has been obtained in terms of two flexural modes, which are assumed to be coupled via the one-to-one internal resonance.

For the first two natural modes of flexural vibrations, the cases of the 1:2 and 1:3 internal resonances have been also studied in [14].

Another type of the internal resonance has been investigated by Rossikhin and Shitikova [15-18], when one frequency of in-plane vibrations is equal (the 1:1 internal resonance [17,18]) or two times larger (the 1:2 internal resonance [15,18]) than a certain frequency of out-of-plane vibrations. As this takes place, a set of three nonlinear differential equations in terms of three mutually orthogonal displacements has been used considering inertia of all types of vibrations, what allows the authors to study further the combinational resonances of the additive and difference types [16,19-20]. Combinational types of the internal resonance result in the energy exchange between three or more subsystems. It should be noted that investigations in this direction were initiated by Witt and Gorelik [21], who pioneered in the theoretical and experimental analysis of the energy transfer from one subsystem to another using the simplest two-degree-of-freedom mechanical system, as an example.

Moreover, in order to study nonlinear free damped vibrations of a thin plate, the viscoelastic Kelvin-Voigt model involving fractional derivative [22] has been utilized, since this model possesses the advantage over the conventional Kelvin-Voigt model [10-14], because it provides the results matching the experimental data. Thus, for example, experimental data on ambient vibrations study for the Vincent-Thomas [23] and Golden Gate [24] suspension bridges have shown that different modes of vibrations possess different magnitudes of damping coefficients. Besides, the increase in the natural frequency results in the decrease in the damping ratio. In order to lead the theoretical investigation in the agreement with the experiment, in 1998 it was suggested in [25] to utilize the fractional derivatives to describe the processes of internal friction occurring in suspension combined systems, what allowed the authors in a natural

way to obtain the damping ratios, which depend on natural frequencies.

Nowadays fractional calculus is widely used for solving linear and nonlinear dynamic problems of structural mechanics, what is evident from numerous studies in the field, the overview of which could be found in the state-of-the-art articles by Rossikhin and Shitikova [26,27], wherein the examples of adopting the fractional derivative Kelvin-Voigt, Maxwell and standard linear solid models are provided for single-mass oscillators, rods, beams, plates, and shells.

In particular, linear vibrations of Kirchhoff-Love plates with the Kelvin-Voigt fractional damping were considered for rectangular and circular plates, respectively, in [28] and [29] using one equation for vertical vibrations, while utilizing three equations of in-plane and transverse vibrations in [7,30], and later multiplate systems were analyzed in [26,31]. It has been proved [27,32] that if viscoelastic properties of plates are described by the Kelvin-Voigt model assuming the Poisson's ratio as the time-independent value (though for real viscoelastic materials the Poisson's ratio is always a time-dependent function [33]), then this case coincides with the case of the dynamic behaviour of elastic bodies in a viscoelastic medium. Thus, the authors of [28,29], and not only them, replaced one problem with another, namely: a problem of the dynamic response of viscoelastic Kirchhoff-Love plates in a conventional medium with a problem of dynamic response of elastic Kirchhoff-Love plates in a viscoelastic medium, damping features of which are governed by the fractional derivative Kelvin-Voigt model. The vibration suppression of fractionally damped thin rectangular simply supported plates subjected to a concentrated harmonic loading has been studied recently in [34] in order to minimize the plate deflection, in so doing the vibration suppression is accomplished by attaching multiple absorbers modelled as the Kelvin-Voigt fractional oscillators, i.e. generalizing the approach suggested in [26,31].

As for the analysis of nonlinear vibrations of plates, then except the above mentioned papers [15-20], the fractional derivative Kelvin-Voigt model was used in [35-40] and fractional derivative standard linear solid model in [6,41,42] but without considering the phenomena of the internal resonance. Thus, free and forced vertical vibrations of an orthotropic plate have been studied in [35] considering first four modes of flexural vibrations, and during the analysis of force driven vibrations the frequency of a harmonic force was assumed to be equal to one of natural frequencies. The von Karman plate equation with fractional derivative damping was utilized in [36] for analyzing the cases of primary, subharmonic and superharmonic resonance conditions, when the harmonic force frequency, respectively, is approximately equal, three times less or larger than the first or second natural frequency of vertical vibrations. Nonlinear random vibrations of the same plate was studied in [39]. Dynamic nonlinear response to random excitation of a simply supported rectangular plate based on a foundation, damping features of which are described by the fractional derivative Kelvin-Voigt model, has been considered in [38]. The analysis of chaotic vibrations of simply supported nonlinear viscoelastic plate with fractional derivative Kelvin-Voigt model has been carried out in [40] for the case when the plate is subjected to an in-plane harmonic force in one direction and a transverse harmonic force. The Galerkin decomposition has been used to obtain the modal equation of the system, in so doing the authors restricted themselves only by the first mode. The fractional derivative standard linear solid model has been utilized in [42] for a viscoelastic layer for active damping of geometrically nonlinear vibrations of smart composite plates using the higher order plate theory and finite element method with discretizing the plate by eight-node isoparametric quadrilateral elements.

In the present paper, the approaches suggested in [18] for solving the problem on free nonlinear vibrations of elastic plates in a viscoelastic

medium, damping features of which are governed by the Riemann-Liouville derivatives of the fractional order, and in [43] for studying the dynamic response of the fractional Duffing oscillator subjected to harmonic loading are generalized for the case of forced vibrations of a simply-supported nonlinear thin elastic plate under the conditions of different combinational internal resonances, when three natural modes corresponding to mutually orthogonal displacements are coupled.

2. PROBLEM FORMULATION

2.1. Governing equations.

Let us consider the dynamic behavior of a simply supported nonlinear thin rectangular plate, vibrations of which in a viscoelastic fractional derivative medium are described by the following three differential equations in the dimensionless form [44, 45]:

$$u_{xx}+\frac{1-\nu}{2}\beta_1^2 u_{yy}+\frac{1+\nu}{2}\beta_1 v_{xy}+\frac{1+\nu}{2}\beta_1^2 w_y w_{xy}+ +w_x\left(w_{xx}+\frac{1-\nu}{2}\beta_1^2 w_{yy}\right)=\ddot{u}+æ_1 D_{0+}^{\gamma}u, \tag{1}$$

$$\beta_1^2 v_{yy}+\frac{1-\nu}{2}v_{xx}+\frac{1+\nu}{2}\beta_1 u_{xy}+\frac{1+\nu}{2}\beta_1 w_x w_{xy}+ +\beta_1 w_y\left(\beta_1^2 w_y+\frac{1-\nu}{2}w_{xx}\right)=\ddot{v}+æ_2 D_{0+}^{\gamma}v, \tag{2}$$

$$\begin{aligned}&\frac{\beta_2^2}{12}(w_{xxxx}+2\beta_1^2 w_{xxyy}+\beta_1^4 w_{yyyy})-\\ &-w_{xx}(u_x+\nu\beta_1 v_y)-w_x(u_{xx}+\nu\beta_1 v_{xy})-\\ &-\frac{1-\nu}{2}\beta_1\left[w_{xy}(\beta_1 u_y+v_x)+w_y(\beta_1 u_{xy}+v_{xx})\right]-\\ &-\beta_1^2\left[w_{yy}(\nu u_x+\beta_1 v_y)+w_y(\nu u_{xy}+\beta_1 v_{yy})\right]-\\ &-\frac{1-\nu}{2}\beta_1\left[w_{xy}(\beta_1 u_y+v_x)+w_x(\beta_1 u_{yy}+v_{xy})\right]-\\ &-\hat{F}\delta(x-x_0)\delta(y-y_0)\cos(\Omega_F t)=\\ &=-\ddot{w}-æ_3 D_{0+}^{\gamma}w,\end{aligned} \tag{3}$$

(4)

where $u=u(x,y,t)$, $v=v(x,y,t)$, and $w=w(x,y,t)$ are the displacements of points located in the plate's middle surface in the *x*-, *y*-, and *z*-directions, respectively, ν is the Poisson's ratio, $\beta_1=a/b$ and $\beta_2=h/a$ are the parameters defining the dimensions of the plate, *a* and *b* are the plate's dimensions along the *x*- and *y*-axes, respectively, *h* is the thickness, *t* is the time,

$$F=\hat{F}\delta(x-x_0)\delta(y-y_0)\cos(\Omega_F t)$$

is the harmonic force applied at the point with the coordinates x_0, y_0, $\hat{F}$ and Ω_F are its amplitude and frequency, respectively, δ is the Dirac delta function,

$$æ_i=\varepsilon\mu_i\tau_i^{\gamma}\ (i=1,2,3)$$

are damping coefficients, ε is a small dimensionless parameter of the same order of magnitude as the amplitudes, μ_i are finite values, τ_i is the relaxation time of the *i*th generalized displacement, D_{0+}^{γ} is the Riemann-Liouville fractional derivative of the γ-order [46], an overdot denotes the time-derivative, and lower indices label the derivatives with respect to the corresponding coordinates.

For solving nonlinear governing equations of motion (1)-(3), the procedure resulting in decoupling linear parts of equations has been proposed with the further utilization of the method of multiple scales [18,44,45], in so doing the amplitude functions are expanded into power series in terms of the small parameter and depend on different time scales. It has been shown that the phenomenon of internal resonance could be very critical, since in the thin plate under consideration the internal resonance is always present. Moreover, its type depends on the order of smallness of the viscosity involved into consideration [18]. The

following types of the internal resonance have been revealed:
of the order of ε:
the two-to-one internal resonance (1:2)

$$\begin{aligned}&\omega_1 = 2\omega_3 \quad (\omega_2 \neq \omega_1, \omega_2 \neq 2\omega_3),\\ &\omega_2 = 2\omega_3 \quad (\omega_1 \neq \omega_2, \omega_1 \neq 2\omega_3);\end{aligned} \tag{5}$$

the one-to-one-to-two internal resonance $(1:1:2)$

$$\omega_1 = \omega_2 = 2\omega_3; \tag{6}$$

of the order of ε^2:
the one-to-one internal resonance (1:1)

$$\begin{aligned}&\omega_1 = \omega_2 \quad (\omega_3 \neq \omega_1, \omega_3 \neq \omega_2),\\ &\omega_1 = \omega_3 \quad (\omega_2 \neq \omega_1, \omega_2 \neq \omega_3),\\ &\omega_2 = \omega_3 \quad (\omega_1 \neq \omega_2, \omega_1 \neq \omega_3);\end{aligned} \tag{7}$$

the one-to-one-to-one internal resonance $(1:1:1)$

$$\omega_1 = \omega_2 = \omega_3; \tag{8}$$

the combinational resonance of the additive-difference type

$$2\omega_3 = \omega_1 + \omega_2, \tag{9}$$

$$2\omega_3 = \omega_1 - \omega_2, \tag{10}$$

$$2\omega_3 = \omega_2 - \omega_1, \tag{11}$$

where ω_1 and ω_2 are the frequencies of certain modes of in-plane vibrations in the *x*- and *y*-axes, respectively, and ω_3 is the frequency of a certain mode of vertical vibrations.
Note that the cases of the internal resonances (4)-(7) have been studied recently by the authors in [44,45,47,48]. Thus, below we will examine in detail all possible cases of the combinational resonances (8)-(10).

2.2. Combinational resonance of the additive type $2\omega_3 \simeq \omega_1 + \omega_2$

Now let us consider the case of the additive internal combinational resonance (8) accompanied by the external resonance, i.e.,

$$2\omega_3 = \omega_1 + \omega_2 + 2\varepsilon^2\sigma$$

and

$$\Omega_F = \omega_3 + \varepsilon^2\sigma_F,$$

where σ is the detuning parameter characterizing the nearness between the natural frequencies of the coupled modes, and σ_F is the second detuning parameter defining the difference between the frequency of vertical vibrations and the frequency of the external force Ω_F.
Using the set of solvability equations to eliminate secular terms similarly to the case of free vibrations considered in [18] and adding the external resonance, we obtain the following solvability equations for the case of force driven vibrations:

$$\begin{aligned}&2i\omega_1 D_2 A_1 + \mu_1 (i\omega_1\tau_1)^{\gamma} A_1 + 2\zeta_1 (k_5 + k_7) A_1 A_3 \bar{A}_3 +\\ &+2\zeta_1 k_8 \bar{A}_2 A_3^2 \exp(2i\sigma T_2) = 0,\end{aligned} \tag{12}$$

$$\begin{aligned}&2i\omega_2 D_2 A_2 + \mu_2 (i\omega_2\tau_2)^{\gamma} A_2 + 2\zeta_2 (k_6 + k_8) A_2 A_3 \bar{A}_3 +\\ &+2\zeta_2 k_7 \bar{A}_1 A_3^2 \exp(2i\sigma T_2) = 0,\end{aligned} \tag{13}$$

$$\begin{aligned}&2i\omega_3 D_2 A_3 + \mu_3 (i\omega_3\tau_3)^{\gamma} A_3 +\\ &+\left[\zeta_{13}(k_1 + 2k_2) + \zeta_{23}(k_3 + 2k_4)\right] A_3^2 \bar{A}_3 +\\ &+\zeta_{13}(k_5 + k_7) A_1 \bar{A}_1 A_3 + \zeta_{23}(k_6 + k_8) A_2 \bar{A}_2 A_3 +\\ &+(\zeta_{13} k_8 + \zeta_{23} k_7) A_1 A_2 \bar{A}_3 \exp(-2i\sigma T_2) -\\ &-2f \exp(i\sigma_F T_2) = 0,\end{aligned} \tag{14}$$

where $D_2 = \partial / \partial T_2$ is the time-derivative due to the utilization of the generalized method of

multiple time scales [18], $A_j(T_2)$ $(j=1,2,3)$ are unknown complex functions, $\zeta_1, \zeta_2, \zeta_{13}, \zeta_{23}$ are coefficients depending on the plate dimensions and numbers of excited modes [18], k_p $(p=1,2,...8)$ are coefficients depending on the natural frequencies of plate, and f is a finite value.

To eliminate $\exp(\pm 2i\sigma_1 T_2)$ from equations (11)-(13), let us introduce the substitution

$$A_3(T_2) = A_3 \exp(-i\sigma T_2). \tag{15}$$

Representing the functions $A_i(T_2)$ in equations (11)-(13) in the polar form

$$A_i(T_2) = a_i(T_2)\exp\lfloor i\varphi_i(T_2)\rfloor \quad (i=1,2,3)$$

and separating real and imaginary parts yield

$$\left(a_1^2\right)' + s_1 a_1^2 = -2\omega_1^{-1}\zeta_1 k_8 a_1 a_2 a_3^2 \sin\delta, \tag{16}$$

$$\left(a_2^2\right)' + s_2 a_2^2 = -2\omega_2^{-1}\zeta_2 k_7 a_1 a_2 a_3^2 \sin\delta, \tag{17}$$

$$\left(a_3^2\right)' + s_3 a_3^2 = -2f\omega_3^{-1} a_3 \sin\beta_a + \\ +\omega_3^{-1}\left(\zeta_{13}k_8 + \zeta_{23}k_7\right) a_1 a_2 a_3^2 \sin\delta, \tag{18}$$

$$\dot{\varphi}_1 = \frac{1}{2}\lambda_1 + \omega_1^{-1}\zeta_1\left(k_5 + k_7\right) a_3^2 + \\ + \omega_1^{-1}\zeta_1 k_8 a_1^{-1} a_2 a_3^2 \cos\delta, \tag{19}$$

$$\dot{\varphi}_2 = \frac{1}{2}\lambda_2 + \omega_2^{-1}\zeta_2\left(k_6 + k_8\right) a_3^2 + \\ +\omega_2^{-1}\zeta_2 k_7 a_1 a_2^{-1} a_3^2 \cos\delta, \tag{20}$$

$$\dot{\varphi}_3 = \frac{1}{2}\lambda_3 + \frac{1}{2}\omega_3^{-1}\zeta_{13}\left(k_5 + k_7\right) a_1^2 + \\ + \frac{1}{2}\omega_3^{-1}\zeta_{23}\left(k_6 + k_8\right) a_2^2 + \\ + \frac{1}{2}\omega_3^{-1}\left[\zeta_{13}\left(k_1 + 2k_2\right) + \zeta_{23}\left(k_3 + 2k_4\right)\right] a_3^2 + \\ + \frac{1}{2}\omega_3^{-1}\left(\zeta_{13}k_8 + \zeta_{23}k_7\right) a_1 a_2 \cos\delta - \\ - f\left(\omega_3 a_3\right)^{-1}\cos\beta_a + \sigma, \tag{21}$$

where a dot denotes differentiation with respect to T_2, a_i and φ_i are amplitudes and phases, respectively,

$$\delta = 2\varphi_3 - \varphi_2 - \varphi_1$$

is the phase difference,

$$s_i = \mu_i \tau_i^{\gamma}\omega_i^{\gamma-1}\sin\psi, \ \psi = \pi\gamma/2,$$
$$\lambda_i = \mu_i \tau_i^{\gamma}\omega_i^{\gamma-1}\cos\psi, \text{ and } \beta_a = \varphi_3 - (\sigma_F + \sigma)T_2.$$

The set of Eqs. (15)-(20) describes the phase-amplitude modulations at nonlinear forced vibrations (1)-(3) in the case of the additive combinational resonance (8), and it is the generalizations of the case of free vibrations considered in detail in [19].

2.3. Combinational resonances of the difference type $2\omega_3 \simeq \omega_1 - \omega_2$

Now let us consider the difference combinational resonance (9) accompanied by the external resonance, i.e. when

$$2\omega_3 = \omega_1 - \omega_2 + 2\varepsilon^2\sigma$$

and

$$\Omega_F = \omega_3 + \varepsilon^2\sigma_F.$$

Then eliminating secular terms, we obtain the following solvability equations:

$$2i\omega_1 D_2 A_1 + \mu_1\left(i\omega_1\tau_1\right)^{\gamma} A_1 + 2\zeta_1\left(k_5 + k_7\right) A_1 A_3 \bar{A}_3 + \\ +2\zeta_1 k_6 A_2 A_3^2 \exp\left(2i\sigma T_2\right) = 0, \tag{22}$$

$$2i\omega_2 D_2 A_2 + \mu_2\left(i\omega_2\tau_2\right)^{\gamma} A_2 + 2\zeta_2\left(k_6 + k_8\right) A_2 A_3 \bar{A}_3 + \\ +2\zeta_2 k_7 A_1 \bar{A}_3^2 \exp\left(-2i\sigma T_2\right) = 0, \tag{23}$$

$$2i\omega_3 D_2 A_3 + \mu_3 (i\omega_3\tau_3)^{\gamma} A_3 + \left[\zeta_{13}(k_1+2k_2)+\zeta_{23}(k_3+2k_4)\right]A_3^2\bar{A}_3 + +\zeta_{13}(k_5+k_7)A_1\bar{A}_1A_3+\zeta_{23}(k_6+k_8)A_2\bar{A}_2A_3 + (24) +\left(\zeta_{13}k_6+\zeta_{23}k_7\right)A_1\bar{A}_2\bar{A}_3\exp(-2i\sigma T_2) - -2f\exp(i\sigma_F T_2)=0.$$

Applying to (21)-(23) the same procedure as it has been done above for (11)–(13), as a result, we have

$$\left(a_1^2\right)' + s_1 a_1^2 = -2\omega_1^{-1}\zeta_1 k_6 a_1 a_2 a_3^2 \sin\delta, \quad (25)$$

$$\left(a_2^2\right)' + s_2 a_2^2 = 2\omega_2^{-1}\zeta_2 k_7 a_1 a_2 a_3^2 \sin\delta, \quad (26)$$

$$\left(a_3^2\right)' + s_3 a_3^2 = -2f\omega_3^{-1}a_3\sin\beta_a + +\omega_3^{-1}\left(\zeta_{13}k_6+\zeta_{23}k_7\right)a_1a_2a_3^2\sin\delta, \quad (27)$$

$$\dot{\varphi}_1 = \frac{1}{2}\lambda_1 + \omega_1^{-1}\zeta_1(k_5+k_7)a_3^2 + +\omega_1^{-1}\zeta_1 k_6 a_1^{-1}a_2a_3^2\cos\delta, \quad (28)$$

$$\dot{\varphi}_2 = \frac{1}{2}\lambda_2 + \omega_2^{-1}\zeta_2(k_6+k_8)a_3^2 + +\omega_2^{-1}\zeta_2 k_7 a_1 a_2^{-1}a_3^2\cos\delta, \quad (29)$$

$$\dot{\varphi}_3 = \frac{1}{2}\lambda_3 + \frac{1}{2}\omega_3^{-1}\zeta_{13}(k_5+k_7)a_1^2 + +\frac{1}{2}\omega_3^{-1}\zeta_{23}(k_6+k_8)a_2^2+\sigma_1 + +\frac{1}{2}\omega_3^{-1}\left[\zeta_{13}(k_1+2k_2)+\zeta_{23}(k_3+2k_4)\right]a_3^2 + +\frac{1}{2}\omega_3^{-1}\left(\zeta_{13}k_6+\zeta_{23}k_7\right)a_1a_2\cos\delta - -f(\omega_3 a_3)^{-1}\cos\beta_a, \quad (30)$$

where $\delta = 2\varphi_3+\varphi_2-\varphi_1$

is the phase difference.

The set of Eqs. (24)-(29) describes the phase-amplitude modulations at nonlinear forced vibrations (1)-(3) in the case of the difference combinational resonance (9).

2.4. Combinational resonances of the difference type $2\omega_3 \simeq \omega_2 - \omega_1$

Now let us consider the difference combinational resonance (10) subjected to the external resonance, i.e. when

$$2\omega_3 = \omega_2 - \omega_1 + 2\varepsilon^2\sigma$$

and

$$\Omega_F = \omega_3 + \varepsilon^2\sigma_F .$$

In this case the solvability equations have the form

$$2i\omega_1 D_2 A_1 + \mu_1(i\omega_1\tau_1)^{\gamma}A_1 + 2\zeta_1(k_5+k_7)A_1A_3\bar{A}_3 + +2\zeta_1 k_8 A_2\bar{A}_3^2\exp(-2i\sigma T_2)=0, \quad (31)$$

$$2i\omega_2 D_2 A_2 + \mu_2(i\omega_2\tau_2)^{\gamma}A_2 + 2\zeta_2(k_6+k_8)A_2A_3\bar{A}_3 + +2\zeta_2 k_5 A_1 A_3^2\exp(2i\sigma T_2)=0, \quad (32)$$

$$2i\omega_3 D_2 A_3 + \mu_3(i\omega_3\tau_3)^{\gamma}A_3 + +\left[\zeta_{13}(k_1+2k_2)+\zeta_{23}(k_3+2k_4)\right]A_3^2\bar{A}_3 + +\zeta_{13}(k_5+k_7)A_1\bar{A}_1A_3+\zeta_{23}(k_6+k_8)A_2\bar{A}_2A_3 + (33) +\left(\zeta_{13}k_8+\zeta_{23}k_5\right)\bar{A}_1A_2\bar{A}_3\exp(-2i\sigma T_2) - -2f\exp(i\sigma_F T_2)=0.$$

Applying to (29)-(31) the same procedure as it has been done above for (11)–(13), as a result, we have

$$\left(a_1^2\right)' + s_1 a_1^2 = 2\omega_1^{-1}\zeta_1 k_8 a_1 a_2 a_3^2 \sin\delta, \quad (34)$$

$$\left(a_2^2\right)' + s_2 a_2^2 = -2\omega_2^{-1}\zeta_2 k_5 a_1 a_2 a_3^2 \sin\delta, \quad (35)$$

$$\left(a_3^2\right)' + s_3 a_3^2 = -2f\omega_3^{-1}a_3\sin\beta_a + +\omega_3^{-1}\left(\zeta_{13}k_8+\zeta_{23}k_5\right)a_1a_2a_3^2\sin\delta, \quad (36)$$

$$\dot{\varphi}_1 = \frac{1}{2}\sigma_1 + \omega_1^{-1}\zeta_1(k_5+k_7)a_3^2 + +\omega_1^{-1}\zeta_1 k_8 a_1^{-1}a_2a_3^2\cos\delta, \quad (37)$$

$$\dot{\varphi}_2 = \frac{1}{2}\lambda_2 + \omega_2^{-1}\zeta_2\left(k_6 + k_8\right)a_3^2 + \\ + \omega_2^{-1}\zeta_2 k_5 a_1 a_2^{-1} a_3^2 \cos\delta, \tag{38}$$

$$\dot{\varphi}_3 = \frac{1}{2}\lambda_3 + \frac{1}{2}\omega_3^{-1}\zeta_{13}\left(k_5 + k_7\right)a_1^2 + \\ + \frac{1}{2}\omega_3^{-1}\zeta_{23}\left(k_6 + k_8\right)a_2^2 + \sigma_1 + \\ + \frac{1}{2}\omega_3^{-1}\left[\zeta_{13}\left(k_1 + 2k_2\right) + \zeta_{23}\left(k_3 + 2k_4\right)\right]a_3^2 + \\ + \frac{1}{2}\omega_3^{-1}\left(\zeta_{13}k_8 + \zeta_{23}k_5\right)a_1 a_2 \cos\delta - \\ - f\left(\omega_3 a_3\right)^{-1}\cos\beta_a, \tag{39}$$

where $\delta = 2\varphi_3 + \varphi_1 - \varphi_2$

is the phase difference.

The set of Eqs. (33)-(38) describes the phase-amplitude modulations at nonlinear forced vibrations (1)-(3) in the case of the difference combinational resonance (10).

3. NUMERICAL CALCULATIONS

The differential equations (15)-(20), (24)-(29) and (33)-(38) describing the phase-amplitude modulation for the additive and difference combinational resonances (8)-(10) have been solved numerically using the Runge-Kutta fourth-order algorithm at different magnitudes of the fractional parameter γ. The geometrical parameters of the plate utilized for calculations are given in Table 1 for three types of the combinational resonance for three types of plates: square, rectangular and oblong.

The envelopes of the amplitudes for all nine examples presented in Table 1 are shown in Figures 1-9 for free ($f = 0$) and forced ($f \neq 0$) vibrations, wherein solid, dotted and dashed lines correspond to the functions $a_3(T_2)$, $a_2(T_2)$ and $a_1(T_2)$, respectively, allowing one to trace the energy exchange between three interacting modes coupled by the additive-difference combinational resonances (8)-(10).

The time T_2-dependence of the amplitude envelopes for a rectangular plate with the dimensions a = 0.57 m and b = 0.1425 m (cases № 1, 4 and 7 in Table 1) are shown in Figures 1, 4 and 7 at $f = 10$ for three types of the combinational resonance. It is seen that the most unfavorable is the difference combinational resonance

$$2\omega_3 \simeq \omega_2 - \omega_1,$$

Table 1. Plate parameters which satisfy the combinational resonance condition.

№	ω_1	m_1	n_1	ω_2	m_2	n_2	ω_3	m_3	n_3	a, m	b, m	h, m	ν
Combinational resonance: $2\omega_3 \simeq \omega_1 + \omega_2$ *and force amplitude level* $f = 10$													
1	15.7	3	1	9.29	3	1	13.33	6	1	0.57	0.1425	0.0513	0.3
2	37.83	9	1	44.953	3	3	41.668	3	3	1.14	0.1425	0.0285	0.3
3	16.92	5	2	11.9	4	5	14.25	4	3	0.25	0.25	0.05	0.3
Combinational resonance: $2\omega_3 \simeq \omega_1 - \omega_2$ *and force amplitude level* $f = 10$													
4	42.15	6	3	14.985	1	2	13.324	6	1	0.57	0.1425	0.0513	0.3
5	100.58	1	4	14.985	1	1	41.65	3	3	1.14	0.1425	0.0285	0.3
6	32.345	9	5	4.156	1	2	14.245	4	3	0.25	0.25	0.05	0.3
Combinational resonance: $2\omega_3 \simeq \omega_2 - \omega_1$ *and force amplitude level* $f = 1$													
7	26.842	3	2	47.639	9	6	10.51	5	1	0.57	0.1425	0.0513	0.3
8	25.328	1	1	61.783	9	4	18.3	1	2	1.14	0.1425	0.0285	0.3
9	7.025	1	1	13.142	5	5	2.85	2	1	0.25	0.25	0.05	0.3

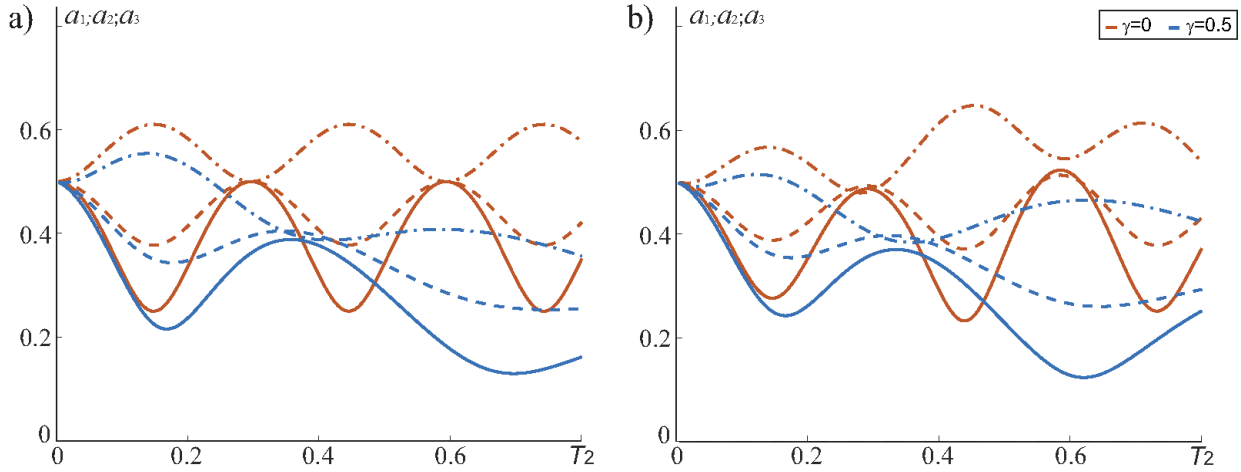

Figure 1. Amplitude envelopes of (a) free and (b) forced vibrations for plate №1 at the initial amplitudes $a_{i0} = 0.5$.

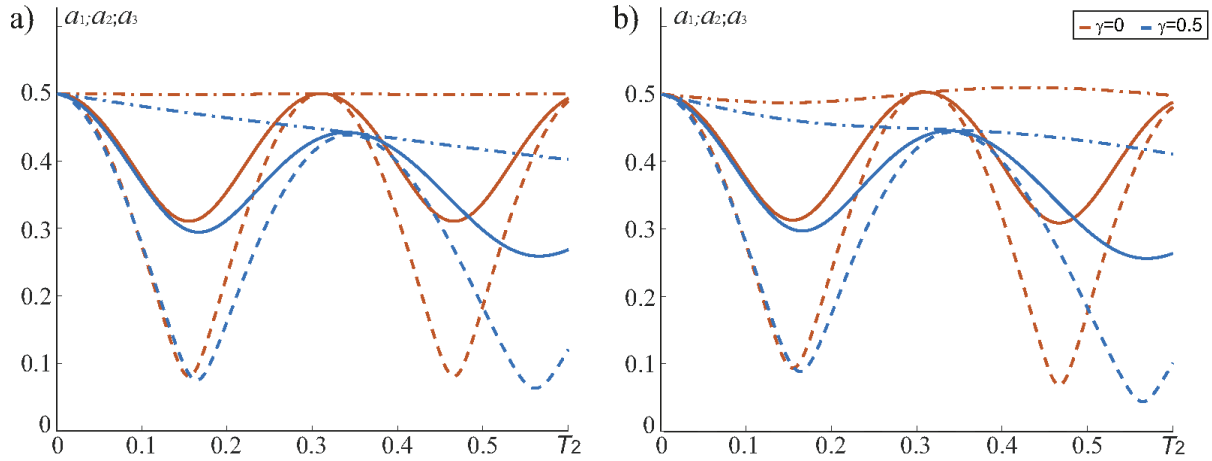

Figure 2. Amplitude envelopes of (a) free and (b) forced vibrations for plate №2 at $a_{i0} = 0.5$.

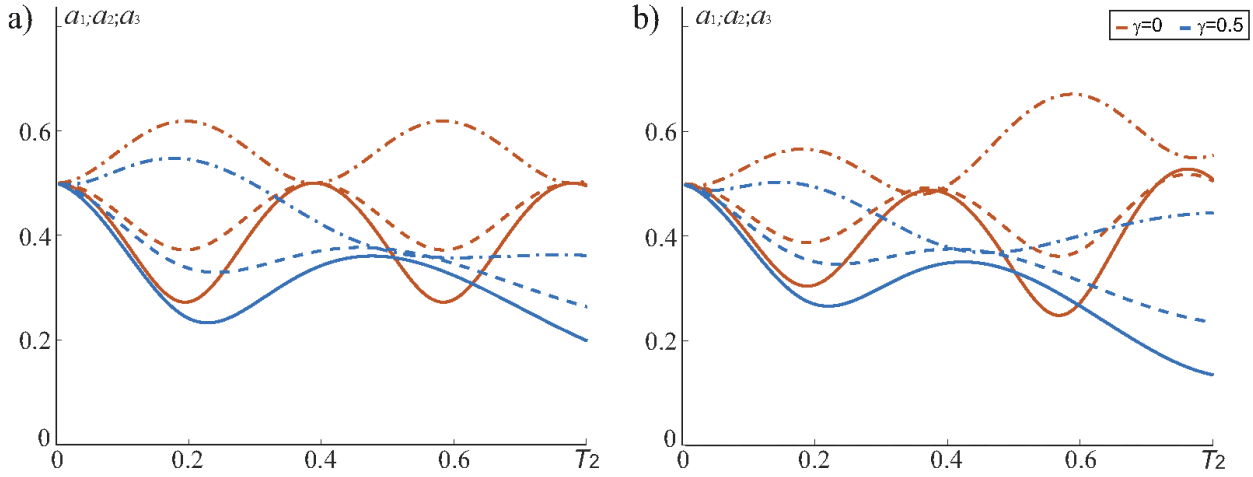

Figure 3. Amplitude envelopes of (a) free and (b) forced vibrations for plate №3 at $a_{i0} = 0.5$.

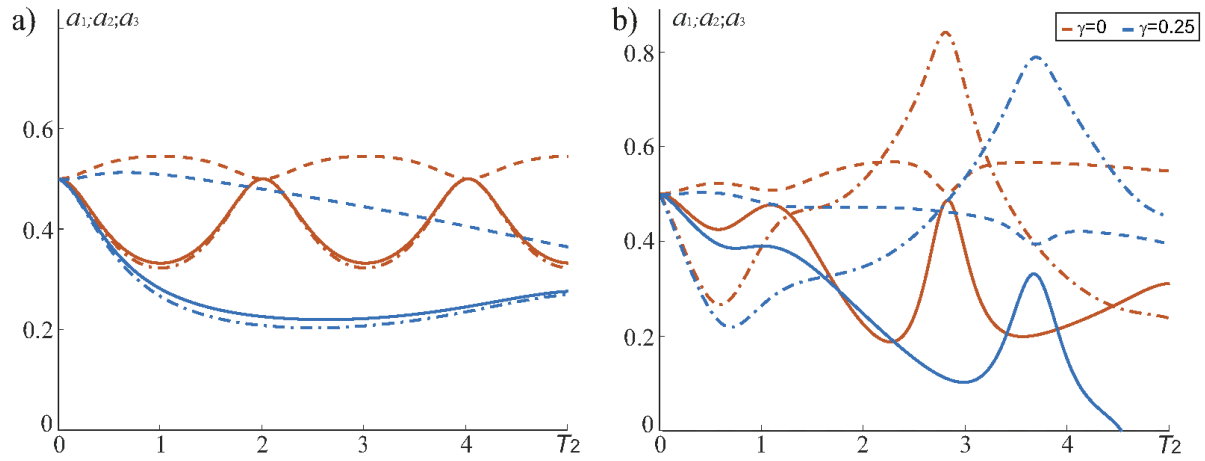

Figure 4. Amplitude envelopes of (a) free and (b) forced vibrations for plate №4 at $a_{i0} = 0.5$.

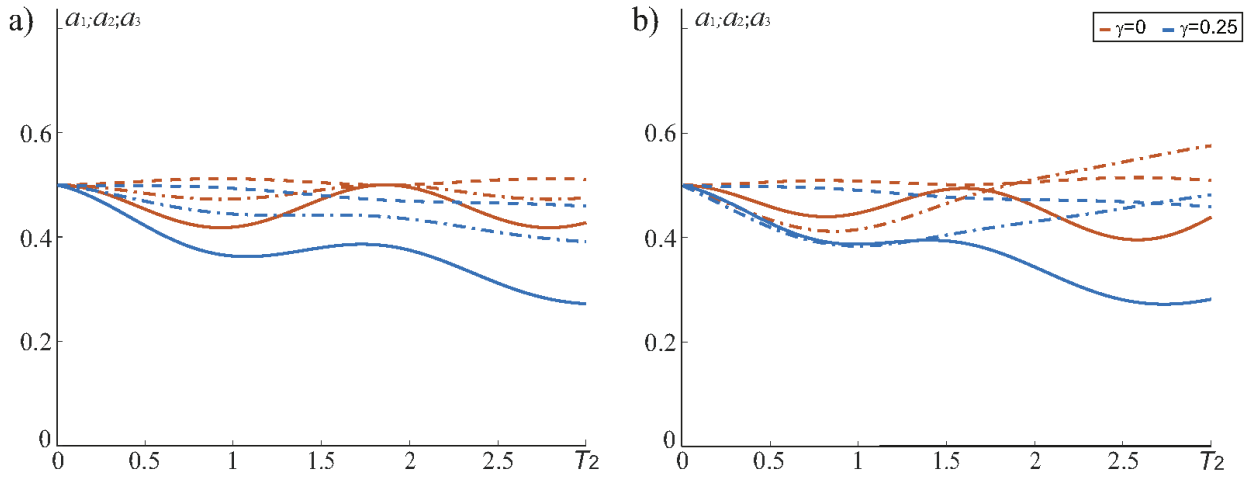

Figure 5. Amplitude envelopes of (a) free and (b) forced vibrations for plate №5 at $a_{i0} = 0.5$.

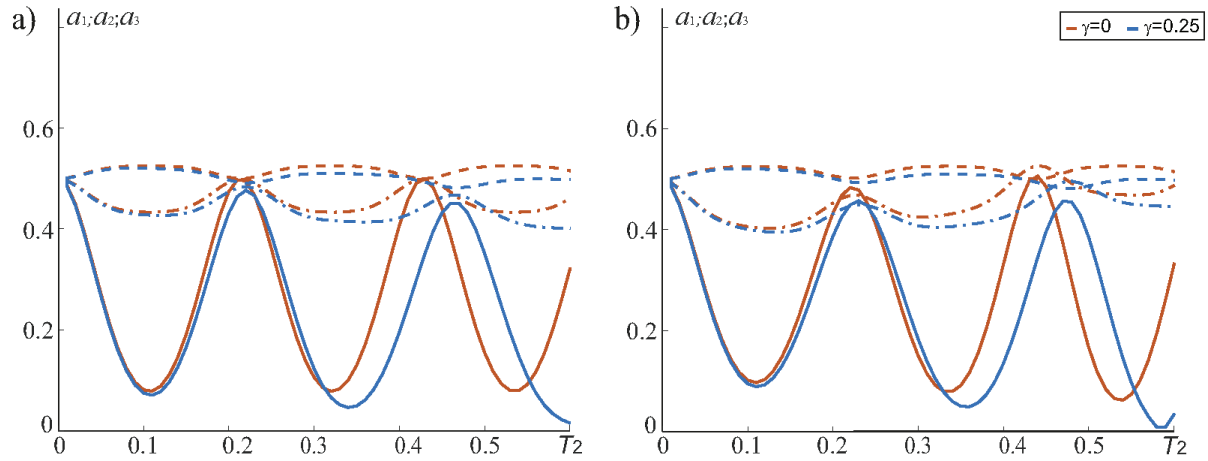

Figure 6. Amplitude envelopes of (a) free and (b) forced vibrations for plate №6 at $a_{i0} = 0.5$.

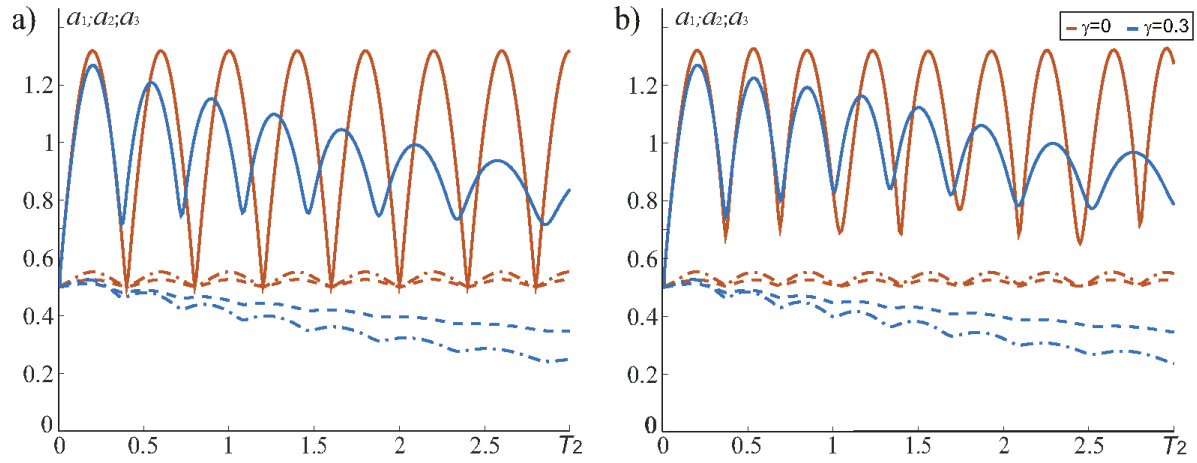

Figure 7. Amplitude envelopes of (a) free and (b) forced vibrations for plate №7 at $a_{i0} = 0.5$.

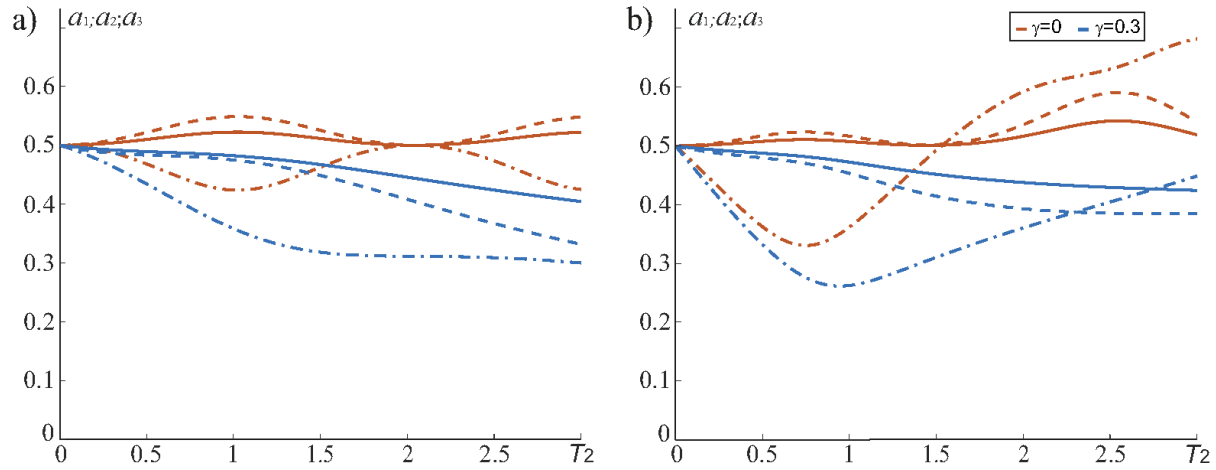

Figure 8. Amplitude envelopes of (a) free and (b) forced vibrations for plate №8 at $a_{i0} = 0.5$.

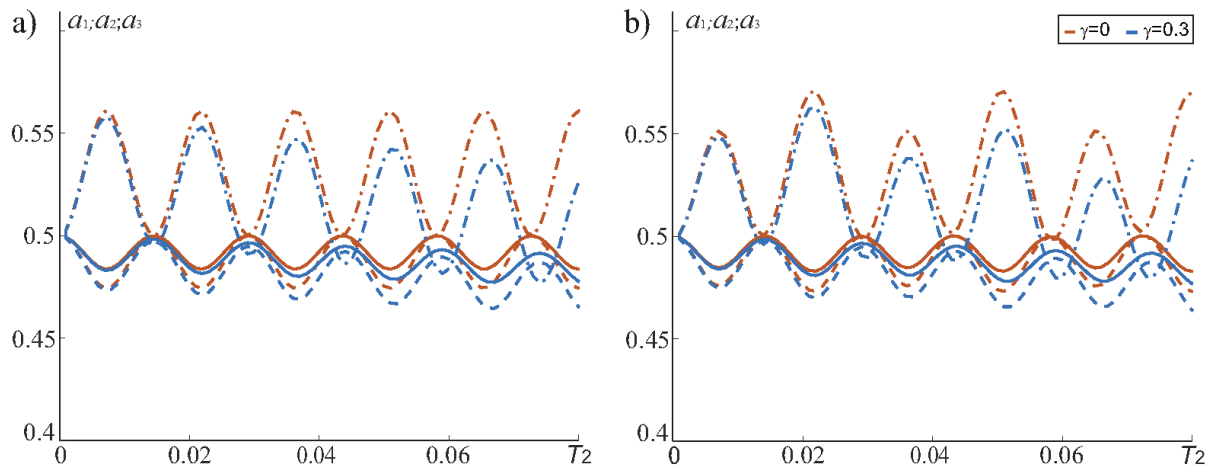

Figure 9. Amplitude envelopes of (a) free and (b) forced vibrations for plate №9 at $a_{i0} = 0.5$.

since it provides the essential increase in dimensionless amplitudes, resulting in high level of stresses and strains.

The time T_2-dependence of the amplitude envelopes for an oblong plate with dimensions a=1.14 m and b=0.1425 (cases 2, 5 and 8 in Table 1) is presented in Figures 2, 5 and 8 at $f=10$, whence it follows that the additive combinational resonance is the most unfavorable, while the difference resonances result in the monotonic variation of dimensionless amplitudes.

As for a square plate (cases 3, 6 and 9 in Table 1), then all types of the combinational resonance influence equally on the amplitudes variation with time.

4. CONCLUSION

In the present paper, nonlinear force driven vibrations of thin plates in a viscoelastic medium have been studied, when the motion of the plate is described by a set of three coupled nonlinear differential equations subjected to the condition of the combinational resonance accompanied by the external resonance. Nonlinear sets of resolving equations in terms of amplitudes and phase differences have been solved numerically using the Runge-Kutta fourth-order algorithm. The influence of viscosity on the energy exchange mechanism between interacting modes has been analyzed. It has been revealed that plates of different dimensions behave in a different manner under the additive and difference combinational resonances. Rectangular plates are more sensitive to plate's dimensions than square ones.

FUNDING

This research has been supported by the Ministry of Education and Science of the Russian Federation (Project 9.5138.2017/8.9).

REFERENCES

1. **Amabili M.** Nonlinear vibrations of rectangular plates with different boundary conditions: theory and experiments. // *Computers & Structures*, 2004, 82, pp. 2587-2605.
2. **Amabili M.** Nonlinear Vibrations and Stability of Shells and Plates. Cambridge University Press, London, 2008, 391 pages.
3. **Breslavsky I.D.**, **Amabili M.**, **Legrand M.** Physically and geometrically non-linear vibrations of thin rectangular plates. // *International Journal of Non-Linear Mechanics*, 2014, Vol. 58, pp. 30-40.
4. **Amabili M.** Nonlinear vibrations of viscoelastic rectangular plates. // *Journal of Sound and Vibration*, 2016, Vol. 362, pp. 142–156.
5. **Amabili M.** Nonlinear damping in nonlinear vibrations of rectangular plates: Derivation from viscoelasticity and experimental validation. // *Journal of the Mechanics and Physics of Solids*, 2018, Vol. 118, pp. 275–292.
6. **Amabili M.** Nonlinear damping in large-amplitude vibrations: modelling and experiments. // *Nonlinear Dynamics*, 2018, Vol. 93(1), pp. 5–18.
7. **Rossikhin Yu. A.**, **Shitikova M.V.** Thin bodies embedded in fractional derivative viscoelastic medium. // *Dynamic response, In: Encyclopedia of Continuum Mechanics*, edited by H. Altenbach, A. Ochsner, Springer, Berlin, Heidelberg, 2019.
8. **Clough R.W.**, **Penzien J.** Dynamics of Structures. McGraw-Hill, New York, 1975.
9. **Hedrih K.R.**, **Simonovic J.D.** Structural analogies on systems of deformable bodies coupled with non-linear layers. // *International Journal of Non-Linear Mechanics*, 2015, Vol. 73, pp. 18-24.
10. **Ribeiro P.**, **Petyt M.** Nonlinear free vibration of isotropic plates with internal resonance // *International Journal of Non-Linear Mechanics*, 2000, Vol. 35, pp. 263-278.

11. **Nayfeh A.H**. Nonlinear interaction: Analytical, computational, and experimental methods. New York, Wiley, 2000.
12. **Chang S.I.**, **Bajaj A.K.**, **Krousgrill C.M.** Non-linear vibrations and chaos in harmonically excited rectangular plates with one-to-one internal resonance. // *Nonlinear Dynamics*, 1993, Vol. 4(5), pp 433-460.
13. **Anlas G.**, **Elbeyli O.** Nonlinear vibrations of a simply supported rectangular metallic plate subjected to transverse harmonic excitation in the presence of a one-to-one internal resonance. // *Nonlinear Dynamics*, 2002, Vol. 30(1), pp. 1-28.
14. **Hao Y.X.**, **Zhang W.**, **Ji X.L.** Nonlinear dynamic response of functionally graded rectangular plates under different internal resonances. // *Mathematical Problems in Engineering*, 2010, Vol. 33, Article ID 738648.
15. **Rossikhin Yu.A.**, **Shitikova M.V.** Free damped non-linear vibrations of a viscoelastic plate under the two-to-one internal resonance. // *Materials Science Forum*, 2003, Vols. 440-441, pp. 29-36.
16. **Rossikhin Yu.A., Shitikova M.V., Ovsjannikova E.I.** Free damped vibrations of a nonlinear rectangular thin plate under the conditions of internal combinational resonance. // *Nonlinear Acoustics at the Beginning of the 21st Century*, *Proceedings of the 16th International Symposium on Nonlinear Acoustics* (O.V. Rudenko and O.A. Sapozhnikov, eds.), August 19-23, 2002, Moscow, Russia, Vol. 2, pp. 693-696.
17. **Rossikhin Yu.A.**, **Shitikova M.V.** Analysis of free non-linear vibrations of a viscoelastic plate under the conditions of different internal resonances. // *International Journal of Non-Linear Mechanics*, 2006, Vol. 2, pp. 313-325.
18. **Rossikhin Yu.A.**, **Shitikova M.V., Ngenzi J.Cl.** A new approach for studying nonlinear dynamic response of a thin plate with internal resonance in a fractional viscoelastic medium. // *Shock and Vibration*, 2015, Article ID 795606.
19. **Rossikhin Yu.A.**, **Shitikova M.V., Ngenzi J.Cl.** Phenomenological analysis of the additive combinational internal resonance in nonlinear vibrations of fractionally damped thin plates. // *WSEAS Transactions on Applied and Theoretical Mechanics*, 2015, Vol. 10, pp. 260-276.
20. **Rossikhin Yu.A.**, **Shitikova M.V.**, **Ngenzi J.Cl**. Fractional calculus application in problems of non-linear vibrations of thin plates with combinational internal resonances. // *Procedia Engineering*, 2016, Vol. 144, pp. 849-858.
21. **Witt A.A.**, **Gorelik G.S.** Oscillations of an elastic pendulum as an example of the oscillations of two parametrically coupled linear systems. // *Journal Technical Physics*, 1933, Vol. 3(2-3), pp. 294-307.
22. **Rossikhin Yu.A.**, **Shitikova M.V.** Applications of fractional calculus to dynamic problems of linear and nonlinear hereditary mechanics of solids. // *Applied Mechanics Reviews*, 1997, Vol. 50, pp. 15-67.
23. **Abdel-Ghaffar A.M.**, **Housner G.W.** Ambient vibration tests of suspension bridge. // *Journal of the Engineering Mechanics Division*, 1978, Vol. 104(5), pp. 983-999.
24. **Abdel-Ghaffar A.M.**, **Scanlan R.H.** Ambient vibration studies of Golden Gate bridge: I. Suspended structure. // *ASCE Journal of Engineering Mechanics*, 1985, Vol. 111, pp. 463-482.
25. **Rossikhin Yu.A.**, **Shitikova M.V.** Application of fractional calculus for analysis of nonlinear damped vibrations of suspension bridges. // *Journal of Engineering Mechanics*, 1998, Vol. 124, pp. 1029-1036.
26. **Rossikhin Yu.A.**, **Shitikova M.V.** Application of fractional calculus for dynamic problems of solid mechanics: novel trends and recent results. // *Applied*

Mechanics Reviews, 2010, Vol. 63, Article ID 01081.

27. **Rossikhin Yu.A.**, **Shitikova M.V.** Fractional calculus in structural mechanics, In: Handbook of Fractional Calculus with Applications. Vol 7: Applications in Engineering, Life and Social Sciences, Part A, edited by D. Baleanu, A.M. Lopes (De Gruyter, Berlin, 2019), pp. 159-192.
28. (**Stevanovic**) **Hedrih K.** Partial fractional differential equations of creeping and vibrations of plate and their solutions (First part). // *Journal of Mechanical Behavior of Materials*, 2005, Vol. 16, Issue 4-5, pp. 305-314.
29. **Ingman D.**, **Suzdalnitsky J.** Response of viscoelastic plate to impact. // *ASME Journal of Vibration and Acoustics*, 2008, Vol. 131(7), pp. 763-767.
30. **Rossikhin Yu.A.**, **Shitikova M.V.** Analysis of damped vibrations of linear viscoelastic plates with damping modeled with fractional derivatives. // *Signal Processing*, 2006, Vol. 86(10), pp. 2703-2711.
31. (**Stevanovic**) **Hedrih K.** Dynamics of coupled systems. // *Nonlinear Analysis: Hybrid Systems*, 2008, Vol. 2, pp. 310-334.
32. **Rossikhin Yu.A.**, **Shitikova M.V.**, **Trung P.T.** Application of the fractional derivative Kelvin–Voigt model for the analysis of impact response of a Kirchhoff-Love plate. // *WSEAS Transactions on Mathematics*, 2016, Vol. 15, pp. 498-501.
33. **Hilton H.H.** Implications and constraints of time-independent Poisson ratios in linear isotropic and anisotropic viscoelasticity. // *Journal of Elasticity*, 2001, Vol. 63(3), pp. 221-251.
34. **Ari M.**, **Faal R.T.**, **Zayernouri M.** Vibrations suppression of fractionally damped plates using multiple optimal dynamic vibration. // *International Journal of Computer Mathematics*, 2019, DOI: 10.1080/00207160.2019.1594792.
35. **Mashrouteh S.** Nonlinear vibration analysis of viscoelastic plates with fractional damping. Master Thesis, University of Ontario, Institute of Technology, 2017.
36. **Permoon M. R.**, **Haddadpour H.**, **Javadi M.** Nonlinear vibration of fractional viscoelastic plate: primary, subharmonic, and superharmonic response. // *International Journal of Non-Linear Mechanics*, 2018, Vol. 99, pp. 154-164.
37. **Babouskos N.G.**, **Katsikadelis J.T.** Nonlinear vibrations of viscoelastic plates of fractional derivative type: An AEM solution. // *The Open Mechanics Journal*, 2010, Vol. 4(8), pp. 8-20.
38. **Hosseinkhani A.**, **Younesian D.**, **Farhangdoust S.** Dynamic analysis of a plate on the generalized foundation with fractional damping subjected to random excitation. // *Mathematical Problems in Engineering*, 2018, ID 3908371.
39. **Malara G.**, **Spanos P.D.** Nonlinear random vibrations of plates endowed with fractional derivative elements. // *Probabilistic Engineering Mechanics*, 2018, Vol. 54, pp. 2-8.
40. **Nwagoum Tuwa P.R.**, **Miwadinou C.H.**, **Monwanou A.V.**, **Chabi Orou J.B.**, **Woafo P.** Chaotic vibrations of nonlinear viscoelastic plate with fractional derivative model and subjected to parametric and external excitations. // *Mechanics Research Communications*, 2019, Vol. 97, pp. 8-15.
41. **Litewka P.**, **Lewandowski R.** Steady-state non-linear vibrations of plates using Zener material model with fractional derivative. // *Computational Mechanics*, 2017, Vol. 60, pp. 333-354.
42. **Datta P.**, **Ray M.C.** Fractional order derivative model of viscoelastic layer for active damping of geometrically nonlinear vibrations of smart composite plates. // *CMC*, 2015, Vol. 49-50(1), pp. 47-80.
43. **Rossikhin Yu.A.**, **Shitikova M.V.**, **Shcheglova T.A.** Forced vibrations of a nonlinear oscillator with weak fractional damping. // *Journal of Mechanics of Materials and Structures*, 2009, Vol. 4(9), pp. 1619-1636.

44. **Shitikova M.V.**, **Rossikhin Yu.A.**, **Kandu V.** Interaction of internal and external resonances during force driven vibrations of a nonlinear thin plate embedded into a fractional derivative medium. // *Procedia Engineering*, 2017, Vol. 199, pp. 832-837.
45. **Shitikova M.V.**, **Kandu V.V.** Chislennyj analiz vynuzhdennyh kolebanij nelinejnyh plastinok v vjazkouprugoj srede pri nalichii vnutrennego rezonansa odin k odnomu [Force driven nonlinear vibrations of a thin plate in one-to-one internal resonance in a fractional viscoelastic medium]. // *News of higher educational institutions. Construction*, 2018, 12, pp. 9-22.
46. **Samko S.G.**, **Kilbas A.A.**, **Marichev O.I.** fractional integrals and derivatives. theory and applications. Gordon and Breach Science Publishers, Amsterdam, 1993.
47. **Kandu V.V., Shitikova M.V., Rossikhin Yu.A.** Chislennyj analiz vynuzhdennyh kolebanij nelinejnyh plastinok v vjazkouprugoj srede pri nalichii vnutrennego rezonansa 1:1:2 [Numerical analysis of forced nonlinear vibrations of plates in a viscoelastic medium at the presence of the 1:1:2 internal resonance]. // *Proceedings of the X All-Russian Conference on Mechanics of Deformable Solids*, Samara, 18-22 September 2017, Vol. 2, pp. 10-12.
48. **Shitikova M.V., Kandu V.V.** Modelirovanie vynuzhdennyh kolebanij nelinejnyh plastinok v vjazkouprugoj srede pri nalichii vnutrennego rezonansa 1:1:1 [Modelling of forced vibrations of nonlinear plates in a viscoelastic medium at the 1:1:1 internal resonance]. // *Proceedings of the International Conference on Actual Problems of Applied Mathematics, Informatics, and Mechanics*, Voronezh, 17–19 December, 2018. Voronezh, Publishing House “Research Publications”, 2019, pp. 1295-1300.

СПИСОК ЛИТЕРАТУРЫ

1. **Amabili M.** Nonlinear vibrations of rectangular plates with different boundary conditions: theory and experiments. // *Computers & Structures*, 2004, 82, pp. 2587-2605.
2. **Amabili M.** Nonlinear Vibrations and Stability of Shells and Plates. Cambridge University Press, London, 2008, 391 pages.
3. **Breslavsky I.D.**, **Amabili M.**, **Legrand M.** Physically and geometrically non-linear vibrations of thin rectangular plates. // *International Journal of Non-Linear Mechanics*, 2014, Vol. 58, pp. 30-40.
4. **Amabili M.** Nonlinear vibrations of viscoelastic rectangular plates. // *Journal of Sound and Vibration*, 2016, Vol. 362, pp. 142–156.
5. **Amabili M.** Nonlinear damping in nonlinear vibrations of rectangular plates: Derivation from viscoelasticity and experimental validation. // *Journal of the Mechanics and Physics of Solids*, 2018, Vol. 118, pp. 275–292.
6. **Amabili M.** Nonlinear damping in large-amplitude vibrations: modelling and experiments. // *Nonlinear Dynamics*, 2018, Vol. 93(1), pp. 5–18.
7. **Rossikhin Yu. A.**, **Shitikova M.V.** Thin bodies embedded in fractional derivative viscoelastic medium. // *Dynamic response, In: Encyclopedia of Continuum Mechanics*, edited by H. Altenbach, A. Ochsner, Springer, Berlin, Heidelberg, 2019.
8. **Clough R.W.**, **Penzien J.** Dynamics of Structures. McGraw-Hill, New York, 1975.
9. **Hedrih K.R.**, **Simonovic J.D.** Structural analogies on systems of deformable bodies coupled with non-linear layers. // *International Journal of Non-Linear Mechanics*, 2015, Vol. 73, pp. 18-24.
10. **Ribeiro P.**, **Petyt M.** Nonlinear free vibration of isotropic plates with internal resonance // *International Journal of Non-Linear Mechanics*, 2000, Vol. 35, pp. 263-278.

11. **Nayfeh A.H**. Nonlinear interaction: Analytical, computational, and experimental methods. New York, Wiley, 2000.
12. **Chang S.I.**, **Bajaj A.K.**, **Krousgrill C.M.** Non-linear vibrations and chaos in harmonically excited rectangular plates with one-to-one internal resonance. // *Nonlinear Dynamics*, 1993, Vol. 4(5), pp 433-460.
13. **Anlas G.**, **Elbeyli O.** Nonlinear vibrations of a simply supported rectangular metallic plate subjected to transverse harmonic excitation in the presence of a one-to-one internal resonance. // *Nonlinear Dynamics*, 2002, Vol. 30(1), pp. 1-28.
14. **Hao Y.X.**, **Zhang W.**, **Ji X.L.** Nonlinear dynamic response of functionally graded rectangular plates under different internal resonances. // *Mathematical Problems in Engineering*, 2010, Vol. 33, Article ID 738648.
15. **Rossikhin Yu.A.**, **Shitikova M.V.** Free damped non-linear vibrations of a viscoelastic plate under the two-to-one internal resonance. // *Materials Science Forum*, 2003, Vols. 440-441, pp. 29-36.
16. **Rossikhin Yu.A., Shitikova M.V., Ovsjannikova E.I.** Free damped vibrations of a nonlinear rectangular thin plate under the conditions of internal combinational resonance. // *Nonlinear Acoustics at the Beginning of the 21st Century, Proceedings of the 16th International Symposium on Nonlinear Acoustics* (O.V. Rudenko and O.A. Sapozhnikov, eds.), August 19-23, 2002, Moscow, Russia, Vol. 2, pp. 693-696.
17. **Rossikhin Yu.A.**, **Shitikova M.V.** Analysis of free non-linear vibrations of a viscoelastic plate under the conditions of different internal resonances. // *International Journal of Non-Linear Mechanics*, 2006, Vol. 2, pp. 313-325.
18. **Rossikhin Yu.A.**, **Shitikova M.V., Ngenzi J.Cl.** A new approach for studying nonlinear dynamic response of a thin plate with internal resonance in a fractional viscoelastic medium. // *Shock and Vibration*, 2015, Article ID 795606.
19. **Rossikhin Yu.A.**, **Shitikova M.V., Ngenzi J.Cl.** Phenomenological analysis of the additive combinational internal resonance in nonlinear vibrations of fractionally damped thin plates. // *WSEAS Transactions on Applied and Theoretical Mechanics*, 2015, Vol. 10, pp. 260-276.
20. **Rossikhin Yu.A.**, **Shitikova M.V.**, **Ngenzi J.Cl**. Fractional calculus application in problems of non-linear vibrations of thin plates with combinational internal resonances. // *Procedia Engineering*, 2016, Vol. 144, pp. 849-858.
21. **Witt A.A.**, **Gorelik G.S.** Oscillations of an elastic pendulum as an example of the oscillations of two parametrically coupled linear systems. // *Journal Technical Physics*, 1933, Vol. 3(2-3), pp. 294-307.
22. **Rossikhin Yu.A.**, **Shitikova M.V.** Applications of fractional calculus to dynamic problems of linear and nonlinear hereditary mechanics of solids. // *Applied Mechanics Reviews*, 1997, Vol. 50, pp. 15-67.
23. **Abdel-Ghaffar A.M.**, **Housner G.W.** Ambient vibration tests of suspension bridge. // *Journal of the Engineering Mechanics Division*, 1978, Vol. 104(5), pp. 983-999.
24. **Abdel-Ghaffar A.M.**, **Scanlan R.H.** Ambient vibration studies of Golden Gate bridge: I. Suspended structure. // *ASCE Journal of Engineering Mechanics*, 1985, Vol. 111, pp. 463-482.
25. **Rossikhin Yu.A.**, **Shitikova M.V.** Application of fractional calculus for analysis of nonlinear damped vibrations of suspension bridges. // *Journal of Engineering Mechanics*, 1998, Vol. 124, pp. 1029-1036.
26. **Rossikhin Yu.A.**, **Shitikova M.V.** Application of fractional calculus for dynamic problems of solid mechanics: novel trends and recent results. // *Applied*

Mechanics Reviews, 2010, Vol. 63, Article ID 01081.

27. **Rossikhin Yu.A.**, **Shitikova M.V.** Fractional calculus in structural mechanics, In: Handbook of Fractional Calculus with Applications. Vol 7: Applications in Engineering, Life and Social Sciences, Part A, edited by D. Baleanu, A.M. Lopes (De Gruyter, Berlin, 2019), pp. 159-192.
28. (**Stevanovic**) **Hedrih K.** Partial fractional differential equations of creeping and vibrations of plate and their solutions (First part). // *Journal of Mechanical Behavior of Materials*, 2005, Vol. 16, Issue 4-5, pp. 305-314.
29. **Ingman D.**, **Suzdalnitsky J.** Response of viscoelastic plate to impact. // *ASME Journal of Vibration and Acoustics*, 2008, Vol. 131(7), pp. 763-767.
30. **Rossikhin Yu.A.**, **Shitikova M.V.** Analysis of damped vibrations of linear viscoelastic plates with damping modeled with fractional derivatives. // *Signal Processing*, 2006, Vol. 86(10), pp. 2703-2711.
31. (**Stevanovic**) **Hedrih K.** Dynamics of coupled systems. // *Nonlinear Analysis: Hybrid Systems*, 2008, Vol. 2, pp. 310-334.
32. **Rossikhin Yu.A.**, **Shitikova M.V.**, **Trung P.T.** Application of the fractional derivative Kelvin–Voigt model for the analysis of impact response of a Kirchhoff-Love plate. // *WSEAS Transactions on Mathematics*, 2016, Vol. 15, pp. 498-501.
33. **Hilton H.H.** Implications and constraints of time-independent Poisson ratios in linear isotropic and anisotropic viscoelasticity. // *Journal of Elasticity*, 2001, Vol. 63(3), pp. 221-251.
34. **Ari M.**, **Faal R.T.**, **Zayernouri M.** Vibrations suppression of fractionally damped plates using multiple optimal dynamic vibration. // *International Journal of Computer Mathematics*, 2019, DOI: 10.1080/00207160.2019.1594792.
35. **Mashrouteh S.** Nonlinear vibration analysis of viscoelastic plates with fractional damping. Master Thesis, University of Ontario, Institute of Technology, 2017.
36. **Permoon M. R.**, **Haddadpour H.**, **Javadi M.** Nonlinear vibration of fractional viscoelastic plate: primary, subharmonic, and superharmonic response. // *International Journal of Non-Linear Mechanics*, 2018, Vol. 99, pp. 154-164.
37. **Babouskos N.G.**, **Katsikadelis J.T.** Nonlinear vibrations of viscoelastic plates of fractional derivative type: An AEM solution. // *The Open Mechanics Journal*, 2010, Vol. 4(8), pp. 8-20.
38. **Hosseinkhani A.**, **Younesian D.**, **Farhangdoust S.** Dynamic analysis of a plate on the generalized foundation with fractional damping subjected to random excitation. // *Mathematical Problems in Engineering*, 2018, ID 3908371.
39. **Malara G.**, **Spanos P.D.** Nonlinear random vibrations of plates endowed with fractional derivative elements. // *Probabilistic Engineering Mechanics*, 2018, Vol. 54, pp. 2-8.
40. **Nwagoum Tuwa P.R.**, **Miwadinou C.H.**, **Monwanou A.V.**, **Chabi Orou J.B.**, **Woafo P.** Chaotic vibrations of nonlinear viscoelastic plate with fractional derivative model and subjected to parametric and external excitations. // *Mechanics Research Communications*, 2019, Vol. 97, pp. 8-15.
41. **Litewka P.**, **Lewandowski R.** Steady-state non-linear vibrations of plates using Zener material model with fractional derivative. // *Computational Mechanics*, 2017, Vol. 60, pp. 333-354.
42. **Datta P.**, **Ray M.C.** Fractional order derivative model of viscoelastic layer for active damping of geometrically nonlinear vibrations of smart composite plates. // *CMC*, 2015, Vol. 49-50(1), pp. 47-80.
43. **Rossikhin Yu.A.**, **Shitikova M.V.**, **Shcheglova T.A.** Forced vibrations of a nonlinear oscillator with weak fractional damping. // *Journal of Mechanics of Materials and Structures*, 2009, Vol. 4(9), pp. 1619-1636.

44. **Shitikova M.V., Rossikhin Yu.A., Kandu V.** Interaction of internal and external resonances during force driven vibrations of a nonlinear thin plate embedded into a fractional derivative medium. // *Procedia Engineering*, 2017, Vol. 199, pp. 832-837.
45. **Шитикова М.В., Канду В.В.** Численный анализ вынужденных колебаний нелинейных пластинок в вязкоупругой среде при наличии внутреннего резонанса один к одному. // *Известия высших учебных заведений. Строительство*, 2018, №12(720), с. 9-22.
46. **Samko S.G., Kilbas A.A., Marichev O.I.** fractional integrals and derivatives. theory and applications. Gordon and Breach Science Publishers, Amsterdam, 1993.
47. **Канду В.В., Шитикова М.В., Россихин Ю.А.** Численный анализ вынужденных колебаний нелинейных пластинок в вязкоупругой среде при наличии внутреннего резонанса 1:1:2. // Сборник материалов всероссийской конференции по механике деформируемого твердого тела, 2017, с. 10-12.
48. **Шитикова М.В., Канду В.В.** Моделирование вынужденных колебаний нелинейных пластинок в вязкоупругой среде при наличии внутреннего резонанса 1:1:1. // Сборник трудов Международной научной конференции «Актуальные проблемы прикладной математики, информатики и механики», 2018, с. 1295-1300.

Marina V. Shitikova, Advisor of the Russian Academy of Architecture and Construction Sciences, Prof., Dr.Sc., Research Center on Dynamics of Solids and Structures; Voronezh State Technical University; 20-letiya Oktyabrya 84, Voronezh, 394006, Russia;
phone +7 (473) 271-42-20; fax +7 (473) 277-39-92;
E-mail: mvs@vgasu.vrn.ru.

Vladimir V. Kandu, Ph.D. student; Junior Researcher; Research Center on Dynamics of Solids and Structures; Voronezh State Technical University; 20-letiya Oktyabrya 84, Voronezh, 394006, Russia;
phone +7 (473) 271-42-20; fax +7 (473) 277-39-92;
E-mail: kandu8vladimir@gmail.com.

Шитикова Марина Вячеславовна, советник РААСН, профессор, доктор физико-математических наук; руководитель международного научного центра по фундаментальным исследованиям в области естественных и строительных наук имени Заслуженного деятеля науки РФ, профессора Россихина Ю.А.; Воронежский государственный технический университет; 394006, Россия, г. Воронеж, ул. 20 лет Октября, д. 84;
E-mail: mvs@vgasu.vrn.ru

Владимир В. Канду аспирант, младший научный сотрудник международного научного центра по фундаментальным исследованиям в области естественных и строительных наук имени Заслуженного деятеля науки РФ, профессора Россихина Ю.А.; Воронежский государственный технический университет; 394006, Россия, г. Воронеж, ул. 20 лет Октября, д. 84;
E-mail: kandu8vladimir@gmail.com

DOI:10.22337/2587-9618-2019-15-3-149-160

CONSTRUCTION OF DEFORMATION DIAGRAMS OF CONCRETE UNDER SHEAR BASED ON THE AUTHOR'S THEORY OF ANISOTROPIC MATERIALS POWER RESISTANCE TO COMPRESSION AND DEFORMATION THEORY OF PLASTICITY

Boris S. Sokolov [1], Oleg V. Radaikin [2]

[1] JSC "Kazan GIPRONIIAVIAPROM", Kazan, RUSSIA

[2] Kazan State University of Architecture and Engineering, Kazan, RUSSIA

Abstract: The Aim of this work was the construction of a concrete deformation diagrams under shear on the basis of two approaches: the theory of anisotropic materials force resistance in compression and deformation theory of plasticity with the use of state diagrams of concrete under tension and compression, obtained by the authors jointly with Acad. N.I. Karpenko earlier. For this purpose, in the framework of the first approach, the main computational expression of the author's model was written in the current deformations, which ultimately allowed to establish a relationship between the diagrams σ_b-ε_b, σ_{bt}-ε_{bt} and τ_b-γ_b and reveal the mechanics of destruction of concrete elements under compression. The second approach additionally takes into account the change in the coefficient of transverse deformations, μ_b, and shear modulus of deformations, G_b, as the load increases, but does not take into account the presence of normal stresses affecting the stress-strain state. This approach recreates the conditions of pure shear, which is possible only theoretically, and in real designs is applicable with a certain degree of error. Nevertheless, both approaches provide almost identical data in the construction of diagrams «τ_b-γ_b», which differ from the experiment by no more than 13-15%. In this regard, they are recommended for implementation: the first-to perform engineering calculations «manually», the second –to develop computer programs that allow you to automate the calculation.

Keywords: theory of anisotropic materials force resistance in compression, deformation theory of plasticity, diagram of concrete deformation at shear, shear strength

К ПОСТРОЕНИЮ ДИАГРАММ ДЕФОРМИРОВАНИЯ БЕТОНА ПРИ СДВИГЕ НА ОСНОВЕ АВТОРСКОЙ ТЕОРИИ СИЛОВОГО СОПРОТИВЛЕНИЯ АНИЗОТРОПНЫХ МАТЕРИАЛОВ СЖАТИЮ И ДЕФОРМАЦИОННОЙ ТЕОРИИ ПЛАСТИЧНОСТИ

Б.С. Соколов [1], О.В. Радайкин [2]

[1] АО «Казанский Гипроинавиапром», г. Казань, РОССИЯ

[2] Казанский государственный архитектурно-строительный университет, г. Казань, РОССИЯ

Аннотация: Целью данной работы ставилось построение диаграммы деформирования бетона при сдвиге на основе двух подходов: теории силового сопротивления анизотропных материалов сжатию и деформационной теории пластичности с использованием диаграмм состояния бетона при растяжении и сжатии, полученных авторами совместно с акад. Н.И. Карпенко ранее. Для этого в рамках первого подхода основное расчётное выражение авторской модели было записано в текущих деформациях, что в конечном итоге позволило установить взаимосвязь между диаграммами σ_b-ε_b, σ_{bt}-ε_{bt} и τ_b-γ_b и раскрыть механику разрушения бетонных элементов, находящихся в условиях сжатия. Во втором подходе дополнительно учитывает изменение коэффициента поперечных деформаций, μ_b, и сдвигового модуля деформаций, G_b, по мере увеличения нагрузки, но не учтено наличие нормальных напряжений, влияющих на напряжённо-деформированное состояние. Этот подход воссоздаёт условия чистого сдвига,

что возможно лишь теоретически, а в реальных конструкциях применимо с определённой долей погрешности. Тем не менее оба подхода дают практически совпадающие данные при построении диаграмм «τ_b-γ_b», которые отличаются от эксперимента не более, чем на 13-15%. В связи с этим они рекомендованы для внедрения: первый – для выполнения инженерных расчётов «вручную», второй –для разработки компьютерных программ, позволяющих автоматизировать расчёт.

Ключевые слова: теория силового сопротивления анизотропных материалов сжатию, деформационная теории пластичности, диаграмма деформирования бетона при сдвиге, прочность на срез

The problem of reliable construction of diagrams of concrete deformation under shear arises when solving a number of practical and theoretical problems. For example, this concerns the calculations of reinforced concrete elements under bending in the zone of couple action of bending moments and shear forces, the adhesion of reinforcement to concrete, and the application of the theory of power resistance of anisotropic materials under compression to estimate the stress-strain state of structural elements at all stages of loading. This theory has been known for over 30 years, and in practice, it has shown its viability. Its main provisions at the present stage are set forth in the monograph [1]. However, the development potential of the theory is far from exhausted. Therefore, if the ultimate states of compressed concrete and reinforced concrete elements were examined at the stage of destruction in previous publications mainly, then this article attempts to study the intermediate stages of operation of these elements under load using diagrammatic calculation methods.

Below two approaches for constructing concrete shear deformation diagrams are given: 1 – The author's theory of the power resistance of anisotropic materials to compression [1]; 2 – Deformation theory of plasticity and design expressions for diagrams of concrete deforming under tension and compression, proposed in [2-4].

Figure 1 shows the design scheme for assessing the strength of a compressed element (prism and cylinder), reflecting the hypothesis of the author's theory [1] on the fracture mechanics that occurs after overcoming the material's resistance to separation, shear and crushing.

The strength condition according to the theory is written as the inequality:

$$N \le N_{ult} = \frac{N_{bt}\cos\alpha + 2N_{sh}}{\sin\alpha} + N_{ef} \qquad (1)$$

where N_{bt}, N_{sh}, N_{ef} are ultimate internal forces characterizing power resistance in the zones of stretching, shear and crushing; α – wedge angle:

$$\alpha = arctg\left(0,25R_{bn}/R_{btn} - 1,56\right) \qquad (2)$$

These efforts are determined as the product of the corresponding design resistance and area:

$$N_{bt} = R_{bt}A_{bt},\ N_{sh} = R_{sh}A_{sh},\ N_{ef} = R_bA_{ef}, \qquad (3)$$

where R_{bt}, R_{sh}, R_b are respectively design resistance of concrete to tension, shear and compression, and A_{bt}, A_{sh}, A_{ef} are areas of tension, shear and crushing(compression).

Substituting (2) in (1) and accepting

$$N = N_{ult} = R_bA,$$

where A is area of external effort transmitting, we obtain:

$$R_bA = R_{bt}A_{bt}ctg\alpha + \frac{2R_{sh}A_{sh}}{\sin\alpha} + R_bA_{ef}. \qquad (4)$$

At the same time formula (3) is the same for prismatic and cylindrical elements (fig. 1), but there is difference in determination of areas A_{bt}, A_{sh}, A_{ef} and substituting prismatic strength by cylindrical one f_{ck} (according to Eurocode-2), at the same time

$$f_{ck} \approx \frac{R_b}{\gamma_{ck}\gamma_R},$$

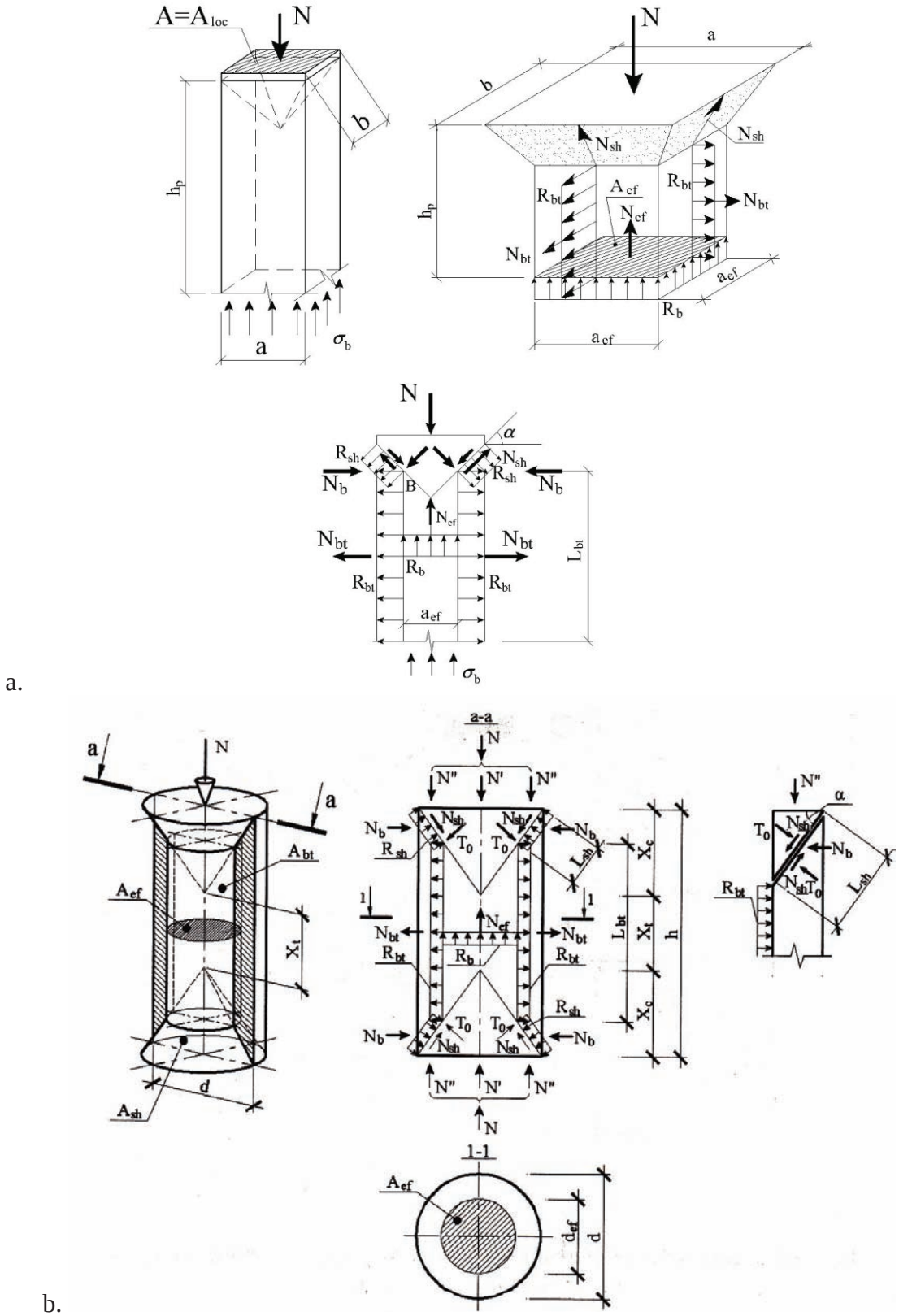

a.

b.

Figure 1. Calculation schemes of concrete prism (a) and cylinder (b) under compression.

where $\gamma_{ck} = 0,8$, $\gamma_R = 0,75$ are respectively coefficients of transition from cylindrical strength to cubic and from cubic to prismatic.
Let us transform expression (4) by following way:

$$R_b\left(A - A_{ef}\right) = R_{bt}A_{bt}ctg\alpha + \frac{2R_{sh}A_{sh}}{\sin\alpha} \Rightarrow R_b = k_1R_{bt}ctg\alpha + \frac{k_2R_{sh}}{\sin\alpha},$$

$$R_b\left(A - A_{ef}\right) = R_{bt}A_{bt}ctg\alpha + \frac{2R_{sh}A_{sh}}{\sin\alpha} \Rightarrow R_b = k_1R_{bt}ctg\alpha + \frac{k_2R_{sh}}{\sin\alpha}, \quad (5)$$

where $k_1 = A_{bt}/\left(A - A_{ef}\right), k_2 = 2A_{sh}/\left(A - A_{ef}\right)$.

Let us note that according to expression (5), it is possible to obtain the calculated value of concrete shear resistance depending on its class after the following transformation:

$$R_{sh} = \frac{R_b\sin\alpha - k_1R_{bt}\cos\alpha}{k_2}. \quad (6)$$

In addition, the same expression can be written through stresses, which will allow us to consider not only the stage of destruction of the concrete element, but also the intermediate stages of its loading:

$$\sigma_b = k_1\sigma_{bt}ctg\alpha + \frac{k_2\tau_b}{\sin\alpha}. \quad (7)$$

The resulting expression can now be written through the corresponding deformations:

$$\varepsilon_bE_b = k_1\varepsilon_{bt}E_{bt}ctg\alpha + \frac{k_2\gamma_bG_b}{\sin\alpha}. \quad (8)$$

According to Building standard of Russian Federation SP 63.13330.2012, it is: $E_{bt} = E_b$, $G_b = 0,4E_b$, and at calculation by deformations, it is $E_{bt} \approx 0,5E_b$, then equality (8) can be written in the form:

$$\varepsilon_b = 0,5k_1\varepsilon_{bt}ctg\alpha + \frac{0,4k_2\gamma_b}{\sin\alpha}, \quad (9)$$

From equality (9), it follows: if we know the relative deformations of concrete under compression and tension, and their diagrams are given in the regulatory documents (Fig. 3, a-b), we can determine the relative deformations under shear:

$$\gamma_b = \frac{\left(\varepsilon_b - 0,5k_1\varepsilon_{bt}ctg\alpha\right)\sin\alpha}{0,4k_2}. \quad (10)$$

Substituting shear deformations in the expression

$$\tau_b = G_b\gamma_b \approx 0,4E_b\gamma_b,$$

we obtain diagram "$\tau_b - \gamma_b$". In this case, a significant difference in the values of ultimate deformation of concrete under compression and tension should be taken into account. The consequence of this is that when testing real samples (prisms or cylinders) for compression, vertical cracks appear, indicating the exhaustion of the tensile strength of concrete. In this case, in condition (10), from a certain level of loading, tensile deformations ε_{bt} should be excluded. Then the transverse expansion of the sample occurs due to the opening of vertical cracks, and at the moment immediately before the formation of these cracks, condition (10) will look like:

$$\gamma_{b1} = \frac{\left(\varepsilon_{b1} - 0,5k_1\varepsilon_{bt2}ctg\alpha\right)\sin\alpha}{0,4k_2}, \quad \tau_{b1} = 0,4E_b\gamma_{b1}, \quad (11)$$

where ε_{bt2} is ultimate deformation of concrete at tension ($\varepsilon_{bt2} = 0,00015$);

$$\varepsilon_{b1} = \frac{0,6R_b}{E_b}$$

is the boundary of elastic stage of compressed concrete work.
Value γ_{b1}, according to (11), is the abscissa of the first point from the parametric points in the

diagram "$\tau_b - \gamma_b$", which corresponds reaching value

$$\tau_b \approx 0,2R_{sh}$$

by tangential stresses.

The second parametric point is determined for conditions

$$\varepsilon_b = \varepsilon_{b0} = \frac{R_b}{E_b} \text{ and } \varepsilon_{bt} = 0$$

that means concrete in tension excluded from work, and transverse expansion of a sample occurs due to opening of vertical cracks. At the same time, tangential stresses reaches maximum values:

$$\gamma_{b0} = \frac{\varepsilon_{b0} \sin\alpha}{0,4k_2},\ \tau_{b0} = R_{sh}. \qquad (12)$$

The third parametric point corresponds to the ultimate strain of compressed concrete

$$\varepsilon_b = \varepsilon_{b2} = 0,002$$

and, by analogy with the previous one, we obtain:

$$\gamma_{b2} \approx \frac{\varepsilon_{b2} \sin\alpha}{0,4k_2},\ \tau_{b2} = \tau_{b0} = R_{sh}. \qquad (13)$$

With a further increase in load, we assume that the concrete shear resistance is overcome and the compressed core continues to work. However, the friction and engagement forces arising between concrete surfaces along inclined platforms should also provide some resistance up to the complete destruction of the compressed element.

The verification of the calculated expressions was carried out according to the results of concrete samples of a cylindrical shape [1]. The nature of the formation and development of cracks for specimens of the 5.1 series (d × h = 0.1 × 0.2 m, concrete B30) is shown in Fig. 2, from which one can see their compliance with the design scheme and the hypothesis of the fracture mechanism.

For the specimens of the considering series, the results of calculating the parameters included in formula (6), as well as their breaking load, are given in the table below, which also shows a comparison of theoretical and experimental data.

From table, it is seen:

$$R_{sh}/R_{bt} = 2,944$$

that proves known relationship

$$R_{sh}/R_{bt} = \sqrt{R_b/R_{bt}} \approx 3,0$$

[5]. Besides, difference between theoretical and experimental values of ultimate force N_{ult} is 13.5 % that can be accepted as satisfactory result for such a material with high variability of properties as concrete.

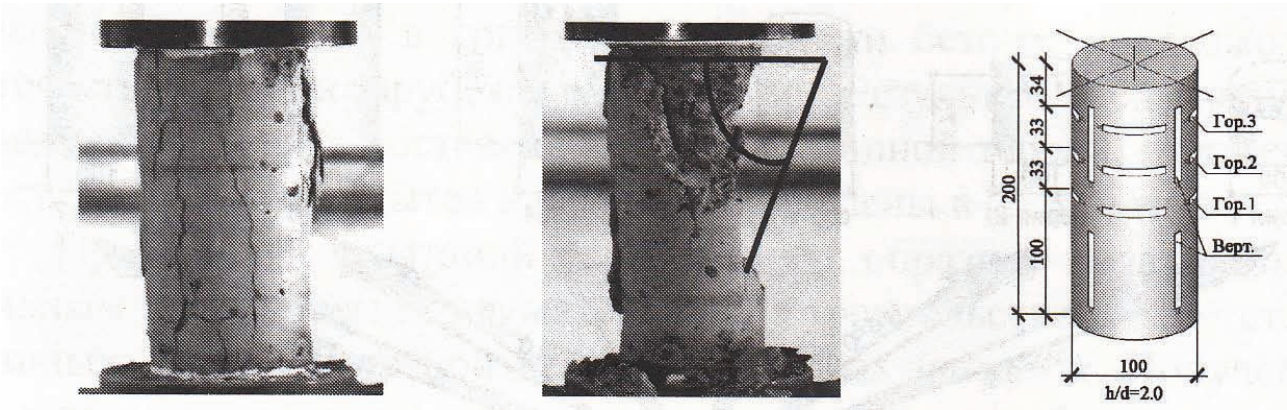

Figure 2. The nature of the destruction of cylindrical specimens under compression [1].

Table 1. Comparison of theoretical and experimental data for specimens series of 5.1 [1].

Parameter	R_b, MPa	R_{bt}, MPa	α, ^{0}	k_1	k_2	R_{sh}, MPa	N_{ult}, ton
Theory	-	-	54^0	10,14	3,43	5,01	21,0
Experiment	20,1	1,7	57^0	-	-	-	18,5

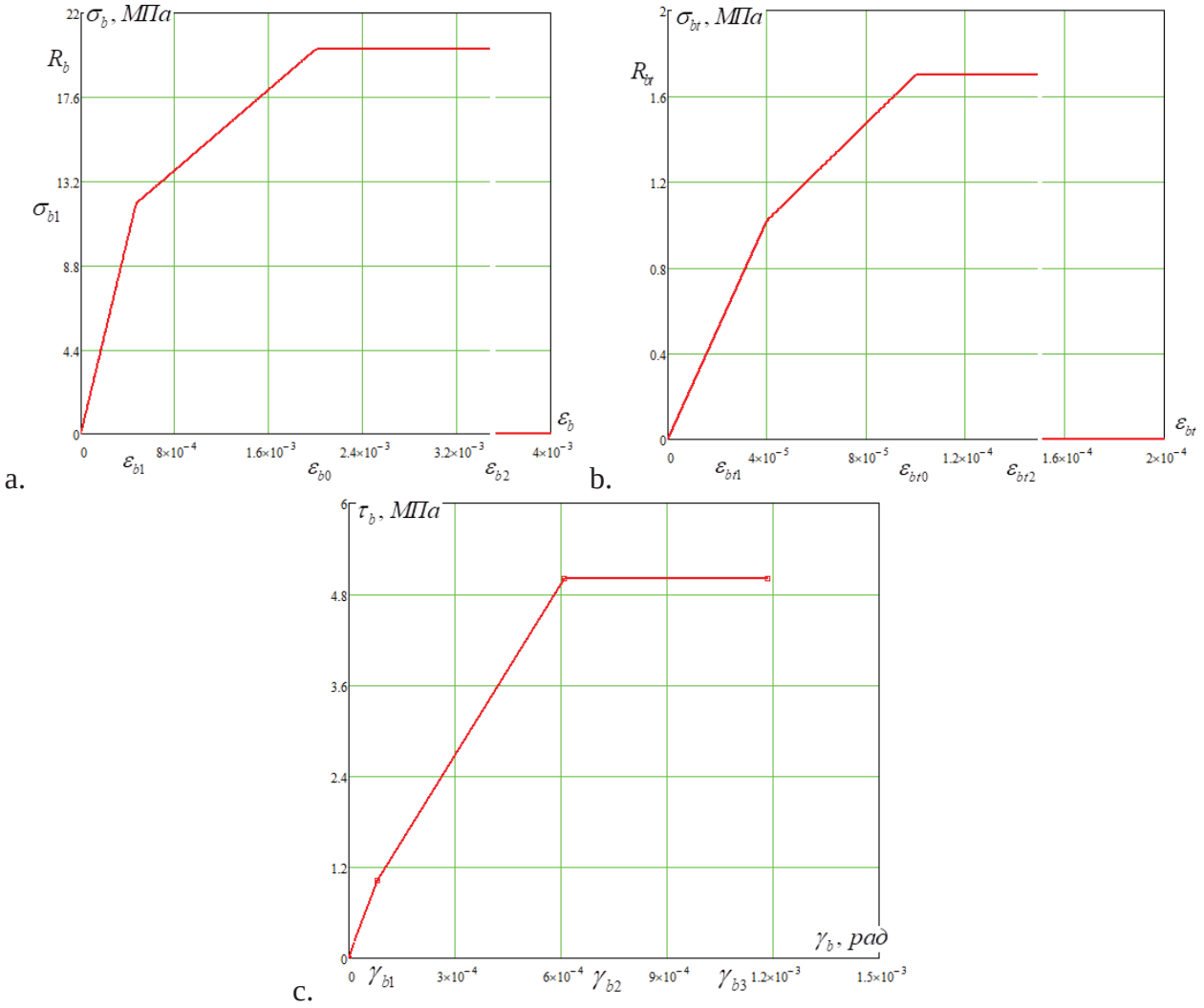

Figure 3. Concrete deformation diagrams for a cylindrical specimen of the 5.1 series [1] made of class B30 concrete under compression (a), tension (b) and shear (c).

In addition, fig. 3, a-b show the so-called working (three-line) diagrams of concrete deforming under compression and tension, which are constructed according to the formulas of SP 63.13330.2012. Figure 3,c shows the diagram "$\tau_b - \gamma_b$" obtained from dependencies (11)-(13).

To identify the relationship between the diagrams of deformation of concrete under compression, tension and shear with each other, we superimposed all three graphs in Figure 3 to one coordinate plane. In order to do this, for each diagram we took our scale of the stress axis, and we expressed the tensile and shear strains through compression strains:

$$\varepsilon_{bt} = \mu\varepsilon_b \approx 0,2\varepsilon_b\,,\ \gamma_b = \frac{\varepsilon_b \sin\alpha}{0,4k_2}\,.$$

Then we obtain diagram presented in Figure 4.

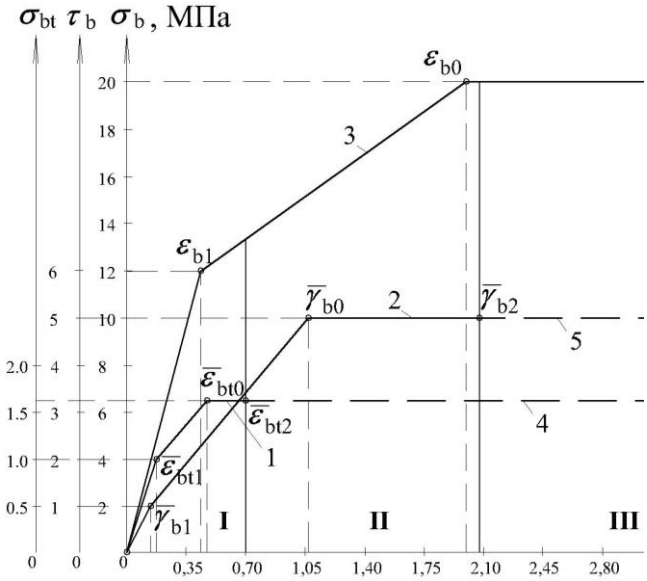

Figure 4. Diagrams of deformation of a cylindrical specimen of a series 5.1 [1] of concrete of class B30 under tension - 1, shear - 2 and compression - 3; 4 - section of the disclosure of vertical cracks; 5 - plot of resistance due to friction and engagement of concrete surfaces; I, II, III - areas of the characteristic operation of the element at different stages of loading.

In this figure, for diagrams 1 and 2, parametric points are indicated by deformations, which are determined using the above dependencies:

$$\bar{\varepsilon}_{bt} = \frac{\varepsilon_{bt}}{0,2}, \quad \bar{\gamma}_b = \frac{0,4k_2}{\sin\alpha}\gamma_b .$$

At the same time, three characteristic areas can be distinguished in compression diagram 3: I – the area of joint resistance to compression of the separation, shear and crushing zones; II – the area of switching off the separation zone from work and further joint resistance to compression of the shear and crushing zones; III - the area of switching off the shear zone from work and further resistance to compression of only the crushing zone.

Figure 4 also shows that the abscissas of the majority of the parametric points of the three strain diagrams practically coincide (excluding $\bar{\gamma}_{b0}$):

– $\bar{\varepsilon}_{bt1} = \bar{\gamma}_{b1}$ is the condition of the beginning of inelastic deformations in the separation zone;

– $\bar{\varepsilon}_{bt0} = \varepsilon_{b1}$ is condition of nucleation of vertical cracks of transverse separation, their development, continuing up to deformations $\bar{\varepsilon}_{bt2}$, after that stretched zone removing from work (boundary between areas I and II);

– $\bar{\gamma}_{b2} = \varepsilon_{b0}$ – after the shear zones are completely turned off, crushing of the concrete core begins (the boundary between regions II and III).

Moreover, after the magnitude reached in the stretched zone of deformations $\varepsilon_{bt} = \varepsilon_{bt2}$, the tensile diagram 1 continues in the form of a dashed section 4, which characterizes the opening of vertical cracks. In addition, for the shear diagram 2 after reaching the deformations $\gamma_b = \gamma_{b2}$, the dashed section 5 characterizes the work of the friction forces and the engagement of concrete surfaces on inclined platforms.

Thus, using the author's theory, we obtained analytical expressions for determining concrete deformations under shear and tangential stresses during fracture of the material, which allowed us to finally represent the dependence "$\tau_b - \gamma_b$" (Figure 3, c). In addition, the mechanics of concrete deformation under compression up to its destruction were explained on the basis of this theory, which became possible due to the establishment of the relationship of concrete

deformation diagrams for tension, compression and shear.

The second approach to constructing the "$\tau_b - \gamma_b$" dependence is using the provisions of the deformation theory of plasticity [6] and the diagrams proposed by Acad. Karpenko N.I. together with the authors of this article [2-4]. This theory is based on the results of testing concrete prisms for compression with the determination of longitudinal and transverse strains (ε_b and ε'_b). Using well-known expressions [6], the desired parameters for describing the diagrams can be obtained by the following algorithm:

$$\text{Initial experimental data: } \sigma_b = f(\varepsilon_b),\ \mu_b = \frac{\varepsilon'_b}{\varepsilon_b};$$
$$\text{Solution algorithm: } \gamma_b = (1+\mu_b)\varepsilon'_b \rightarrow E'_b = \frac{\sigma_b}{\varepsilon_b} \rightarrow G'_b = \frac{E'_b}{2(1+\mu_b)} \rightarrow \tau_b = G'_b\,\gamma_b, \tag{14}$$

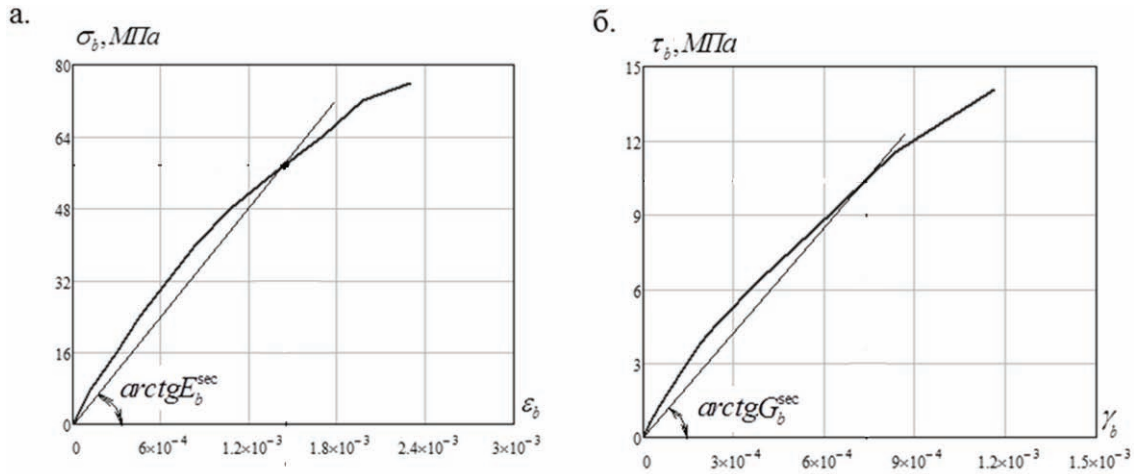

Figure 4. Deformation diagrams for high-strength concrete of class B100: a – experimental "σ_b-ε_b" [8]; b – "τ_b-γ_b", constructed on the basis of algorithm (14).

where μ_b is coefficient of transverse deformations, which increases from initial value $\mu_b^0 = 0{,}15...0{,}2$ up to 0.5.

Figure 4b shows a curve constructed according to the proposed algorithm (14) based on experimental data [8] for high-strength concrete of class B100.

When there are not experimental data, this coefficient can be obtained analytically by the formula proposed Acad. N.I. Karpenko [7]:

$$\mu_b = \bar{\mu}_b \pm (\mu_b^0 - \bar{\mu}_b)\sqrt{1-\eta^2}, \tag{15}$$

where

$$\bar{\mu}_b = \mu_b^0 + 1 - \sqrt[3]{\frac{R_{bn}}{\varepsilon_{b0} E_b}}$$

is the lateral strain coefficient at the top of the compression diagram;

$$\varepsilon_{b0} \approx 0{,}002$$

is the relative compressive strains at the same point;

$$\mu_b^0 = 0{,}2$$

is Poison coefficient;

$$\eta = \frac{\sigma_b}{R_{bn}}$$

is current level of stresses.

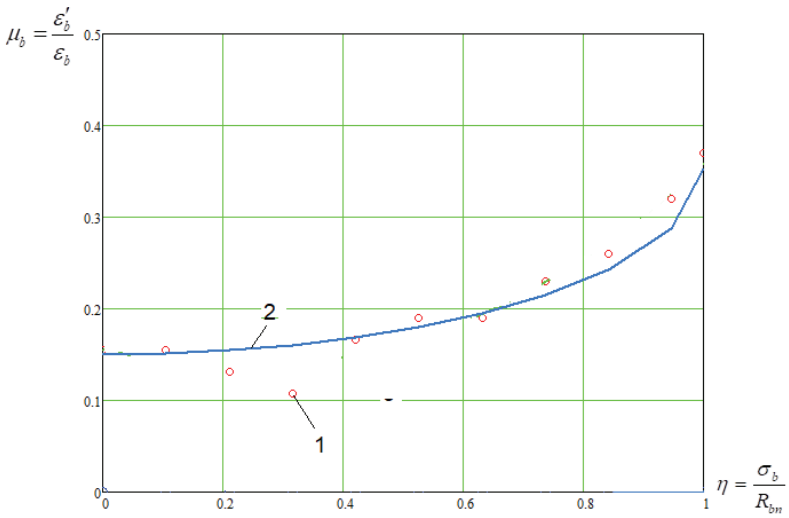

Figure 5. Change in the coefficient of transverse deformations "μb" during loading a compressed prism of concrete class B100: 1 – experimental data [8]; 2 – curve constructed by the formula (15).

For concrete of class B100, the experimental and theoretical dependences for μ_b are shown in Figure 5.

The curves obtained in this figure qualitatively and to some extent quantitatively coincide with the previously obtained data in the works of O. J. Berg [9,10], which have already become classics and confirms the validity of the proposed expressions.

In the case of applying the analytical dependence for μ_b, the algorithm (14) is slightly modified:

Initial analytical data: $\sigma_b = f(\varepsilon_b)$ [2-4], $\mu_b = \varphi(\eta)$;

$$\text{Solution algorithm: } \mu_b = \varphi\left[\frac{f(\varepsilon_b)}{R_{bn}}\right] = \psi(\varepsilon_b) \rightarrow \gamma_b = (1+\mu_b)\mu_b\varepsilon_b \rightarrow E'_b = \frac{\sigma_b}{\varepsilon_b} \rightarrow \quad (16)$$

$$G'_b = \frac{E'_b}{2(1+\mu_b)} \rightarrow \tau_b = G'_b\,\gamma_b$$

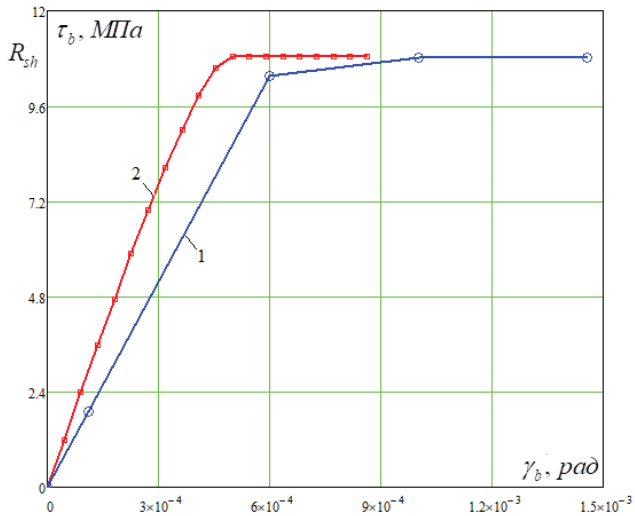

Figure 6. The diagram "τb-γb" for heavy concrete of class B100, constructed according to formulas (8)-(11) – curve 1 - and on the basis of the algorithm (16) – curve 2.

As a result of the implementation of this algorithm for concrete of class B100, we obtain the dependence "τ_b-γ_b", presented in Figure 6 (curve 2). At the same time, for comparison, curve 1 is shown in the same figure, constructed according to formulas (8)-(11) of the previously considered approach.

Unlike Figure 4b, the curves in Figure 6 were built according to the normative strength characteristics of concrete. Nevertheless, the difference between the experimental and theoretical shear strength turned out to be

$$R_{sh}^{ex} / R_{sh}^{th} = 14/11 = 1,27,$$

which approximately corresponds to the material safety factor $\gamma_m = 1,3$. And despite the fact that, in contrast to the experimental curve, the diagrams in Figure 6 have a horizontal section (theoretically possible), however, in general, the values of the parametric points of the compared curves practically coincide.

Thus, the second approach to the construction of shear strain diagrams is considered. This approach is based on the provisions of the deformation theory of plasticity and the dependences of [2-4, 7]. It takes into account the change in the transverse strain coefficient, μ_b, and the shear strain modulus, G_b', as the load increases. However, the presence of normal stresses affecting the stress-strain state is not taken into account.

CONCLUSIONS

1. Two approaches to determining the diagrams of concrete deformation under shear are considered:
   - the author's theory of the power resistance of anisotropic materials to compression;
   - the deformation theory of plasticity and the provisions of [2-4, 7] developed by academician N.I. Karpenko together with the authors of this article.
2. The peculiarity of the first approach is that it takes into account the specifics of concrete work under compression, reveals the mechanics of its destruction from overcoming the peel, shear and crush resistance and is based on piecewise-linear diagrams of material deformation under compression and tension.
3. The second approach is based on the provisions of the deformation theory of plasticity and dependences for diagrams [2-4, 7], in addition, it takes into account the change in the coefficient of transverse deformations, μ_b, and the shear modulus of deformations, G_b', as the load increases. However, the presence of normal stresses affecting the stress-strain state is not taken into account, since the pure shear conditions are recreated in the calculation model of this approach, which is possible only theoretically, and in real designs it is applicable with a certain degree of error.
4. Comparing the mathematical apparatus of both approaches, we can conclude that the first one is more applicable for performing engineering calculations "manually", while the second one can be recommended for the development of computer programs that automate the calculation (including programs based on the Finite Element Method). Nevertheless, both approaches give practically the same data when constructing the "τ_b-γ_b" diagrams, which differ from the experiment by no more than 13-15%. Therefore, the proposed approaches are recommended for implementation in the regulatory literature on the design of concrete and reinforced concrete elements and structures.

REFERENCES

1. **Sokolov B.S.** Teoriya silovogo soprotivleniya anizotropnykh materialov szhatiyu i yeyo prakticheskoye primeneniye [The theory of force resistance of anisotropic materials to compression and its practical application]. Moscow, Izd-vo ASV, 2011, 160 pages (in Russian).
2. **Karpenko N.I., Sokolov B.S., Radaykin O.V.** Analiz i sovershenstvovaniye

krivolineynykh diagramm deformirovaniya betona dlya rascheta zhelezobetonnykh konstruktsiy po deformatsionnoy modeli [Analysis and improvement of curved concrete deformation diagrams for calculating reinforced concrete structures using the deformation model]. // *Promyshlennoye i grazhdanskoye stroitel'stvo,* 2013, No. 1, pp. 25-27 (in Russian).

3. **Karpenko N.I., Sokolov B.S., Radaykin O.V.** Sovershenstvovaniye metodiki rascheta izgibayemykh zhelezobetonnykh elementov bez predvaritel'nogo napryazheniya po obrazovaniyu normal'nykh treshchin [Improving the methodology for calculating bent reinforced concrete elements without prestressing the formation of normal cracks]. // *Zhurnal Stroitel'nyye materialy*, 2013, No. 6, pp. 54-55 (in Russian).
4. **Karpenko N.I., Sokolov B.S., Radaykin O.V.** K raschotu prochnosti, zhostkosti i treshchinostoykosti vnetsentrenno szhatykh zhelezobetonnykh elementov s primeneniyem nelineynoy deformatsionnoy modeli [To the calculation of strength, rigidity and crack resistance of eccentrically compressed reinforced concrete elements using a nonlinear deformation model]. // *Izvestiya KazGASU*, 2013, No. 4 (26), pp. 113-120 (in Russian).
5. **Bazhenov YU.M., Korol' Ye.A., Yerofeyev V.T., Mitina Ye.A.** Ograzhdayushchiye konstruktsii s ispol'zovaniyem betonov nizkoy teploprovodnosti [Building envelopes using concretes of low thermal conductivity]. Moscow, Izd-vo ASV, 2008, 320 pages (in Russian).
6. **Teregulov I.G.** Soprotivleniye materialov i Osnovy teorii uprugosti i plastichnosti. Uchebnik dlya studentov vuzov [Resistance of materials and Fundamentals of the theory of elasticity and plasticity. Textbook for university students]. Moscow, Vysshaya shkola, 1984, 472 pages (in Russian).
7. **Karpenko N.I.** Obshchiye modeli mekhaniki zhelezobetona [General models of reinforced concrete mechanics]. Mosocow, Stroyizdat, 1996, 416 pages (in Russian).
8. **Punagin V.V.** Svoystva i tekhnologiya betona dlya vysotnogo monolitnogo stroitel'stva [Properties and technology of concrete for high-rise monolithic construction]. // *Elektronnyy arkhiv Khar'kovskogo natsional'nogo universiteta imeni V.N. Karazina* [Electronic archive of V.N. Karazin Kharkiv National University]. Khar'kov, 2012. URL: http://dspace.snu.edu.ua:8080/jspui/bitstream/123456789/357/32/Punagin.pdf (available on 12.05.2014). (in Russian).
9. **Berg O.J., Shcherbakov Ye.N., Pisanko G.N.** Vysokoprochnyy beton [High strength concrete]. Moscow, Stroyizdat, 1971, 208 pages (in Russian).
10. **Berg O.J.** Fizicheskiye Osnovy teorii prochnosti betona i zhelezobetona [Physical Fundamentals of the theory of strength of concrete and reinforced concrete]. Moscow, Gosstroyizdat, 1962, 98 pages (in Russian).

СПИСОК ЛИТЕРАТУРЫ

1. **Соколов Б.С.** Теория силового сопротивления анизотропных материалов сжатию и её практическое применение. – М.: Издательство АСВ, 2011. – 160 с.
2. **Карпенко Н.И., Соколов Б.С., Радайкин О.В.** Анализ и совершенствование криволинейных диаграмм деформирования бетона для расчета железобетонных конструкций по деформационной модели. // *Промышленное и гражданское строительство*, 2013, №1, с. 25-27.
3. **Карпенко Н.И., Соколов Б.С., Радайкин О.В.** Совершенствование методики расчета изгибаемых железобетонных элементов без

предварительного напряжения по образованию нормальных трещин. // *Журнал Строительные материалы*, 2013, №6, с. 54-55.
4. **Карпенко Н.И., Соколов Б.С., Радайкин О.В.** К расчёту прочности, жёсткости и трещиностойкости внецентренно сжатых железобетонных элементов с применением нелинейной деформационной модели. // *Известия КазГАСУ*, 2013, №4 (26), с. 113-120.
5. **Баженов Ю.М., Король Е.А., Ерофеев В.Т., Митина Е.А.** Ограждающие конструкции с использованием бетонов низкой теплопроводности. – М.: Издательство АСВ, 2008. – 320 с.
6. **Терегулов И.Г.** Сопротивление материалов и Основы теории упругости и пластичности. – М.: Высшая школа, 1984. – 472 с.
7. **Карпенко Н.И.** Общие модели механики железобетона. – М.: Стройиздат, 1996. – 416 с.
8. **Пунагин В.В.** Свойства и технология бетона для высотного монолитного строительства. // *Электронный архив Харьковского национального университета имени В.Н. Каразина*. – Харьков, 2012. URL: http://dspace.snu.edu.ua:8080/jspui/bitstream/123456789/357/32/Punagin.pdf (дата обращения: 12.05.2014).
9. **Берг О.Я., Щербаков Е.Н., Писанко Г.Н.** Высокопрочный бетон. – М.: Стройиздат, 1971. – 208 с.
10. **Берг О.Я.** Физические Основы теории прочности бетона и железобетона. – М.: Госстройиздат, 1962. – 98 с.

Sokolov Boris Sergeevich, Correspondent Member of the Russian Academy of Architecture and Construction Sciences, Professor, Doctor of technical Sciences; scientific adviser, JSC “Kazan Giproniiaviaprom”; 420127, Russia, Republic of Tatarstan, Kazan, Dementyev St., 1; e-mail: sbs.1942@mail.ru.

Radaikin Oleg Valerjevich, Candidate of Technical Sciences, Associate Professor of the Department of Zhbikk, Kazan state University of Architecture and Construction; 420043, Russia, Republic of Tatarstan, Kazan, Zelenaya str., 1; e-mail: olegxxii@mail.ru.

Соколов Борис Сергеевич, член-корреспондент Российской академии архитектуры и строительных наук, профессор, доктор технических наук; научный консультант Акционерного общества «Казанский Гипрониавиапром»; 420127, Россия, Республика Татарстан, г. Казань, ул. Дементьева, 1; E-mail: sbs.1942@mail.ru.

Радайкин Олег Валерьевич, кандидат технических наук, доцент кафедры ЖБиКК Казанского государственного архитектурно-строительного университета; 420043, Россия, Республика Татарстан, г. Казань, ул. Зеленая, 1; e-mail: olegxxii@mail.ru.

УШЕЛ ИЗ ЖИЗНИ ПРЕЗИДЕНТ РОССИЙСКОЙ АКАДЕМИИ АРХИТЕКТУРЫ И СТРОИТЕЛЬНЫХ НАУК, ЧЛЕН РЕДАКЦИОННОЙ КОЛЛЕГИИ ЖУРНАЛА «INTERNATIONAL JOURNAL FOR COMPUTATIONAL CIVIL AND STRUCTURAL ENGINEERING» АЛЕКСАНДР ВИКТОРОВИЧ КУЗЬМИН

Научная и творческая общественность России понесла тяжелую утрату. 26 сентября 2019 года на 69-м году жизни скончался выдающийся советский и российский архитектор, президент Российской академии архитектуры и строительных наук (РААСН), академик РААСН, академик Российской академии художеств (РАХ), Народный архитектор Российской Федерации, Заслуженный архитектор Российской Федерации, Почетный строитель России, Почетный строитель Москвы, Почетный строитель Московской области Александр Викторович Кузьмин.

Александр Викторович родился 12 июля 1951 в Москве. С раннего детства он увлекался рисованием. Позже это увлечение переросло в серьезное занятие, рисунки, чертежи, и планирование стали профессией. А.В. Кузьмин сам решил стать архитектором, хотя изначально мечтал быть художником-иллюстратором. Еще в школе он узнал о наборе в подготовительную группу при Московском архитектурном институте, и все старшие классы усиленно посещал обучающие курсы.

О таких, как Александр Викторович Кузьмин, принято говорить — человек-эпоха. Вся его жизнь была примером самоотверженного служения профессии. В 1974 году Александр Викторович окончил в 1974 году Московский архитектурный институт. С 1974 по 1991 годы работал в НИиПИ Генерального плана г. Москвы, прошел путь от архитектора до главного архитектора института. С 1991 по 1996 годы – заместитель и

первый заместитель Председателя Комитета по архитектуре и градостроительству г. Москвы (Москомархитектура), начальник ГлавАПУ г. Москвы. С сентября 1996 года по июль 2012 года – председатель Москомархитектуры, главный архитектор города Москвы. Следует отметить, что А.В. Кузьмин никогда не ограничивался только лишь руководящей работой, многие проекты в Москве и области он создавал сам или в соавторстве с другими архитекторами. В 2009 году Александр Викторович был избран вице-президентом РААСН, в марте 2014 года был назначен генеральным директором Научно-исследовательского центра «Строительство».

В апреле 2014 года А.В. Кузьмин был избран Общим собранием членов РААСН президентом РААСН и утвержден в этой должности Правительством Российской Федерации. В апреле 2019 года Александр Викторович был также избран и утвержден в должности президента РААСН на второй срок.

А.В. Кузьмин известен в нашей стране и за рубежом как руководитель, автор и соавтор десятков крупных градостроительных проектов и научных трудов, реализованных архитектурных проектов. В его активе большое количество книг, научных статей, аналитических публикаций по различным проблемам архитектуры, градостроительства и строительных наук.

Александр Викторович совмещал свою профессиональную деятельность с педагогической работой. В течение многих лет он вкладывал большой труд в дело подготовки высококвалифицированных кадров в Московском архитектурном институте (государственной академии). Под его руководством и при его деятельном участии были защищены сотни выпускных квалификационных работ, была воспитана целая плеяда талантливых архитекторов и градостроителей.

А.В. Кузьмин долгие годы являлся членом Президиума правления Союза архитекторов России и Союза московских архитекторов, Председателем Совета главных архитекторов субъектов Российской Федерации и муниципальных образований, Председателем Совета главных архитекторов столиц стран СНГ.

Александр Викторович имеет благодарность Президента России, является обладателем золотой медали им. В.Г. Шухова, золотых медалей РААСН и РАХ, Лауреатом Государственной премии Российской Федерации в области архитектуры, премии Правительства Российской Федерации, двух премий правительства Москвы, Кавалером ордена Франции «За заслуги в области искусств и литературы» и Инженерного общества Бельгии «За заслуги в изобретениях», награжден Знаком отличия «За безупречную службу городу Москве», четырьмя орденами и медалью Русской Православной Церкви.

Светлая память о выдающемся мастере архитектуры, одареннейшем педагоге и наставнике, замечательном человеке Александре Викторовиче Кузьмине будет вечно жить в сердцах и памяти тех, кто его знал.

Выражаем искренние соболезнования родным, близким и коллегам в связи с невосполнимой утратой.

Редакционная коллегия и редакционный совет журнала
International Journal for Computational Civil and Structural Engineering